Suffusion Phenomenon in Widely Graded Soils Influence of Homogeneity

Dissertation

zur Erlangung des akademischen Grades

Doktor-Ingenieur

an der Fakultät Bauingenieurwesen

der

Bauhaus-Universität Weimar

vorgelegt von

M.Sc. M.Sc. Mohamad Reza Salehi Sadaghiani

aus Teheran (Iran)

Gutachter:

1. **Prof. Dr.-Ing. Karl Josef Witt**
2. **Prof. Dr.-Ing Eckhart Kraft**
3. **Senior Lecturer Dr.-Ing Alexander Scheuermann**

Tag der Dissputation: 08 Juni 2016

Vorwort des Herausgebers

Das Phänomen der Suffosion in weitgestuften Böden ist seit vielen Jahren ein wesentliches Forschungsfeld an der Professur Grundbau der Bauhaus-Universität Weimar. Nach den grundlegenden Arbeiten von Herrn Semar bis 2009 hat nun Herr Salehi Sadaghiani in Fortsetzung dieser Forschung eine Dissertation mit einer sehr speziellen und neuen Fragestellung vorgelegt. Aus vielen experimentellen Untersuchungen, die in Zusammenhang mit einem DFG-Forschungsprojekt und einer deutsch-französischen Kooperation zu den Erosionsrisiken der Seitendämme am Oberrhein durchgeführt wurden, hat sich gezeigt, dass die Homogenität der Bodenproben, somit auch die Homogenität der Schüttung in einem Erdbauwerk, ein wesentlicher Aspekt des Grenzzustandes der inneren Erosion und speziell der Suffosion weitgestufter Böden ist. Dieser Aspekt ist zwar jedem Experimentator als Erklärung der eher unbefriedigenden Reproduzierbarkeit der Ergebnisse bekannt, es gab aber in der Geotechnik bisher keinen Ansatz zur Quantifizierung. Was ist Homogenität in Zusammenhang mit Suffosion? Wie ist die Definition? Wie viel Inhomogenität, unvermeidliche Entmischung, ist akzeptabel? Wie lässt sich der Zusammenhang zwischen dem Grad der Entmischung und dem Erosionspotential quantitativ darstellen?

Herr Salehi Sadaghiani hat mit Experimenten begonnen, hat die Bedingungen des Grenzzustandes aufgezeigt, theoretische Zusammenhänge hergeleitet. Und er hat versucht, den unbestimmten Begriff der Homogenität in Hinblick auf das Potential einer inneren Erosion quantitativ zu greifen und zu bewerten. Dabei hat er in vielen Punkten neue Wege beschritten oder zumindest geebnet. Zum einen ist es das verbesserte Experiment, mit dem er die Einflüsse und die Grenzen der Homogenität aufgezeigt hat, zum andern ist dies die Simulation mit diskreten numerischen Modellen in Zusammenhang mit digitaler Bildverarbeitung. Seine Definition der Homogenität über das repräsentative Einheitsvolumen ist nicht neu, aber die Quantifizierung des Einflusses der Homogenität auf die Suffusion ist originär. Und am Ende seiner Arbeit definiert er ein neues Suffosionskriterium, das den Grad der Homogenität berücksichtigt.

Für mich blieben am Ende der Lektüre dieser Dissertation zwei Fragen, (i) kann es denn bei weitgestuften Böden in der Praxis überhaupt Homogenität in einem befriedigenden Grad geben und (ii) treffen wir mit unseren bisherigen Ansätzen zum Suffosionsnachweis den überhaupt den Nagel oder ist bei weitgestuften Böden die Durchströmung wie auch der Partikeltransport nicht vielmehr eine Frage der zufälligen Aneinanderreihung entmischter Zonen? Wenn dem so wäre, ist jeder deterministische Nachweis der inneren Erosion weitgestufter Böden unter hydraulischer Beanspruchung unzutreffend. Die Strategie kann dann nur in der Elimination des Risikos liegen, in der Kontrolle der potentiellen Transportwege.

Weimar, Juni 2016   Karl Josef Witt

Acknowledgments

I strongly believe that this thesis with all its side effects has been worth it. I did not know that at the beginning how much effort and hardship my family, friends and I had to invest in this thesis. Truly, sometimes it is better not to know what the future holds. I have had a very deep process in self and world recognition during my time here in Bauhaus-Universität Weimar.

I don't know how can I thank all friends, events and processes that guide me to this point. The best summarized way is to thank life, for all of these beauties. Nevertheless, I would like to take this opportunity to express my appreciation to the following people who, over the years, have made a significant contribution to the completion of this thesis as well as my self knowledge. Of course, many others deserve mention too; to you, I can only promise that you are really appreciated. If you don't believe it, it is also appreciated. Thanks go to:

- **Prof Karl Josef Witt**, thesis supervisor (Department of Geotechnical Engineering, Bauhaus-Universität Weimar). You have been a patient critic and a gracious academic guide.You have taught me, both consciously and unconsciously, a lot of lessons about life and geotechnical engineering. I appreciate all his contributions of time, ideas, jokes and funding to make my PhD experience productive and stimulating. The joy and enthusiasm you got for your work, teaching and research was contagious and motivational for me, even during tough times in the life situations. I am also thankful for the excellent example you have provided as a successful geotechnical engineer, professor and kind human being. Thanks for persevering with me through this chapter of my life. You have also become a wonderful friend. I will never forget the Christmas 2009 at your house with your lovely wife. It has brought a whole new dimension to the contemplation of dialogue the cultures.

- **Arvin Salehi Sadaghiani** my son, who taught me how to be present and collect creative energy from the present moment and forced me always to laugh. He taught me to laugh without having any reason and living without expectations

- **Hosseingholi Salehi Sadaghiani** my father, who almost forced me to resign my job in Iran and supported me lovingly to come to Germany and get my PhD.

- **Paul Winkler** my good friend and colleague, I would like to acknowledge you for working along side me, I very much appreciated your enthusiasm, intensity, willingness to do the numerical simulations. Your interests on modeling and programming have inspired me to work more in this direction.

- **Robert-Baltazar Wuttke** my good friend and colleague, your enthusiastic engineering skills plus your many objections have made me think highly hard and very carefully, the

result of which is I am confident, a much stronger dissertation.

- **Hennes Jentsch** my good friend and colleague, your seriousness and way of thinking plus your many ideas have made me work on those ideas hard the result of which is I am confident, a well throughout thesis. I would also thank you for working along side me on different experiments.

- **Thomas Wolf** my good friend and colleague, your penetrating questions and comments have been truly helpful, adding clarity to my thesis; and your unfailing humor and personal warmth have always lifted my spirit. I have learned a lot from you, how to write and how to make a good diagram.

- **Dr.-Ing Alexander Scheuermann**, I would like to thank you for the constructive conversations. I appreciate also the time that we worked together on the research proposal. I have learned some very good important points on suffusion from you.

- **Prof Dr.-Ing Eckhard Kraft**, I would like to thank you for your thesis and interesting usage of voronoi-tesselation method, which inspired me a lot to research on this topic and find a way for quantification of homogeneity. The scientific and friendly conversations with you have brought a lot of insight to my work.

- **Prof Dr.-Ing Dimitrios Kolymbas**, I would like to thank you for your enthusiasm about physic. It is always amazing to see you presenting your ideas about geotechnical engineering.

I would also like to acknowledge the lab of the Department of Geotechnical Engineering, Bauhaus-Universität Weimar, Frank Hoppe and Gabriele Tscheschlok as well as MFPA Weimar, where I made several probes and a lot of experiments, Jens Köditz and Thorsten Schäfer and other good friends of the MFPA Weimar lab.

Foreword of Author

I would like to give an introduction to soil behavior to clear my point of view in this thesis. I start to describe the soil strength, because all engineers are familiar with the concept of strength. From former works or studies, it may be apparent that soil strength is not unique values as it tends to be for steel and concrete, two materials that are specified by engineer and carefully controlled during manufacture, so their strength and behavior can be predicted with a good accuracy.

It is not on common to measure the soil strength on the identical side that differs in value by in order of magnitude. For example, two tests on same soil but on samples in various depth may give strength that differ by 100%. If such variations were found from test on steel, something must be wrong. Typically, we would expect the strength of steel to vary by no more than a few percent. Geotechnical engineers are dealing with results of a large variation. It is because of the inherent variability of nature, what is really amazing and interesting for me. One cannot probably find two grains which are totally the same. This is like the fingerprints of different person which are definitely different. As a matter of fact, for steel and concrete if one chooses a smaller scale (micro-scale), the behavior encounters spatial variability too. Structural Engineers are used to work with the small range of result's variations. It is because of the manufactured materials. If someone tries to go deeper into the roots of both disciplines, one will see that this is much more to do with inherent variability in nature and representative elementary volume of both material than a philosophical difference between two disciplines. So, this was one of the reasons, that I wanted to do my PhD in geotechnical engineering, and it was really satisfactory to try to understand the nature.

The research studies in soil mechanics unfortunately had one undesirable effect. The attentions of many researchers and even lecturers are diverted from diverse limitations imposed by nature on the application of mathematics to soil mechanic's problems. Consequently, more and more focus has been placed in refinements sampling and testing on those very few problems which can be solved with enough accuracy. However, accurate solution can be obtained only if the soil strata is stochastically homogeneous and continuous in horizontal direction. Furthermore, since the investigations leading to exact solution involve highly specialized methods of sampling and testing, they are justified in exceptional cases. It must be considered that on the majority of different projects, no more than approximate prediction or forecast is needed and if such a prediction cannot be made by simple means, it cannot be made at all. I believe, if it is impossible to make an approaching forecast, the behavior of the soil must be observed during the construction, and the design has to be modified in accordance with the field situations. These facts have been thought over in the background of my PhD thesis.

Abstract

In this study, the behavior of a widely graded soil prone to suffusion and necessity of homogeneity quantification for such a soil in internal stability considerations are discussed. With the help of suffusion tests, the dependency of the particle washout to homogeneity of sample is shown. The validity of the great influence of homogeneity on suffusion processes by the presentation of arguments and evidences are established. It is emphasized that the internal stability of a widely graded soil cannot be directly correlated to the common geotechnical parameters such as dry density or permeability. The initiation and propagation of the suffusion processes are clearly a particle scale phenomenon, so the homogeneity of particle assemblies (micro-scale) has a decisive effect on particle rearrangement and washout processes. It is addressed that the guidelines for assessing internal stability lack a fundamental, scientific basis for quantification of homogeneity. The observation of the segregation processes within the sample in an ascending layered order (for downwards flow) inspired the author to propose a new packing model for granular materials which are prone to internally instability.

It is shown that the particle arrangement, especially the arrangement of soil skeleton particles or the so-called primary fabric has the main role in suffusiv processes. Therefore, an experimental approach for identification of the skeleton in the soil matrix is proposed. 3D models of Sequential Fill Tests using Discrete Element Method (DEM) and 3D models of granular packings for relative, stochastically and ideal homogeneous particle assemblies were generated, and simulations have been carried out.

Based on the numerical investigations and in dependency on the soil skeleton behavior, an approach for measurement of relevant scale, the so-called Representative Elementary Volume (REV) for homogeneity investigation is proposed. The development of a new testing method for quantification of homogeneity is introduced (in-situ). An approach for quantification of homogeneity in numerically or experimentally generated packings (samples) based on image processing method of MATLAB has been introduced. A generalized experimental method for assessment of internal stability for widely graded soils with dominant coarse matrix is developed, and a new suffusion criterion based on ideal homogeneous internally stable granular packing is designed.

My research emphasizes that in a widely graded soils with dominant coarse matrix, the soil fractions with diameters bigger than D_{60} build essentially the soil skeleton. The mass and spatial distribution of these fractions governs the internal stability, and the mass and distribution of the fill fractions are a secondary matter. For such a soil, the homogeneity of the skeleton must be cautiously measured and verified.

Kurzfassung

Problemstellung und Zielsetzung der Arbeit

Dämme und Deiche für z.B. Fluß-, Kanal- oder Speicherbauten sind Erdbauwerke mit großer Kubatur, die meistens großen Platzbedarf und enormen Materialverbrauch erfordern. Aus der Vielfalt von Materialien die uns zur Herstellung der Dämme zur Verfügung stehen, muss immer die wirtschaftlichste Lösung gefunden werden. Aus diesem Grund werden im Dammbau, die im Umfeld natürlich anstehenden Böden verwendet. Meist handelt es sich um weitgestufte Böden, so dass bei der Herstellung der Erdbauwerke eine potenzielle Gefahr der Entmischung besteht. Bei einer hydraulischen Beanspruchung solcher Böden können verschiedene Prozesse der inneren Erosion auftreten, deren Phänomene in Filtration, Suffosion, Kolmation und rückschreitende Erosion unterschieden werden.

In der Geotechnik beschreibt man den Transport von Feinteilen aus einem Erdstoff mit dem Begriff "Suffosion". Kommt es zum Materialtransport innerhalb des Bodens, verursacht dies eine Erhöhung der Wasserdurchlässigkeit und des Porenanteils. Gleichzeitig nehmen die Raumdichte des Bodengefüges und die Tragfähigkeit des Bodens ab. Suffosion ist geometrisch möglich, wenn die Porenengstellen der groben, skelettbildenden Fraktionen größer als die Korngrößen der mobilen feinen Fraktionen des Bodens sind. Sobald ein kritischer hydraulischer Gradient erreicht wird, werden die mobilen feinen Partikel transportiert.

Wegen des starken Einflusses der Struktur spielt die Homogenität des Korngefüges bei allen Prozessen der inneren Erosion eine große Rolle. Die Effekte der Suffosion können bei verschiedenen Erdbauwerken unterschiedliche Wirkung haben und zur Beeinträchtigung der Funktion oder zu Schäden führen. Zu den Aufgaben der Ingenieure zählt die Abschätzung, inwiefern die hydrodynamischen Einwirkungen einen standsicherheitrelevanten Einfluss haben.

Die Rolle der Partikelzusammensetzung zur Initialisierung und Fortsetzung des Materialtransportes (Suffosion) wurde noch nicht vollständig untersucht. Alle gängigen Kriterien gehen von einer Homogenität des Gefüges aus. Daher ist das Hauptziel dieser Arbeit, ein analytisches Suffosionskriterium unter Berücksichtigung der Homogenität abzuleiten. Das Kriterium soll in der Lage sein, die mobilen, lokal beweglichen, sowie die suffosiven, global beweglichen Fraktionen eines weitgestuften Bodens einzuschätzen.

Stand der Wissenschaft

Geometrische Suffosionskriterien basieren auf Untersuchungen, die zur Dimensionierung von Erdstofffiltern im Dammbau entwickelt wurden. Als Eingangsparameter werden die Korngrößenverteilungen der Böden herangezogen. Fundamentale geometrische Suffosionskriterien wurden u. a. von Ziems (1969), Burenkova (1993), Kenney & Lau (1986), Wan und Fell (2008) und Witt (2013) entwickelt.

Mit den verfügbaren Kriterien zur Beurteilung der inneren Suffosionsbeständigkeit kann die Wahrscheinlichkeit eines Materialtransportes nicht quantitativ beurteilt werden. Die zahlreichen Kriterien basieren im Wesentlichen auf empirischen Ansätzen und sind nur für spezifische Bodenarten und Randbedingungen anwendbar. Die Anwendungsgrenzen der Suffosionskriterien werden hinsichtlich der Bodenart und des Ungleichförmigkeitsgrades meist überschritten.

Darüber hinaus ist das Phänomen "Suffosion" in erster Linie ein Problem, das auf der Partikelebene untersucht werden muss. Die Homogenität der Kornzusammensetzung der Erdstoffe findet explizit keine Rolle in den verfügbaren Kriterien und die aktuellen internationalen Forschungsaktivitäten zeigen, dass hauptsächlich weitere empirische Ansätze entwickelt werden.

Eingesetzte Methoden

Für die analytische Beschreibung von suffosiven Materialtransportprozessen in weitgestuften Erdstoffen unter Berücksichtigung der Homogenitätseffekte, muss das Phänomen auf der Partikelebene beschrieben werden. Dies setzt drei Arbeitsschritte und Teilziele voraus: i) Die Kenntnis und Beschreibung der Gefügestruktur ii) Beschreibung und Dimensionierung eines repräsentativen Volumens iii) Konstruktion einer homogenen Packung für beliebige Korngrößenverteilungslinien und Quantifizierung des vorhandenen Homogenitätsgrads.

Die granularen Packungen wurden sowohl experimentell als auch numerisch anhand sequentieller Mischversuche (SFT) untersucht. In einer stochastisch homogenen Packung werden der Anteil der skelettbildenden und der mobilen Fraktionen identifiziert und ein Bereich als Trenndurchmesser, der Skelett und mobile Feinteile abgrenzt, bestimmt. Dadurch kann die Gefügestruktur in suffosiv und nicht suffosive Gruppen klassifiziert werden. Der experimentelle Ansatz wurde numerisch mittels Diskreter Element Methode (DEM) simuliert, um die Kontaktkräfte und Anzahl der Nachbarn für verschiedene Bodenfraktionen (Skelett und bis zu gewissen Bereichen auch die Füllung) zu finden. Das kleinste repräsentative Volumen (REV) für solch eine Bodenpackung wird numerisch bestimmt. Eine Methode zur Festlegung der relevanten Skala zur Quantifizierung der Homogenität wurde vorgeschlagen.

Als Bindeglied wurden 2D-Aufnahmen der experimentell oder numerisch erzeugten Packungen angefertigt, um mit Methoden der digitalen Bildverarbeitung die relevanten Kennwerte der Packung und die Anzahl der skelettbildenden Partikel zu ermitteln. Die erfassten Oberflächen dienen der statistischen Analyse der räumlichen Streuung skelet-

tbildender Partikel. Anhand der Berechnung der Varianz können die unterschiedlichen Parameter miteinander verglichen werden. Eine Varianz von Null bedeutet totale Homogenität. Ein Programm wurde in MATLAB geschrieben, um die Bildanalyse und die Varianzkalkulationen anhand unterschiedlicher Eingangsparameter durchzuführen. Ein analytisch beschreibbares Packungsmodell wird vorgeschlagen, um Homogenität und REV mit Suffosion in Verbindung zu bringen. Basierend auf diesem Modell wird ein Suffosionskriterium entwerfen, das in der Lage ist die Masse des ausgespülten Materials aus einem weitgestuften Boden zu prognostizieren.

Wesentliche Ergebnisse

Suffosion ist ein Phänomen der Partikelskala und der Partikeltransport ist abhängig von der Partikelanordnung. Die Zusammensetzung der skelettbildenden Partikel bestimmt die Eigenschaft des Porenraums. Die charakteristischen Parameter der Bodenstruktur eines weitgestuften Bodens wurden anhand sequentieller Mischversuche (SFT) festgestellt. Dadurch kann ein weitgestufter Boden in suffosiv oder nicht-suffosiv eingestuft werden.

Das granulare Material formt ein Skelett, wenn die benötigte Mindestmasse oder das repräsentative Volumen erreicht wird. Dies ist eine notwendige Bedingung für die weiteren Untersuchungen. Diese Mindestmasse bzw. das repräsentatives Volumen wurde numerisch mittels DEM Simulationen ermittelt.

Eine statistische Methode für die Quantifizierung der Homogenität für 2D-Aufnahmen in Abhängigkeit der Größe des repräsentativen Volumens wurde vorgeschlagen. Diese Methode wurde für komplexe stochastisch homogene, segregierte sowie für homogene Gitter-Packungen getestet. Die Ergebnisse sind vergleichbar mit dem bekannten Verfahren des Voronoi-Diagramms. Der Vorteil dieser Methode ist, dass viele Parameter berücksichtigt und in den Code integriert werden können.

Eine in-situ Versuchsmethode für die Quantifizierung der Homogenität wurde vorgeschlagen. Darüber hinaus wurde gezeigt, dass der lockerste und der dichteste Zustand eines weitgestuften Bodens, welcher gemäß den Standardrichtlinien ermittelt werden kann, nicht die ultimativen Zustände sind. Die ultimativen Zustände können durch die vorgeschlagene Probenvorbereitung ermittelt werden. Ein homogenes Packungsmodell für weitgestufte Böden mit dominanter Grobmatrix wurde vorgestellt. Die Idee dieses Packungsmodells basiert auf der immer wiederkehrenden Natur der Homogenität und des Segregationsprozesses. Dieses Modell wurde durch Suffosionsversuche getestet und validiert.

Basierend auf dem vorgeschlagenen Packungsmodell wurde eine neue experimentelle Methode zur qualitativen Beurteilung der Suffosionsanfälligkeit vorgestellt. Ein neues analytisches Suffosionskriterium, basierend auf dem vorgeschlagenen Packungsmodel unter Berücksichtigung der Homogenität im REV wurde entworfen. Damit können die mobilen sowie suffosiven Fraktionen eines weitgestuften Bodens ermittelt werden.

Contents

List of Figures

List of Abbreviation

STL   StereoLithography is a file format native to the stereolithography CAD software created by 3D Systems. STL is abbreviation of "Standard Triangle Language" and/or "Standard Tessellation Language".

SUFFOS   The aim of the SUFFOS project, which was supported by the German Research Foundation (*DFG*), was to study suffusion processes in gradated soils. The main purpose was the numerical simulation of the erosion phenomena to derive suffusion criteria and boundary conditions based on the statistical data. Project duration (1st phase): August 2007 - October 2010

Yade   Yade is an extensible open-source framework for discrete numerical models, focused on Discrete Element Method

List of symbols

v	$\mathrm{m\,s^{-1}}$	velocity of Fluid
V	$\mathrm{m^3}$	volume
V_{sat}	$\mathrm{cm^3}$	the needed volume of water for saturation of the sample
$V_{w,outlet}$	$\mathrm{cm^3}$	the measured volume of water at the outlet of the test apparatus
W_{dio}	$\mathrm{cm^3}$	the needed volume of dionized water sample preparation
W_{tap}	$\mathrm{cm^3}$	the needed volume of tap water for saturation
σ	$-$	standard deviation
σ^2	$-$	variance

List of Tables

1. Introduction

1.1. Relevance of the study

The effect of particle arrangement in micro-structures is widely understood to be a major feature in controlling behavior of all materials. In soil, this is the most important issue because of its three-phase structure and its local variations. Often non-homogeneity dispersed in a particle segregation, deformable matrix, leading to poor mechanical and hydraulical properties. Homogeneous distributions of the soil particles are well documented as improving the soil mechanical and hydraulical characteristics when compared to segregated soils (Saucke et al., 1999). For instance, the resulted micro-structure of the soil body have a decisive influence on the internal stability of the widely graded soils. In the recent years, different soil placement techniques and specifications for preparation of soil materials have been employed to improve homogeneity.

However, there are still reports of dam and embankment failures (Bonelli, 2012). Because of uncertainties, the thickness of soil layers, even filter layers, has been increased by guidelines to ensure a more uniform average property. The homogeneous distribution of the particles at the micro-structure level is unpredictable, despite all of the current considerations. The reality of the particle arrangement is much more complicated, and in-situ particle distributions are highly dependent on placement parameters during construction (i.e., the moisture content of the soil, drop height, geometry, particle coarseness, the relation between particle diameters, dynamical vibrations). There is a general assumption in geotechnical communities that the particle arrangement of poorly graded soils, like filter materials, is always homogeneous. Even so, after Kenney and Westland (1993) the poorly graded soils are also very vulnerable to segregation.

Improved ability to define and quantify the homogeneity of soil (particle arrangement) is required so that homogeneity measurement of specimens can be more directly correlated to material's mechanical and hydraulical performance. This study focuses on the development of a quantification methodology in this area through numerical, experimental, image analysis as well as statistical approaches. Ultimately, an improved homogeneity assessment method may lead to more systematic methods for soil placement techniques and tool design to get a higher coefficient of homogeneity not only in a laboratory controlled specimens but also in field conditions.

1.2. Motivation

In flow through soil materials, there is always the risk of internal erosion. The seepage can cause particle migration, rearrangement and thus structural changes. Wherever soil exists, internal erosion of the soil can lead to catastrophic consequences. According to Foster et al. (2000), 136 large dams in the world, which were constructed until 1986, have failed. Almost half of them due to different internal erosion processes. This study did not take into account the channels and flood protection dikes. Suffusive processes usually occur in supporting body of the dams and dikes, which is built using widely graded soils (see Figure 1.1). If the supporting body is segregated, the suffusion can occur even for an internally stable widely graded soil.
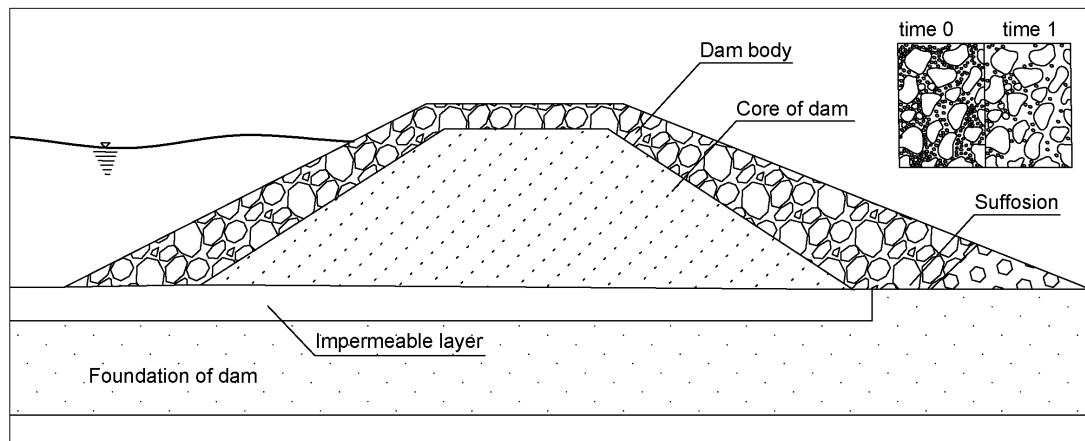
Figure 1.1.: Schematic view of an embankment dam

Despite all of the recent researches and proposed design methods, the failure frequency is still high and constant during the past years, as Fell and Fry (2007) reported that it is approximately one failure per annum. Moreover, ecological and economical damages can be reported due to the internal erosion of technical flood protection constructions. Even in the natural underground, internal erosion leads to subsidence and sinkholes. When internal erosion is to occur, the time until the failure happens is difficult to predict. To be able to develop adequate emergency action plans preventing casualties, it is necessary to comprehend the phenomena of internal erosion.

Indisputably, overviews of current research on internal erosion exist, and many laboratory studies have been carried out on this subject just by looking at, for instance, the conference proceedings in last decade. All these studies show that the internal erosion is not entirely understood yet. The author believes that this phenomenon cannot be understood without the homogeneity consideration as well as its quantification. It can be seen that in the most accepted experimental and even though theoretical studies for assessment of internal stability in soils, there is an assumption that the investigated soil is homogeneous or is to be placed in a homogeneous manner without any checking and proof for this hypothesis. However, after Ripley (1986), the potential for internal erosion

instability of a specific *PSD* can significantly be higher than indicated by such a laboratory test if the soil material is susceptible to segregation. Moreover, the criteria based on these studies which are widely used in engineering guidelines has almost no consistency in the internal stability predictions. For instance, for different *PSDs* which are shown in Figures 1.2,1.3,1.4, these criteria predict different assessments. (see Table 1.1).
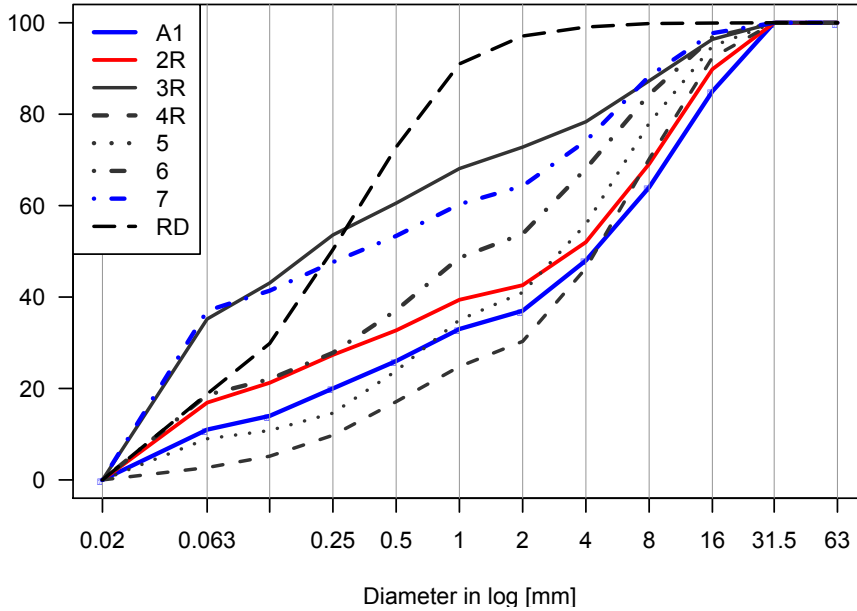
Figure 1.2.: PSDs of theoretically analyzed soils by authors - stable soils
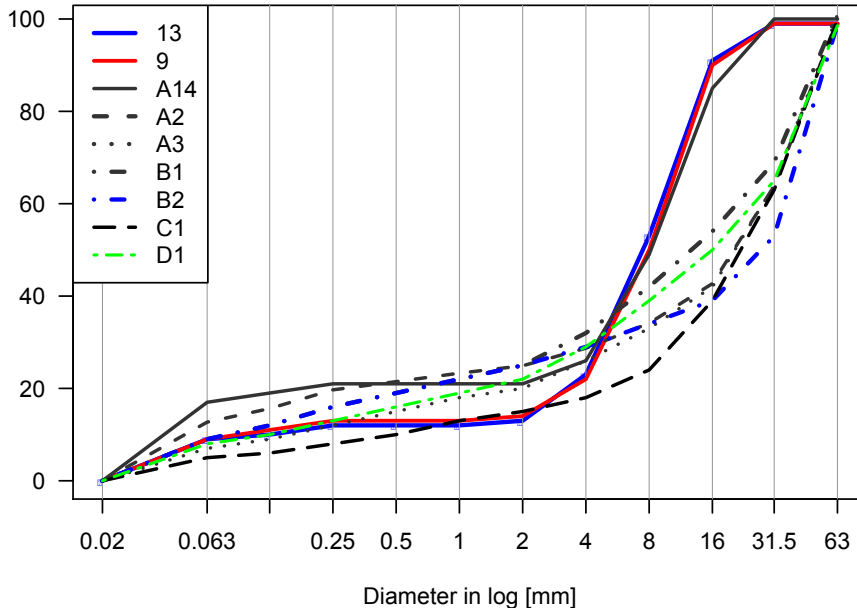
Figure 1.3.: PSD of theoretically analyzed soils by authors - unstable soils

In almost all of published experimental studies were written that the soil specimen was homogenized, or soil was placed in a homogeneous manner into the test device. Nevertheless, the term homogeneity is not clear and is not quantified by experts. The prepared and investigated specimens were always assumed to be homogeneous. But all experiments show that it is still one of the main challenges to building a soil specimen of a widely graded soil without segregation.
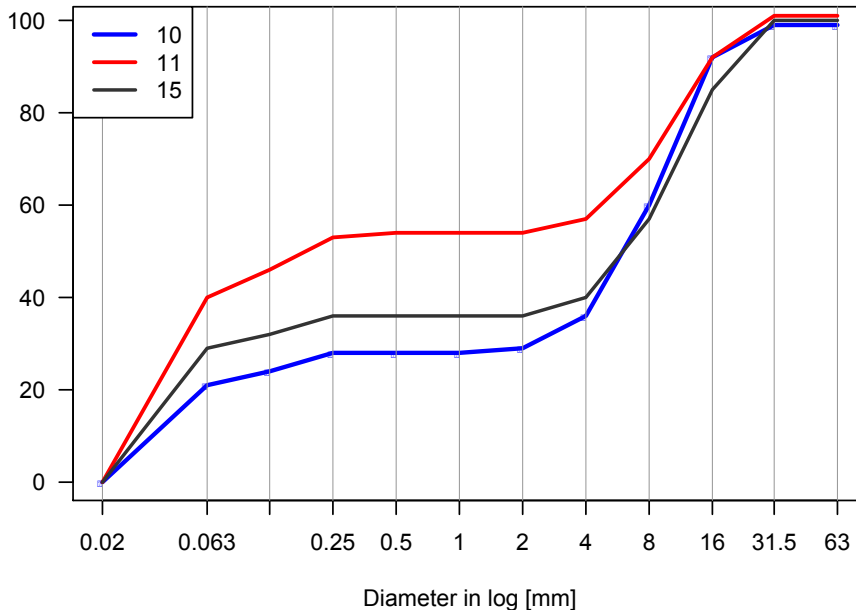
Figure 1.4.: PSD of theoretically analyzed soils by authors - soils with marginal stability

By the construction of flood protection dikes and earthworks, the soil will be placed in a random way. Therefore, the results of laboratory tests under controlled specimen preparation cannot be used for field situations, even if the assumption of homogeneity is a realistic assumption and has been met. In Table 1.1, it can be seen that the results of suffusion criteria for different widely graded soils vary significantly. In this Table, the following symbols are used: Stable (*S*), Unstable (*U*), Marginal (*M*), Different prediction (*) and more than 5% cohesive soil (**).

In controlling of the soil shear strength, settlement, permeability, internal erosion and many other aspects, the most highly important criterion is the homogeneity of particles in the soil. There is no placement technique for earthworks, which can assure a consistent quality of the compacted soil material. The reason for that is the mechanism of particle motion. It is still unclear, and no standard concise method exists for quantifying and comparing homogeneity for field and laboratory tests as well as for numerically generated specimens based on *DEM*. The guidelines and recent studies are not able to consider the homogeneity of the soil quantitatively. There is also no standard way for the production of a homogeneous specimen for experimental purposes. It is necessary to find a method for quantification of the soil homogeneity before starting to assess the internal stability or even compare results of different experimental or numerical methods.

PSD	Sherard (1979)	Kenny-Lau (1984, 1985)	Burenkova (1993)	Wan-Fell (2008)	Sadaghiani-Witt (2012)
A1	U*	U*	S	S	S
2R	U*	U*	U,M*	S	S
3R	U*	S,M	S	S	S
4R	U*	U*	S	S	S
5**	U*	U*	U,M*	S	S
6**	U*	U*	U,M*	S	S
7**	U*	U*	U*	S	S
RD	U*	U*	S	S	S
10	U	S*	U	U	U,M
11	U	U	S	S	S,M
15**	U	U	U	U	U,M
9	U	U	S*	S*	U
13**	U	U	S*	S*	U
14A**	U	U	U	U,M	U
A2	U	U	U	U	U
A3	U	U	U	U	U
B1	U	U	S*	U	U
B2	U	U	U	U	U
C1	U	U	U	U	U
D1	U	U	S*	U	U

Table 1.1.: Comparison of results of some suffusion criteria used for internal stability assessment of different widely graded soils.

1.3. Research aim

The research is focused on suffusion phenomenon and the description of homogeneity influences on internal stability of the widely graded soils. Therefore, the quantification of the soil homogeneity (particle arrangement) within the framework of direct image analysis methods based on mathematical tools is considered. For *3D* numerical granular packings, coefficient of homogeneity (C_H) should be calculated based on the *2D* image analysis and statistical methods. To achieve these aims, Author has studied different disciplines to quantify the homogeneity of widely graded soils with a coarse dominant matrix.

Topics studied included experimental identification and evaluation of soil matrix, Discrete Element Method *DEM* for modeling different granular packings with a coarse dominant matrix, image analysis as well as statistical tools of *MATLAB* (see Fig. 1.5. Additionally, case studies are elaborated to demonstrate the application of homogeneity quantification in numerically generated packings and laboratory tests. These established calculation procedures for homogeneity quantification are seen as basic for internal stability assessment and construction quality control by earthworks. It is intended to propose a new granular packing for ideal homogeneous widely graded soil. The implementation of homogeneity consideration in internal stability leads to a more reliable risk assessment. Finally, based on all investigations an empirical analytical criteria should be proposed.
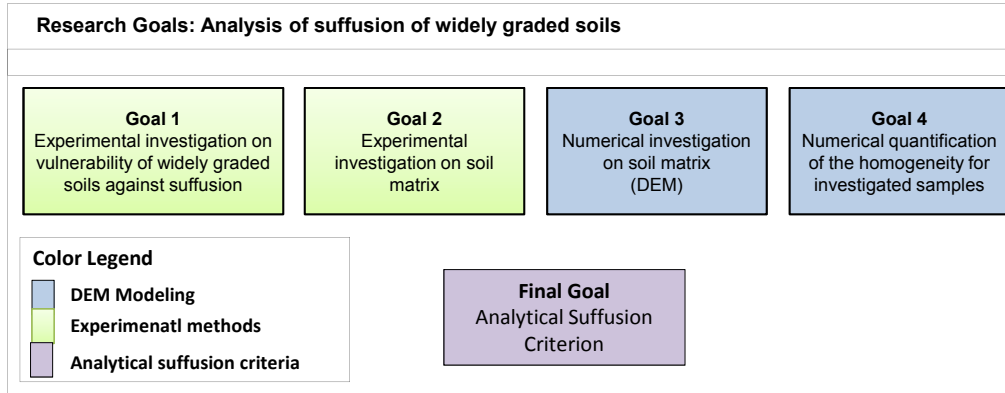
Figure 1.5.: Research aims

1.4. Literature review

1.4.1. Previous studies on internal erosion and filtration

Seepage flow can cause the different shapes of internal erosion in soils. Often, it is followed by piping failure and soil structure collapse, or if soil is protected by a filter, then it can cause clogging of the zone in front of the filter. Although internal erosion can be controlled by filters if they are already available, it is necessary to investigate soil vulnerability against internal erosion. Among poorly graded cohesion-less soils, silty sands and silts are considered as prone to internal erosion. The widely graded soils with a small amount of fine content are also susceptible to internal erosion. Cohesive soils and widely graded soils with a dominant fine matrix are more resistant to internal erosion, due to cohesion of such a soil (inter-particle forces).

For assessment of the soil internal stability, many empirical, experimental and numerical approaches are presented. In Tables 1.2 to 1.5 several examples of empirical methods can be found, which are still used for the evaluation of soil safety against different types of internal erosion and piping. However, all of them are suitable for an overall estimation, because they do not take into account the gap grading of the particular *PSD* and the water flow concentration due to the possible segregation. Even though, for the uniform filters as it is shown in the Tables 1.2 to 1.5, carried out experiments on a certain *PSD* cannot be supported fully by other researchers, that emphasize the importance of homogeneity in laboratory scale again. Although, the experimental methods are, to some extent, suitable for internal erosion investigation of widely graded soils, they are too time-consuming and expensive. To obtain the expertise for carrying out such an experiment cannot be easily achieved.

In the following, different expressions and terms are used when referring to a *PSD* curve. A certain diameter of the particle is indicated by D with a numeric subscript that corresponds to a point on the curve equivalent to the percentage of particles passing through the imaginary sieve with the openings of the same size. If the particle diameter of PSD at 10% passing (D_{10}) equals to 0.075 mm. This means 10 percent, by dry mass of

soil, is composed of particles smaller than 0.075 mm. The 10-percent size (D_{10}-sizes) is also called the effective particle size by Hazen. This term was introduced by Hazen in connection with his work on sanitary filters (Fair et al., 1933). Hazen found that sizes smaller than the effective particle size affected the functioning of filters as much or more than did the remaining 90 percent of sizes. Other sizes, such as D_5, D_{15}, D_{50}, D_{85} and D_{90}, are also used in filter design. The sizes D_{10}, D_{30}, and D_{60} are used in defining the *PSD* or gradation characteristics of a soil. One could say, the gradation curve is used to designate various particle fractions by particle size.

Reference/Title	study Type	Major conclusions
Karl Terzaghi [1939]/Soil Mechanics: A New Chapter in Engineering Practice (Terzaghi et al., 1996)	Empirical/Filter tests	- Soil retentaion criterion (piping)$D_{15F}/D_{85B} < 4 \sim 5$ - Permeability criterion $D_{15F}/D_{85B} > 4$ - the particle diameter of filter at 15% passing (D_{15F}) - the particle diameter of base at 85% passing (D_{85B})
G.E. Bertram [1940]/An Experimental Investigation of Protective Filters (Bertram, 1940)	Empirical/Filter tests	- Stability condition: $D_{15F}/D_{85B} = 6$ - The dependency of ratio D_{15F}/D_{85B} on shape of the soil's particle - Suitability of ratio D_{15F}/D_{85B} for $i = 6 \sim 20$ - hydraulic gradient (i)
K.P. Karpoff [1955]/The Use of Laboratory Tests to Develop Design Criteria for Protective Filters (Terzaghi et al., 1996)	Empirical/Filter tests	- the particle with maximum diameter of the filter ($D_{max,F}$) < 75 mm to minimize segregation and bridging during placement - $D_{5F} > 0.075$ mm to prevent excessive movement of fines in the filter - D_{5F} the particle diameter of filter at 5% passing - *PSD* of filter and base should be approximately parallel to the range of finer sizes - Some extra recommendations for ratio D_{15F}/D_{85B} and D_{15F}/D_{15B} - the particle diameter of base at 15% passing (D_{15B})
Davidenkof [1964]/Deiche und Erddämme (Davidenkoff, 1964)	Empirical	- Importance of cohesion – usage of aggregate sizes in filter criteria instead of particle sizes
P.R. Vaughan [1978]/Design of Filters for the Protection of Cracked Dam Cores against Erosion (Vaughan and Soares, 1982)	Empirical/ Discussion	- The way that the Balder-head-Dam core in Northern England behaved during failure suggests that filter design criterion based on intact homogeneous core clay is invalid - To prevent the erosion of the smallest core clay particle, at least 2.5% of the filter should pass the sieve number 200 (0.075 mm) - The filter permeability is a good measurement for filter design - For effective uniform filters the mean value of $k = 7 \cdot 10^{-5} cm/s$ - For effective graded filters the mean value of $k = 2 \cdot 10^{-5} cm/s$ - Accomplishment of sand castle tests is recommended to determine the amount of cohesion in filter - coefficient of permeability (k)

Table 1.2.: Selected studies on filtration and internal erosion without homogeneity consideration - part 1

Reference/Title	study Type	Major conclusions
J.L.Sherard [1979]/Sinkholes in Dams of Coarse, Broadly Graded Soils (Sherard, 1979)	Case Study	- Importance of filtration of the silt-size fractions - Problem soils are usually glacial in origin and have linear gradation curves - Assessment of internal stability for broadly (widely) graded soils using a separation point by one mm and checking the stability of the Base-Filter combination
U.S. Department of the interior [1980,1998]/Earth Manual second and third edition	Review of Filter Design Criteria	- Stability condition: $D_{50F}/D_{50B}= 5 \sim 10$ for uniform filters - If there is gravel in base Soil, modify the PSD so that PSD minus sieve number 4 fraction - in the third edition of the Earth Manual the ratio D_{15F}/D_{85B} is used
K. Arulandan and E.B. Perry [1983]/Erosion in Relation to Filter Design Criteria in Earth dams (Arulanandan and Perry, 1983)	Review of previous studies: Discussion of current filter design	- With reference to Terzaghi's filter criteria, for D_{15F}, the void column and permeability of the filter material decrease with increasing of the PSD Width. The filter permeability can then become equivalent to that of the base material. - The consequence of using a widely graded sand gravel filter is that, if it contains a significant percentage of fines passing the 200 sieve, combined with particle interlock, the filter may be able to sustain a crack - The main dilemma is that it is necessary to have some percentage of fines in the filter material to prevent erosion of base material, but this in turn allows the filter to behave as a cohesive material - Base material erodes due to a surface shear stress caused by water flow through the material
J. Lafleur [1984]/Filter Testing of Broadly Graded Cohesionless Tills (Lafleur, 1984)	Case study	- Suggests that the Filter permeability is a suitable criterion for determination of the success or failure of a filter
J.L. Sherard et al.[1984]/Basic Properties of Sand and Gravel Filters (Sherard et al., 1984)	Empirical/ Discussion	- $D_{15F}/D_{85B}<5$ is conservative for most uniform filters, but should continue to be used as the main criterion for filter assessment - D_{15F}/D_{85B} and D_{50F}/D_{50B} considerations established by USBR tests, which are performed in 1955 are not supported by these experiments

Table 1.3.: Selected studies on filtration and internal erosion without homogeneity consideration - part 2

Reference/Title	Study Type	Major conclusions
T.C. Kenney et al. [1985]/ Controlling Construction Sizes of Granular Filters (Kenney et al., 1985)	Theoretical/ Review of previous studies	- Mathematical analysis to the maximum and minimum constriction with the assumption of total homogeneity - The parameter of the controlling constriction diameter of the filter (D_c^*) is defined as the controlling constriction size of the filter, which is the same as the maximum particle size that can pass through a filter of particular thickness - The capability of a filter is dependent on the minimum constriction sizes along the flow path. - Base particle bigger than D_c^* cannot pass through the filter - It is recommended that two criteria should be satisfied for the cohesionless bases:$D_{5F}/D_{50B} < 4$ and $D_{15F}/D_{50B} < 5$

T.C. Kenney and D. Lau [1985]/Internal Stability of Granular Filters (Kenney and Lau, 1985)	Empirical	- The Bi-modal Theory for Widely graded Soils is proposed, in which there is definitely a soil skeleton and a fill:
		
		   − soil transmits the stresses through its skeleton (skeletal fabric, coarse or primary fabric)
		
		   − the coarser particles are assumed to have relatively fixed position and form the skeleton of the soil for a coarse dominant matrix
		
		   − potentially mobile particles are embedded in the pores of the soil skeleton (fine's or secondary fabric).
		
		- With respect to *PSD* of filters, there are Stable and Unstable *PSD*
		- Vibration of the test specimens during the tests causes a large increase in migration of fill particles at the bottom of the specimen

K.J. Witt [1986]/ Filtration Behavior and Dimensioning of Granular Filters (Witt, 1986)	Empirical	- Investigation on the mechanism of the filtration based on bi-modality nature of the soil - Quantification of conditions for geo-material retention of eroded base particles in filters - Development of an equation for reliability analysis of base-filter combinations considering different *PSDs* - Estimation of expected depth of penetration for clogging of the filter - Estimation of expected loss of material before clogging

Table 1.4.: Selected studies on filtration and internal erosion without homogeneity consideration - part 3

Reference/Title	Study Type	Major conclusions
V.V. Burenkova [1993]/Assessment of suffusion in non-cohesive and graded soils (Burenkova, 1993)	Empirical	- The Bi-modal Theory for Widely graded Soils is considered. A test procedure for identification of soil skeleton fractions and fill fractions is proposed: - Soils can be evaluated for their internal stability by their location in a logarithmic diagram. The limit ratios for stable and unstable conditions can be described analytically. - Analytic approximation of the separation point is proposed: $$D_s < 1.87(D_{90}/D_{15})^{-1.5} \, \& \, D_s > 0.55(D_{90}/D_{15})^{-1.5}$$ - A domain for internal stable soils is proposed $$0.76(D_{90}/D_{15}) + 1 \, < \, (D_{90}/D_{60}) \, < \, 1.86(D_{90}/D_{15}) + 1$$ - the particle diameter of PSD at 15% passing (D_{15}) - the particle diameter of PSD at 60% passing (D_{60}) - the particle diameter of PSD at 90% passing (D_{90})
C. F. Wan and R. Fell [2008]/Assessing the potential of internal stability and suffusion in embankment dams and their foundations (Wan and Fell, 2008)	Empirical	- Improved procedures (Modified Burenkova Method) for predicting the internal instability of sand gravel soils with silty and clayey fines based on *PSD* are proposed. - They show that the most widely used methods to assess whether a soil is internally unstable are conservative. Minor differences in the shape of the PSD affect, whether a soil is internally stable. - Soils that have less than 15% finer fraction (20% for the alternative method) may not be adequately assessed by these methods. While it has not been proven by tests, if the slope of the finer fraction is used in lieu of the D_{20}/D_5 ratio, the alternative method should be applicable. - the particle diameter of PSD at 20% passing (D_{20}) - the particle diameter of PSD at 5% passing (D_5) - the particle diameter of PSD at 10% passing (D_{10})

Table 1.5.: Selected studies on filtration and internal erosion without homogeneity consideration - part 4

1.4.2. Previous studies on homogeneity in science

Homogeneity is of obvious importance in a variety of fields wherein the effect of the different parameters must be characterized and quantified. Homogeneity and microstructure of the mixtures or particle assemblies determine the product quality in the food science, pharmaceutical, and chemical engineering industries. The mixture local properties must be measured, and a departure from variability with a finite limit can be defined as stochastic homogeneity. These fields encounter mixtures of many types, for instance, suspensions, the particle containing visco-plastics or powders, but face the same obstacles in defining and measuring homogeneity, which is often termed mixedness (the quality or state of being mixed) or mixture quality. In geotechnical engineering, the soil can be considered as a mixture or assembly of particles with different diameters. Therefore, it seems to be appropriate to implement the same procedure in this field of engineering. Nevertheless, in all of the mentioned areas, there are some difficulties in micro-structural investigations. They can be categorized into:

1. **Measurable parameters**: which parameters must be measured?

2. **Suitable length scale**: which length scale should be used for the characterization of the mixture?

The challenge is the implementation of an appropriate method for measuring the suitable parameters on a definite length scale. Here the length scale can be extended to area (A) or volume (V) which can be considered as REV. In the food industry, the homogeneous dispersion is essential to recipes and therefore, product quality. Food products typically require blending of fluids and particulate materials, e.g., a mixture that consists of flour or meal and a liquid (as milk or water) and is stiff enough to knead or rolled must be prepared with particles of varying size and rigidity. Large industrial mixers use various impeller blades to blend and homogenize materials. Many studies have been done in this area to maximize mixing efficiency, depending on the constituent materials.

In chemical engineering, polymer composite mixing involves many of the same principles just discussed. Many practical examples in this field exist, which can be compared with food-industry productions. Food or a chemical product is often analyzed during processing to ensure that the process is operating efficiently. Therefore, during processing, if a complication develops it can be instantly detected, and the process adjusted so that the properties of the product are not negatively affected. Techniques used to monitor the process, and different controlling methods are capable of producing precise outcomes in a short time. Manufacturers use either analytic methods that measure the food quality on-line, or they select and remove specimens and test them in a quality assurance laboratory (Nielsen et al., 1998). After all, these techniques for homogeneity quantification based on the product package which has a well-defined and limited scale cannot be used for geotechnical engineering, because the circumstances of food or chemical mixture production are highly controlled, which is not the case in geotechnical engineering.

In welding engineering, alloys are of great importance. An alloy is a mixture of metals or a mixture of a metal and another element. Alloys are defined by metallic bonding

character. An alloy may be a solid solution of metal elements (a single phase) or a mixture of metallic phases (two or more solutions). Inter-metallic compounds are alloys with a defined crystal structure (Callister et al., 2007). The stiffness of such a composite material depends directly on the distribution of different phases of the alloy in a more-solution mixture. (Woertz et al., 2013) compared the various alloy processing methods such as advective mixing, diffusional processes, and discontinuous shearing of alloys based on quantitative measures of homogeneity. The quantification method is based on a *2D* image analysis method. They mentioned that a homogeneity index was developed based on the variance of several morphological parameters, and this index will be published in greater detail in later publication.

Concrete is one of the most widely used construction materials. All kinds of structures and structural elements can be built using concrete. In construction practice, quite often in some parts of concrete structural elements defects occur due to concrete in-homogeneity. Defects of this kind affect negatively massive structural elements on their durability and compression strength. There are many kinds of concrete non-homogeneity, but the most common problem is the so-called honeycombing, i.e. parts of concrete characterized by different compaction degrees, occurred as a cause of the improper concrete compaction. Contrary to defects occurring on the surface of structural elements, the internal defects are difficult to detect. They may appear only during the serviceability of such a structure, whereby a repair is required to remove them. Therefore, nondestructive test methods are increasingly used to evaluate the homogeneity of concrete elements (Bungey et al., 2006; Beutel et al., 2008). The state of the art for acoustic impulse response method is nondestructive and particularly suitable for this purpose. The method is described in detail in the study of Hoła and Schabowicz (2010). Such a nondestructive method for controlling of concrete homogeneity respectively its quality is developed based on the ability of the concrete for transmitting the acoustic response. The material continuity plays the leading role for the mentioned method. On the other hand, it can be assumed that the sand and gravel particles in the concrete do not touch each other. The cement does not allow the contact between the sand and gravel particles. Due to that, there will be no-contact forces and no particle interactions after solidification of the concrete. It can be concluded that these methods are unsuitable for geotechnical engineering usage.

1.4.3. Previous studies on homogeneity in geotechnical engineering

There are a few studies related to soil homogeneity. Two significantly relevant studies related to internal erosion, which were carried out by Kenney and Westland (1993) and Saucke et al. (1999) have focused experimentally on quantifying the rate of segregation in poorly and widely graded soils as well as for mineral filters. Ripley (1986) discussed the study of Kenney and Lau (1985, 1986) to encourage them in their research into a new field which is according to him more consequential than internal stability. He recommended them to investigate the relationship between the width of PSD of a soil material and its susceptibility to harmful segregation. He emphasized that the laboratory prepared specimens, which have been placed under controlled conditions cannot give the insight of vulnerability of the internal erosion phenomena in the field situation. The laboratory specimens are always prepared to prevent segregation and horizontal layering

effects within the sample. Ripley addressed that the test results and the analyses are applicable to idealized conditions for the group of widely graded filter materials, which are tested.

PSD investigated by Kenney and Westland (1993)
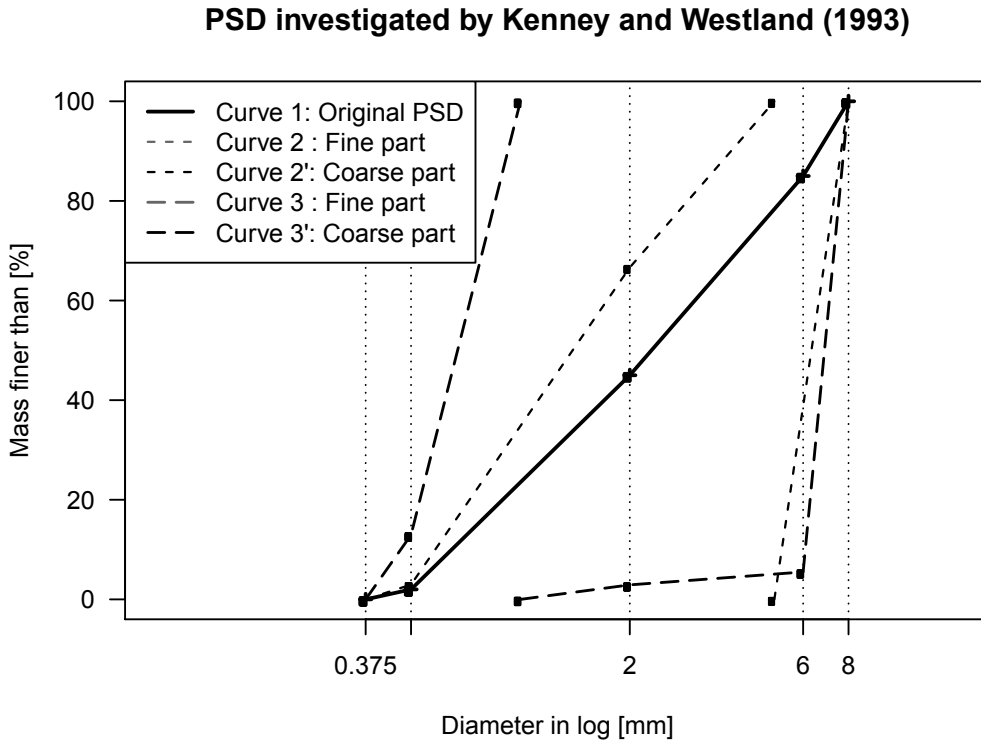
Figure 1.6.: Initial and segregated PSDs; curve 1 initial PSD; curve 2 and 2' relatively segregated; curve 3 and 3' perfect segregated after (Kenney and Westland, 1993)

The authors Kenney and Lau (1985) have correctly acknowledged that the test conditions of significant seepage velocity and mild vibrations were more severe than would be expected in practice. However, Ripley (1986) believed that the controlled homogeneity of the test materials was the most significant variation from actual field conditions. Afterward, Kenney and Westland (1993) published the results of a new study of segregation of granular filter materials. They concluded that the dry soils consisting of sand and gravels readily segregate at small discharge rates with a full segregation under a fall height of less than 1.00 m. They found out that almost all sands and gravels segregate so that they can be reproduced independent of their *PSD*. The *PSD* which contains fine particles (<0.06 mm) segregates to a smaller extent than soils not containing fine particles. Experimentally, they showed that wet sands are less vulnerable to segregation than dry sands. However, moisture contents had little influence over the segregation behavior of gravels. Kenney and Westland (1993) also commented that the particles bigger than D_{60} have a significant influence on the soil segregation.

In Figure 1.6, it is shown that a poorly graded filter (curve 1) segregates easily due to

placement. The question arises, when can a lightly segregated soil be considered as its initial PSD? Milligan (2003) warned the geotechnical communities that the issue of segregation is a critical uncertainty. It is poorly recognized and dealt with in geotechnical engineering. In lots of projects, the problem of segregation is handled by an indicative statement in the specifications saying that soil materials must be placed without any segregation taking place. However, this is in many practical situations very difficult to fulfill and the specifications thereby place an obligation on the contractor who cannot be met. Milligan (2003) indicates that much of the uncertainty associated with appropriate filter placement be to a large extent by specifying the use of widely, narrowly graded, sand-rich filters, of a gradation finer than the following limits and placed wet in thin layers.

$$\forall\, D\,\varepsilon\, PSD \;\Rightarrow\; \left\{ \begin{array}{rcl} D_{max} & < & 30\,mm \\ D_{15} & \leq & 0.7\,mm \end{array} \right. \tag{1.1}$$

where:

D_{max} : the maximum particle diameter of a PSD

D_{15} : the particle diameter of PSD at 15% passing

1.4.4. Summary of literature review

Different experimental, analytical, statistical methods used by previous researchers and a brief description of their approach and their results are given in section 1.4.1. Embankment dams or flood protection dikes having broadly-graded clay-silt-sand-gravel mixtures with cohesive or non-cohesive fines are very common. For example, glacial and alluvial materials and many alluvial soils in dam foundations found in some American, Swedish, German and Norwegian flood protection dikes are widely graded and have significant fines content.

Most of the proposed criteria, as introduced in section 1.4.1, for assessing the internal stability of soil, were based on laboratory tests on cohesionless sand-gravel mixtures. These criteria may not be applicable to widely graded silt-sand-gravel mixtures or materials with significant fine content. Most previous researchers have ignored the effect of compaction and density, which is directly related to homogeneity on the internal stability of soil. The idea behind of all these studies indicate that, for suffusion to occur, the following three criteria have to be satisfied:

1. the void volume of the soil skeleton formed by the coarser particles has to be bigger than the volume of fine particles. If there are larger amounts of fine soil particles for void filling, the coarser particles will be floating in the matrix of fine soil particles, instead of forming the soil skeleton (matrix criterion).

2. the size of fine fractions must be smaller than the size of the equivalent diameter of pore spaces between the coarser particles, which is assumed to form the skeleton of the soil (geometrical criterion).

3. the velocity of flow through the soil matrix must be high enough to move the loose fine soil particles through the constrictions between the larger soil particles. (hydraulical criterion).

The first two criteria, which is called geometrical criterion, are related to the *PSD* of soil, whereas the third criterion, hydraulical criterion, is related to the hydraulic force causing movement of the fine soil particles. As stated by the author (Salehi Sadaghiani and Witt, 2011), for the reliable assessment of internal stability, another criterion must be satisfied. The most important criterion prior evaluating the *PSD* of the soil can be stated as:

·   there must be no considerable segregation or observable stratification within the soil body. If a layer with a significant thickness of fine particles normal to the flow direction exists, then there are two distinctive types of soil with different equivalent diameters of pore constriction that may stagnate or initiate the suffusion process (homogeneity criterion)

1.5. Investigation strategies and methods

This study is restricted to granular materials with a dominant coarse matrix. Such a granulated material with a small amount of fine content can be classified as widely graded soil. Under the assumption of homogeneity, the dominant coarse matrix is a matrix by which finer soil particles are embedded into the soil skeleton. However, soil can experience segregation during placement, compaction as well as other dynamical man-made impacts. If the soil is segregated, the finer particles do not fill the pores of the soil skeleton. Therefore, they can transmit the stresses and behave as the soil skeleton.

It is known that soils with a portion of fines less than about thirty percent have a dominant coarse matrix (Burenkova (1993), Kenney and Lau (1985) and Witt (2013). The fractions, which belong to the soil skeleton respectively the separation diameter between skeleton and fill, change if fine fractions are added above this limit. It is caused by the physical presence of additional fine particles between the skeleton particles. As they come together, fines force the lock-in of the skeleton particles and changing the matrix of the soil. There is a point in which by adding the fine particles more than the void capacity of the soil skeleton after Binner et al. (2010) and Witt (2013), about thirty percent of the total weight for the shown *PSD* in Figure 2.2), the skeleton rearranges itself so that the soil builds a new matrix. In such a matrix, fines can transmit stresses and behaves as the skeleton (Jentsch et al., 2014). Therefore, the first step is to diagnose if a soil matrix is susceptible to suffusion. Here, the primary focus must be on the soils which have a dominant coarse matrix with a small amount of the fill fractions.

In all of the experiments in this study, if the specimen placement method is not clarified, the particular sample placement technique is used to ascertain the most practical possible degree of homogeneity. Several *SFTs* were carried out for identification of the most reliable D_s between the soil skeleton and the soil fill with bimodal particle frequency distribution (Salehi Sadaghiani and Witt, 2012) and (Salehi Sadaghiani et al., 2012). The skeleton of soil can be formed if a minimum mass of related fractions is available. This least mass respectively *REV* must be measured for such a soil. On the other hand, for the quantification of homogeneity, the length scale is an important point which depends directly on the size of *REV*.

The main idea for homogeneity investigation either in numerically generated packings

or for the in-situ condition is based on the theory of the soil bimodality for the dominant coarse matrix with fines. The author believes that if the soil skeleton fractions are stochastically homogeneous, the potential mobile particles which can be transported inside the soil skeleton will always reach to a combination of skeleton particles with the smallest pore constriction size, which could eventually stop the particle washout. This idea should be validated experimentally using the *SFT* method. The homogeneity of the soil skeleton can prevent the internal erosion if the soil *PSD* is internally stable according to geometrical criteria. Moreover, the specimen volume must be representative for the defined *PSD*. For the *PSDs* which are not internally stable, the potentially mobile particles of soil can be washed out even if the skeleton fractions are homogeneously distributed. As far as the problem of internal stability is concerned, homogeneity is in the first line a matter of position and distances of the particles in soil skeleton and not a question of similarity in the gradation.

If the specimen is large enough to maintain adequate scale conditions, the C_H can be determined, but in the practical point of view, the minimum size of the sample must be ascertained to reduce the unnecessary work. The author's approach for quantification of homogeneity is in the first-line independent of scale. Nevertheless, various scales can be used for different assessment. For instance, the relevant scale for C_H related to internal stability must be a C_H with a *REV* size of minimum $5 \times D_{max}$ in each dimension of the specimen based on own investigation (Salehi Sadaghiani et al., 2014). The sample can be divided into five times five blocks, and the variation of different factors can be calculated in all the sub-images. Through comparison of the sub-images with each other, the C_H can be calculated. Because the internal stability of the soil is dependent on the skeleton forming fractions, the D_{max} is a suitable characteristic parameter for the behavior of the soil skeleton. This method can be used for the smaller fractions of the skeleton as well which is also performed. Nevertheless, the REV of the soil is numerically determined.

As another example, for quantification of homogeneity related to soil permeability a REV size of $5 \times D_{10}$ seems to be a good approximation. After Hazen (1943) the permeability of the granular materials is governed by diameter D_{10} (Carrier III, 2003).

The coefficient of homogeneity C_H based on D_{max} can be calculated for numerically generated packings as well as for images captured from computer tomography sections or images taken with normal cameras from the surface of the soil. In this study, an implicit sectional method for quantification of C_H is presented. The homogeneity quantification is based on a multivariate parameters analysis. For determination of C_H theoretically all soil fractions can be analyzed in dependency on image resolution.

For the investigation of the suffusion, it is needed to study carefully a sample which is generated according to its REV and is stochastically homogeneous. Otherwise, the suffusion phenomenon cannot be investigated properly. Homogeneity of the numerically generated packings produced using *DEM* can be analyzed by capturing the *2D* cross sections of the packing. The homogeneity of each cross section can be quantified, and the mean value of the homogeneity of a whole specimen is measurable. The *3D* homogeneity analysis which is also possible, but it is very time-consuming if one wants to analyze all of the fractions. An experimental method based on *SFT* is proposed for quantification of

Homogeneity in the field for existing embankment dams and dams under construction. A new analytically packing model which is homogeneous and has the minimal necessary dimensions (REV) should be proposed.

The primary objective of this thesis is to propose a new suffusion criterion which is derived analytically. The analytically derived criterion should be validated with a new *ST* procedure, which is reproducible. The new suffusion criterion, as well as test method, should consider the soil matrix, its homogeneity and the *REV* size of the soil.

2. Suffusion Phenomenon

2.1. Effect of homogeneity on initiation of suffusion

The Author started to investigate the factors affecting internal erosion processes in embankment dikes and their foundations as part of a research project funded by German Waterways and Shipping Office Freiburg (*WSA*). The finer soil particles, which are smaller than the smallest diameter of pore constriction, are moved through the soil skeleton by seepage forces, the process what is called suffusion. Soils susceptible to suffusion are described as internally unstable after Kenney and Lau (1985). Internally unstable soils are typically widely or gap-graded soils with particles from silt or clay to gravel size, or widely graded soils, which are segregated. Within an embankment core, supporting body or the foundation of a dam suffusion can occur. This process results in a coarser soil structure, leading to increased permeability and leakage forces, a possible settlement of the embankment, and a higher likelihood of downstream slope stability problems, which may result in failure of the dam by continuation and propagation of the particle washout. Dam body constructed of internally unstable materials will have a potential for washout of the finer particles. This problem cannot be solved by taking the coarser particles out of the *PSD* which is less efficient in protecting the core materials from erosion. The slope stability and the soil stability against piping depend on the amount of the coarser particles within the soil (Skempton and Brogan, 1994; Wan and Fell, 2008).

To be able to identify the soil vulnerability to suffusion under hydrodynamic conditions, laboratory tests are necessary. The degree of particle transport or washout of soil is closely correlated to the local stratification and segregation of the particles inside the soil. It depends on the homogeneity which is a reflection of local particle arrangement and fraction distribution within the soil. These form the preferred flow paths, which increases material transport along these paths that often result to further local segregation.

The challenge in assessing the internal erosion processes is to find out or to estimate the related parameters of soil under consideration of spatial uncertainty due to non-homogeneity of the soil skeleton. If the relevant parameters cannot be determined with the desired accuracy, the quantitative risk assessment against internal erosion cannot be estimated correctly. Even though, by carrying out laboratory tests the risk assessment of internal erosion for field situations remains unknown. Because without capturing the degree of soil homogeneity in field conditions, one cannot be sure that the assumed *PSD* in different points of the embankment exists or not.

The phenomenon of suffusion of sand-gravel soils has been studied by a number of researchers, including Kenney et al. (1985); Kenney and Lau (1985, 1986); Sun (1989); Burenkova (1993); Lafleur et al. (1993) and Chapuis (1992). The investigated soils by most of these authors are sand gravels free of silty fines. The exception is Burenkova (1993) who

investigated silt-sand-gravel soils and Sun (1989) who investigated clay-silt-sand soils but tested them under very high gradients, which will not occur in dams or their foundations. Suffusion of clay-silt-sand-gravel has been studied by Wan and Fell (2008) but they tested these samples under a constant hydraulic gradient of 8, which seems to be very high even for the transition zones within an embankment. With this, it has to be taken into consideration that the samples are not 100 percent homogeneous, and only the average values could be measured, which means, within the sample higher local gradients might occur.

Author's experiments on silt-sand-gravel soil indicated that for suffusion to occur, four criteria, matrix or quantity, geometrical, homogeneity and finally hydraulic criterion has to be satisfied (See section 1.4.4).

2.2. Suffusion phenomenon

2.2.1. Suffusion tests on soils prone to suffusion

The identification and determination of mobile particles within the fill fractions of a widely graded soil are necessary to assess the internal stability of a certain PSD. There is still no standard way for identification or measurement of mobile particles. There are some attempts for the analysis of the internal stability of the soil based on the soil bimodal theory and identification of the soil Separation Point (D_s) (i.e. after Ziems.J. (1969)).
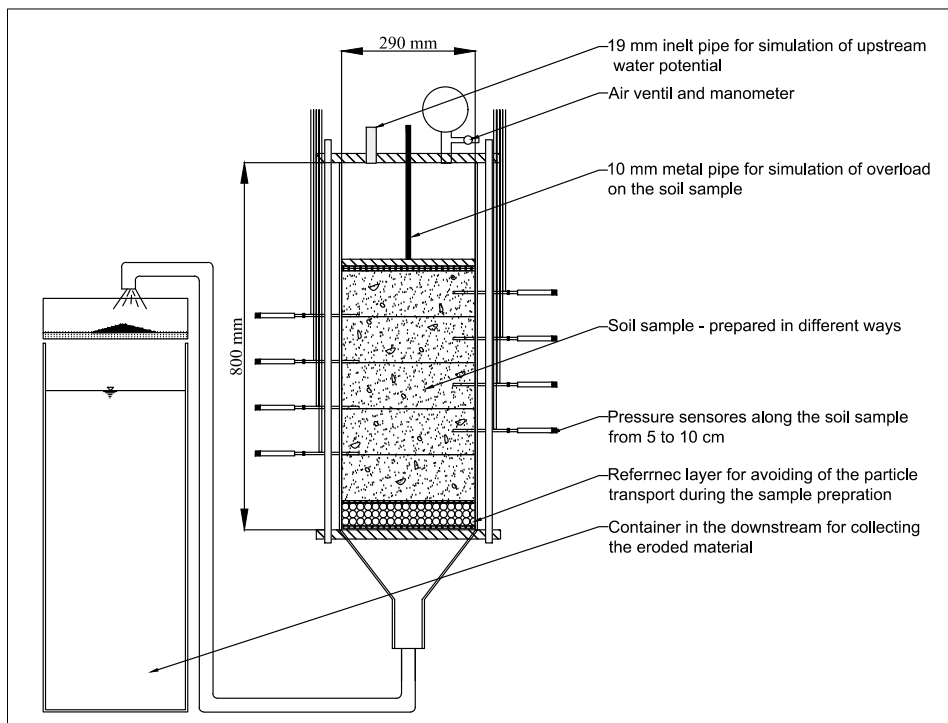
Figure 2.1.: Principle sketch of the suffusion test procedure

The boundary between soil skeleton (skeletal fabric) and potentially mobile particles (loose fractions or fill) on a soil *PSD* is defined somewhat arbitrary, which is still used in the assessment of the internal stability. For example, the Federal Waterways Engineering and Research Institute in Germany proposed in the latest guideline Bun (2013) a direct method for describing and quantifying mobile particles for proof of the geometrical stability with a combination of the different criterion of Kenney and Lau (1985); Kenney et al. (1985), Burenkova (1993) and Ziems.J. (1969). In the background of all these criteria, there is a method for separating soil into the skeleton and fill particles. In the case of widely-gap graded soils, it could be a safe assumption that the D_s is a particle diameter within the range of missed soil fractions. This assumption can be made for homogeneous soils, but it is known that such a gap graded soil is very vulnerable to segregation and in a practical point of view, this is almost impossible to build a homogeneous layer of such a soil.

Investigated Particle Size distributions
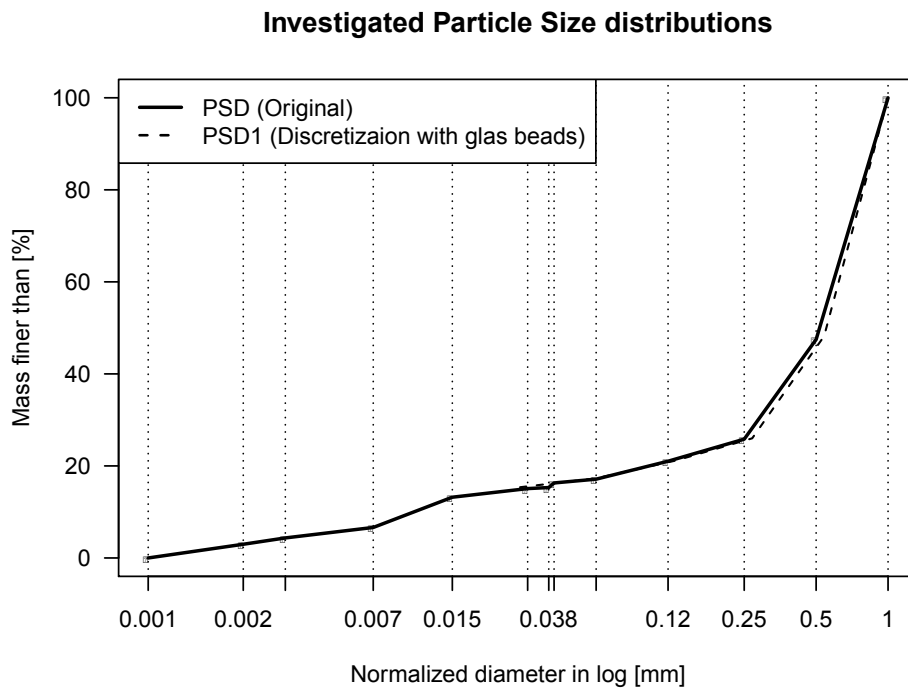
Figure 2.2.: Used soil for suffusion tests - the reconstitution of the *PSD* with glass beads is called *PSD1*. It shows a small variation in comparison to original *PSD*

The author has carried out more than 50 suffusion tests on widely graded and widely-gap graded soils. The test device was a relatively big device with a height of 50 cm and a diameter of 50 cm (see Fig. 2.1). For the acquisition of potential changes within the specimen, ten pressure sensors were installed in the device. Additionally, piezometer pipes were attached to the specimen, for controlling of the total head within the specimen. A distance between the individual pressure sensors and piezometers of 5 cm permits a detailed recording of the pore water pressure as well as the total head changes

in the soil specimen. The pore water pressures along the soil column were measured at points with distance of 10 cm from the center of the column, to exclude boundary effects (Salehi Sadaghiani and Witt, 2011).

d<0.06 mm	D_{10}	D_{30}	D_{60}	C_U	C_C	k	Soil Group (DIN18196)
1.05	0.35	5	10.5	30	6.8	$1.23 * 10^{-2}$	GL

Table 2.1.: Geotechnical properties of *PSD1*

For the suffusion tests specimens with a mass of ca. 40 to 65 kg of the investigated *PSD* is used (see Fig.2.2). The geotechnical properties of the samples using *PSD1* were obtained from standard laboratory tests can be obtained from Table 2.1. The experimentally investigated *PSD1* represents a soil at the limit state of the suffusion according to common geometrical internal stability criteria (Semar et al., 2010; Witt, 2013)).

2.2.2. Results of Suffusion tests

There were different results for the same test procedures on the *PSD1*. The material washout has shown a variety between 2.92 to 10.3 % of the total mass for the final hydraulic gradient of i equal to one ($i = 1$). The different particle arrangement in each sample could be the reason for the variation of the test results.

In Figure 2.3, the total head surface is shown, which is observed during suffusion tests on relatively and stochastically homogeneous specimens. For better visualization of the results of pressure sensors and piezometers, the total head surface is shown as 2D and 3D contours (see Fig. 2.5 and 2.4). The hydraulic gradient i is obtained by dividing the head loss ($\triangle h$) by the length (L) of the specimen over which this head is lost ($i = \triangle h/L$) (see Fig. 2.3). In the case of horizontal seepage the $\triangle h$ is entirely a loss in the pressure head ($P/(\rho g)$). In the case of seepage in a downward suffusion test the $\triangle h$ is derived from a loss of elevation (elevation head (h_e)) and water pressure. It is sometimes incorrectly assumed that the $\triangle h$ in all cases is either a pressure head loss or an elevation head loss. In fact, it is the loss of the total head where according to Bernoulli's equation:

$$H_{total} = P/(\rho g) + v^2/2g + h_e \tag{2.1}$$

where:

H_{total} : total head
P : pressure
ρ : density
g : earth's gravity
v : velocity of Fluid
h_e : elevation head

The *2D* and *3D* contours of the total head for two different specimens during the suffusion test are shown in Figures 2.5 and 2.4. These Figures show the gradual change of the soil matrix during the time. Each test was started with a similar hydraulic gradient of i

equal to 0.1. The following gradient was applied, when the coefficient of permeability (k) was constant for more than 10 minutes, and no particle washout could be observed.
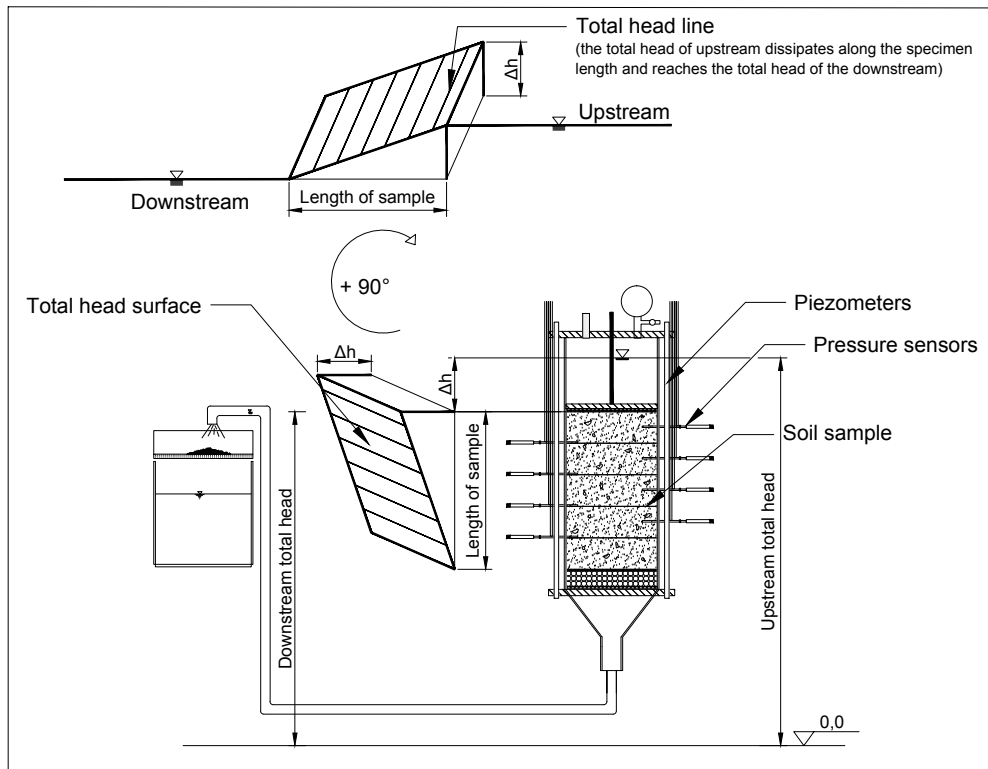
Figure 2.3.: Schematic illustration of total head surface for suffusion tests

The sample A was not placed in a layered manner (at once), relatively various *PSDs* in different layers could be observed. At the end of this test, a solid amount of 10.3 % of particle washed out could be measured. Sample B was placed in four layers. For each layer of sample B, the same amount of fractions based on *PSD1* was mixed and placed into the test device. In sample B, the contours are more symmetrical about the vertical axis of the sample. The sample B was qualitatively a more homogeneous sample. At the end of the test, the particle washout was about 2.92 % of the total mass of the specimen. In Figure 2.5, it can be easily seen that the total head dissipates at a uniform rate, and the contours build almost parallel lines. Higher amount of finer particles at the bottom of sample A could be observed from the beginning of the suffusion tests in comparison to sample B.

Generally, in suffusion tests, it could be observed that murky water appeared after starting the test. It again disappeared after the initiation phase of the water percolation through the soil sample. The soil sample after a while during became stable and built segregated local nests along flow paths. They could be observed on the sides of the sample. It could also be found that the soil was segregated in an ascending superimposed order in those nests. For the upward flows, it must be with the same behavior in descending order. On the top of these local ascending layered segregated nests, which replicate Ascending

layered segregated (*ALS*), some fine particles moved in the pore spaces in a rotational manner due to the water flow. Those particles sometimes could be transported locally to the next pore. However, occasionally the ascending layered particles existed in all of the directions so that the fine particle on the top could not be transported, even for higher hydraulic gradients.

From these suffusion test results, it can be concluded that even in a large sample, the local changes of the particle arrangement can influence the results enormously, and homogeneity of the samples are of obvious importance in laboratory scales.

2.3. Insufficiency of homogeneity assumption in practice

In the engineering community, the homogeneity is related to consistency. If soils are of a definite classification - for instance, Poorly graded sand (*SP*), Poorly graded silty sand (*SP-SM*), Poorly graded clayey sand (*SP-SC*), etc. and there is a record of near consistency in soil *PSD*, moisture-density relationship, unconfined compression strength, direct shear and triaxial shear strength, then it is likely legitimately to assume homogeneity for most purposes. However, these considerations are not sufficient for the assumption of homogeneity in soils with a dominant coarse matrix which is vulnerable to internal erosion.

In the numerical studies, the definition of homogeneity is also not clear, and there is no standard way to quantify it. The engineers do a statistical analysis of differences and look for small *COV*. However, that cannot reflect the importance of spatial distribution in macro and micro scale. It seems that constructed embankment dams are one, for instance, where the assumption of homogeneity could be appropriate. Although, it is needed to describe a way for quantification of homogeneity. In the embankment dams, the engineers may be concerned with seepage, for which permeability is very sensitive to small changes in particle sizes. It must be mentioned that the permeability is guaranteed to be anisotropic due to variations in the borrow pit and compaction. There is also the problem of placing materials in a homogeneous fashion. It is always in the specs but hard to do. Take a grader leveling off the sub-base layer with sizes up to 32 mm and bigger (also larger size in other directions of the particle). The surface of each layer must be graded to $\pm 10\,mm$ If one watches the grading, undoubtedly find that the bigger fractions get graded off to the sides, while the PSD of the stack may be similar from sample to sample, the placement factor is hard to control.

In other cases, the engineers may be concerned with uniformity of the material for its ability to act as a filter throughout the dam. Let us consider a filter layer which has a uniformly graded *PSD* with two particle fractions. There are two undisturbed samples of the soil available. In the first sample (Sample 1), almost all of smaller particles are under the bigger fraction (segregated). In the second sample (sample 2) there is a proper distribution of smaller particles within the pore spaces of the bigger fraction of PSD (*F*). In this case, it can be easily proven that the coefficient of uniformity or grain size distribution cannot provide any information about soil homogeneity. Even the permeability is an average value which is for both samples in vertical direction equal. As a matter of fact, homogeneous soils in earthworks as well as in nature do not exist. Even very uniformly

graded soils vary somewhat from point to point horizontally but much more vertically. It is an assumption made for computational purposes, based on engineering judgment.

In the opinion of many researchers, the best qualitative definition of the homogeneity can be written as the following statement. Something can be assumed as homogeneous in the analysis without affecting the results of the analysis too much, and that is site specific. This statement is to qualitative and general. In this study, the author focuses on the description and quantification of the homogeneity related to internal erosion. However, the method can be generalized with some modifications for any material.

Based on yearlong first-hand experiences from several projects in the field of material transport (Suspension, Contact erosion, Suffusion and Filtration tests), the author states that the main reason for the result variations by different studies in the case of widely graded soils is the heterogeneity of the samples (experimental scale). It can also be stated that the particle transport problems occur not in case of bad design, but they typically happen in the field scale because of local segregation.
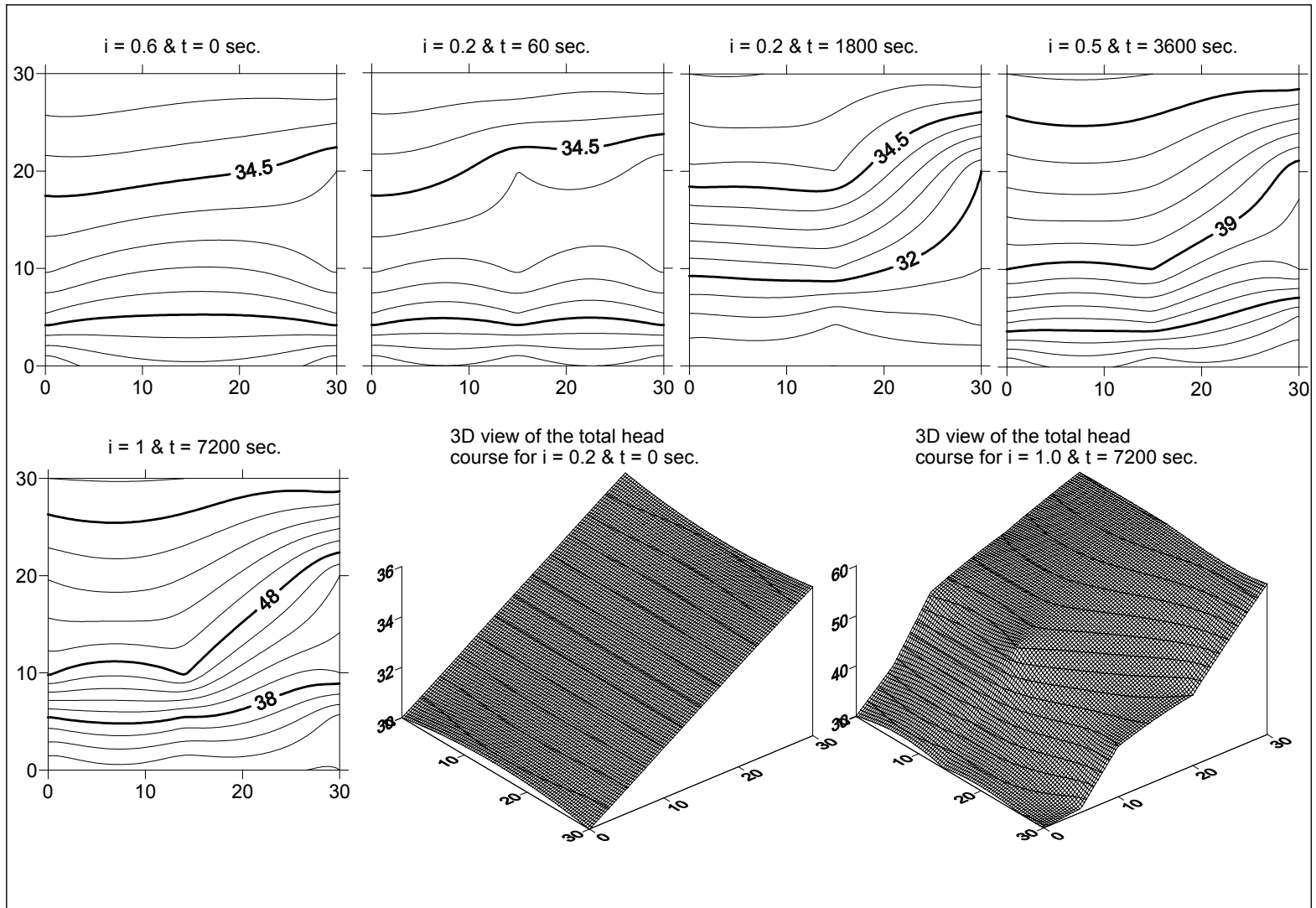
Figure 2.4.: Contours of total head for specimen A, it was placed into the test device at once, it can be imagined that each layer had a different *PSD* in comparison to *PSD1* but the whole specimen represents the original *PSD1* (specimen non-homogeneous).
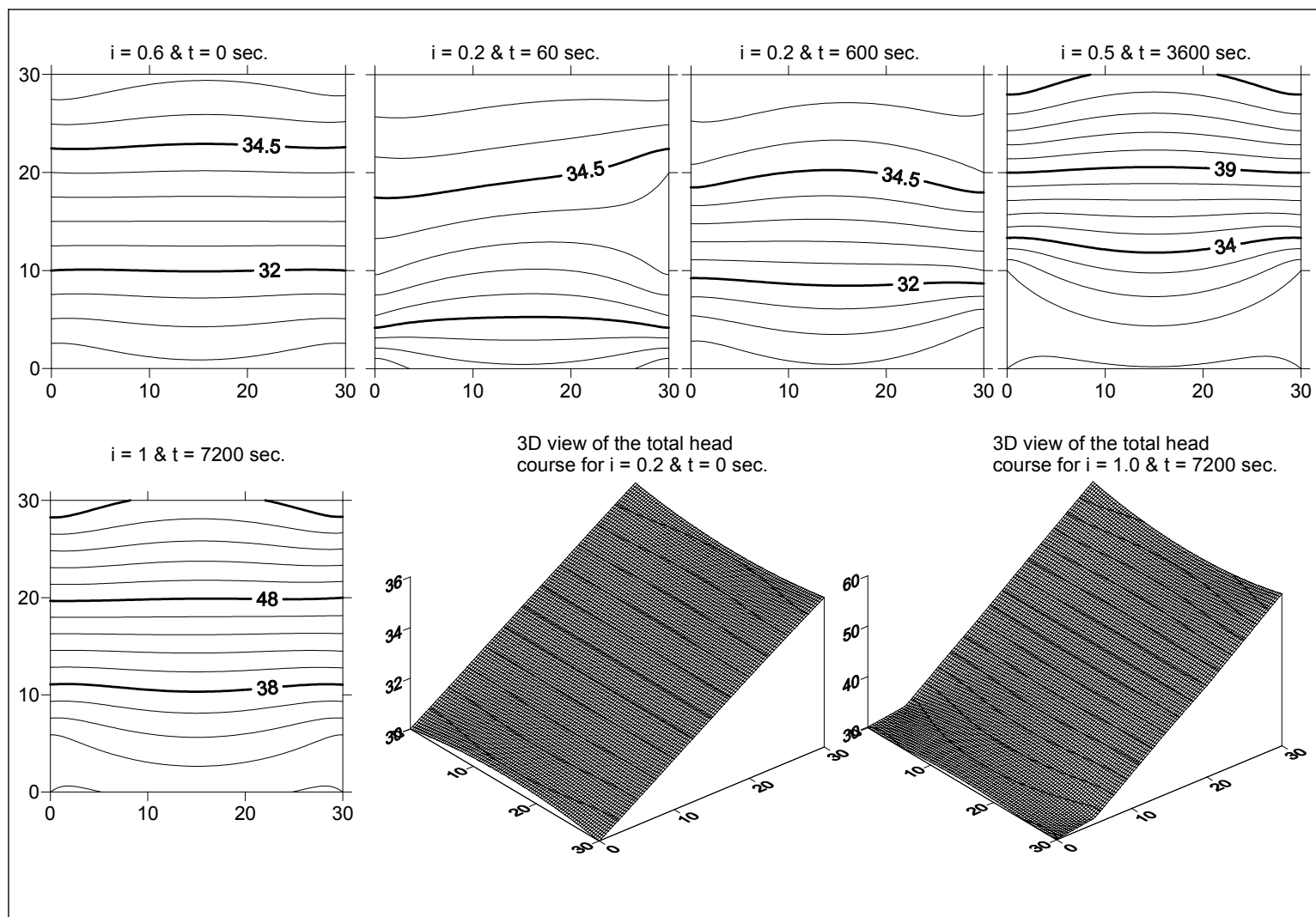
Figure 2.5.: Contours of total head for specimen B, during the suffusion test, it was placed into the test device in 4 layers, each layer had exactly the same *PSD* as original *PSD1* (specimen stochastically homogeneous).

3. Experimental identification of dominant soil matrix

3.1. Definition of soil matrix

Despite the recent progress and better understanding of many phenomena of granular matter, a governing theorem or foundation for particle assemblies (packings) which consist of different fractions (poly-disperse) like widely graded soils remains still unknown. It is impossible to set detailed statements about the skeleton and fill properties of such a packing. For assessment of the internal stability of soil, the participation of its fractions on forming the skeleton and identification of mobile and suffusive fractions seems to be necessary. The mobile particles are those particles which can move through the soil skeleton but cannot be washed out. The suffusive particles are those who can be washed out from the soil body. The matrix of soil can qualitatively be classified into four main groups and a transition phase which is called dual or Transition Matrix (*TM*)(see Fig.3.1).
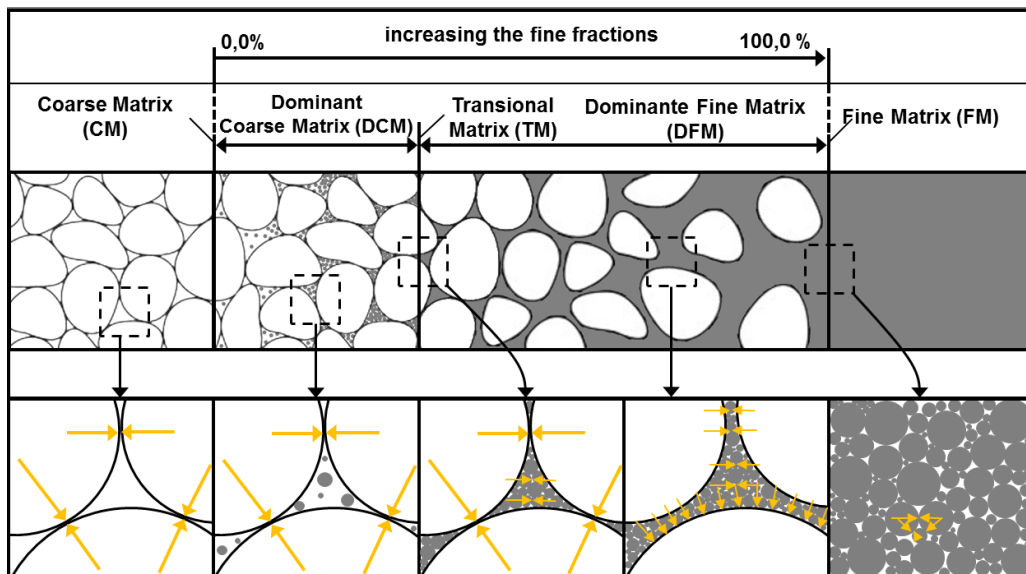
Figure 3.1.: Different soil matrix classified based on skeletal behavior (transmitting of stress) of the matrix (Jentsch et al., 2014)

Figure 3.1 shows how the structure changes during a gradual increase of fine content (amount of fill fractions). These stages are characterized as follows:

· **Skeleton without fine content**: the matrix consists of just skeletal fractions. All fractions can transmit stresses (Coarse Matrix (*CM*)).

· **Skeleton with fine content**: the matrix consists of skeletal fractions, which can transmit stresses and fill fractions, which do not carry any stress. The fill fractions are embedded in the pore spaces of the skeletal fabric and are potentially mobile (Dominat Coarse Matrix (*DCM*)).

· **Fine fractions behave as the skeleton**: the matrix consists of skeletal fractions and fill fractions. In this stage, both can transmit stresses. The finer fractions fill 100% the pore spaces of the skeletal fabric (*TM*). An example of such a case is Fuller curve.

· **Fine fractions with coarse content**: the matrix consists of fine and coarse fractions. In this stage, both can transmit stresses. The finer fractions are the dominant matrix, and coarser fractions swim in the Dominant Fine Matrix (*DFM*). An example for such a case can be sandy-silt and sandy-clay soils.

· **Skeleton with fine and coarse fractions**: the matrix consists of just skeletal fractions. All fractions can transmit stresses (Fine Matrix (*FM*)).

3.2. Identification of soil matrix by Sequential Fill Test (*SFT*)

Soil structure could be analyzed experimentally, analytically, numerically as well as based on image processing of the images captured from computer tomography (Vincens et al., 2014). The analysis of soil structure consisted of particles and pore spaces by considering its *PSD* is a complicated procedure.
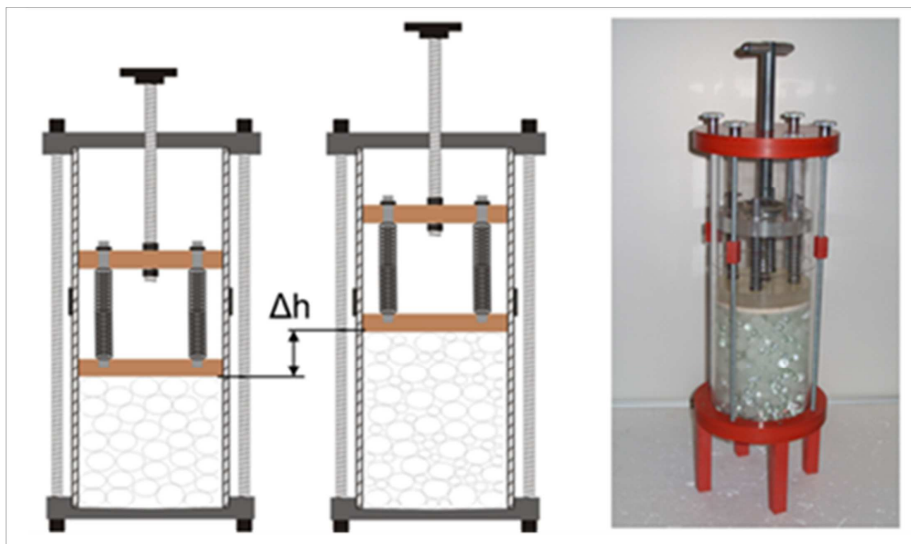
Figure 3.2.: Schematic view of the used test apparatus by Binner et al. (2010).

Investigations based on the Probability Distribution Function (*PDF*) and the Number Distribution Function (*NDF*), which can be easily derived from *PSD* of the soil, delivers

more information about soil structure. All above that the bimodality characteristic of widely-gap graded soils which can be successfully found by *SFT* is a suitable attribute for measuring the most liable D_s between the soil skeleton and its fill. The nature of such a packing (polydisperse particle assembly) is so complicated that it cannot be modeled with defining an exact separation point D_s between its skeleton and fill. One reason can be the local segregation in the different location of a specimen. To et al. (2014) showed numerically that the soil fractions generally could belong to both groups of the skeleton and fill. To et al. (2014) emphasized that the soil fractions also build a transition zone between skeletal and fill. The degree of homogeneity of the investigated packings is not mentioned. Due to that the author always defines a complete fraction as the Separation Point point of a soil gradation.

The *SFT* idea is mentioned, firstly, by Burenkova (1993). It is a very simple method for identification of the Separation Point for a particular *PSD* Burenkova (1993) has developed a test procedure, in which the soil was sieved and divided into its fractions. First, the coarsest fraction D_{max} was built into a device. After that, the next finer fraction was added. In each step, the volume of the soil was measured. The test is finished when all fractions are added to the test apparatus. If the volume of the soil in each step is increased, the fractions are considered to belong to the soil skeleton. There is no published image or illustration of the Burenkova's test device.

This procedure was followed by Witt and his colleagues, and they have shown for the first time a simple apparatus, in which the *SFT* test was accomplished (Binner et al., 2010). The used apparatus was designed by Federal Institute for Materials Research and Testing (*BAM*) as a part of *DFG* research project *SUFFOS* for identification of granular soil structure. The same apparatus was adapted and used for measurement of homogeneity of soil structure at Bauhaus-Universität Weimar. A schematic diagram of the apparatus for the tests is given in Figure 3.2. The experiments were performed with the assumption that the particle fractions, which do not belong to the supporting skeleton, cannot change the height of soil column (see Equation (3.1)). Samples were collected from the supporting body of a river dike. The samples were washed, rinsed, sun-dried and next placed in an oven. The samples were later sieved into different fraction sizes using sieve series: 63, 31.5, 16, 8, 4, 2, 1, 0.5, 0.25, 0.125 and 0.063 *mm* according to DIN18123 (2011).

The permeability of the soil was determined in the laboratory using a vertical form of Darcy's permeability constant head test. Distinctly different homogeneous as well as various segregated samples were used for the permeability, *SFT* and *ST* experiments (see also section 6.4 and Table 6.3). Two different types of segregated samples were prepared. They were *ALS* sample and Descending layered segregated (*DLS*) sample. The *ALS* sample is built by layers of the fractions in ascending (D_{max} at the bottom of the sample). The *DLS* sample is built inversely in comparison to the *ALS* sample. From the experiment, the porosity of the sample was determined using the volumetric method, while the fluxes were determined from vertical permeameter set up with the constant head method after DIN18130 (1998).

3.3. *SFT* on homogeneous samples

Salehi Sadaghiani and Witt (2012) have proposed a new sample placement method based on Sample Reconstitution Technique (*SRT*) to minimize the soil segregation. Moreover, the effective porosity is measured in each layer to ascertain the relative homogeneity in the soil skeleton for each step. The objective of the reconstitution technique is to produce a sample with a higher degree of homogeneity for widely graded soils (*DCM*). A more homogeneous sample was achieved through a sequential sample placement method based on *SRT*. In this technique, the sample is reconstituted in four layers using four batches consisted of the same mass of each fraction of the *PSD1*. The number of layers is dependent D_{max}. The layer thickness can be selected in range of 2 to 3 D_{max}.

Each layer can be prepared using a batch of granular material or glass beads according to the target *PSD1*. Each layer is built in the apparatus with the same mass of particle size fractions (Salehi Sadaghiani and Witt, 2012). This is to replicate the stochastical homogeneity of particle fractions in each layer. Placement of successive layers was carried out under the identical conditions. When each batch of material was ready, it was placed directly into the apparatus cell using a pipe and a funnel.
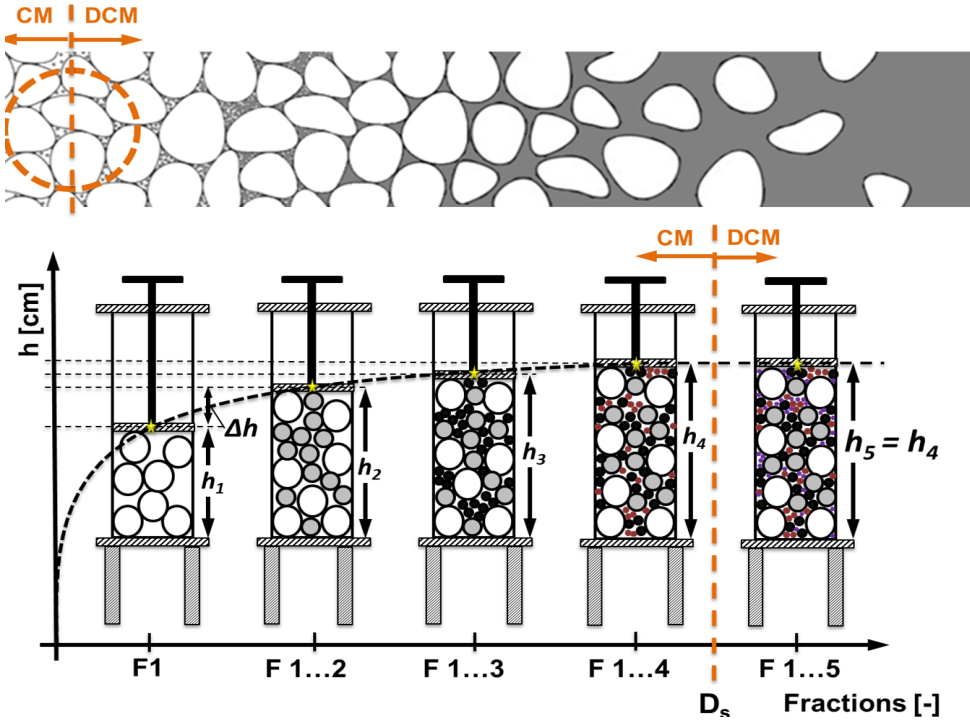
Figure 3.3.: SFT test procedure for identification of soil matrix and separation point D_s - Soil matrix: Dominant Coarse Matrix (DCM)

The relative height is computed to make the comparison of the several tests with different masses possible. If the height of the sample consisted of a certain fraction or a cumulative number of fractions is h_i, and the maximum height of the sample in the test

apparatus h_{max}, the relative height h_r in percent is defined by the formula:

$$h_r = \frac{h_i}{h_{max}} \; ; \; (i \, \varepsilon \, Z) \tag{3.1}$$

in which, i is the cumulative fraction numbers. Additionally, the permeability and effective porosity measurements were undertaken.

3.4. *SFT* on segregated samples

The test procedure is as same as the procedure of *SFT* (see section 3.2. After sieving the soil sample and dividing it into its fractions, the soil fractions will be placed into the test apparatus layer by layer from the minimum fraction diameter the minimum particle diameter of a PSD (D_{min}) to the maximum fraction diameter D_{max} for *DLS* samples and inversely for *ALS* samples.

After placement of the sample, the height of the layered segregated specimen was measured (Figure 3.4). The *ALS* and *DLS* samples represent a fully segregated soil sample. In the case of a widely graded soil with a dominant coarse matrix, it is needed to measure the total segregated height only for the skeleton fractions. The homogeneous and segregated samples undergo the same axial pressure during the *SFT*.
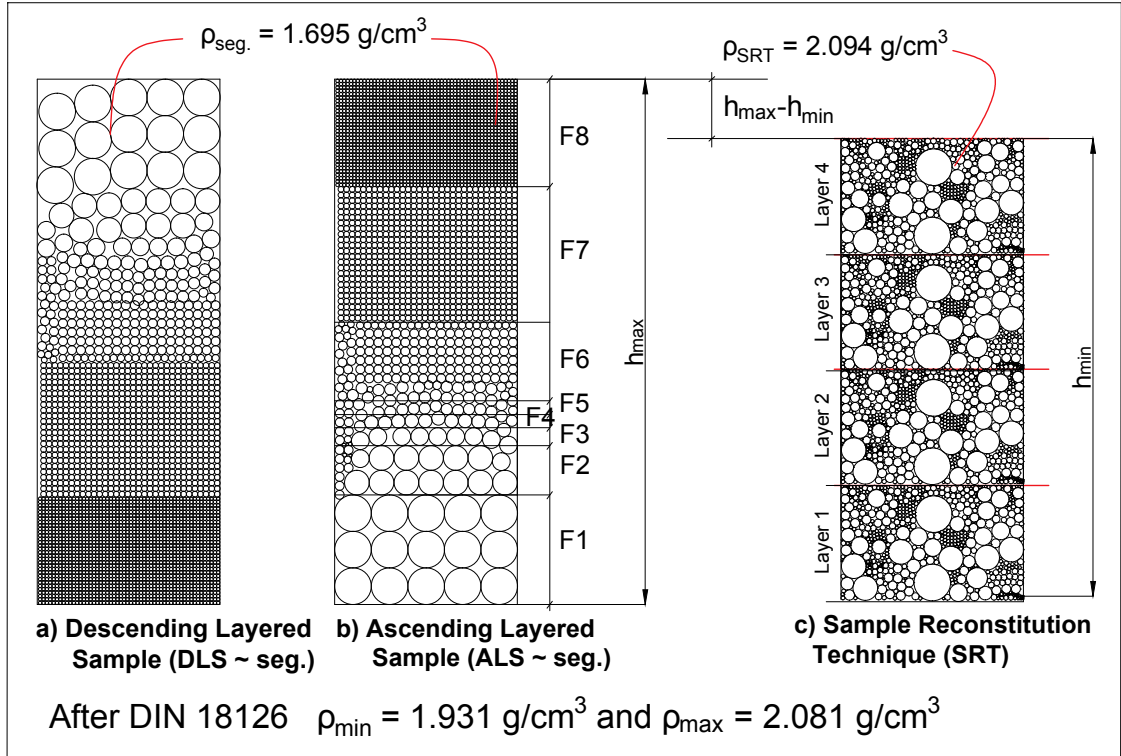
Figure 3.4.: SFT on ascending and descending layered samples (ALS and DLS - Loosest and densest packings in a polydisperse material)

3.5. The real loosest and densest state of a sample

By comparison of the results of the *SFT* tests for homogeneous and segregated samples, one can obviously see the effect of homogeneity on the skeleton height. The more homogeneous the skeleton of the sample of soil with a Dominat Coarse Matrix (*DCM*) is, the less the height of the sample. These tests seem to be related to the maximum and minimum density, which reflect the density of a soil respectively when it is fully compacted (without particle breakage), and the loosest density. The second one can be obtained by gently pouring the material into the mold (no compaction).

However, it is shown that the loosest and densest states of a sample based on the test procedures recommended by guidelines are not the extremes of these states. After Salgado (2007), in granular materials, it is almost impossible to define experimentally minimum and maximum porosities. The minimum porosity (n_{min}) corresponds to the state of densest or closest packing in which a sample of such a soil can be formed without significant particle breakage. The maximum porosity (n_{max}) corresponds to the loosest possible packing which is statically stable. Cases of packings can be generated with n_{max} which are not stable and collapse quickly. The guidelines have proposed methods for the determination of n_{min} and n_{max}, which can result in consistent values for poorly graded soils. For widely graded soils, there will be some fluctuation in the measurements.

The loosest and densest densities of the selected *PSD* is as following:

$$for\ (PSD \cong PSD1) \Rightarrow \begin{cases} \rho_{min} &= 1.931\,g/cm^3 \\ \rho_{max} &= 2.081\,g/cm^3 \\ G_s &= const. \end{cases} \qquad (3.2)$$

where:

ρ_{min} : standard minimum density

ρ_{max} : standard maximum density

G_s : specific gravity of soil refers to the specific gravity of the its solid matter

The measurements of the density for segregated sample *DLS* was significantly less than the loosest density, and the density of the homogeneous sample based on *SRT* (see also 3.3) was slightly higher than the densest density of the soil. The density values for those samples are listed as following:

$$for\ (PSD \cong PSD1) \Rightarrow \begin{cases} \rho_{seg.} &= 1.695\,g/cm^3 \\ \rho_{SRT} &= 2.094\,g/cm^3 \\ G_s &= const. \end{cases} \qquad (3.3)$$

where:

ρ_{SRT} : stochstically homogeneous density based on SRT

$\rho_{seg.}$: density based on ALS or DLS

It can be shown that by the implementation of the mentioned *SRT*, the sample experiences a more efficient particle arrangement and results a lower density ρ_{SRT}. The same argument, explains why the total height of the totally segregated sample (*ALS* or *DLS*) is more than the height of the sample using the tests for finding the loosest density. By Proctor test or even by numerically generated packings, if the arrangements of the particles are disadvantageous, the sample cannot reach the maximum density with the compaction energy (Winkler et al., 2014). Thus, for a widely graded soil, different results can be obtained by conducting density tests. The effect of sample mass, container size, particle arrangement on the maximum height of the skeleton of a numerically generated packing is investigated by the author in the next chapter.

3.6. Summary of this chapter

For investigation of the internal stability of a widely graded soil, the homogeneity of the soil must be quantified. Firstly, the soil matrix must be classified into internally stable or unstable. For soils with a Dominat Coarse Matrix (*DCM*) which are prone to suffusion, the soil can be divided into the skeleton and fill fractions. It can be done by the *SFT* method. The height of the skeleton fractions is statistically a constant value, so that the soil fractions which build the maximum height, can be defined as the soil skeleton. The range of that fraction is referred as the separation point. The *SFT* must be carried out for a stochastically homogeneous sample which is constructed by sample preparation method Sample Reconstitution Technique (*SRT*). The sample height for maximum segregation can also be measured (*ALS*). It is shown that with these proposed sample preparation methods, the loosest and densest state of soil can be estimated more precisely in comparison to the standard methods for determination of n_{min} and n_{max}. In section 5.6, method for quantification of homogeneity numerically and experimentally based on these two height measurements ($h_{max,ASL}$ and $h_{max,SRT}$) for a calculated Representative Elementary Volume (*REV*) is proposed.

4. Numerical identification of REV

4.1. Discrete Element Method (DEM)

There is no perfect method to measure the geomechanical parameters of the single particles in a particle assembly in laboratory experiments. Therefore, in geotechnical engineering, a great number of criteria are driven empirically. The *DEM* is a robust numerical method, which can compute the motion and interaction of several particles in each time step of the simulation (Cundall, 1971). It enables the determination of discrete parameters of particle assembly. Although *DEM* is originally designed for molecular dynamics, the *DEM* method can be distinguished from molecular dynamics because it can assign to particles rotational degrees of freedom as well as contact. The application of the *DEM* in geomechanics was proposed by Cundall and Strack (1979). Allen and Tildesley (1989) added thermodynamic to the *DEM* and this extension made the coupling of *DEM* to Computational Fluid dynamic (*CFD*) and Finite Element Method (*FEM*) possible. Today, in geomechanics research, the *DEM* is a well-established method (O'Sullivan, 2011). The *DEM* simulations are computationally intensive. To make the simulations faster, some *DEM* codes use parallel processing. With advances in computing power and optimization algorithms for nearest neighbor sorting, it has become possible to increase the number of particles and to run simulations of longer duration.

The *DEM* simulations start with the user inputs of the geometry of the system. This includes particle coordinates, boundary conditions and material properties by specifying the contact model parameters like the stiffness and friction coefficients. The user can also determine the schedule for loading or deforming the system by adding loads, deformations or settlements. The simulation can be started as a transient or dynamic analysis until a specified number of time steps is over. After insertion of particles into the simulation box, there is an overlap check procedure, which is performed based on the geometry and coordinates of the particles. After starting the simulation of motions, the particles that come into contact with each other are identified, and the contact forces are calculated at each time step. The distance between the contacting particles relates to the magnitude of the particle forces. From these data the resultant force including, body forces, external forces and moment acting on each particle can be determined.

Moreover, there is one exception when the particle rotation is blocked, then two sets of equations for the dynamic equilibrium of the particles are solved at every time step. The resultant applied force determines the translational movement of each particle and from the resultant applied moment the rotational movement is calculated. Now knowing the inertia of the particles, the translational and rotational accelerations for the particles can be calculated. Hence, the particle positions and orientations are updated and ready for the next time step after their new contact forces are calculated. This process will be

repeated for all number of time steps. Although this system seems to respond in an almost static manner, it can be seen that the Discrete Element Method is a transient or dynamic analysis.
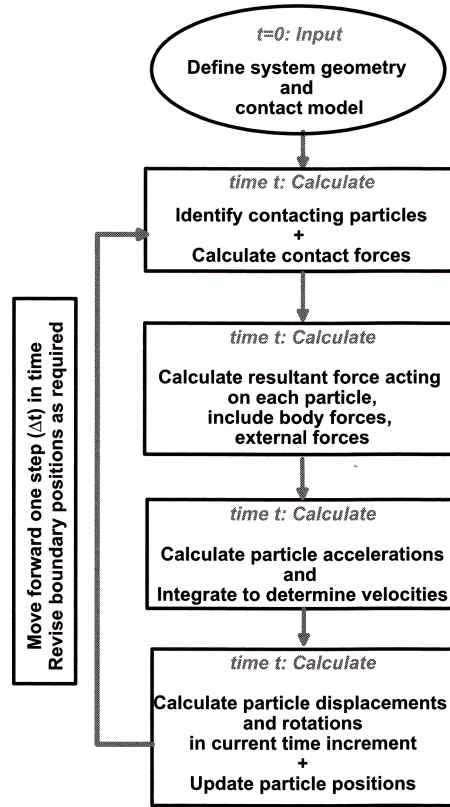
Figure 4.1.: Indication of calculation sequence within a DEM time step O'Sullivan (2011)

The series of calculations within a time step are illustrated in Figure 4.1. The first set starts with the calculation of the particle velocities and incremental displacements. Here, the equilibrium of each particle in the sequence is considered. When the system geometry is updated, in the second series, then the forces at each contact in the whole system are calculated. The normal contact force as well as the tangential component of the contact force, produce the particle rotational moment. From these moments and forces, the new particle position is generated for the next time step, and the series of calculation starts all over again.

For every particle-based *DEM* simulation the following fundamental assumptions are typical. The first condition is that there are rigid particles, which possess a finite inertia and can be described analytically. Moreover, the particles can move independently of each other and can translate and rotate. The identifications of new contacts between the particles are automatically made by a geometry check algorithm. Those contacts commonly take place over an infinitesimal area based on the allowed overlapping and involve only

two particles each time. Analogous to the deformation that occurs between the particles, in reality, particles in *DEM* simulations are authorized to overlap slightly at the contact point. The magnitude of the overlapping at each contact point needs to be small. From this overlapping value, the compressive inter-particle forces can be calculated.

Tensile and compression forces can be transmitted at the contact points of particles in the contact normal direction as well as a tangential force orthogonal to the normal contact force. There is furthermore, a separation distance between two particles from what tensile inter-particle forces are calculated. When particles bump into each other, this force exceeds its maximum, and the particles move away from each other, which also means that the contact is deleted and no longer considered during contact force calculations. The selected time step must be small enough that the motion of a particle within this time step only affects its immediate neighboring particles. The last key assumption is that clusters of the rigid base particles can be used to represent a single particle. A measurable deformation of the composite particles is caused by the relative motion of the base particles within the cluster. These agglomerates may be rigid themselves.
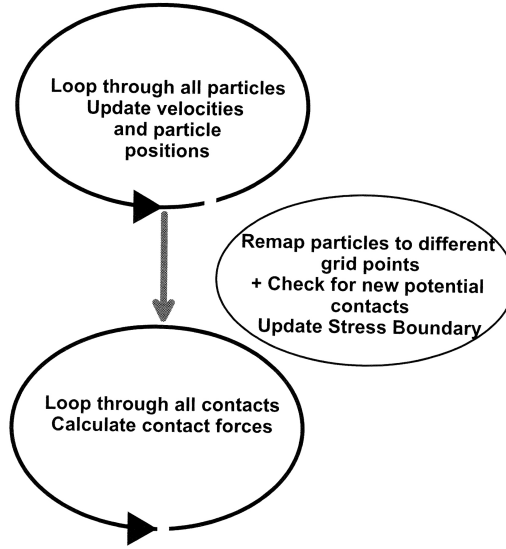
Figure 4.2.: Schematic diagram of sequence of calculations in a DEM simulation O'Sullivan (2011)

The contacts between two particles can also be mathematically described by a simple linear spring-damping model shown in Figure 4.4. The rigid particles are either in a spherical shape or another geometrically well-defined volume or a combination of them. As it can be seen from the assumptions above, the translational and angular accelerations of a sphere are based on the corresponding equilibrium. The normal force at the contact point p, which pushes the particles away from each other can be calculated from the overlapping length (Δx_p) and the normal relative velocity at the contact point (Δu_p).

The is given by the following formula.

$$F_n = -k_n * \Delta x_p + c_n * \Delta u_{p,n} \tag{4.1}$$
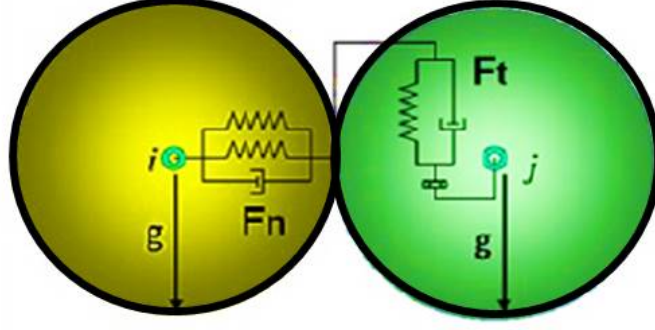
Figure 4.3.: Simple spring-dashpot model Goniva et al. (2010)

where:

Δx_p : overlapping length

Δu_p : normal relative velocity at the contact point

F_n : normal force

k_n : spring stiffness

c_n : viscous damping coefficient

The magnitude of the tangential contact force F_t can be calculated by the relative tangential velocity of the particles in contact $\Delta u_{p,t}$.

$$F_t = min\{|-k_t * \int_t^{t_{c,0}} \Delta u_{p,t} * \delta t + c_t * \Delta u_{p,t}\} \tag{4.2}$$

where:

F_t : tangential force

k_t : tangential spring stiffness

c_t : the tangential dissipation parameter

$t_{c,0}$: time of contact between two particles

The incremental spring that stores energy from the relative tangential motion is represented by the integral term. It is evident that the limits of the integral stand for the elastic tangential deformation of the particle surfaces which happened since particles touched at $t = t_{c,0}$ The damper represents the energy dissipation of the tangential contact. Particles incline to slip over each other when the Coulomb frictional limit is reached. This is also the limit for the magnitude of the tangential force (O'Sullivan, 2011).

As it can be seen from the fundamental assumptions above, a *DEM* simulation might be very comparable to a continuum model. One of the differences is that the difficulty in the continuum-based analysis like *FEM* is to generate meshes for highly complex geometries whereas, for *DEM* models, it is the time step which is difficult to choose. Both simulation

types can be computationally intensive and therefore, time-consuming. For instance, with *DEM* analysis, one has to use small time steps and a large number of particles due to its non-linearity. Another difference is that a *DEM* simulation does not generate stress and strain values but basic results for particle positions and inter-particle contact forces After data input or pre-processing and solution of these data a post processing has to take place to see the results. Like *FEM* analysis, the *DEM* method needs to satisfy theoretical requirements as well. In *DEM* the equilibrium is accounted for by considering the dynamic balance of each particle at each time increment during the analysis. In a *FEM* analysis holes and overlaps should not develop during the deformation. This compatibility requirement is of course not fulfilled for a particulate *DEM* simulation. The constitutive matrix in a continuum-based modeling relates the stresses and strains whose relationships can be linear or not. In a *DEM* model this is not required, the constitutive model rather emerges from the simulation results. To conclude this comparison between *DEM* and *FEM* a statement of the boundary conditions is required. Both concepts are similar and only differ in details.

To conclude this introduction to *DEM* a few codes should be mentioned. The codes BALL (*2D* code) and Trubal (*3D* code) were the first ones outlining a *DEM* algorithm and published by Cundall and Strack (1979). Up until now, the most *DEM* simulations in geotechnical engineering are based on those two codes or on the commercially available *PFC2D* and *PFC3D* which are linked to other two (Cundall, 2004). Another commercial code is *EDEM*, however, it is more widespread in mining engineering (EDEM, 2006). For the use in research the open sources *DEM* codes like ESyS-Particle Simulation (Weatherley et al., 2013), *Yade* (Šmilauer and Chareyre, 2010), Virtual Geoscience Workbench (VGW)(Latham et al., 2010) and OVAL (Kuhn, 2006) have been developed recently.

The code of the program *LIGGGHTS* is written based on the molecular dynamics method, *LAMMPS* (Plimpton et al., 2007) simulator and is extended to support granular media (Kloss and Goniva, 2011). The models for the simulation and the assignment of the material properties are provided in an input script file, which allows easy modifications of the model. The program is an open-source program, and the code can be modified and extended to the different variety of problems. It is possible to import complex geometry from Computer Aided Design (*CAD*) programs in *STL*-data format into the simulation, which is a relatively good compensation for lacking a graphical user interface (GUI). Because the *DEM* simulation only provides calculation, a post-processing software, for instance, ParaView, an open-source, multi-platform data analysis, and visualization application, can be used (Henderson et al., 2004) In this thesis, ParaView and *MATLAB* are utilized for the post-processing of the data.

4.2. Relevant scale for homogeneity investigations

One of the important questions that arise when considering the quantification of homogeneity for such a discontinuous porous media is whether or not the particle assembly behaves like the real physical medium and replicates the response of bigger volumes. In other words, can the three-phase system of a granular material be modeled in a way that the characteristics of its pore network and pore paths are replicated? In sampling or the

numerical modeling of a granular material, it is very influential in introducing a stochastically comparable porous medium to represent good equivalence properties of the actual strata.

It is crucial to establish the theoretic porosity of the medium, which represents the real porosity as much as possible. If this porosity is set based on small-volume samples, it is possible randomly to select either a too small or a too high porosity. The volume of the sample is not representative to allow the characterization of the whole soil. The minimum volume randomly selected, which keeps, for example, the porosity features of the entire volume of the site, is called Representative Elementary Volume (*REV*). Increasing the sample volume over this representative elementary one, the sample properties have to remain at least for small changes constant. However, for large volumes, the characteristic feature is lost because of the inherent heterogeneity of the considered domain (Bear, 2012).

For quantification of static parameters of an environment, a closed system which is representative of that environment must be defined. In general terms, the closed system can be referred as a volume. This representative volume is an element of the system and has a definite volume. It is therefore called the *REV*. For proposed homogeneity quantification method, *REV* is a very important parameter and the C_H can be determined in dependency of *REV* sizes.

The size of the *REV* can be defined in dependency of the soil *PSD* and the container shape and its volume. The relation between the container diameter, i.e. in a cylindrical container and the maximum particle diameter of the *PSD* (D_{max}) is here numerically investigated. If one could use the optimum mass for the *SFT* test, the optimized *PSD* can be undertaken. The *REV* helps to decrease the duration of the simulation as well as for laboratory tests by reducing the total mass respectively volume of sample. Besides, the number of particles in the numerical simulation can be decreased enormously, and the boundary effects stay within an acceptable range. In this thesis *SFTs* on two *PSDs* were modeled and required mass for forming a soil skeleton is determined.
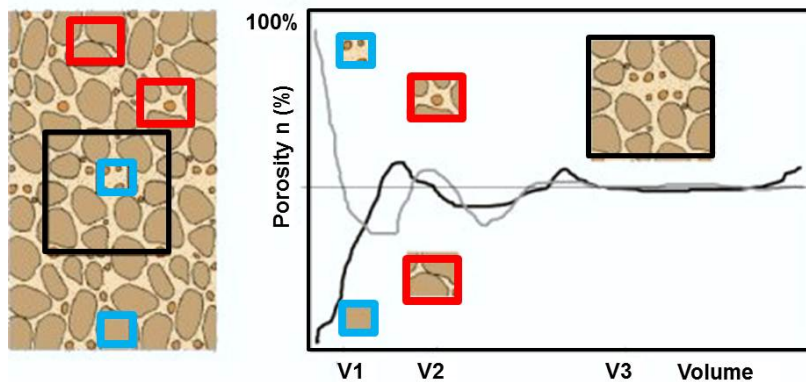
Figure 4.4.: Representative Elementary Volume (*REV*)(modified after Bear (2012))

4.3. Simulation approach SFT

A series of *3D DEM* simulations were carried out. The numerical model is a model of a physical experimental procedure (Salehi Sadaghiani and Witt, 2012). Here the open source code LAMMPS improved for general granular and granular heat transfer simulations. (*LIGGGHTS*) 2.3.6 was used for the simulations (Kloss et al., 2012). All the soil fractions were poured into a cylindrical container. Rigid boundaries were applied to the simulation cylinder (cylindrical and bottom walls). The created sample should be considered with boundary effects associated with rigid boundaries and bridging effects of particles. The experimental device which was modeled is shown in Figure 3.2. The model parameters of the simulations are presented in Table 4.1. The Hertz-Mindlin contact model was used (Jaeger, 2005) for the generation of a packing (particle assembly).

Parameter	Symbol	Units	Value
Particle density	ρ	kg/m^3	2500
Young's Modulus	E	GPa	50
coefficient of Restitution	ς	-	0.3
Coefficient of inter-particle fraction	μ	-	0.1
Length of timestep	Δt	sec.	10^{-7}
Poison ratio	ν	-	0.3

Table 4.1.: DEM model parameters for numerical simulations.

In the scientific literature related to *DEM* modeling, the pouring of the particles in a container is known as the sedimentation algorithm. In the sedimentation algorithm (Tory, 1990), which belongs to the group of sequential construction algorithms, particles of different diameters can be inserted randomly in a volume (V) and falling due to gravity. It must be mentioned that Tory (1990) used this algorithm to create a stochastic model for slow sedimentation of small particles in a viscous fluid. For finding the *REV*, the author used mainly the same algorithm but without a viscous liquid. Therefore, this algorithm is called Pouring-Algorithm (*PA*).

The normalized particle size distributions were inserted randomly into the simulation cylinder by *LIGGGHTS*. After insertion of the particle in the cylinder, gravity was activated, and the particles were poured downwards. The particles reach their stable positions after required time steps. In this way, the sample was created. The particles were compacted with a plate to form a dense packing after pouring. Whereby the particles were allowed to rearrange and come to the static equilibrium. The compaction was continued until a desired percolating system at the defined stress, which was used for the experimental procedure. The segregation neither could be avoided in the experiment nor the simulation, but a packing was generated, in which the *COV* of the porosity in 4 layers was ca. 19%. Also, a moderate density was obtained. The parameters with a *COV* of 19% in geotechnical engineering after Phoon (2008) can be classified as a parameter with satisfactory quality.

4.3.1. Investigated PSDs

The normalized *PSDs* used in simulations are presented in Figure 4.5 and the data set of these *PSDs* are displayed in Tab.4.2.

Fraction	F1	F2	F3	F4	F5	F6
D/D_{max} PSD2 [-]	1	0.8	0.315	0.2	0.1	0.05
D/D_{max} PSD3 [-]	1	0.8	0.25	0.15	0.065	0.0375

Table 4.2.: Different fractions of the normalized PSDs
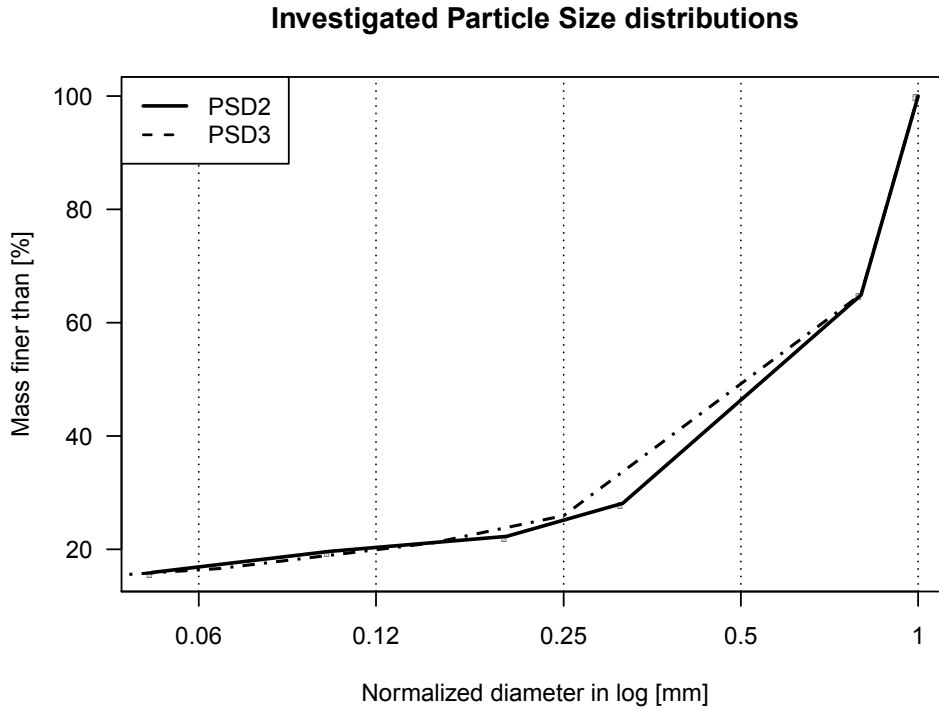
Figure 4.5.: Normalized Particle Size Distribution (*PSD*) used in *DEM* simulations

The *PSD2* and *PSD3* are slightly different from the *PSD1* which was investigated in chapter 2. Nevertheless, they belong to the same soil material of various locations from dikes of river Rhein. These types of soil with the given *PSDs* can be considered as a *DCM* (see section 4.3). This group of *PSDs* were comprehensively investigated by Binner et al. (2010) and by the author in previous chapters. These widely graded soils can be considered according to common suffusion criteria as a soil prone to suffusion (Witt, 2013; Wan and Fell, 2008; Kenney et al., 1985; Kenney and Lau, 1985).

In all numerical simulations, the investigated particles are restricted to the diameter of particles higher than 0.1 *mm*. This diameter is approximately the size limit at which

the particle behavior becomes dominated by inertia of the particle, i.e. the magnitude of the surface interaction forces became negligible in comparison to the particle inertia (O'Sullivan, 2011).

4.3.2. Results

The *PSDs* are cut at the smallest possible particle size for the simulations to keep the particle numbers to a practical level (computing time). Whereby, these particles (smaller than sixth fraction of PSD (*F6*)) do not have any influence on the total height of the sample (compare to Fig. 4.6, see also 3) The parameter study with the different mass of samples was carried out. The optimal mass which represents the *REV* was derived from these investigations.

Experimental results SFT (Relative height and porosity)
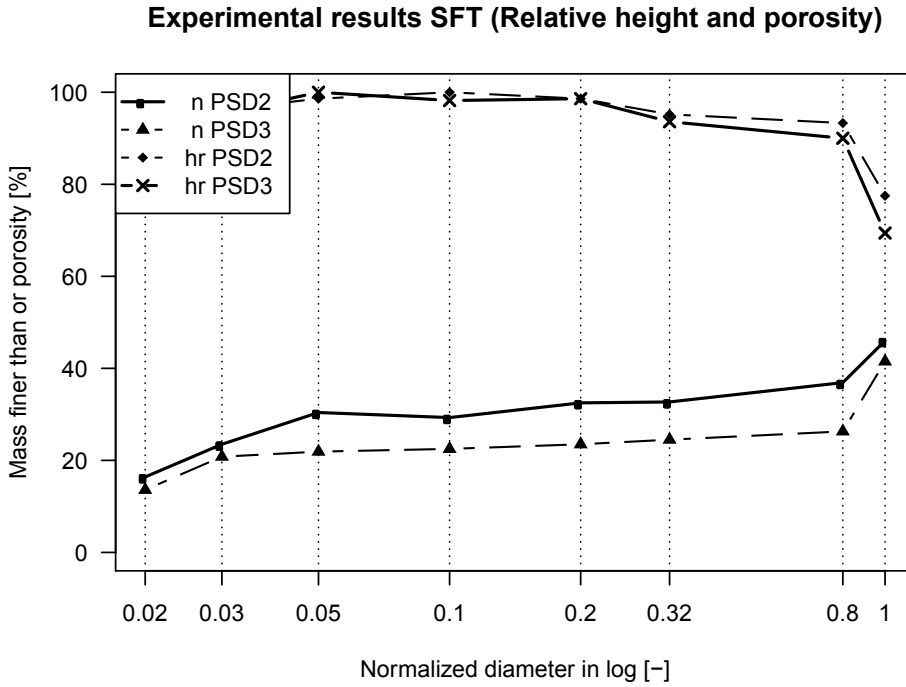
Figure 4.6.: *SFT* result for *PSD2* and *PSD3*, h_r : relative height n : porosity

Figure 4.6 shows the experimental identification of the separation point of samples generated using glass beads based on the *PSD2* and the *PSD3* (Salehi Sadaghiani and Witt, 2012). The *SFT* tests using glass beads were further validated using fluviatile soils. The measured porosity in dependency of added fractions is illustrated in Figure 4.6. Moreover, the experimental *SFT* and numerical *SFT* show a decent agreement for the chosen discretization. The discretization of the *PSD* for both numerical and experimental procedures have a significant effect on the identification of the separation point D_s. This point represents a fraction range. Due to that, a moderate discretization with relatively small span of fraction range should be considered for *SFT* method.
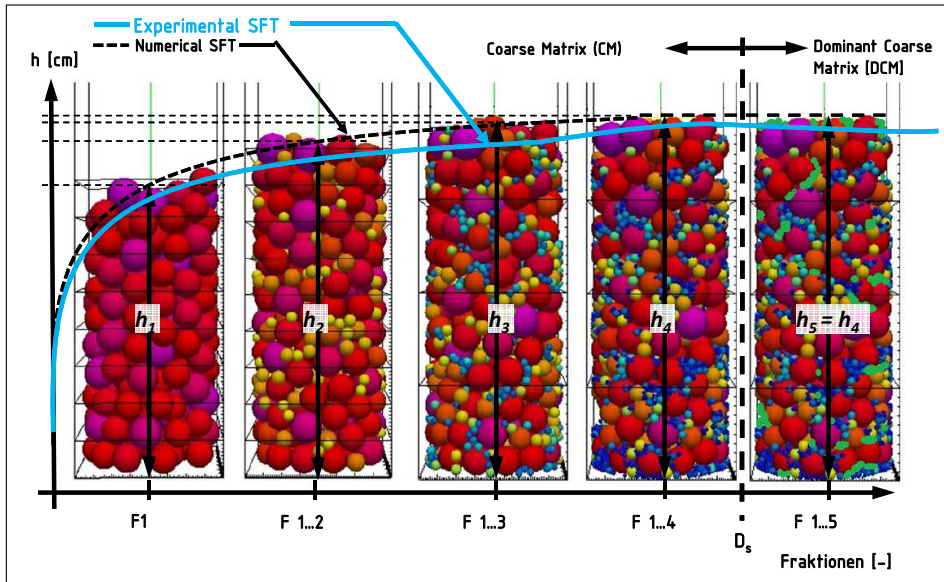
Figure 4.7.: Comparison of simulated absolute height and *SFT* results with a mass of *M* and cylinder diameter of $7 \times D_{max}$ for *PSD2*
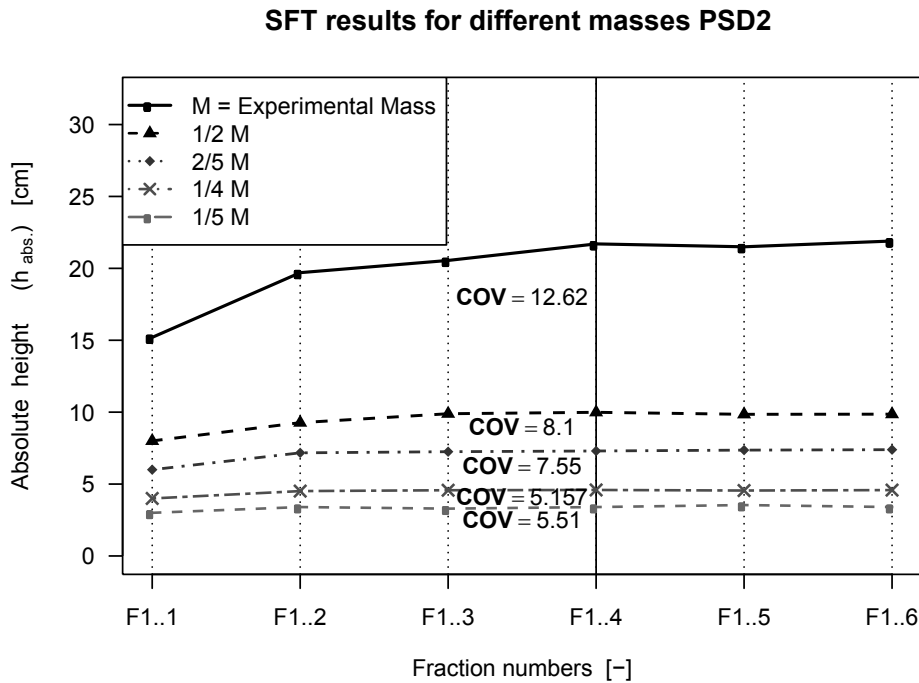
Figure 4.8.: Comparison of simulated absolute height for different masses using *PSD2*

As a matter of fact, for forming the soil skeleton, a minimum amount of mass based on the given *PSD* is needed. For example, if just 1 particle of the D_{max} is chosen and based on its mass, the mass of other fractions are determined regarding its *PSD*, this sample represents only the soil Particle Size Distribution (*PSD*) but not the soil behavior, especially its skeletal behavior. For identification of the *REV*, the packings were evaluated based on the absolute height of the samples in the simulation cylinder. If the relative height is chosen, one cannot see the significance differences between height-fraction graphs of the various samples. In Figure 4.8, the measured absolute heights for *PSD2* for the different amount of sample masses are presented.

It can be seen that by adding the *F6* to the sample the maximum height was obtained. All graphs show at the beginning a steep upward increase and in the middle a flat course. They can be approximated by a linear line for the sharp rise (skeleton; $F < F_{1..4}$) and a constant line for horizontal part (fill; $F > F_{1..4}$). The first part, which is assumed to be the soil skeleton is responsible for transmitting stresses. The average contact number of each particle show strictly the same result. The second part which shows the potential mobile particles (fill) consists of the smaller fractions. Almost the identical course of the graphs is obtained for *PSD3* (see Fig.4.9). The absolute heights of the simulations with more mass are more variable than those with less mass as confirmed by the computed *COV*.
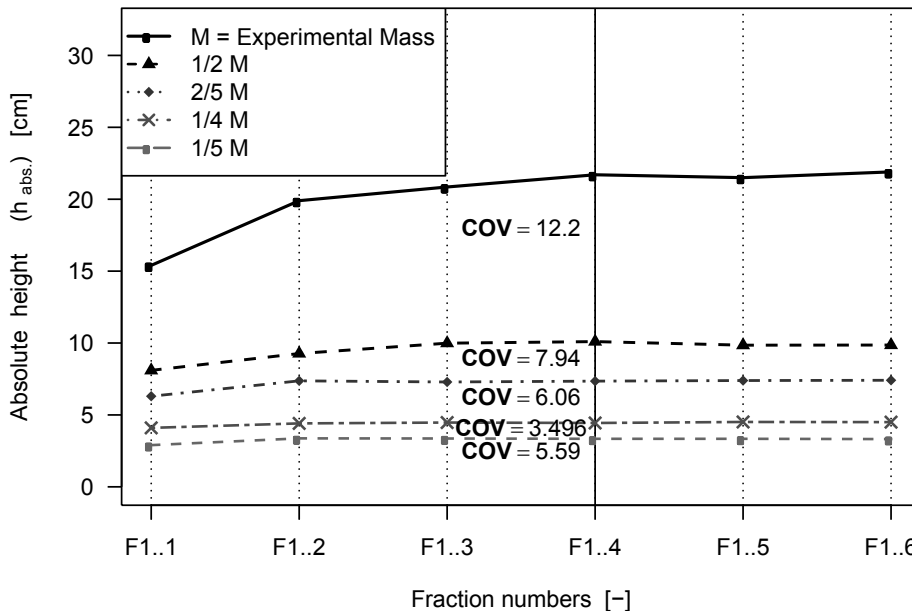
Figure 4.9.: Results of SFT simulation - Comparison of absolute height for different masses using *PSD3*
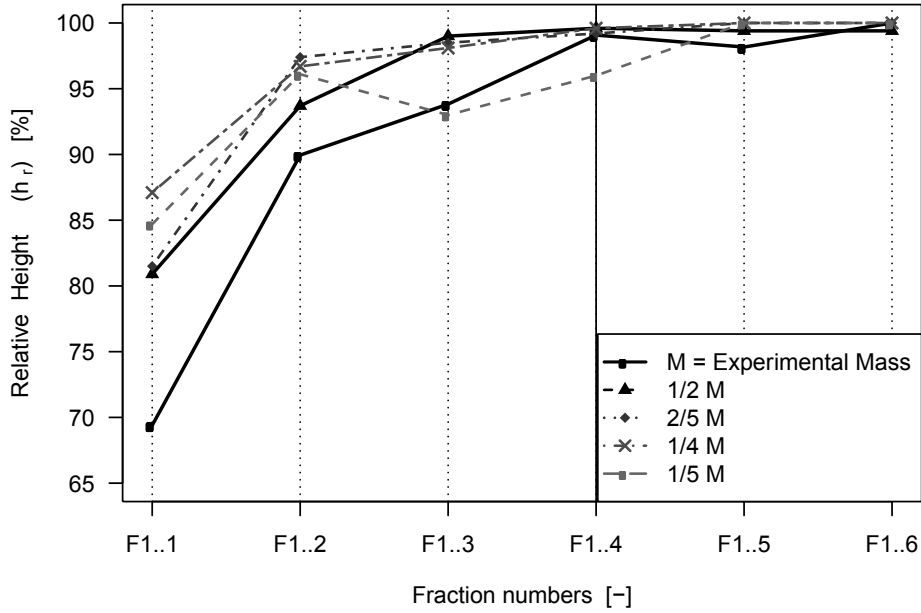
Figure 4.10.: Results of SFT simulation - Comparison of absolute height for different masses using *PSD3*
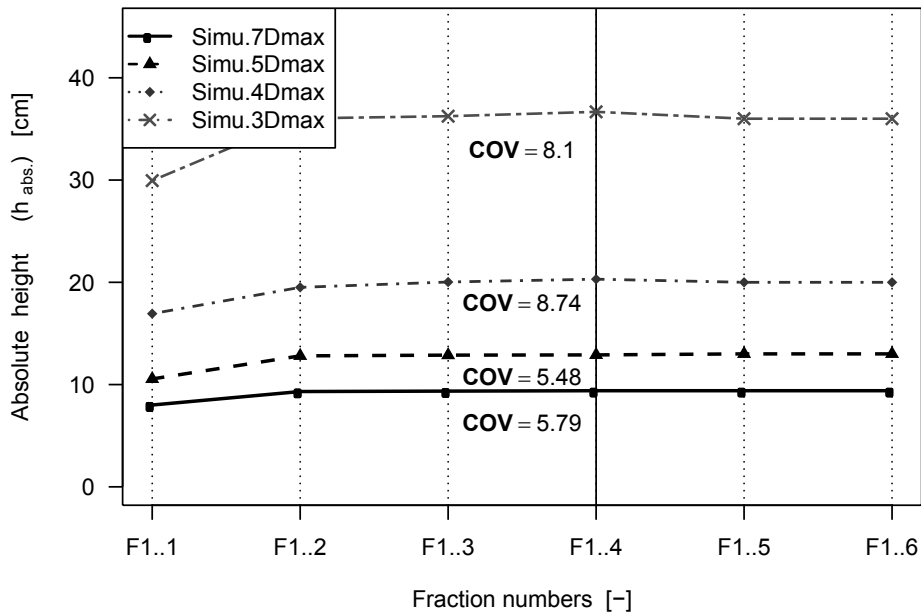
Figure 4.11.: Results of SFT simulation - Comparison of simulated absolute height for different radii of cylinder for the constant mass $1/2\,M$ using *PSD2*

The results of the *DEM* simulations for relative height h_r are shown in Figure 4.10. Using *DEM* simulation and by changing of total mass for a relatively big cylinder with $7 \times D_{max}$ of diameter, the parameter study for finding the minimum possible mass was performed. Theis mass, the so-called *REV* for such a widely graded soil, which can form the skeleton, was obtained. For the further investigations, the diameter of simulation cylinder ($D_{Cylinder}$) was varied for the optimization of the $D_{Cylinder}$. The $D_{Cylinder}$ was varied in dependency of the maximum diameter of the biggest fraction of the *PSD* (D_{max}), between 3 to $7 \times D_{max}$ (see Fig. 4.11).
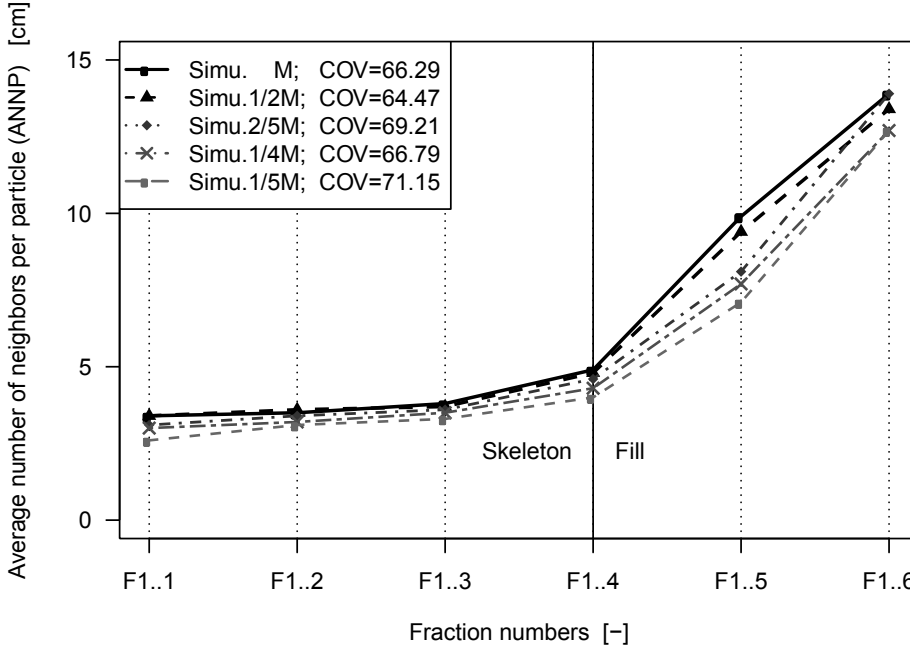
Figure 4.12.: Results of SFT simulation - Comparison of *ANNP* for different masses using *PSD2*

In this way, the minimum amount of mass and the optimized cylinder diameter can be determined. In Figure 4.12, the *ANNP* for *PSD2* is illustrated. The diagram indicates that *ANNP* is a good index for identification of the skeleton and fill. After addition of finer particles, here, addition of fraction *F5*, the *ANNP* increases suddenly. It means that the coarser particles are locally getting more neighbors while the finer ones have fewer neighbors in comparison. In fact, a particle with non-co-linear 4 neighbors is a stable particle according to Silveira (1965). The number of neighbors can be used for identification of a stable particle. The sudden increase in *ANNP* can be an essential criterion for the determination of the separation point D_s in a packing. The results of *ANNP* and height variation concerning the cumulative fraction numbers show a perfect correlation.

The same course of changes in *ANNP* was observed in different simulations. It must be considered that the number of neighbors is not equal to the number of particle contacts. Neighbors are particles in a given region around one particle. Hence, the first four frac-

tions can be assumed as the soil skeleton, and the following fractions can be considered as fill or secondary fabric of the investigated *PSD2*.

4.3.3. Discussion and summary

The analyses at the particle scale for packings generated with Pouring-Algorithm (*PA*) using two widely graded *PSDs* were carried out. Idealized numerically generated packings with spherical particles can be compared with glass beads used for the experimental *SFT* The results between the *DEM* simulations and the experiments prove the comparability of the real physical test with the simulation. The average densities of generated packings, with the half and two-fifths of the experimental mass ((1//2 *M* and 2/5 *M*) for *PSD2* as well as for *PSD3* were calculated. There are small differences between densities of the simulations with those of the experimental measurements. The density of the samples in experiments shows higher values than those in the simulations. The experimental samples are compressed with a relatively low compaction energy, to avoid segregation. Moreover, the plexiglass-cylinder (test apparatus) allowed us a minimal degree of compaction. Nevertheless, the compaction procedure did not change the height of samples significantly, especially by coarser fractions (see also section 3 and A.1.1) .
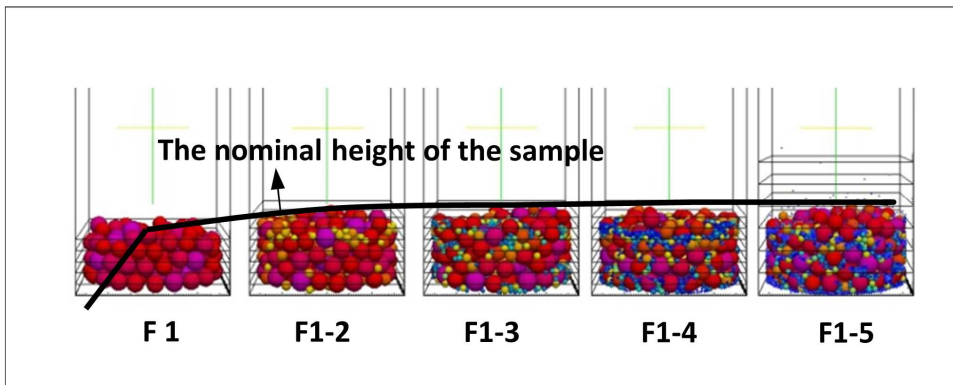
Figure 4.13.: Numerically simulated SFT results for PSD1 h_r relative height is illustrated with a continues line

To et al. (2014) presented a numerical approach for determination of the soil skeleton of granular soils. To et al. (2014) showed that the soil structure could be divided into three parts, primary or skeletal, transitional and fill. The transitional part consists of some locally fixed particles of fill fractions, which can transmit stresses and some particles of skeleton fractions, which are loose in the soil structure. The fifth and sixth fractions (*F5* and *F6*) represent only two percent of the maximum height (0.02 $\times h_{max}$). That two percent variation can be considered to be induced by the arching or boundary effect or according to To et al. (2014), it can be considered as the transitional fabric.

The higher the cylinder is filled with particles, the larger is the boundary effect. The more significant effect of the boundaries was proven by a correlation analysis of half of

the experimental mass ($1/2\,M$) for *PSD2* with changing the $D_{Cylinder}$. Due to the rigid boundary, arching effects occurred which increase the sample height.

Another correlation analysis shows that the absolute sample height, number of particles and Average number of neighbors per particle (*ANNP*) for *PSD2* as well as *PSD3* have a linear relationship. None of the correlations lied below 92% The numerically generated packings replicate soil behavior if the diameter of simulation cylinder ($D_{Cylinder}$) is bigger than $5{\times}D_{max}$ and the mass must always be more than 3.2 *kg* for such a widely graded soil. It can be concluded that by *ANNP* higher than 6 in a *SFT* process all coarser fractions belong to the soil skeleton. The changing of the sample height during the addition of fractions in *SFT* is equally significant as the number of neighbors per particle for identification of skeleton and fill of a widely graded soil.

As it can be seen from all presented results, all the graphs from numerically simulated *SFT* begin with a steep rise. This steep rise is similar to the results by the experimental *SFT*.For *PSD2*, all the graphs seem to have a good agreement until adding Fraction 4 *F4* The graphs from *PSD3* show more irregularities. The results of simulations with half and two-fifth of experimental mass ($1/2\,M$ and $2/5\,M$) for both *PSDs* illustrate the same course and very high correlation with the results of experimental *SFT*. In the tests with lower masses than $2/5\,M$, the particles are not able to form the soil skeleton and make a representative packing. By a lower amount of mass, the boundary effects as well as the segregation of the smaller particles increases, so that the height varies in an irregular way. Due to the segregation, it is possible that the finer fractions build the bottom layer in the cylinder, and the coarser fractions lie on top of them. This explains why curves with $1/4\,M$ and $1/5\,M$ reach their absolute maximal height by addition of the *F2*. Although, the mass increases by addition of next smaller fractions, the added particles are not able to increase the height of the sample (see Fig.4.13).

Therefore, the mass of simulation with half of the experimental mass ($1/2\,M$) was chosen to perform the second series of simulations with varying diameter of the diameter of simulation cylinder ($D_{Cylinder}$). In Figure 4.11, the results of simulation (*Sim.*) with a diameter of $5{\times}D_{max}$ show the same trend of height development like experimental *SFT* results. However, the *Sim.* $3{\times}D_{max}$ and *Sim.* $4{\times}D_{max}$ did not show the significant growth of height, which has been observed by experiments. For the simulation with the diameter bigger than $5{\times}D_{max}$, the mass must be increased. This increase indicates that the $D_{Cylinder}$ affects the formation of the soil skeleton. The $D_{Cylinder}$ of $5{\times}D_{max}$ can be chosen for the *REV*.

In Figure 4.13 the absolute height of the sample in relation to the cumulative fraction numbers for the simulation with the mass of $2/5M$ is illustrated. The necessary condition to obtain *REV* for such a widely graded soil (*PSD1*, *PSD2* and *PSD3*) with a Dominat Coarse Matrix (*DCM*) is to have a mass more than 3.2 *kg*.

$$M_{REV} > 3.2\,[kg] \tag{4.3}$$

Figure 4.14 shows the trend line for an effective formation of the soil skeleton. The following equations 4.4 must be satisfied in order to achieve a *REV* for further analysis:

$$REV = \begin{cases} Mass\ of\ REV\ [kg] & > & 1.01 \times (D_{cylinder}/D_{max}) - 1.66 \\ D_{cylinder}/D_{max} & \geqslant & 5 \\ D_{cylinder,\ min} & \geqslant & 5.D_{max} \end{cases} \qquad (4.4)$$

in which the *Mass of REV* is in kilogram. This equation is just for the investigated *PSDs*. To verify the experimental data and to determine a *REV*, over fifty single *DEM* simulations were made using the program *LIGGGHTSs* Generally, the greater the contact surface between granular material and rigid boundaries, the higher the boundary effects, for instance, due to arching.

Relationship between REV, cylinder diameter and D_{max}
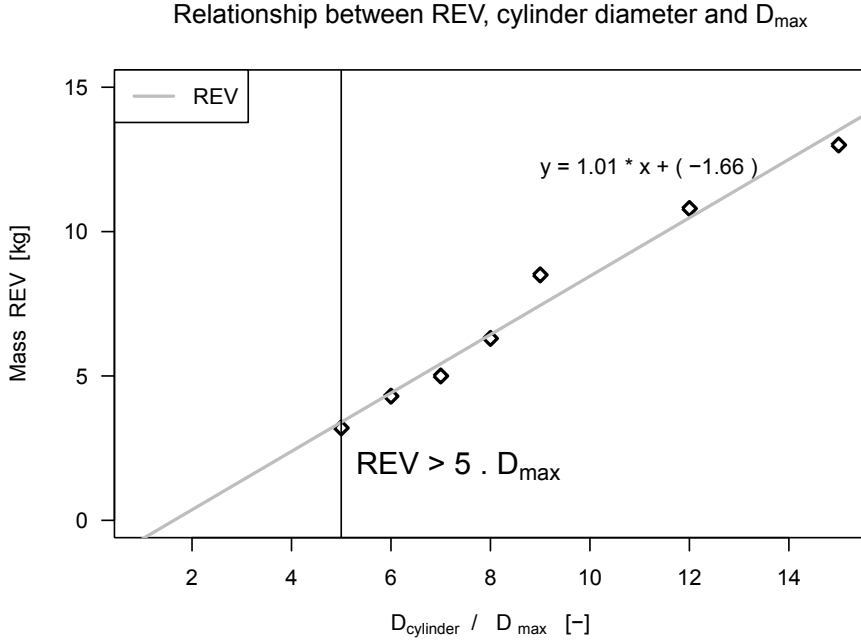
Figure 4.14.: Trend line of allowed REV related to maximum particle size D_s of investigated *PSDs*

Based on the result of simulations the lower mass limit for identification of the soil skeleton is recommended. The results indicate that the samples with a mass less than recommended mass are segregated so that the height of the sample did not significantly increase. The segregation of fine particles changes the height in an inconsistent manner by reduction of the mass. The investigated mass of simulation with $3.2\ kg$ and the radius of the $D_{Cylinder}$ of $5 \times D_{max}$ are defined as the *REV*. The suggested mass also agrees with the minimum specimen mass after DIN18123 (2011), which is recommended for sieve analysis.

By analysis of the Average number of neighbors per particle (*ANNP*), the soil skeleton is considered to be built predominantly by the first four fractions $F_{1..4}$ and eventually the fifth fraction of PSD (*F5*). The number of neighbors for each particle can be used to

find the Separation Point (D_s) between the soil skeleton and its fill. With the proposed method the size of the largest mobile particles of widely graded soils with a Dominat Coarse Matrix (*DCM*) can also be determined.

4.4. Simulation approach MFBA

Packing generation based on the *MFBA* which is originally built on the Collective Re-arrangement (*CR*) method offers all degrees of freedom to single particles. In this way, the realistic behavior of such a particle assembly with its special micro-mechanic can be modeled.

(a)	(b)
(c)	(d)
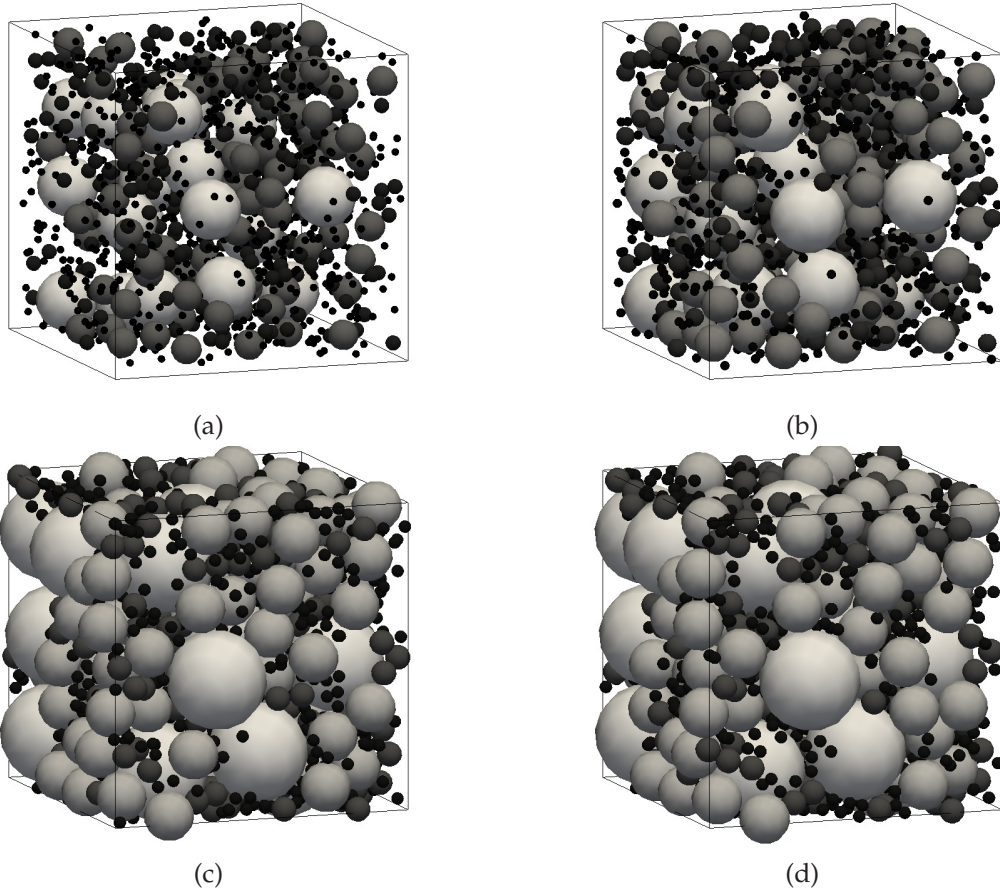
Figure 4.15.: *MFBA* Simulation for generation of a packing for investigated *PSD1* - Images show the insertion, growing and relaxation processes (a) first step: Insertion (b) second step: Start growing (c) second step: Middle of growing (c) third step: End of growing

By using the periodic boundaries, this method even provides the degree of freedom more than *PA* (see section 4.3) There are different algorithms, with various initial states of the particles and the process of densification. The author proposed *MFBA* based on

modification of *CR* methods, can model granular packings with arbitrary *PSD* and high density (Winkler et al., 2014).

The *MFBA* has three steps, particle insertion, particle growth and relaxation of the packing. In the first step, all particles of a predefined *PSD* are inserted by the Random Sequential Addition (*RSA*) method in the simulation box. The simulation box is cube shaped, which can be used easily for image-sectioning and image processing. The packing has periodic boundary conditions (Meier et al., 2008) There is an upper limit of the packing density, which can be reached. Due to randomly chosen insertion points, finding empty spaces for particle insertion between already inserted particles will be more time-consuming. These effects increase with raising packing density. The Particle Insertion Density (*PID*) can be improved by placing the biggest particles first. Consequently depending on the *PSD*, a *PID* up to 60% can be achieved. The wider the grading (*PSD*) is, the lower is the obtainable *PID* . In the presenting model, a porosity of 25% is targeted. The result of the first step is a loose particle cloud (Figure 4.15).

To increase the volume of particles, in the second step of the *MFBA*, the particle growth technique based on *CR* method is used. The diameters of the inserted particles are increased by a factor which is iteratively adopted on every time step. Thereby, the ratios between the diameter of particles stay unchanged, which results the same normalized *PSD* at the end of growing process (Fig. 4.15).

Whilst the particles grow, they start to contact and overlap with each other, the contact forces arise. Due to these forces, the particles rearrange and the packing becomes denser. The number of contacts increases and porosity decreases, until a state of equilibrium. To compare the obtained packing densities for different *PSDs*, a benchmark of compaction effort is needed, as in the proctor test, where the energy for compaction is standardized. In a thermodynamic model (Extended *DEM*), the temperature, enthalpy, pressure and many other parameters can be determined and controlled. These molecular dynamic parameters are not equivalent for granular systems. However, by keeping the marginal conditions constant, the particle movements and velocities inside of the packing can be imagined. To define a stop criterion for growing process, the confined pressure is used. The process of growing and rearrangement are continued until a percolating system, for instance, at a pressure of 10 MPa for a certain *PSD* was obtained. The more the particles grow, the more the particles overlap. Particle-overlap is not meant to be prevented, it is the fundamental idea of modelling by Discrete Element Method (*DEM*). Since, the intersection of real physical particles is impossible, overlapping causes an error in the model. An algorithm has been developed to control the particle-overlap and minimize it.

The expended energy for compaction is converted to kinetic energy of the packing. For further investigations assuming a stationary state, the packing should contain minimal kinetic energy. In the third step of the evolved algorithm, the particle growth is followed by a relaxation of the packing (Fig. 4.15). The kinetic energy is absorbed by damping, which is active between particles. Because of the overlapping of particles, the apparent porosity is lower than the actual obtained real porosity. The error can be estimated, and the actual porosity can be calculated after Raschdorf (2010). For the simulations with the *MFBA*, the difference of the real and apparent porosity is a value of ca. 1% and this value

is for the geotechnical applications negligible.

The *MFBA* method is comprehensively discussed by the authors in Winkler et al. (2014). The *MFBA* based packings were successfully generated and the section images in all three directions for the image analysis were captured (see Appendix B.2)

4.5. *REV* based on *MFBA*

For finding the *REV*, in this particular analysis, the porosity of the packing is chosen. The porosity value should reach approximately to a constant value by increasing the size of the packing. Figure 4.16 shows the fluctuation of the packing porosity in relation to its size. For identification of the size of the *REV*, statistical calculations based on the maximum likelihood method (*MLM*) have been carried out. The statistical analysis shows clearly that for the packings with an *REV* bigger than $4\times D_{max}$, the packing shows almost a constant porosity.

Change of the packing volume in dependency on porosity
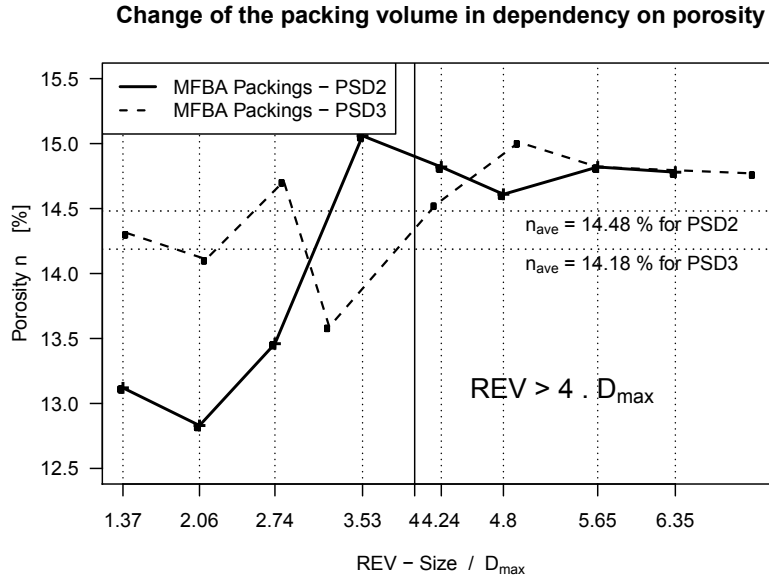
Figure 4.16.: finding the *REV* size for *PSD2* and *PSD3* based on consistency of packing porosities

4.6. Summary of this chapter

The numerical methods like *DEM* is an excellent and sophisticated method to analyze granular materials. In this chapter, two different approaches for making a packing is presented. The relevant scale for homogeneity quantification of widely graded soils, which are prone to suffusion was investigated. The *REV* of such a soil was determined. Based on

the numerical simulations, the soil skeleton can be successfully be identified. The changing of the sample height during the addition of fractions in *SFT* is equally significant as the number of neighbors per particle for identification of skeleton and fill of a soil. In the next chapter, the numerically generated packing will be used for calculation and quantification of homogeneity.

5. Quantification of homogeneity

5.1. Fundamental definition of homogeneity

In general, homogeneity is defined as the state of being identical or of a similar nature. It also means having a unvarying structure throughout. For instance, a uniform gravity field, which has the same acceleration and direction at each point can be addressed as a homogeneous field. In this field, all points experience the identical physical property.

The *Webster's Revised Unabridged Dictionary* (2010) defines a homogeneous material in physic as a system or material that has the identical characteristics at every point of the three-dimensional space, or it is uniform without irregularities. Homogeneity describes a conceptualized object whose properties do not vary with position or of the same or a similar nature. Here the conceptualized object means a static model of reality. For example, an object of uniform porosity is sometimes described as homogeneous. Another related definition of a homogeneous material is simply a parameter that is uniform in composition. Homogeneity can be statistically described as a parameter with a standard deviation (σ) equal to zero (*Webster's Revised Unabridged Dictionary*, 2010)(see Equation 5.1). It states that the average of the squared differences from the mean value (μ) is equal to zero. The variable x is 100 % homogeneous if x in its domain (*REV*) satisfies the following equations:

$$\begin{cases} \sigma &= \sqrt[2]{1/N \sum_{n=1}^{N}(x_i - \mu)^2} \; = \; 0 \\ \\ C_H &= (1 - \sigma^2)100 \;\; [\%] \end{cases} \tag{5.1}$$

where:

x_i : takes random values from a finite data set x_1, x_2, ..., x_N with each value having the same probability

C_H : coefficient of homogeneity

σ : standard deviation

σ^2 : variance

μ : mean value ; $\mu = 1/N \sum_{n=1}^{N}(x_i)$

The definition of homogeneity strongly depends on a certain parameter, the context and chosen scale. For example, a composite material is made up of different separate homogeneous materials, called as constituents of the material, but can be defined as a homogeneous material. Earthen embankments consisted of a core and supporting body can generally be considered as a composite material, if they have an identical cross section for a definite length along the river, it can be called as a homogeneous composite. Observing

such a composite material in another length scale, it consists of different aggregate sizes in the core and various particle diameters in its supporting body, compacted layer by layer, would be a very rough assumption. If the same embankment is more closely investigated, the spatial variation of the particles shows definitely a heterogeneous material. By changing the scale or the context the degree of homogeneity varies.

Another basic problem is that of the establishing homogeneity. Homogeneity in the geological context has been discussed by several researchers like Hubbert and Rubey (1959), Scheidegger (1963), Toth (1970) and Hodge and Freeze (1977). Hodge and Freeze (1977) points out that there is really no such thing as a truly homogeneous medium in rock fills. However, in order to have a tractable analysis of different parameters in a soil, a scale of measurement must be chosen, which is suitable for the investigating parameter. For a certain parameter, on the selected scale the quantified C_H is said to be relevant. Thus, the scale at which analysis is appropriate needs to be found out. For example, after Hazen the permeability of a granular material is governed by fractions smaller than D_{10} of its PSD (Krumbein et al., 1943). Consequently, in the first line, the homogeneity of these particles of a specific PSD affect its k It states that the homogeneity scale should be considered in dependency on D_{10}-fraction. It must be noted that, there are several different methods for estimation of permeability. Kozeny-Carman's formula is based on the entire PSD, the particle shape, and the void ratio (Carrier III, 2003). Therefore, in the case of using Kozeny-Carman's formula for estimation of permeability all particles must be considered and the coefficient of homogeneity must be calculated for all three dimensions.

The volume at which the parameter of interest first stops varying, is defined as the REV (see also section 4.2). The REV will be unchanging as the volume of the soil increases, and if it increases still further, the value of the coefficient of permeability (k) may start to vary once more and then become constant again (Long et al., 1982). This implies that the REV may exist on different scales. The REV of a medium related to permeability can be found by measuring the average permeability of increasing volumes of soil until the value does not change considerably with the addition or subtraction of a small volume. There is no guarantee that such a REV exists for every permeable system. Oda (1985) showed theoretically and experimentally that the permeability of fractured rock may continue to increase with the volume tested. For the different layers of the soil, the continuous increasing of the permeability value may also happen. This means the permeability continues to increase with the size of REV.

It is obvious that in any material, a micro-scale structure of the material dictates its macro-scale properties. Furthermore, the local non-homogeneity or in case of granular material local segregation of the material, the distribution of soil skeleton fractions, can significantly change the quality of the earthworks. Homogeneity of a soil sample for laboratory tests, placement strategy for dam embankment construction or methods for segregation prevention is frequently mentioned in the body of geotechnical literature, but most often, it is discussed in qualitative terms only, without any quantitative measurements.

Like all of ideas inspired from nature, the idea of using images for quantification of homogeneity is based on the evidence, that the humans are able to distinguish between homogeneous and non-homogeneous soils. In the soil images from the surface, the homo-

geneity can be investigated quantitatively. The study of Beck (1967) is known as the basis of automated systems that can statistically test the homogeneity of an image. Min et al. (2004) applied such a method to analysis of the structural homogeneity of rock masses based on their fracture's length and orientation. Almost the same method is used for homogeneity of concrete (Masad et al. (2002); Chermant et al. (2001)). This approach has been also applied to the development of facial recognition systems.

The challenge in any recognition or detection method is to discern the appropriate parameters for a discretization of an object, i.e. shape, size, etc. Once an individual object is detected and measured, the relationship to neighboring objects can also be measured and statistically characterized. Automated detection methods, which are able to identify objects can be classified in two main groups:

1. structural technique developed by Yachida et al. (1979)

2. gray scale method developed by Spowart et al. (2001); Spowart (2006)

In this section, edge detection methods , available in the *MATLAB*(2011) Image Analysis Toolbox, are implemented to measure 4 basic characteristics of granular packings: *a*) Particle Number Distribution (*PND*), *b*) porosity (*n*) , *c*) equivalent diameter (D_e) and *d*) particle distance ($Dist_p$)

The quantification method is by some means the identical idea of calculation of variances for several parameters by Woertz et al. (2013). The analysis then compares the statistical variance of each normalized parameter across equally sized sub-images. The effect of varying the sub-image size is also measured. The variances of four parameters are then combined into a single homogeneity coefficient C_H. It should be noted here, that the measurements for C_H consider *2D* data only. There is a possibility to extend this *2D* method for layers above each other and rebuild the *3D* data with some assumptions. The approach could be easily extended to *3D* using well-known computer tomography methods, but that topic would be left for future studies.

5.2. Approach for measuring homogeneity

5.2.1. Obtaining a measurable image

To count and measure particles using edge detection method, a *2D* image should be first transformed into black-and-white monochrome (binary image). In such an image, each pixel represents either a 1 or a 0. The solid phase for this investigation is represented by the 1 values and the pore spaces with 0 values. By examining the connectivity of each pixel with its neighboring pixels, the boundaries of a single particle can be detected. In a very low resolution, two particles can be detected as one aggregate. The defined connectivity will determine whether an neighbor pixel is part of the current object. Adjacent 1 and 0 values would indicate a boundary, whereas all particles with a value equal to one would point out a continuous area of the same particle (MATLAB, 2013). In *2D* either 8 or 4 pixel connectivity may be used, as schematically shown in figure 5.1. In the case of real granular material or numerically generated packings, particles can be connected also at the corners, so 8 pixel connectivity is a more appropriate choice for the detection of the

particle size or shape. The sections of a packing can be analyzed based on this method with a very good accuracy. Because, in case of section-images the particles do not have any overlapping, and the boundaries of a particle can be detected easily. The main reason that the author used image-sections for the *3D* packings is that the recognition of the *V* or surface of a particle would be a very big challenge (Homberg et al., 2009).

(a) connectivity 8   (b) connectivity 4
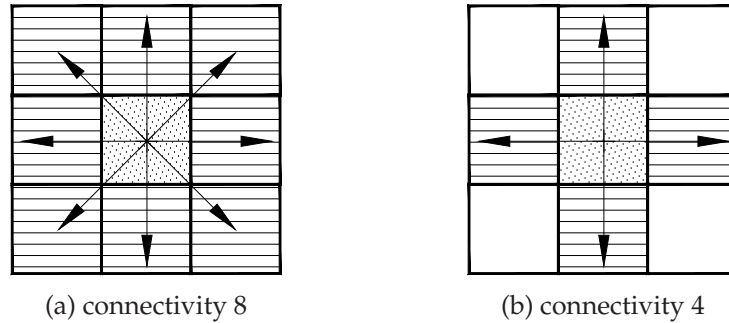
Figure 5.1.: Schematic view of pixel connectivity (a) 8 pixels and (b) 4pixels (MATLAB, 2013)

5.2.2. Image preparation - soil surface and packing sections

The images usually are taken as color (RGB) images, and those from the numerically generated packings can be directly generated as binary images. An additional filtering step is needed to transform RGB image into a gray-scale image Once in the gray-scale image format, based on the existing contrast level, gray thresh-holding transforms the image into a black-and-white image.

(a)   (b)   (c)
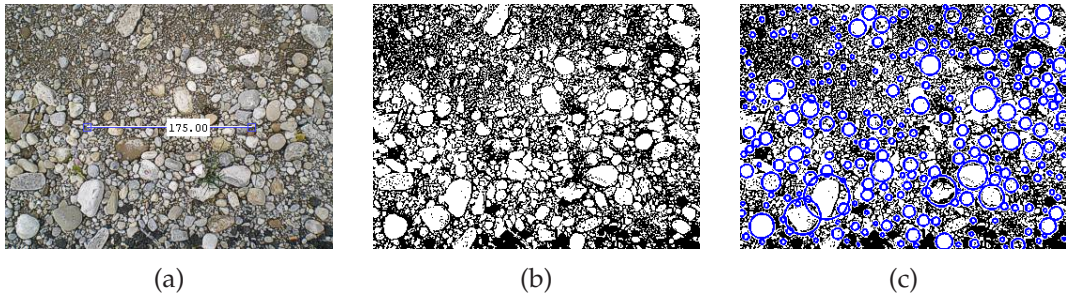
Figure 5.2.: (a)Image of surface of supporting body of a dike (b) filtered image with a threshold of 0.5 (c) detection of skeleton fractions

Note that, this approach is not effective for any images, because the coefficient of homogeneity will be calculated for various locations or heights, so that they can be compared with each other. Nevertheless, for light colored materials weak illumination and for the darker particles, high illuminations (light intensity) are recommended.
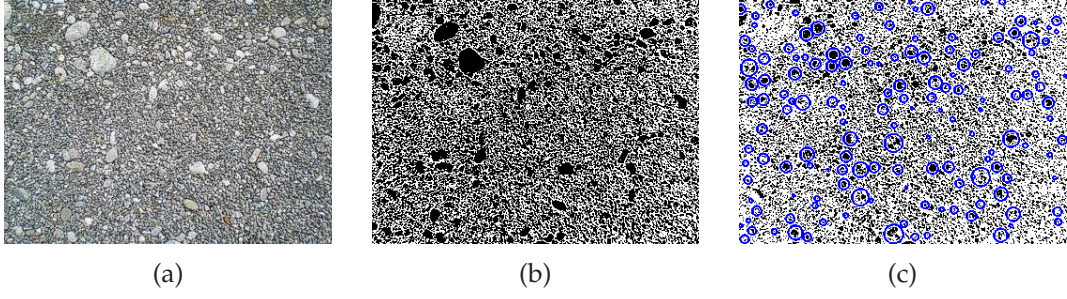
Figure 5.3.: (a)Image of supporting body of dike after layer compaction (b) filtered image with a threshold of 0.5 (c) detection of skeleton fractions

Moreover, the selected filter and threshold values must be chosen with engineering judgement for each image, as they have a large effect on the accuracy of the final binary representation. Figure 5.3 shows an example of an image captured by normal camera, which is accurately transformed to binary representation. In Figures 5.3c and 5.2c, the detection of skeletal fabric of the supporting body of a dike with an accuracy of 88% are represented. The size of the images taken by any camera differs, but they are all rectangular. For calculation of the coefficient of the homogeneity, a square image is cropped.

A *MATLAB* code for visualizing the cubical packings is written. Generally the *3D* numerically generated *MFBA* packings (see section 4.4) or the cubical core of generated packings based on *PA* can be visualized using this code (see Fig.5.4 and 5.5). Another code is written for generating the section-images in horizontal and vertical directions (code can be found in Appendix C).
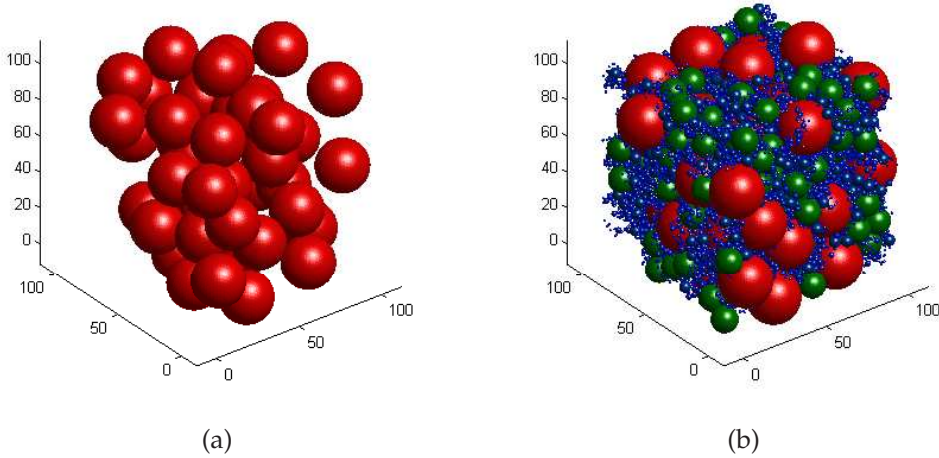
Figure 5.4.: *3D* visualization of the *MFBA* packing by *MATLAB* code for *PSD1*, with dimensions of $100 \times 100 \times 100$ [*pixel*] (a) *F1* of *PSD1* (b) *F1..5* of *PSD1*

(a)   (b)
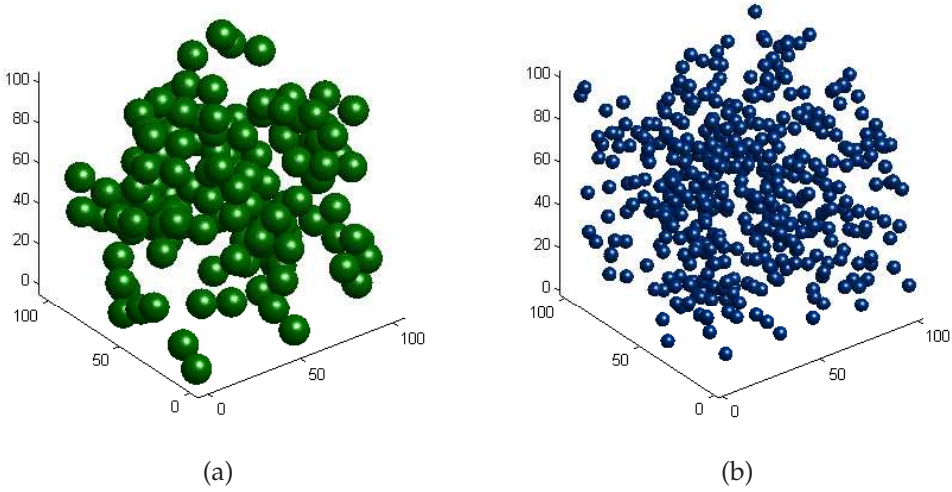
Figure 5.5.: *3D* visualization of the *MFBA* packing by *MATLAB* code for *PSD1*, with dimensions of $100 \times 100 \times 100$ [*pixel*] (a) *F2* of *PSD1* (b) *F3* of *PSD1*

After generating the *2D* section-images, the quantification of homogeneity for the captured section-images as described in section 5.5 is carried out. The *MFBA* packing creates a big data set, which represents an opportunity for the investigator to gain greater insight and to make more informed decisions, but it also presents a number of challenges. Big data sets, like *DEM* output data, may not fit into available memory, may take too long to process for the high amount of particles. Standard algorithms are usually not designed to process big data sets in reasonable amounts of time or memory. Here, for visualization of the packings and section-images, the output of the *LIGGGHTS* has been scaled to $100 \times 100 \times 100$ [*pixel*].

(a)   (b)
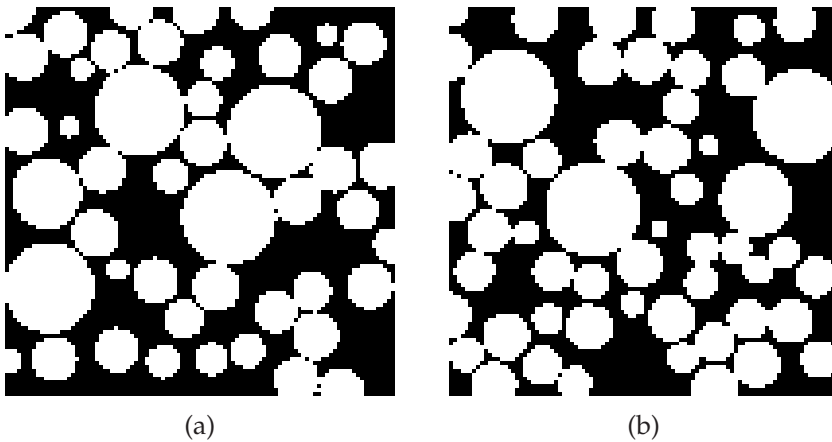
Figure 5.6.: *2D* section images of the *MFBA* packing by *MATLAB* code for *PSD1* and *F1..3* (a) section image $z = 5$ [*pixel*] (b) section image $z = 95$ [*pixel*]

Due to that, in Figure 5.6, the pixels can be seen easily, and the quality is not satisfactory. Nevertheless, the same condition has been applied for all of packings and section-images. Accordingly the quantified C_H of section-images can be compared to each other.

5.2.3. Measuring the binary image

Once the binary image is prepared, 4 particle assembly parameters are measured to assess overall morphological homogeneity. These 5 parametrs are as following:

1. **Equivalent diameter**: Each particle's measured pixel area A_P is converted to an D_e for the circle of same area, given in Equation (5.2). The calculated length can then be scaled if it is necessary.

$$D_e = (\frac{A_P * 4}{\pi})^{0.5} \tag{5.2}$$

2. **Particles distances** : Distances are measured from the centroid of each particle ($Dist_p$). Although, edge-to-edge measurements are more accurate, implementation and choosing the more relevant edge is difficult and computationally very time consuming. Euclidean distance (given by Equation (5.3)) is measured from the centroid coordinates of a particle to those of every other particle in the sub-image ((x_i, y_i) and (x_{i+1}, y_{i+1})), and the process is repeated for each subsequent particle. Repeating distances are ignored for the result.

   It must be mentioned, if the homogeneity of the whole packing is considered, the particle distances have a significant effect on the C_H. For the homogeneity assessment of the soil skeleton, because the particles have a bigger distance to each other, this parameter delivers an exaggerated value. Hence, for the assessment of the soil skeleton, the particle distances are not considered.

$$Dist_p = ((x_{i+1} - x_i)^2 + (y_{i+1} - y_i)^2)^{0.5} \tag{5.3}$$

3. **Porosity**: Each particle area is calculated by finding the entire number of connected pixels for a given object. After it is done for all particles, the total areas of the particles are summed and divided by the total area of the sub-image area.

4. **Particle Number Distribution (*PND*)** The particle number in each sub-image is calculated using edge detection method (MATLAB, 2013)

The following parameters are also calculated in the *MATLAB* code. Though, they do not have significant effect on the C_H for packing, which consists of the skeleton fractions with spherical particles.

   · **Particle Orientation**: This parameter returns a number that defines the angle between the x-axis and the major axis of the ellipse with the similar second-moments as connected pixels. The value is in degrees, ranging from -90 to 90 degrees. With the aid of this parameter, elongated particles and their effect on the homogeneity can also be quantified.

· **Subimage-Centroid**: The subimage centroid (C_i) of each particle is measured. The mean value of the centroid coordinates are measured as the gravity center of the sub-image.

· **Fractal dimension** : If an image displays self-similarity, it is called fractal . It can be split into parts, each of which is at least approximately a reduced-size copy of the original image. The *MATLAB* Image Analysis Toolbox gives the possibility to characterize a fractal set provided by the box-counting method. The number N of boxes of size R needed to cover a fractal set follows a power-law like in equation (5.4).

$$N = N_0 * R^{(-DF)} \text{ , } with \ DF \leq D \tag{5.4}$$

in which, D is the dimension of the space, usually $D = 1, 2$ and 3.

DF is can be calculated by the Minkowski-Bouligand method or box-counting method. There are several examples in *MATLAB* boxcount package, which illustrates how to use the *MATLAB* package *Boxcount* to compute the fractal dimension of $1D$, $2D$ or $3D$ sets, using the box-counting method (MATLAB, 2013).

Depending on the granular material other parameters, like particle shape, orientation and fractal dimension can be added and other parameters that are less relevant may be removed. The author has calculated the coefficient of homogeneity for the same example just by using the fractal dimension of the sub-images (see Appendix C).

5.2.4. Limitations of the approach

Homogeneity in geotechnical materials is frequently discussed in a qualitative manner, but is hardly ever quantified. As stated before, relatively little work has been directed at unifying the geotechnical community in measuring homogeneity or developing standard methods for such a quantification. A difficulty in quantifying homogeneity is identifying the scale at which homogeneity becomes most important for a certain parameter. At low magnification, a material can appear homogeneous, but at smaller length scales, which may control the particle movement of soil and instability growth, the material may be clearly inhomogeneous. The obvious conclusion is that in order to achieve the greatest benefit from homogenizing processes, is imperative to identify: The critical length scale for achieving homogeneity.

As a result of the work in other fields, a variety of statistical approaches is already available to describe the distribution of mixtures. These methods might be eagerly applied to soil subjected to arbitrary in-situ or laboratory homogenizing processes. The statistical aspects are relatively quite simple. The initial activity is to select and apply a set of relevant parameters. These parameters must be identified based on engineering judgment. For permeability of a soil, the whole focus must be on the distribution of the fine particles. These relevant parameters must be normalized. The following basic parameters were selected based on author judgment, such as particle size, porosity of the packing,

particle distances, particle number, clustering tendency. They seem to be the most fundamental logical variables to quantify in a sub-image. The fractal dimension seems to replicate the information of named parameters in itself. Other parameters like centroid of the sub-images, particle shape and orientation can be considered additionally for elongated materials. The color of the material can be used to distinguish different types of materials with varied Young's modulus. Due to the various magnitudes of the parameters, the normalized parameters which can fully characterize the homogeneity of three-phase granular material must be calculated.

To analyze homogeneity, additional steps are required. A microstructure's image must be divided into several sub-images and the distributions of particle parameters within the individual sub-image must be statistically compared. In doing so, a homogeneity index can be generated based on regional variances (C_H). This objective measurement of homogeneity could then be used to compare two images directly and possibly, to connect the measured coefficient of homogeneity (C_H) to a material's expected mechanical performance.

5.3. Assessing Homogeneity

For a variety of mathematical reasons, variance is a convenient parameter to assess homogeneity (Jazwinski (1970) and Morrison (1990)). A variance value of zero indicates that all values within a set of numbers are similar. All variances that are non-zero will be positive numbers. A large variance indicates that numbers in the set are far from the mean and each other, while a small variance indicates the opposite. Statisticians use variance to see how individual numbers relate to each other within a data set, rather than using broader mathematical techniques such as arranging numbers into quartiles.

A general disadvantage to variance is that it gives added weight to numbers far from the mean, since squaring these numbers can skew interpretations of the data. However, for homogeneity assessment, this disadvantage seems to be even an advantage to assess the segregation in a more radical estimation. The parameter of Fractal Dimension was calculated but did not consider in the final C_H estimations, because the variance of Fractal Dimension between different sub-imgaes was very small. The coefficient of homogeneity can be estimated based on DF, but it must be scaled for different soils to achieve a reasonable value for C_H.

5.4. Image segmentation

In Figure 5.7, the sub-images for a 3×3 segmentation are shown. In a perfectly uniform image, all sub-images of the image would have identical values for all measured parameters. By measuring the differences between sub-images, a quantitative evaluation of uniformity can be obtained.

By measuring the statistical variance of the chosen parameters the dissimilarities can be quantified over the range of sub-images respectively different length scales. A low

variance is an index for homogeneity (stochastically homogeneous) for the particular parameter being measured. A combination of all the parameter variances is an index for homogeneity of the image for that length scale. To create systematic sub-images, the cropped binary square image is divided into smaller sub-images. Those sub-images are then statistically analyzed using all of selected parameters (Fig. 5.7).
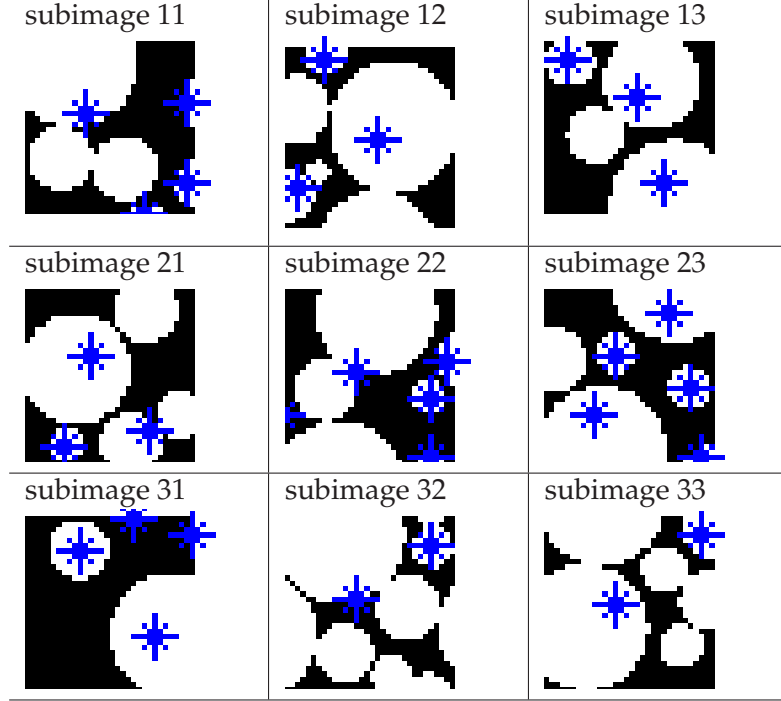
Figure 5.7.: Image segmentation for calculation of C_H (subimage number: 3×3) for *PSD1* for packing with skeleton fractions *F1..3* at $z = 20 \, [pixel]$

5.5. Coefficient of Homogeneity

A suggested coefficient of homogeneity (C_H) for a particular *REV* size can be expressed by the relation shown in equation (5.5). The mean value (μ) of the measurements of the selected parameter (for instance porosity (n)) is obtained across an equal number of sub-images, the mentioned equation is used for calculation of homogeneity or uniformity between sub-images. The index i represents a normalized variation in the sample with respect to all the chosen parameters. Here integer number N represents the number of measured parameters. For example, the calculated coefficient of homogeneity (C_H) for the soil skeleton ($F_{1..3}$) of the *MFBA* packing for *PSD1* is shown in Fig.5.8. For this calculation, because the soil skeleton is considered, the following parameters (D_e, n and *PND*) with $N = 3$ is chosen (see particle distance in section 5.2.3.

$$C_H = (1 - \{\sum_{i=1}^{N} \sum_{j=1}^{N} COV(X_i, X_j)\}) \times 100 \, [\%] \tag{5.5}$$

A total variance in the image can be calculated using the following procedure which has been implemented into a *MATLAB* code with a Graphical User Interface (*GUI*). Certainly the code can be used without the GUI as well.

1. Divide the binary image to a selected number of square sub-images.

2. Calculate the mean values for each measured parameter for all sub-images.

3. Normalize each distribution of sector mean values to 1.

4. Calculate that variance of each normalized distribution.

5. Calculate the covariance for each parameter relation, e.g., $COV(X1, X2)$ to $COV(X2, X3)$. For the three (or any number in dependency of chosen variables) selected parameters, 3 covariance values will result. Sum the covariance values.

6. Sum the calculated covariance values and subtract from 1. Multiplying with 100 the C_H can be expressed in terms of percent.

Since measured values are normalized, the above procedure will result in a coefficient of homogeneity (C_H) ranging from 0 to 100%, with a value of 100% indicating perfect homogeneity, i.e., all variances are zero since all sub-images are identical in their parameter distributions. Note that, using a single image will result in $C_H = 100\%$ since the measured sub-image is compared only to itself.

For a numerically generated packing, the C_H for sections with a maximum distance of half of D_{max} is needed. If one chose higher values for producing the section-images, it is possible to miss some skeleton particles. The less the difference between section-images is the more the results is reliable. By obtaining the C_H for section-images. The COV of the coefficient of homogeneity (C_H) can be calculated.

Phoon (2008) has recommended the values of Table 5.1 for quality assessment of friction angle. He emphasized that the *COVs* of natural geo-materials can be much larger and do not fall within the narrow range of the given table which was originally recommended for concrete quality assessments. For the quality evaluation of the homogeneity, a data base is needed. It is now possible to establish a data base for such a evaluation by using the proposed method.

Quality	COV (%)
Excellent	<10
Good	10-15
Satisfactory	15-20
Bad	> 20

Table 5.1.: Evaluation of the quality for friction angle of the soil samples
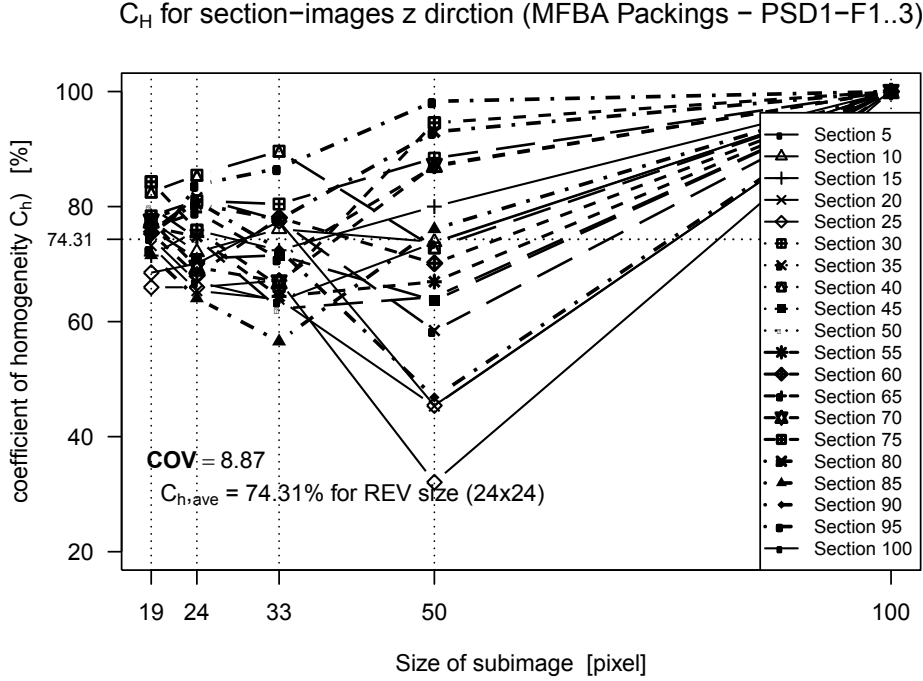
Figure 5.8.: C_H calculations for sections with 5 pixels distances in z direction for *MFBA* using *PSD1* (skeletal fabric *F*1..3 - The calculated *COV* for subimage size of 24×24 pixels equal to 8.87 indicates the excellent quality of the sample. The $C_H = 74.31\%$ represents a stochastically homogeneous sample.

Figure 5.8 shows the effect of scale on homogeneity coefficient using variance measurement. Depending on scale, one material can have complete various regional variances. The calculated C_H for different *REV* sizes showed different values, which can be understood easily. As the *REV* size decreases, however, the sub-image variances should rise in a less uniform material. Another effect is immediately noticeable at smaller *REV* size, in some sub-images the porosity increases, i.e. in pixel scale again the variances begin to decrease from sub-image to sub-image. This trend is important to note for interpretation of the results. This method was tested for complex stochastically homogeneous (*MFBA* packing), segregated (*PA* packing) as well as total homogeneous lattice packing. The results can be compared with the established method of cell porosity calculation based on Voronoi tessellation method. For instance, the calculated *COV* of cell porosities in *MFBA* packing for *PSD1* is equal to 31.17%, which results approximately a coefficient of homogeneity of coefficient of homogeneity = $(1 - 0.3117) \times 100 = 68.83\%$ (Winkler, 2013)

The section-images of a mono-disperse homogeneous packing, which is called here lattice packing is shown in Fig.5.9. The *3D* image of the lattice packing can be found in Appendix C. Figure 5.11 shows again the effect of scale on calculation of C_H. Depending on scale, even lattice packing can have very different regional variances.
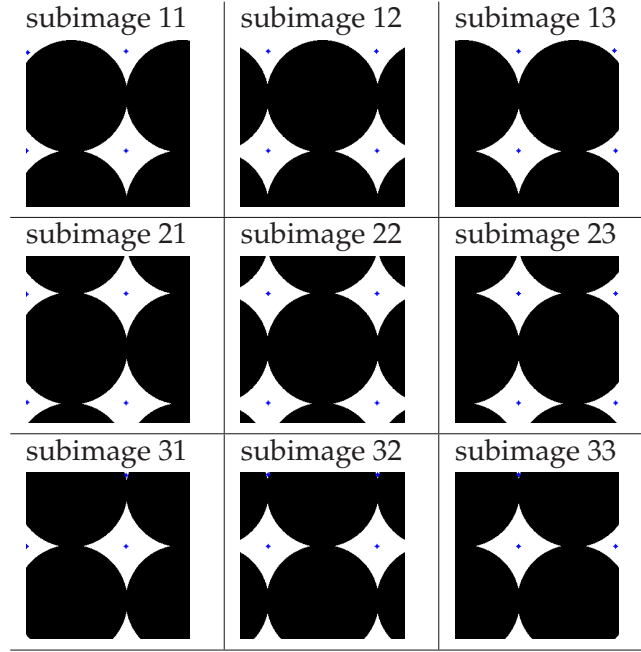
Figure 5.9.: Image segmentation for calculation of C_H of pores (sub-image number: 3×3) for lattice packing at $z = 10$ [$pixel$] The resolution of this image is much higher than the one in Fig. 5.7. Due to the smaller particle numbers in the packing, a higher resolution is chosen.
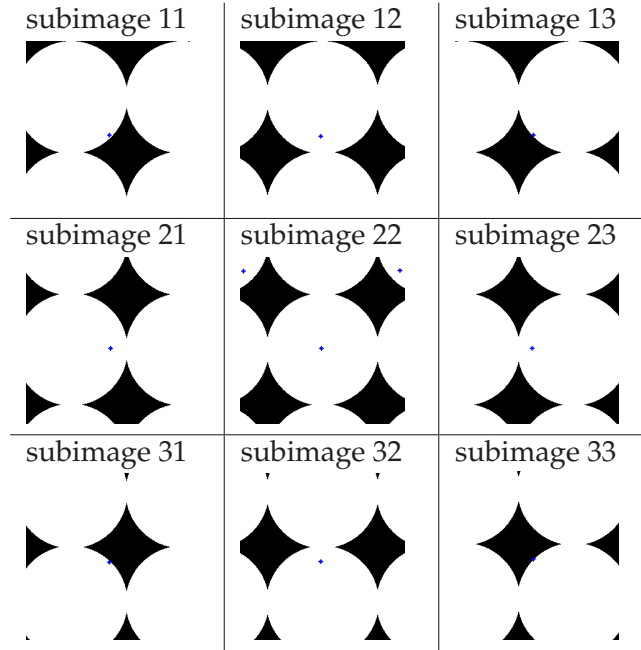
Figure 5.10.: Image segmentation for calculation of C_H of particles (sub-image number: 3×3) for lattice packing at $z = 10$ [$pixel$].

The calculated C_H for various *REV* sizes resulted different values, which can be visually and qualitatively observed. The changes of the values coming from irregularities of the sub-images because of dividing the particles in dissimilar positions. Thus, the equivalent diameter (D_e) and the centroid of the sub-image varies somewhat from sub-image to sub-image. As the *REV* size decreases, however, the variances rise even in a homogeneous section-image. The results can be again compared with the established method of cell porosity calculation. For instance, the calculated *COV* of cell porosities in lattice packing equals to 0.23%, which results approximately a coefficient of homogeneity of coefficient of homogeneity $= (1 - 0.0023) \times 100 = 99.77\%$.
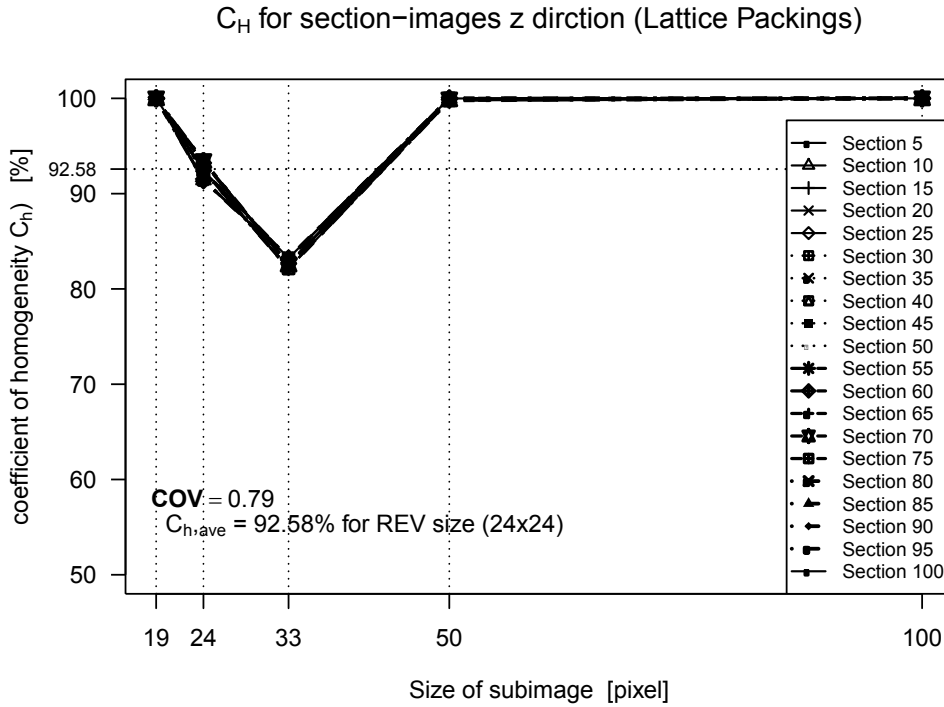
Figure 5.11.: C_H calculations for particles and pores by (see 5.10 and 5.9

Figure 5.11 shows the C_H graphs for particles as well as for pores between particles by sections at 5 pixels distances in z direction for Lattice packing using particles with a constant diameter. The calculated *COV* for sub-image size of 24×24 pixels equal to 0.79 indicates the excellent quality of the sample. The $C_H = 92.58\%$ represents an almost perfect homogeneous sample. The identical C_H results for pore and particles indicate that the developed method respectively, the chosen relevant parameters are appropriately selected.

Parameter matrix	Normalized matrix	Vector of parameter and its mean value

$$PND = \begin{vmatrix} 4 & 3 & 3 \\ 3 & 5 & 4 \\ 4 & 2 & 2 \end{vmatrix} \Rightarrow$$

$$P\hat{N}D = \begin{vmatrix} 0.8 & 0.6 & 0.6 \\ 0.6 & 1.0 & 1.0 \\ 0.8 & 0.4 & 0.4 \end{vmatrix} \Rightarrow$$

$$X_1 = \begin{vmatrix} 0.80 & 0.60 & 0.80 & 0.60 & 1.00 & 0.40 & 0.60 & 1.00 & 0.40 \end{vmatrix}$$

$$\Rightarrow \mu_{X_1} = 0.69$$

$$n = \begin{vmatrix} 0.45 & 0.43 & 0.62 \\ 0.31 & 0.42 & 0.26 \\ 0.40 & 0.39 & 0.28 \end{vmatrix} \Rightarrow$$

$$\hat{n} = \begin{vmatrix} 0.73 & 0.69 & 1.00 \\ 0.51 & 0.68 & 0.42 \\ 0.65 & 0.63 & 0.46 \end{vmatrix} \Rightarrow$$

$$X_2 = \begin{vmatrix} 0.73 & 0.69 & 1.00 & 0.51 & 0.68 & 0.42 & 0.65 & 0.63 & 0.46 \end{vmatrix}$$

$$\Rightarrow \mu_{X_2} = 0.64$$

$$D_e = \begin{vmatrix} 10.29 & 14.92 & 15.89 \\ 14.68 & 9.21 & 11.37 \\ 9.24 & 19.65 & 18.96 \end{vmatrix} \Rightarrow$$

$$\hat{D}_e = \begin{vmatrix} 0.52 & 0.76 & 0.80 \\ 0.75 & 0.47 & 0.58 \\ 0.47 & 1.00 & 0.97 \end{vmatrix} \Rightarrow$$

$$X_3 = \begin{vmatrix} 0.52 & 0.76 & 0.80 & 0.75 & 0.47 & 0.58 & 0.47 & 1.00 & 0.97 \end{vmatrix}$$

$$\Rightarrow \mu_{X_3} = 0.70$$

$$COV(X_1, X_3) = \sum_{i=1}^{N=3} (x_i - \mu_{X_i})(x_{i+1} - \mu_{X_{i+1}})/N \Rightarrow$$

$$COV(X_1, X_3) = \begin{vmatrix} 0.051 & 0.022 & 0.042 \\ 0.022 & 0.030 & 0.028 \\ 0.042 & 0.028 & 0.041 \end{vmatrix} \Downarrow$$

$$\sum(COV(X_1, X_3)) = 0.309 \implies C_H = (1 - sum(COV(X_1, X_3))) \times 100 \implies C_H = 69.14\%$$

Table 5.2.: Calculation method of C_H

5.6. Experimental quantification of coefficient of homogeneity

5.6.1. Purpose and significance

In this section, a new experimental procedure based on *SFT* for quantification of homogeneity in widely graded soils with a Dominat Coarse Matrix (*DCM*) in an already existing or under the construction embankment dam, is proposed. Using this method and measuring $C_{H,Exp}$, particularly the placement techniques can be improved and the risk of internal erosion can be reduced. The $C_{H,Exp}$ of such a soil is the ratio, expressed as a percentage, of the difference between the maximum value of height of the skeleton and the height of the skeleton in-situ to the difference between its maximum and minimum skeleton height according to proposed sample placement techniques (*SRT* and *ALS*; see also section 3.5).

The engineering properties, such as shear strength, compressibility, and permeability, of a soil depend on its compaction index as well as its homogeneity. The vulnerability of such a soil against suffusion depends directly on those factors. In Figure 5.12, it is shown that the Experimental Homogeneity Coefficient ($C_{H,Exp}$) depends all above on the particle arrangement and placement technique of the soil. The various tests on the soil skeleton and skeleton plus fill indicated clearly the effect of segregation by different sample placement and compaction techniques.

5.6.2. Test and evaluation procedure

The test procedure for estimation of the $C_{H,Exp}$ is as following:

1. Considering a sample from the dam body. The minimum diameter of the sample must be $5 \times D_{max}$ and the depth of the sample can be calculated from recommended masses in chapter 4 and equation 4.4.

2. Carrying out the sieve analysis and separate all the soil fractions *F*

3. Carrying out the *SFT* test using *SRT* and classify the soil matrix into *DCM*, *CM*, *TM* or *FM*. If the soil consists of Fine Matrix (*FM*) the soil is not prone to suffusion. If the soil consists of Dominat Coarse Matrix (*DCM*) with a small amount of fines, find the separation point D_s. Determine and record the height of the soil. At this point, the soil sample reaches the maximum height of its homogeneous skeleton ($h_{max,SRT}$).

4. Fill the mold starting with the biggest fraction and ending with the smallest fraction of the soil skeleton as loosely as possible by pouring the soil using a scoop or pouring device (funnel). Determine and record the height of the soil ($h_{max,s,ASL}$) The obtained height of the sample is the maximum height of the segregated skeleton.

It must be noted that for soils with *FM*, the same procedure can be carried out with all fractions to estimate the $C_{H,Exp}$ This coefficient is not as precise as for *DCM*, in which the maximum height of the homogeneous skeleton $h_{max,SRT}$ is an almost unique value. The Experimental Homogeneity Coefficient ($C_{H,Exp}$) can be calculated using the following equation:

$$C_{H,Exp} = \frac{h_{max,ASL} - h_{field}}{h_{max,ASL} - h_{max,SRT}} \tag{5.6}$$

where:

$C_{H,Exp}$: Experimental Homogeneity Coefficient

$h_{max,s,ASL}$: the maximum height of the soil skeleton using DSL

$h_{max,SRT}$: the maximum height of the soil skeleton using SRT

$h_{eq,field}$: the equivalent height of the soil (in-situ)

The equivalent height of the soil $h_{eq,field}$ can be obtained by taking an in-situ sample with a circular surface area A with a diameter of $5 \times D_{max}$ and volume of V. The volume should be about the same experimental volume with a maximum difference of $\pm 2\%$. The $h_{eq,field}$ can be calculated using the following equation:

$$h_{eq,field} = \frac{4}{(\pi \times 5^2)} \times \frac{V_{SFT}}{D_{max}^2} \tag{5.7}$$
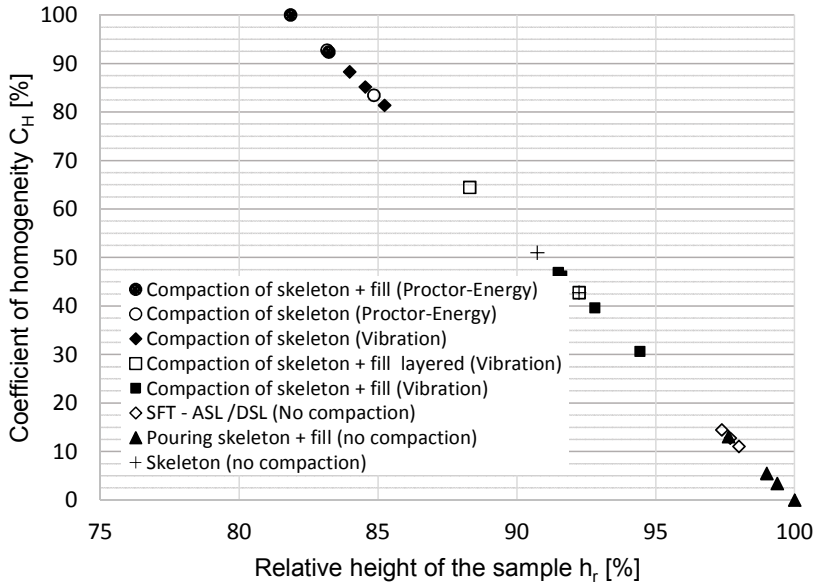
Figure 5.12.: Experimental Homogeneity Coefficient ($C_{H,Exp}$) using different sample prepration techniques and compaction methods

In Figure 5.12, it can be seen that the minimum relative height of the sample h_r respectively maximum density for *PSD1* is independent of compaction energy. One can say that the proctor energy causes more compactions than the other methods. Nevertheless, proctor method or compaction with a high concentrated energy produces a new *PSD* by crushing the coarser particles and resulting predefined channels in the earthworks which is not desirable.

5.6.3. Example data and $C_{H,Exp}$ calculation

The following *SFT* tests were carried out and the equivalent height of the soil (in-situ) ($h_{eq,field}$) is assumed for demonstration of the calculation method for $C_{H,Exp}$

SFT results using *SRT*	*SFT* results using *ALS*	Comment
$h_{max,SRT}$ in $[cm]$	$h_{max,s,ASL}$ in $[cm]$	

$$\begin{vmatrix} h_{F1..1} \\ h_{F1..2} \\ h_{F1..3} \\ h_{F1..4} \\ h_{F1..5} \\ h_{F1..6} \\ h_{F1..7} \end{vmatrix} = \begin{vmatrix} 15.20 \\ 19.70 \\ 20.55 \\ 21.70 \\ 21.50 \\ 21.90 \\ 21.70 \end{vmatrix} \qquad \begin{vmatrix} h_{F1..1} \\ h_{F1..2} \\ h_{F1..3} \\ h_{F1..4} \\ h_{F1..5} \\ h_{F1..6} \\ h_{F1..7} \end{vmatrix} = \begin{vmatrix} 15.20 \\ 21.36 \\ 22.28 \\ 24.93 \\ 25.10 \\ 25.14 \\ 26.7 \end{vmatrix} \qquad D_s = F4$$

$$h_{max,SRT} = 21.70 \qquad\qquad h_{max,s,ASL} = 25.10$$

$$h_{eq,field} = 22.70 \implies (5.6)\ C_{H,Exp} = \frac{25.10 - 22.70}{25.10 - 21.70} = \frac{2.4}{3.4} = 70.6\%$$

Table 5.3.: Calculation method of $C_{H,Exp}$
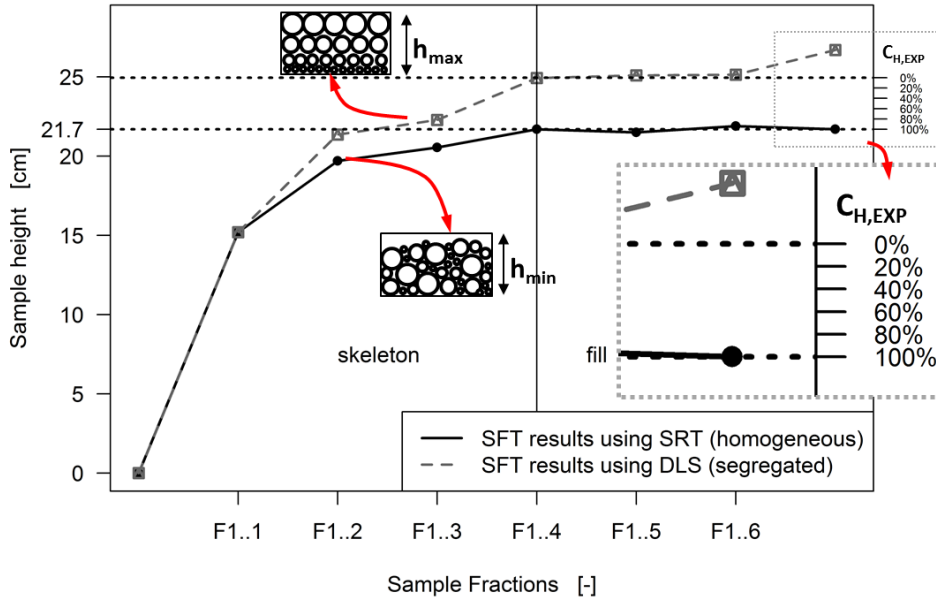
Figure 5.13.: Results of *SFT* for *PSD1* for estimation of $C_{H,Exp}$

Figure 5.13 shows two different paths of the height growths of the soil skeleton. The *SFT* tests using *SRT* were performed with assumption that the particle fractions, which do not belong to the supporting skeleton, cannot change the height of the soil sample. When the soil is segregated, the fine particles are able to contribute to the skeleton. Therefore, the height of the sample increases by addition of each fraction. The *SFT* tests using *ALS* experiments were performed with assumption that all fractions contribute to the soil skeleton. However, for *DCM*, the skeleton fractions are of interest, and the other fractions can be neglected. In the quantification approach the skeleton height is used as an index for homogeneity measurements. In the Appendix D.1, the evaluation of the Coefficient of Homogeneity based on image analysis as well as SFT can be seen.

5.7. Summary of this chapter

This chapter proposes a general new method for quantification of homogeneity in granular material with a *DCM*. Through digital image analysis of a binary 2D image (surface or cross-section) with a representative image size, varieties in particle distributions and several geometrical parameters can be measured. In the proposed method, the following particle parameters are measured: equivalent diameter (D_e), Particle Number Distribution (*PND*), particle distance ($Dist_p$) (distance between particle centroids), porosity (*n*), Fractal Dimension and particle orientation. The method can be extended for other parameters like aspect ratio and the positions of subimage centroid This method can be developed further for *RGB* images to quantify the homogeneity based on different Young's modulus (*E*) or distinctive particle stiffness characteristics. Using the results of the analysis, a coefficient of homogeneity (C_H) was quantified by calculation of normalized covariances in sub-images across an image. Cross sections of granular packings and images of the soil surface are used to demonstrate the application of this technique.

For quantification of C_H for a numerically generated packing, the C_H for sections at various levels in all directions with a maximum distance of half of the D_{max} must be calculated. The *COV* of these C_H can be evaluated using the criteria of Phoon (2008). A new experimental method is proposed for evaluation of Experimental Homogeneity Coefficient ($C_{H,Exp}$) for earthworks in terms of numbers.

6. New suffusion criteria considering homogeneity effect

6.1. An introduction to spherical packings

In mathematics, packing problems are related to optimization problems that involve attempting to pack objects together into containers. The goal is to either pack a single container as densely as feasible or pack all objects using as few containers as possible. In point of view of a geotechnical engineer, the soil particles are the spheres, and the container can be defined as Representative Elementary Volume.

(a) cubic packing   (b) hexagonal packing
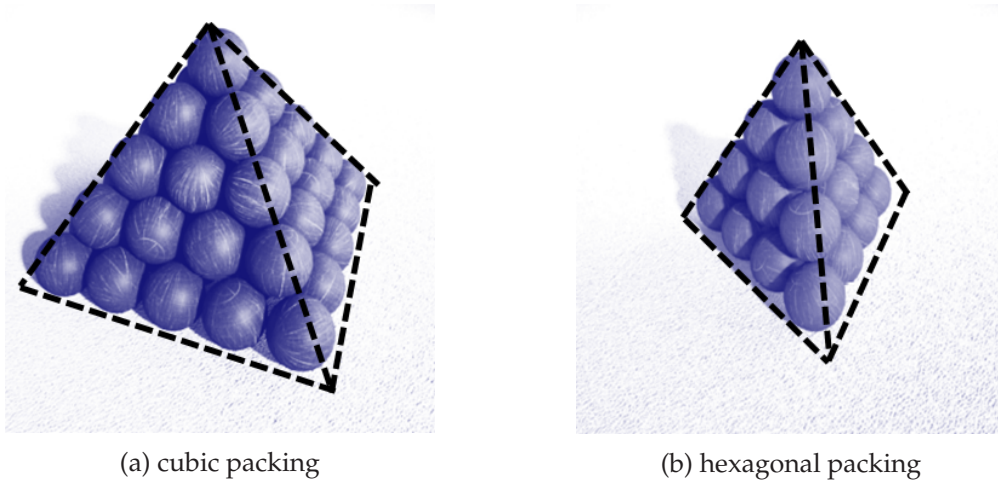
Figure 6.1.: densest packings for mono-disperese spheres

The first known mention of the problem of the densest packing of spheres goes back to Sir Walter Raleigh. He wanted to know if there is a formula for calculation of the maximum cannonballs that can be kept in the storage spaces of his ships. Therefore, he asked Thomas Harriot to find a way to solve this problem. Harriot tried then, to find a way to put cannonballs efficiently into the ships hold. Kepler dealt with the problem for several years. He finally published in 1611 his work "Strena Seu de Nive sexangula", in which he proposed solutions for the problem but without any mathematical proof. This conjecture is famous as Kepler's conjecture. It is a mathematical conjecture about monodisperse sphere packing in three-dimensional Euclidean space. It says that no arrangement of equally sized spheres filling a space can create the densest packing than that of the cubic close packing (face-centered cubic) (Fig.6.1a) and hexagonal close packing arrangements (Fig.6.1b)(Szpiro, 2011).The porosity of these arrangements is around 25.96%.

200 years later, in 1831, succeeded Carl Friedrich Gauss to find some evidence to demonstrate that Kepler's conjuncture can be proven. However, he could bring some mathematical proof for sphere packings on a regular grid (Weisstein, 2003). Thomas Hales in 1998, following an approach suggested by Tóth (1953), announced that he had a proof of the Kepler conjecture. Hale's approach is an evidence based on checking of many individual cases using complex computer calculations. Referees have said that they are almost certain of the correctness of Hale's proof, so the Kepler conjecture is now very close to being accepted as a theorem. In 2011, Hales announced the completion of a formal proof of the Kepler conjecture (Hales et al., 2011).
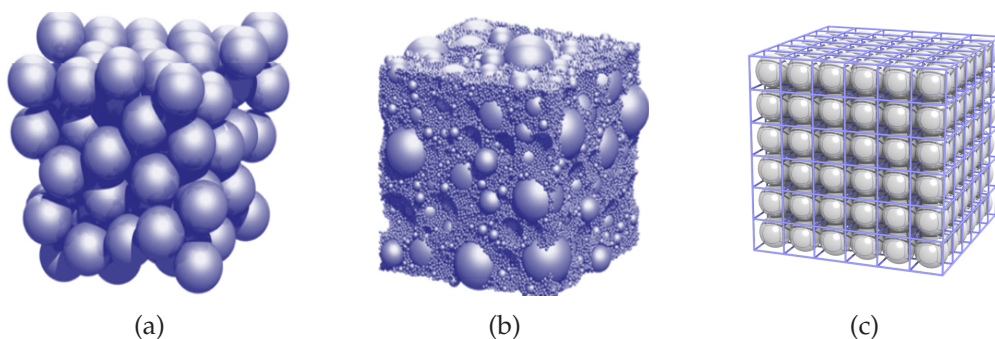
Figure 6.2.: (a) Mono-disperse random packing (b) Poly-disperse random packing (c) Mono-disperse packing on rectangular grid

In addition to the ordered monodisperse packings, there is random monodisperse packings (Fig 6.2a) polydisperse packings (Fig 6.2b) and monodisperse packings on rectangular grid (Fig 6.2c). The first two packings can reach lower densities as Kepler's arrangements. Research is carried out in this direction of finding lower porosities even for monodisperse packings since 1930 (Andreasen, 1930).
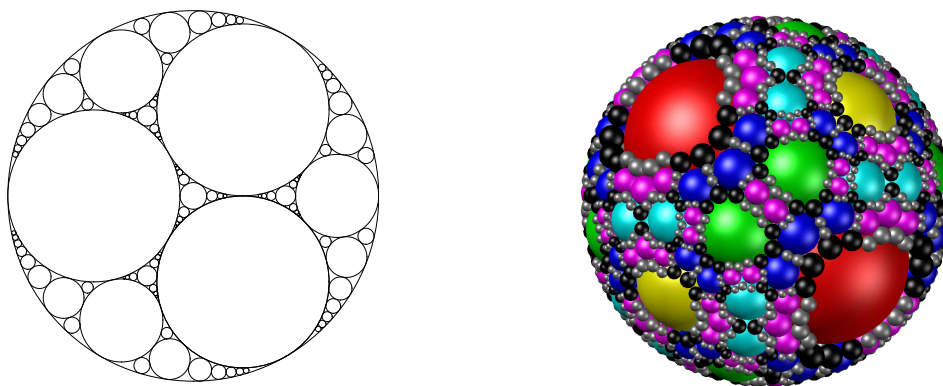
Figure 6.3.: Densest packings for poly-disperse spheres, right) 3D Apollonian Packing and left) 2D Apollonian Gasket

Packings consisted of spheres with different diameters (polydisperse packings) were

studied since the early 20th century. Fuller and Thompson (1907) investigated the Relationship between mass fraction and porosity experimentally and developed the Fuller curve, which represents a continuous particle size distribution. They went from a monodisperse dense packing of spheres and added spheres with smaller diameters to fill the pore spaces. This addition can be continued to fill all of the pores, and the porosity can be theoretically converged to zero. (Fuller and Thompson, 1907).

a) Apollonian Gasket with 3 starting circles   b) Curvilinear triangle - level one

c) Curvilinear triangle - level two   d) Curvilinear triangle - level three
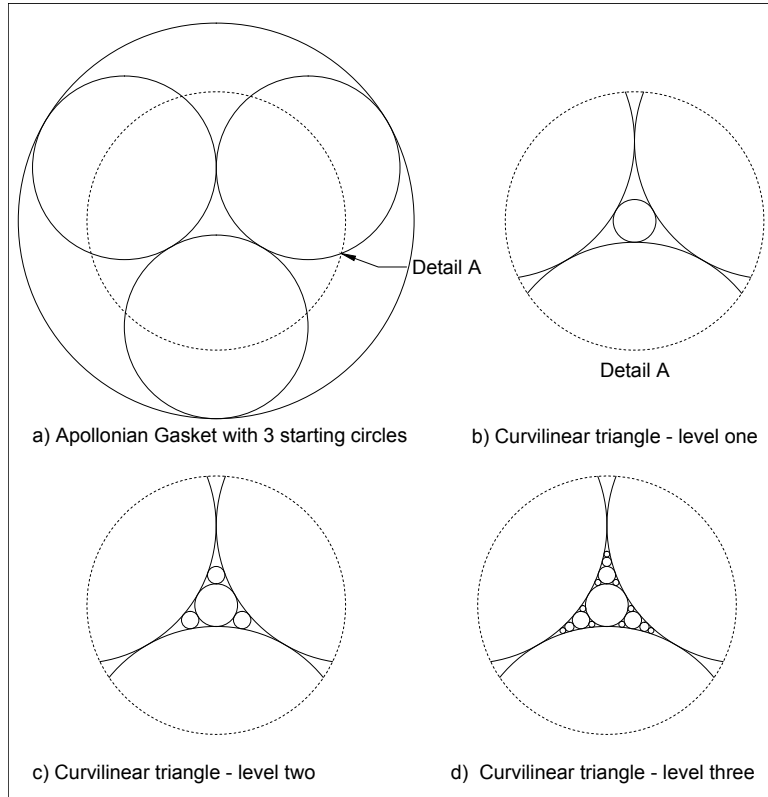
Figure 6.4.: Apollonian Gasket

The empirically achieved formula after Fuller and Thompson (1907) have similarities to Apollonian Gasket respectively to *3D* Apollonian packing. The Apollonian Gasket is named after Apollonius of Perga (ca. 262 to 190 B.C.) who has published a study on tangents to circles with the simple name of "Tangencies". He proved that there are at most eight different circles which are tangent to any three circles on the plane (not necessarily touching).

To construct the Apollonian Gasket, consider the three first circles as holes in a solid disc. The perimeter of the disc is tangent to the first three holes. The fractal is created by interactively drilling out the largest possible circular hole from the remaining solid (Edgar and Measure, n.d.). An alternative but equivalent way of describing this fractal is to consider three identical circles arranged in a triangle (not collinear) so that each circle is tangent to the other two, thus forming a closed region, namely a triangle with curved

edges (Fig. 6.4-a). Two circles are tangent to these three initial circles. They are referred to as the inner and outer circles. Apollonian fractal is created by repeatedly placing inner circles into the gaps between the circles already making up the fractal (Fig.6.4b-d). The Apollonian Gasket is an example of a fractal that is not self-similar. The fractal dimension has been estimated to be 1.305 684 (Mauldin and Urbański, 1998) and if one continues to fill all of the pores, the porosity just like particle arrangement using Fuller curve can theoretically converge to zero.

Based on Fuller curve, *2D*-Apollonina Gasket or *3D*-Apollonian packing one can produce the densest packing, but the resulted *PSDs* are a particular distribution of particles with a Fine Matrix (*FM*) The author has investigated many different arrangements of Apollonian Gasket with varied starting central circles. The author has modified the basic Apollonian algorithm and filled the bigger circle with the same fractal. It is called Nested Apollonian Gasket. The nested Apollonian Gasket was constructed by addition of different level of tangential circles in the middle of initial circles (Fig. 6.5).

b) 3 starting circle - 3 level nested a) 3 starting circle

c) 4 starting circle - 3 level nested c) 4 starting circle
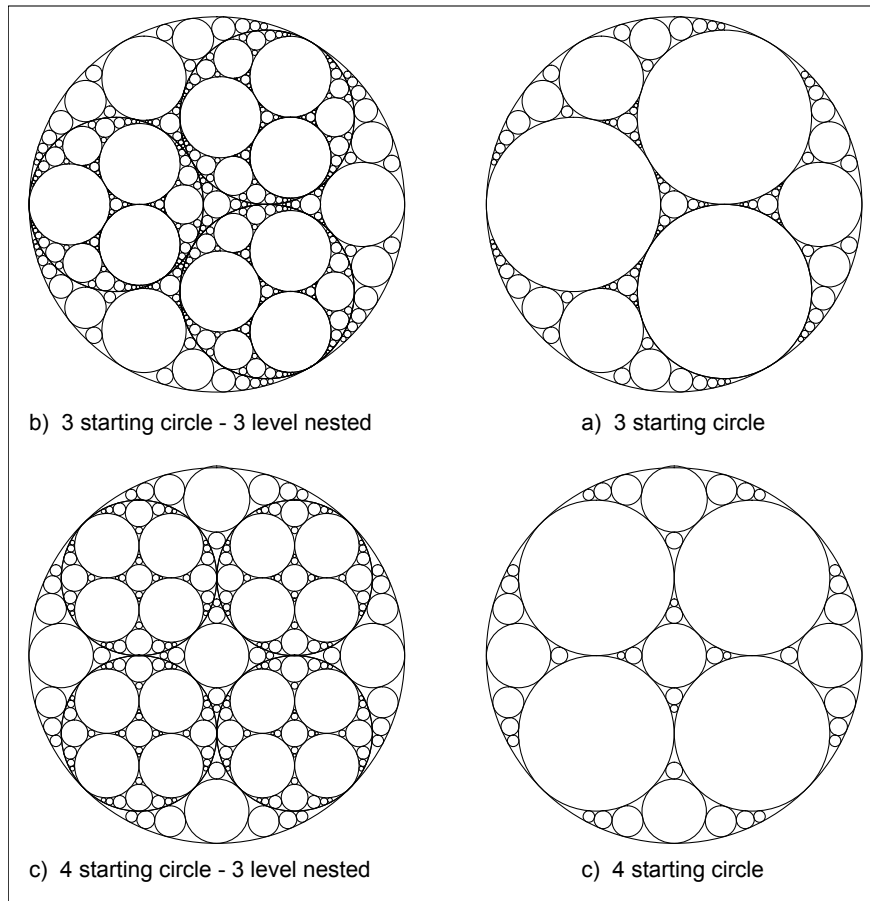
Figure 6.5.: Apollonian Gasket with 3 and 4 starting circles and different level of added tangential circles as well as nested Apollonian circles
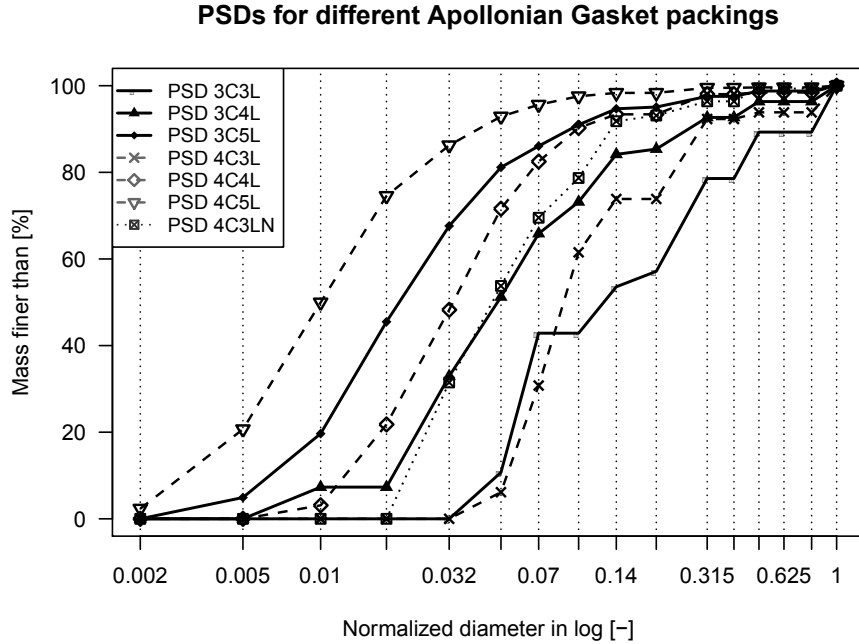
Figure 6.6.: *PSDs* extracted from 2D-Apollonian Gasket packings for different starting circles and levels. In legend of the graph *C* associates with starting circles and *L* means level of particle addition

The resulted *PSDs* of Apollonian Gasket and nested Apollonian Gasket do not show the same course of widely graded soils, which are prone to suffusion, i.e. soils with *DCM*. In Fig. 6.6, it can be seen that in both cases of addition of starting circles and addition of levels of tangential circles, the *PSDs* move in the direction of gradations that represent *FM* This kind of matrix is internally stable and out of scope of this investigation.

6.2. New suffusion criteria based on a new packing model

Standard criteria for assessment of suffusion or internal stability have been derived either empirically based on experimental procedures or analytically by geometrical considerations of pore structure (see section 1.4.1). Despite the remarkable number of different approaches, only a few criteria are recommended and used in practice. It is because of the nonrealistic homogeneity assumptions for the analytical criteria and the boundary conditions of the experimental procedure which cannot be fitted best to each case. In the following, a model based on the loosest state of the soil (based on Ascending layered segregated (*ALS*)) is presented, which is simple and can be used for assessment of suffusion of the granular materials without any limitations. This packing model is based on the geometry of the void constrictions.

Soil with a certain *PSD* can be considered as internally stable if the size of pore constrictions of the soil skeleton is small enough to prevent the fines from washout. Therefore,

there are many approaches based on this idea (e.g. Silveira (1965); Semar et al. (2010); Indraratna et al. (2011)). These researchers tried to determine analytically as well as statistically the pore structure. As a matter of fact, there is an infinite number of possible combinations, because the particles in widely graded soils differ in size and shape. Thus, the use of spherical shaped particles is a common simplification for this kind of calculations. In a soil with the densest packing, a pore is built by three particles. The constriction is within the plane going through the center of these spheres (Fig. 6.7).
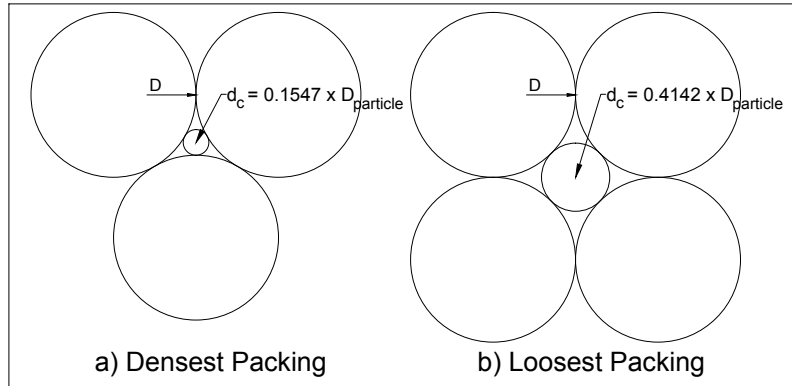
Figure 6.7.: Constriction sizes for densest and loosest packing

The biggest particle which would be able to pass through this constriction can be drawn as a circle, which is tangent to the outer three circles. The diameter of this circle can be calculated with trigonometric considerations. This model was established by Silveira (1965). He published a study, in which all possible combinations of constriction sizes for different fractions were calculated. Such a curve is called Constriction Size Distribution (*CSD*). The use of four connected particles for the calculation of constriction size is a common assumption for the loosest state. The largest possible constriction size is composed, if the centers of all spherical particles are within the same plane. Again, the solution can be found as the solution of a *2D* problem.

6.3. Fundamental assumption of the proposed Packing Model

In all of the suffusion tests carried out by the author, after a while, it could be seen that the water flow builds local segregated nests along preferred paths. It could also be observed that the soil was segregated in an almost ascending superimposed order in those nests. On the top of these segregated nests with ascending layers, which replicate Ascending layered segregated (*ALS*), some fine particles moved in the pore spaces in a rotational manner due to the water flow. Sometimes those particles could be locally transported to the upcoming pore spaces due to the implementation of the next higher hydraulic gradients. However, occasionally the ascending layered particles existed in all directions so that the fine particles could not be transported. The *3D* Apollonian Gasket can give a

good impression about that constellation. The fine particles trapped in the middle coarse particles are not able to move out of the pore spaces formed with coarser particles.

for loosest state
n=47.64%
e=0.9098 Vs=1

a) Model of Loosest state of a soil

b) Dominant coarse matrix

c) Homogeneous Ideal PSD

d) Dominant fine matrix
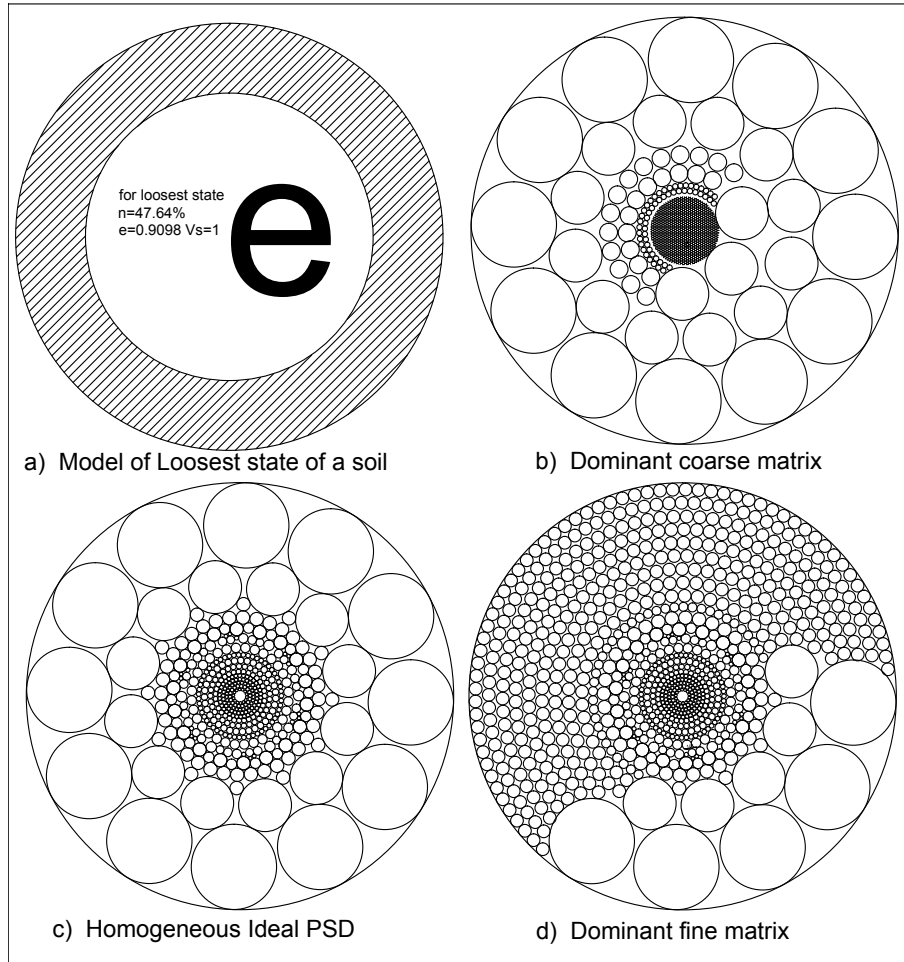
Figure 6.8.: Schematic illustration of packing model for granular poly-disperse soils a) the model of the loosest state of soil $n = 47.67\%$ b) a homogeneous dominant coarse matrix (*PSD1*) c) homogeneous Fuller curve d) homogeneous dominant fine matrix

As mentioned before, because of representing a Dominant Fine Matrix (*DFM*) the Apollonian Gasket with a higher level of tangential circles is not of interest. However, a new circular *2D* model like Apollonian Gasket based on the observations from suffusion tests can be proposed. The fundamental assumption for the packing model is that the homogeneous granular material with any matrix can be treated as an ideal segregated packing. From another point of view this segregated packing represents an entirely homogeneous material (see Fig.6.9). Thus, on another scale, the Ideal Homogeneous Packing (*IHP*) is the same as Ideal Segregated Packing (*ISP*). This packing is internally stable, if enough number (respectively mass) of each fraction F_i are available to filter the upcoming fraction

F_{i+1} (see (6.1)).

$$\forall \, F_i > F_{i+1} \; \Rightarrow \; F_i \sqsupseteq\blacktriangledown \, F_{i+1} \, ; \; (i \, \varepsilon \, Z) \tag{6.1}$$

In Figure 6.8, the bigger outer circle is filled from the outer ring and with particles with a diameter of D_{max}, which represent the diameter of the soil biggest fraction ($D_{max} \cong D_{F_1}$). The next ring will be filled with the following fraction (*F2*) and this continues up to the smallest fraction of the soil. The biggest circle represents the Representative Elementary Volume (*REV*) of the particular material.
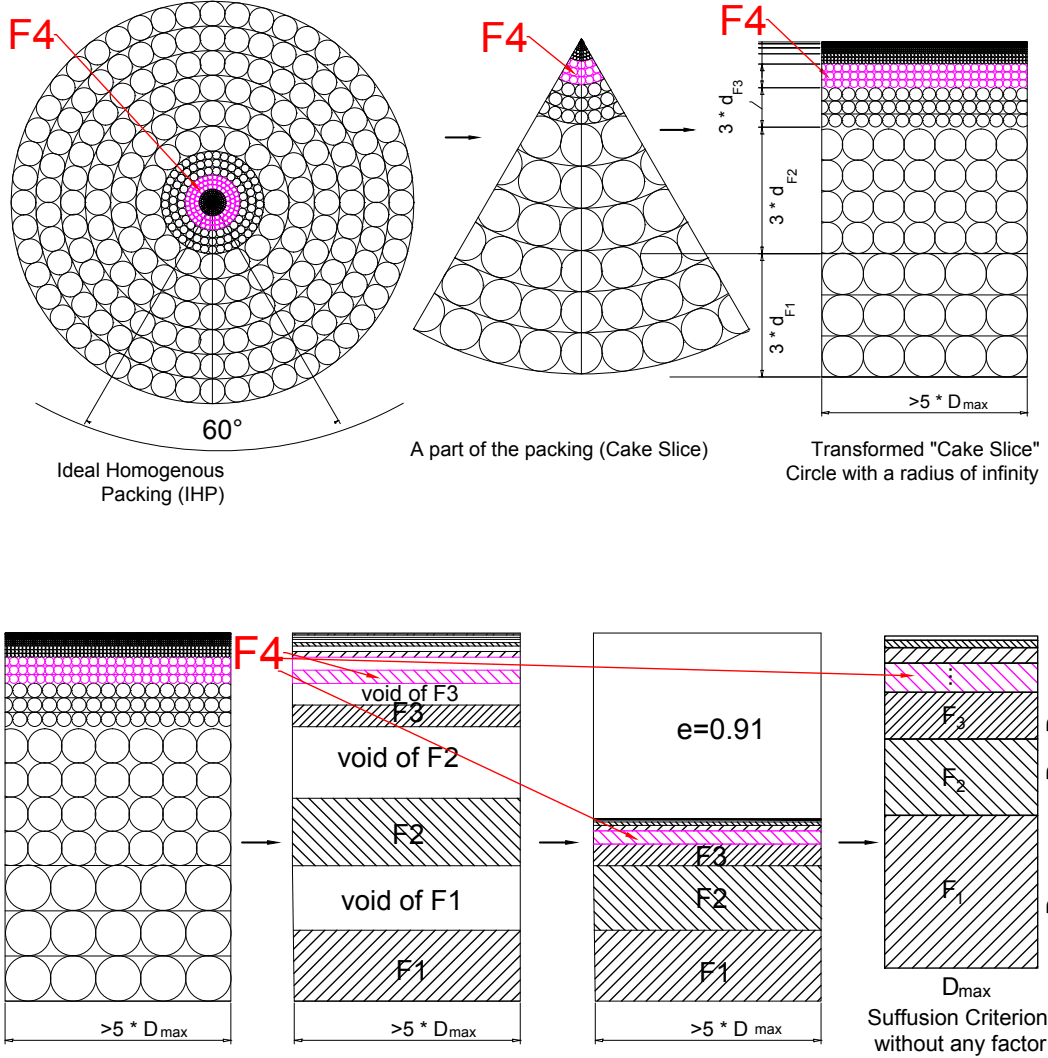
Figure 6.9.: The concept of the *IHIS-PSD*

This model shows that a stable Ideal Homogeneous Packing (*IHP*) is internally stable, self-supporting and independent of flow direction. In the case of soil with a Dominat

Coarse Matrix (*DCM*) (see Fig. 6.8-b), it can be seen that the smaller particles are in contact with the much bigger fractions, and their number is not high enough to fill their reserved area (R_A). It implies the internal instability (*U*) of such a matrix. In the case of Fine Matrix (*FM*), the finer particles are always in contact with the next bigger fraction, and their number is much more than larger fractions, which implies an internally stable matrix. This ideal segregated packing is not a unique packing for the original *PSD* and it changes in dependency of its discretization. It means, slightly different packing by a new *PSD* discretization can be reached. It must be mentioned that the discretization effect has a limit. It seems logical that by reducing the range of the discretization below that limit, all of obtained packings will be identical. If there are relatively few size classes and no reason to believe a particular function fits it well, then only using the standard sieve numbers lead to almost appropriate result. Nevertheless, the effect of discretization must be further investigated.

Likewise, if it is assumed that the whole packing has a radius approaching infinity. The circumference of a circle with the diameter approaching infinity would appear as a straight line. This assumption is a good assumption if one compares the size of the soil particles with the thickness of constructed soil layer. A wedge of this packing (cake slice) can be cut and transformed to a rectangle as a Representative Elementary Volume (*REV*) of such a packing (Fig.6.9). To determine the needed area for each fraction, it is necessary to possess a layer with uniform properties, in which the maximum constriction size for that fraction can be reached. This implies a selecting of a minimum of 3 rows of the given fraction diameter ($3 \times D_{F_i}$). Thus, the R_A for any fraction in *REV* with a minimum width of $5 \times D_{max}$ can be calculated. The reserved area (R_A) for each fraction must be filled by only that fraction to achieve the Ideal Homogeneous Internally Stable Packing (*IHISP*). A sample with all reserved areas filled with associated fraction represents a new *PSD* which is called *IHIS-PSD*. This *PSD* represents a limit function for the given discretization 6.2. All of the used factors are only for better illustraion and the final equation representing the proposed suffusion criterion can be simplified as:

$$f(R_A) = \frac{D_{Fi}}{\sum D_{Fi}} \tag{6.2}$$

For an arbitrary *PSD* and selected discretization, these areas can be calculated as well as its cumulative area distribution. If the density of the solid particles (soil particles) are assumed to be a constant value, the mass of each fraction, which can fully occupy the R_A, can be calculated. In this model, it can be imagined that the particles are meld together, which forms a solid plate and the pore spaces are separated. This can be compared to the classical model of the soil phase diagram, which represents the components of the soil (air, water, solid). To perceive this as a true *3D* volume, these areas can be given one unit length normal to the area. Afterward, their probability or frequency distribution can be compared to the Probability Distribution Function (*PDF*) of the original soil. The differences between the *PDF* of *IHISP* and Original *PDF* for each fraction can be determined by ΔR_A. The filter stability of the fractions which exceeds their reserved areas must be checked. This filter stability can be defined as:

$$\forall\, F_i > F_j \wedge j > i \;\Rightarrow\; D_{F_j}/D_{F_i} \geq 6.46 = \frac{1}{0.1547} \;\Rightarrow\; D_{F_j} \,\exists\blacktriangledown\, D_{F_i} \tag{6.3}$$

F_i	D_{F_i}	$3 \times D_{F_i}$	R_A	$f(R_A)$	PDF	ΔR_A
[-]	[mm]	[mm]	[mm²]	[%]	[%]	[%]
F1	20	60	6000	42.7	52.4	+9.70
F2	16	48	4800	34.2	21.4	-12.8
F3	5	15	1500	10.7	5.10	-5.60
F4	3	9	900	6.40	4.00	-2.40
F5	1.3	3.9	390	2.80	2.00	-0.80
F6	0.75	2.25	225	1.60	2.00	+0.40
F7	0.5	1.50	150	1.10	7.10	+6.00
F8	0.25	0.75	75	0.50	6.00	+5.50
		Σ	14040	100	100	0.0
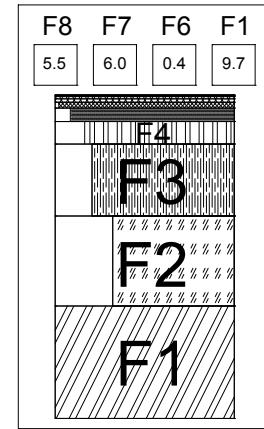
Table 6.1.: Calculation of reserved areas according to discretization of the *PSD* and available areas according to fraction masses for *PSD*1

Figure 6.10.: Graphical calculation for PSD1
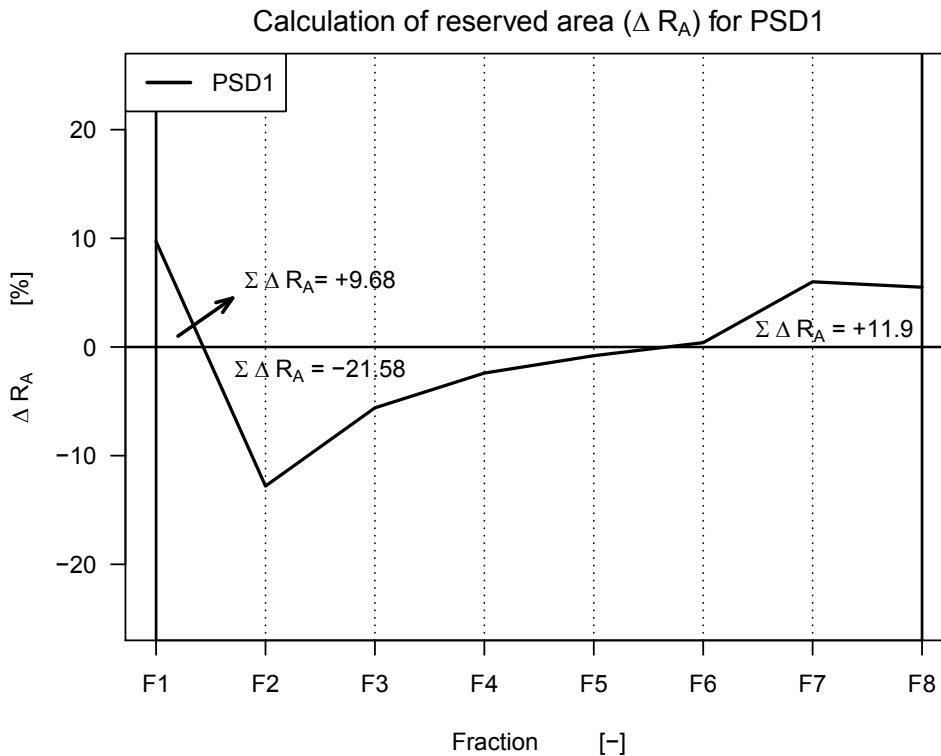
Figure 6.11.: Calculation of difference between ideal homogeneous internally stable packing with packing generated for *PSD1*

This value has no safety factor in itself and is a purely geometrical value which is calculated according to the pore constriction size of 3 identical circles in a surface (see Fig.6.7).

If those fractions are filter stable (∃▼) relative to each other, the *PSD* is stable. Otherwise, the *PSD* is internally unstable. In table 6.1, the width of the *REV* is equal to $5 \times D_{max}$, fractions, fraction diameters, the reserved areas and the difference between reserved area and the masses of the soil *PSD* are represented by *Fi*, D_{F_i}, R_A and ΔR_A respectively.

For an stable *PSD* the distance between two positive areas must be less than 4 to 5 according to common filter criteria. The distance between two positive areas, which must be according to (6.3) lower than 6.46 (stability criterion), as seen in Fig.D.1 is equal to:

$$D_{F1}/D_{F6} = 20/0.75 = 26.66 > 6.46 \tag{6.4}$$

Two examples are calculated in tables Tab. 6.1 and 6.2. In Figure 6.10, the reserved and filled areas for the *PSD1* are illustrated. The graphical presentation indicates that the soil has a Dominat Coarse Matrix (*DCM*). The *PSD1* shows that the middle fractions are not able to fill the reserved areas. Consequently, the fractions *F1*, *F6*, *F7*, *F8* must fill the rest of the R_A. According to equation 6.3, these fractions are not filter stable (∃▼) against *F1*, *F6*, *F7* and *F8* can be washed out through *F1* so they are suffusiv particles. The particles which are smaller than D_s and cannot fill their reserved areas are mobile particles. The mass of the washout is more than 3%. Therefore *PSD1* is internally Unstable (*U*) The calculated ΔR_A can be seen in Fig. D.1.

In Figure 6.12, the Fine Matrix (*FM*) (Fuller curve) can be obviously recognized. For the Fuller curve, it can be seen that there is more than enough of fractions *F4* to *F8* they are all ∃▼ against each other. In Fig.6.13, it can be seen that the positive area is much bigger than negative area. Thus, the *FM* is the dominant matrix, i.e there are not enough coarse fractions to fill their R_A. Furthermore, two positive areas do not exist. Therefore, this *PSD* (the Fuller curve) can be assessed as internally stable.

F_i	D_{F_i}	$3 \times D_{F_i}$	R_A	$f(R_A)$	PDF	ΔR_A
[-]	[mm]	[mm]	[mm²]	[%]	[%]	[%]
F1	25	75	9375	34.9	9.00	-26.4
F2	20	60	7500	28.0	19.0	-9.10
F3	16	48	6000	22.4	18.0	-4.70
F4	5	15	1875	7.0	10.0	+3.20
F5	3	9	1125	4.2	14.0	+10.2
F6	1.3	3.9	487.5	1.80	7.00	+4.90
F7	0.75	2.25	281.3	1.00	5.00	+3.60
F8	0.5	1.50	187.5	0.70	19.0	+18.3
		Σ	26831	100	100	0.0

Table 6.2.: Calculation of R_A according to discretization of the *PSD* and areas filled according to fraction masses for Fuller curve
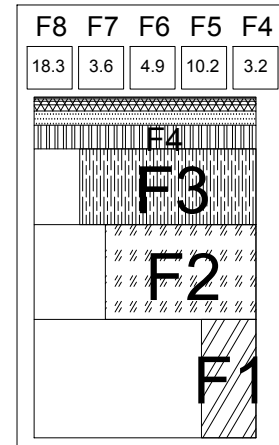
Figure 6.12.: Graphical calculations for Fuller
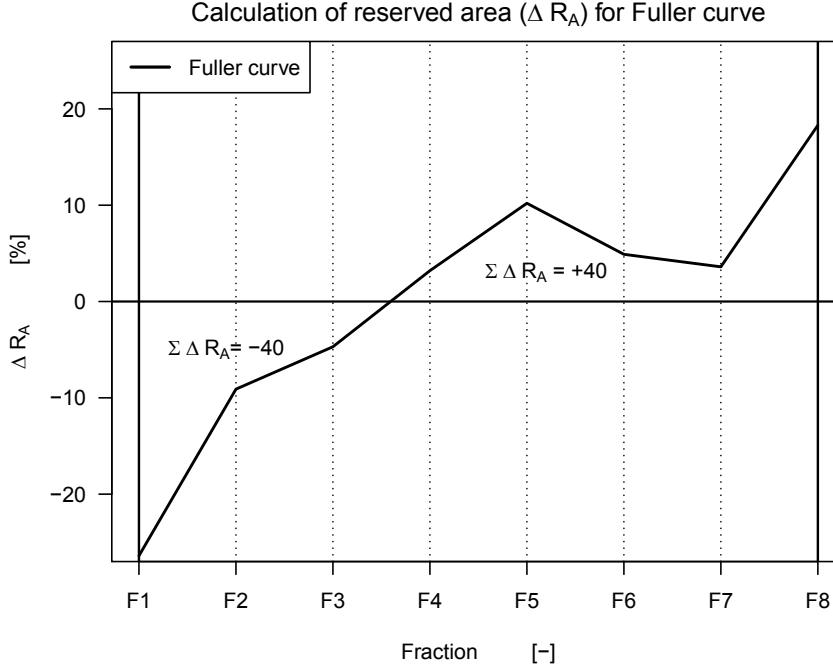
Figure 6.13.: Calculation of difference between ideal homogeneous internally stable packing with packing generated for Fuller curve

It can be said that the necessary condition of internal stability based on the proposed calculation procedure is that the graph of R_A versus fractions of the *PSD* show just one positive area (see Fig.6.13. If there is more than one positive area, those positive areas must be checked for filter stability ⊐▼ against each other. The significance of the suffusion criterion based on a bond of PSDs can be seen in Appendix D.1.

6.4. Experimental validation

6.4.1. Test Procedure

For assessment of internal erosion, the identification of mobile particles is very important. In a soil mass with a certain volume, some particles do not move during loading processes. These particles are known as soil skeleton and the particles that are free to change their positions are called potential mobile particles, which is comprehensively explained in chapters 3 and 4.

Based on the size of these eventually mobile particles the decision can be made, if a soil is internally stable or not. With the intention of validation of the proposed packing model related to suffusion and homogeneity effect, different modified Suffusion Test (*ST*) with various sample preparation techniques were carried out.

The same apparatus, which is introduced in chapter 3, was used for these *STs*. Constant stress of 20 kN/m^2 was applied to the sample during the test. The applied load prevents

the uplift during the saturation process. After each test, the sample is sieved layer by layer. The mass of mobile particles and the transport length of the mobile particles could be estimated for different sample. The samples, after placement into the test apparatus could be visually classified as homogeneous (*SRT*), less homogeneous and segregated (*ALS*) (see section 3.5). During each test, steady flow conditions at the embankment dams were simulated. For the acquisition of potential changes within the soil sample, two piezometers above and below the sample were installed. For additional control, measurements of the head in upstream and downstream water tanks are conducted. The suffusion tests were carried out under high hydraulic gradients ($i_{max} = 2.0$).

Test	sample preparation	Remarks
ST-A1	- Sample placement with tube and funnel - Porous fleece on the surface of each layer - Layers placed separately	stochastically homogeneous (*COV*= 16.85)
ST-A2	- Sample placement with tube and funnel - Without porous fleece - Layers placed separately	stochastically homogeneous (*COV*= 15.36)
ST-A3	- Sample placement with tube and funnel - Dough on the contact area sample-test device - Layers placed separately	stochastically homogeneous (*COV*= 17.17)
ST-B1	- Sample placement with tube and funnel - Without defined layers - All layers placed at once	whole sample at once - less homogeneous (*COV*= 24.89)
ST-C1	- Sample placement with tube and funnel - Dough on the contact area sample-test device - Layers placed separately and divided in 2 sub-layers	sample placement in 8 layers - stochastically homogeneous (*COV*= 13.89)
ST-D1	- Layered Sample placement - Dough on the contact area sample-test device - fractions are placed descending from bottom to top in each layer (Fig.6.14-a)	totally homogeneous after proposed packing model (*COV*= 1.01)
ST-D2	- Layered Sample placement - Dough on the contact area sample-test device - Fractions are placed descending from bottom to top (Fig.6.14-b)	totally homogeneous after proposed packing model (*COV*= 1.89)

Table 6.3.: Different sample preparation for *ST*. The *COV* is calculated based on the C_H of each layer (surface-image)

If a sieve is used at the bottom of the sample, which is often used by researchers in the past studies (see Tab. 1.2 to 1.5), the suffusion process, at least for the bottom of the sample is changed to filtration or contact erosion phenomenon. At the bottom of the sample, a fleece was used to avoid the particle fall (segregation), as well as washout from the bottom layer of the soil. The fleece opening sizes let the water easily percolate but the particles

were blocked at the bottom of the sample. With the selected discretization, clogging could not be observed. The hydraulic gradients at each stage remained almost constant. By placement of the sample into the test apparatus, the change of the *PSD* is already initiated. Therefore, the tests were carried out without any possibility of the particle washout. After completing of each test, the *PSD* of each layer is measured. This allows a conclusion about global and local changes of the sample respectively identification of the mobile particles.

Furthermore, before placing each layer inside the cylinder, they have to be mixed with deionized water, in order to have less particle segregation for the sample placement type *ST*-A, *ST*-B and *ST*-C In this way, the smaller particles can attach to the surface of bigger ones. Thus, the local particle distribution can be assumed as a more uniform distribution.

In Table 6.3, the main features of various types of the sample placement procedures are described. In Figure 6.14, schematically different kind of sample preparation methods can be seen. The test types *ST*-A, *ST*-B and *ST*-C show the common ways of the sample preparation methods. These samples can be classified into stochastic and relative homogeneous samples. The test type *ST*-D1 and *ST*-D2 represent the explained packing model which represents totally homogeneous sample. These samples are placed into the test apparatus in layers, based on *DLS* each of layers represents one fraction (see Fig.6.9). The samples were classified based on the calculated coefficient of homogeneity (C_H) using image analysis of the captured images of each layer. For the *ST*-B1 the sample images were captured when the water percolation through the sample was finished and the sample for the analysis of particle transport was taken out of the test device layer by layer.

6.4.2. Tested material

The experimental investigations were carried out on a widely-gap-graded soil. The same *PSD*, which is used for the simulations and previous experiments were used for these tests (see Fig. 4.5).

Description	F1	F2	F3	F4	F5	F6	F7	F8	F9
D [mm]	27	22	16	12	10	8	5	3	1.5
Mass [g]	194	550	94	49	43	40	47	44	186
Mass [%]	15.5	44.1	7.6	3.9	3.4	3.2	3.8	3.5	15

Table 6.4.: *PSD1* - Mass contribution of fractions for layers 1 to 4 (F: Fraction)

The *PSD1* is typical for sedimentary soils in the medium course of a large river and is considered as a soil with a high risk for suffusion, e.g. after Semar et al. (2010), Witt (2013) and Kenney and Lau (1986). The reconstitution of the *PSD1* was carried out by glass beads based on the given discretization in Table 6.4. The densities of the glass beads are not constant even for the beads with the identical diameter, so that the mass of each layer has very small deviation from the original one (± 2 grams). It should be mentioned that fractions smaller than fraction *F9* ($D < 1.5\,mm$) were taken into account by same weight but with a bigger diameter as same as fraction *F9*. With the assumption that fractions smaller than fraction *F9* ($D < 1.5\,mm$) are with high probability mobile. Therefore, this modification may not change the test results.
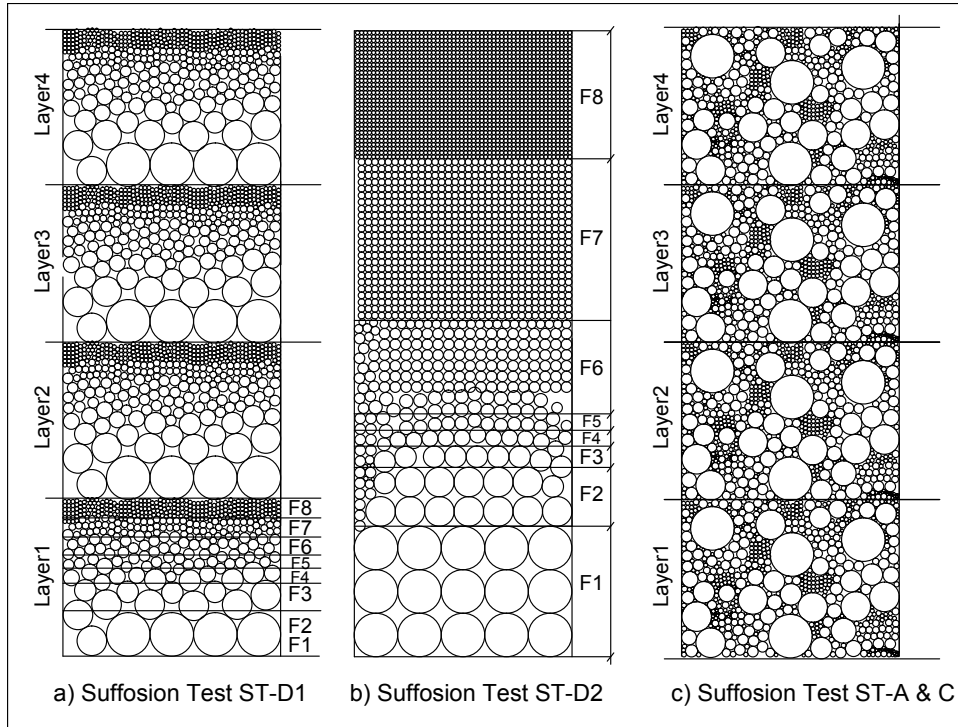
Figure 6.14.: Schematic view of various prepared samples for *STs*

F_i	D_{F_i}	$3 \times D_{F_i}$	R_A	$f(R_A)$	PDF	ΔR_A
[-]	[mm]	[mm]	[mm^2]	[%]	[%]	[%]
F1	27	81	10935	25.8	15.5	-10.3
F2	22	66	8910	21.1	44.1	+23.0
F3	16	48	6480	15.3	7.6	-7.7
F4	12	36	4050	11.5	3.9	-7.60
F5	10	30	3240	9.6	3.4	-6.20
F6	8.0	24	2025	7.7	3.2	-4.50
F7	5.0	15	1215	4.8	3.8	-1.00
F8	3.0	9	607.5	2.9	3.5	+0.60
F9	1.5	4.5	281.3	1.4	15	+13.60
		Σ	42322.5	100	100	0.0

Table 6.5.: Calculation of $R_A s$ according to new discretization of the *PSD1*

A new discretizetion of *PSD1* is shown in Table 6.4. Therefore, the effect of discretiztion can also be investigated in the suffusion tests. For the new discretizetion, the calculations of suffusion based on presented approach can be taken from Table 6.5. The suffusion stability calculations for the *PSD1* for a new discretization based on the given sieve series is shown in Table 6.1. The results in comparison to this discretization did not change the internal stability assessment (see Table 6.5).

6.4.3. Coefficient of homogeneity of the samples

The homogeneity of samples were classified based on the *COV* of the calculated coefficient of homogeneity (C_H). For the C_H calculations, the images taken from each layer were analysed. For all of Suffusion Test (*ST*), the sample images were captured before and after water percolation.The produced section-images of the sample layers for the calculation of the C_H for *ST*-C1 with skeleton fractions (*F1..3*) can be seen in Figure 6.15.
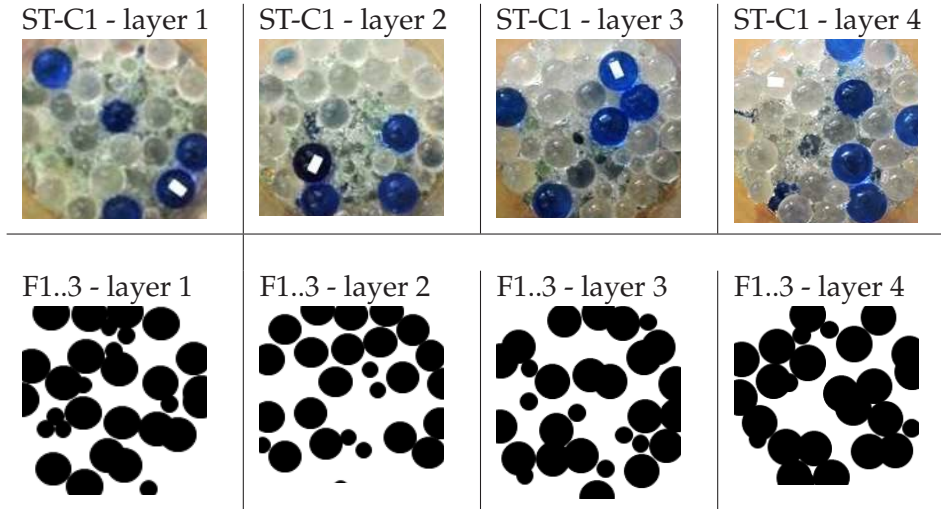
Figure 6.15.: Images of the samples for *ST*-C1 and for quantification of C_H
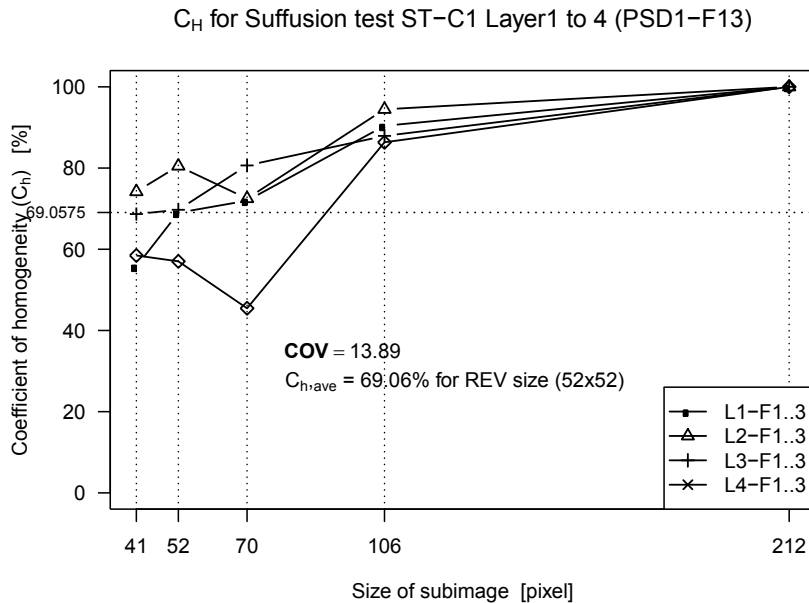
Figure 6.16.: C_H calculations for sample *ST*-C1 for fractions *F1..3*

The sample of *ST*-C1 can be refereed as the worse case of the sample preparation among other samples, because this sample was placed without predefined layers. However, because of using *SRT* the sample is much more homogeneous in comparison with conventional methods. In Figure 6.16 the *COV* of the C_H for layers 1 to 4 can be seen. This sample can be classified as a stochastically homogeneous sample.
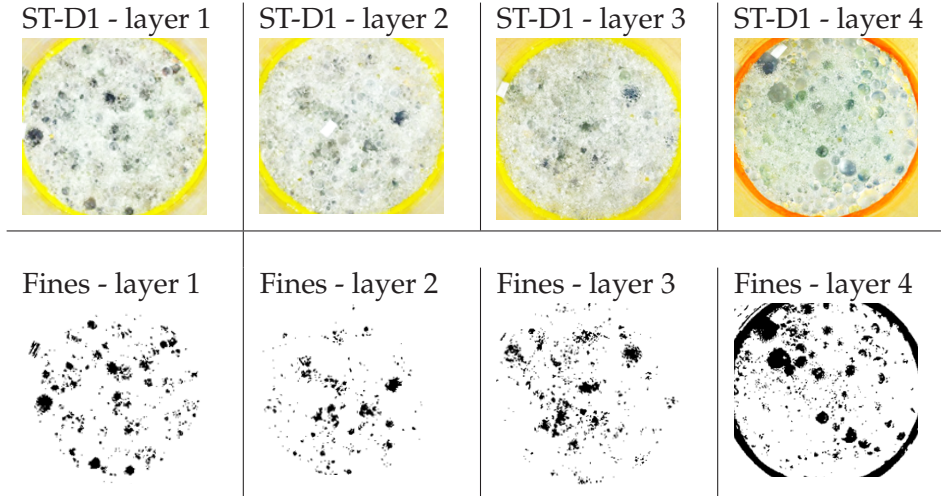
Figure 6.17.: Images of the samples for *ST*-D1 and for quantification of C_H. The surface images were taken after the *ST* was carried out.
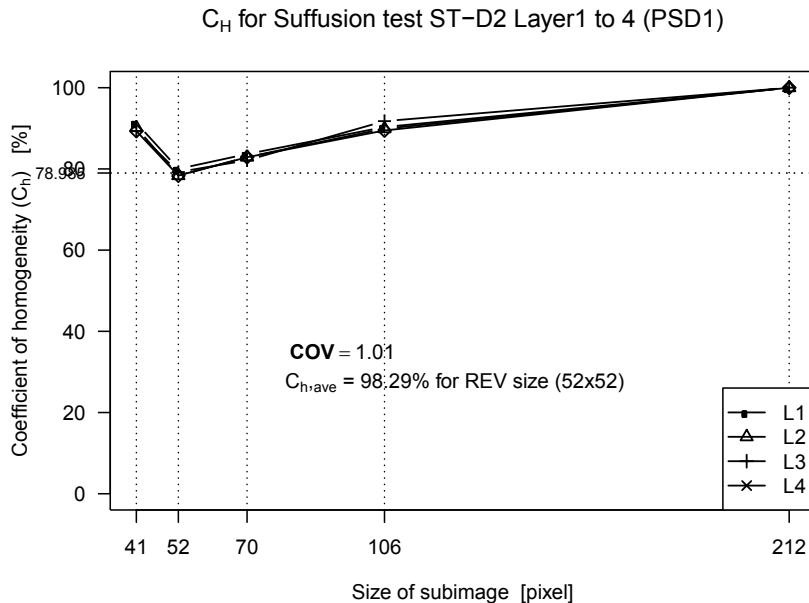
Figure 6.18.: C_H calculations for sample *ST*-D1 for fines on the top of each layer. for the calculations the white ares are calculated

The captured section-images of the sample layers for the C_H calculations by ST-D1 with mainly fill fractions can be seen in Figure 6.17. The section-images were taken after the ST was carried out. As it can be seen, the fines even on the layer 4 (top layer) are not washed out or transported. ST-D1 and ST-D2 samples can be refereed as the maximum homogeneous or totally homogeneous case of the sample, because the whole sample was placed according to the ALS method. In Figure 6.18, the coefficients of homogeneity C_H and the COV of them for layers 1 to 4 can be taken.

6.4.4. Test results

The PSDs of the soil layers after and before water percolation through the sample can be seen in Fig.6.19 and Fig.6.20.
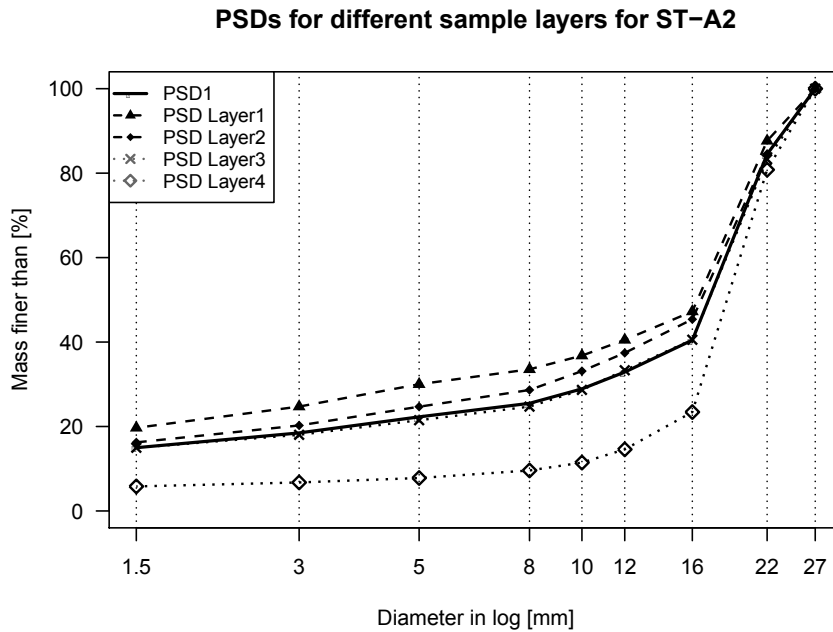
Figure 6.19.: *PSDs* of the sample layers after the ST-A2 and initial *PSD1*

These test results emphasize again the correlation between the degree of the particle washout of a widely graded soil with the degree of homogeneity of the soil matrix. The segregation of the sample builds preferred flow paths. The particle transport along these paths often results in propagation of segregation. In these tests, no global washout could be observed. Nevertheless, the observation of the sample during percolation of water shows that there are mobile particles, which are not fixed in the skeleton and there are suffusive particles, which can be totally washed out respectively transported from layer 4 to layer 1. The mobile particles moved in direction of the flow and were captured within the matrix after passing through a certain path. On the other hand, the suffusive particles moved through the whole sample height, and the soil skeleton was not able to capture

them. In tests *ST*-A1, *ST*-A2 and *ST*-A3 the flow causes a disarrangement of the initial matrix into occasionally a more stable or sometimes unstable one. This is because of random arrangement of the particles. This results in a certain stratification, but any change in flow condition or direction can remobilize the mobile particles.
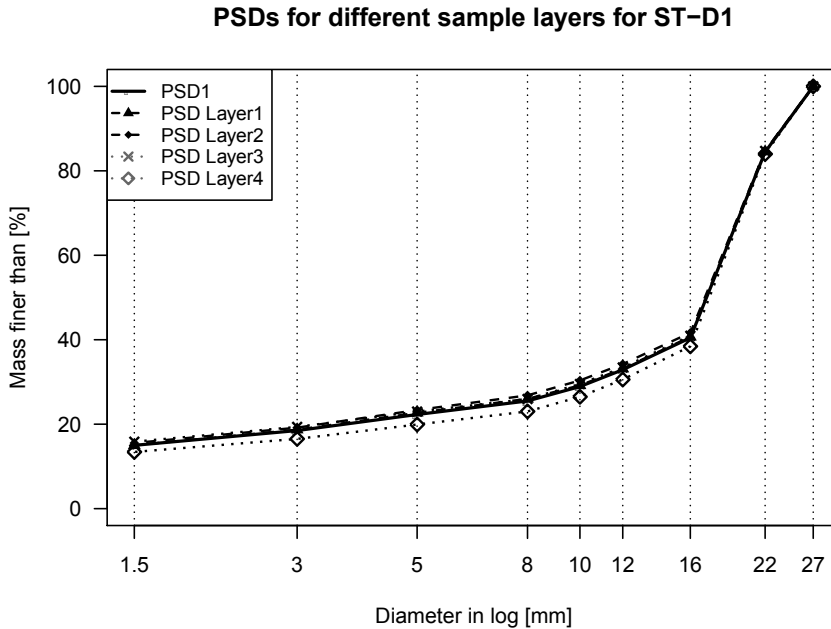
Figure 6.20.: *PSDs* of the sample layers after the *ST*-D1 and initial *PSD1*

The suffusive particles were determined directly from layer 4. The biggest suffusive particle had a diameter of 5 *mm* (*F8*). Moreover, the mobile particles were determined by balancing the weight of the different fractions of each soil layer after and before tests. The biggest mobile particle within the sample was the soil fraction with 8 *mm* diameter.

The author has found that in practical terms, it is too conservative to assume that the whole finer fraction of widely graded soils, and the gap-graded soils will be eroded. The tests showed that more than 50% of the fine particles of the *PSD* are mobile, however they are not suffusive particles. Moreover, the tests *ST*-D1 and *ST*-D2 showed the effect of homogeneity (see Fig.6.19 and Fig.6.20. The amount of suffusive particles are a direct indicator for assessment of suffusion of the sample. There are significant differences between the amount of the mobile and the suffusive ones when the results of *ST*-A, *ST*-B and *ST*-C are compared to *ST*-D tests results. In the stochastically, less and relatively homogeneous samples, more suffusive particles could be measured.
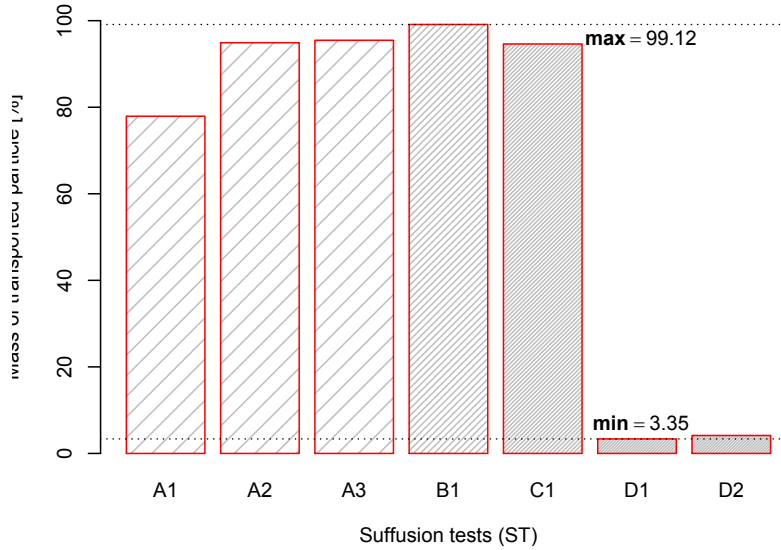
Figure 6.21.: Transported particles from layer 4 to 1 - $D_{F9} = 1.5\,mm$

Figure 6.21 and Figure 6.22 show the variation of transported particles from the top layer to the bottom of sample (from layer 4 to layer 1) for fractions $F8$ and $F9$. The maximum particle transport could be measured by sample ST-B, which was placed into the test device just in one step. It seems that in ST-B the segregation is higher than the other samples. Therefore, the highest particle mobility was occurred. In ST-D1 and ST-D2, the mobile and suffusive particles can be measured, because the layers of many fractions, i.e. $F3$, $F4$, $F5$, $F6$, $F7$ were not able to fill their layers fully, Thus the smaller particles could be easily mobilized and transported to bottom of the sample.
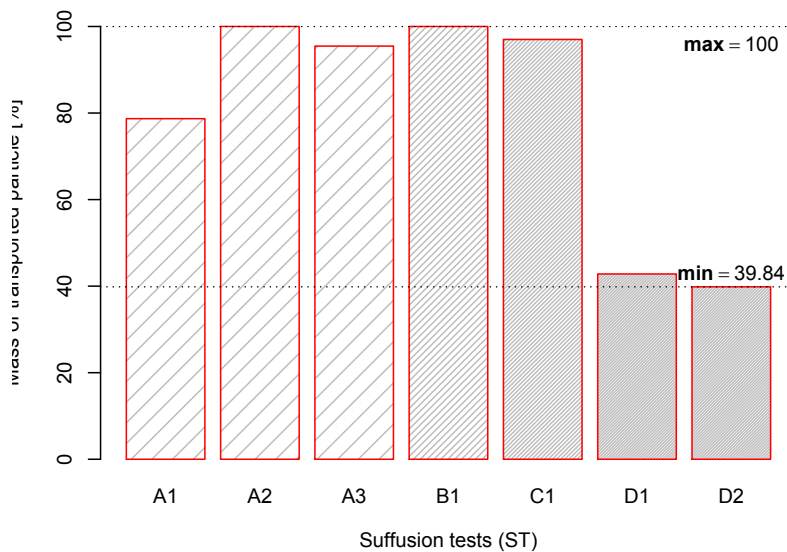
Figure 6.22.: Transported particles from layer 4 to 1 - $D_{F8} = 3.0\,mm$

Figure 6.21 and 6.22 show, that particles of fraction *F9* with the diameter of 1.5 *mm* are less transported than the particles of fraction *F8* with the diameter of 3.0 *mm* Based on the packing model, the particles of fraction ninth fraction of PSD (*F9*) must be filtered by particles of eighth fraction of PSD (*F8*). Considering the calculations of Tab.6.5, it can be seen that the fraction *F8* fills totally its reserved area and even there are 0.6% more than it is needed. Respectively particles of fraction *F8* must be filtered by particles of fraction seventh fraction of PSD (*F7*). However, there are not enough particles of fraction *F7* available. Thus, the particles of fraction *F8* can be easily transported through lower layers. It is also obvious that the other fractions cannot filter effectively the particles of fraction *F8*. Therefore, these particles can reach the bottom of the soil sample.

6.5. Summary of this chapter

The new suffusion criterion based on the proposed packing model is introduced and experimentally validated. The procedure for predicting and determining the mobile and suffusive particles of a widely graded soil based on *PSD* are proposed. The suffusive and mobile particles can be also analytically predicted based on the new suffusion criterion.

Even though for samples with a high degree of homogeneity, fluctuations in particle transport could be observed and were measured experimentally. All of test results for a definite type of sample preparation showed acceptable variation in results. The variation for such selected *PSD* is about 2 to 8% of particle transport. The only sample preparation method which is reproducible and had a good level of consistency in result, is the sample based on the proposed packing model. The seepage force in all of tests (*ST*-A, *ST*-B and *ST*-C) causes a change of the original matrix into sometimes a more stable one *FM* or sometimes an unstable one. The seepage force in Suffusion Test s *ST*-D1 and *ST*-D2 leads the sample for the same percolation direction always to a more stable sample. The particles which cannot be filtered are washed out, and the sample reaches a stable condition.

It is concluded that the degree of particle mobilization is closely related to the arrangement of the particles inside the sample. The extent of suffusion is dependent on the sample homogeneity. These tests emphasize again that the specification for avoidance of segregation in earthworks is not enough and a method for quantification of the homogeneity in terms of numbers is necessary. The more the soil is homogeneous, the less the risk of internal instability.

7. Conclusion and future work

7.1. Findings of the study

The segregation of the widely graded soils during dam construction procedure is unavoidable. It was shown that suffusion criteria based on the empirical methods delivering conservative and contradictory assessment because the soil homogeneity was not considered quantitatively. On the other hand, many researchers recommend that it is necessary to test the internal stability of the widely graded soils for important projects. Though, it was shown that by testing a case scenario can only be replicated, which is not the case in the field situations. It can be stated based on the author's experimental studies that there is a significance effect of the particle arrangement on internal stability of the soil. Different investigations on soils prone to suffusion were conducted. The behavior of such a soil by changing the particle arrangement of the sample was experimentally and numerically studied.

In the experimental studies, an approach for identification of the skeletal behavior of the soil matrix is proposed. Furthermore, these methods were numerically investigated using Discrete Element Method (*DEM*) to find the contact forces, the number of neighbors, cell porosity based on Voronoi-Tesselation method and other relevant parameters for different soil fractions. This has been done for the skeleton and to some extent, fill fraction of the chosen widely graded soil *PSD*. The smallest Representative Elementary Volume (*REV*) for such a soil packing was numerically defined based on two different approaches, Modified-Forced-Biased-Algorithm (*MFBA*) and Pouring-Algorithm (*PA*). A method for finding the relevant scale for identification of the homogeneity is recommended. Laboratory Sequential Fill Test (*SFT*) and Suffusion Test (*ST*) were carried out for documentation of homogeneity effects on internal stability as well as for estimation of Experimental Homogeneity Coefficient ($C_{H,Exp}$).

The homogeneity of the soil was quantified for *2D* section-images of various numerically generated packings. For quantification of homogeneity based an image analysis, the method requires the capability to accurately binerize and examine the section images of the packing. This ability has greatly expanded in *MATLAB* Digital Image Processing Toolbox in the past years. The focus of this effort was to build upon the prior efforts of researchers to assemble a multi-parameter description of homogeneity for two-phase particle-air materials. The coefficient of homogeneity (C_H) quantifies homogeneity by calculating the total variance of multiple normalized particle parameters across the range of sub-images. The sub-images was cropped from section-image based on identified skeletal fractions. The accuracy and consistency of the coefficient of homogeneity depends on the selected sub-image size, *REV*, the characteristic length of the particle size (i.e., D_{max} and D_{min}), the pixel resolution of the image, and the number of parameters in the image

(i.e. particle distances, porosity, etc.). The proposed approach is flexible and parameters may be added or changed, as long as they can be accurately measured. Parameters may also be removed if they are not relevant in a particular case. The method can be extended to other types of soil materials or another shape of particles. The primary requirement is that a parameter must have a distinct boundary to be discerned and measured. For comparative purposes, calculation of the Coefficient of variation (COV) of those C_H of the section-images is advised.

The author proposed a new packing model based on the acquired knowledge and comprehension of his observations. In all of the suffusion tests, it could be seen that the soil sample (*PSD1*), after a while during water percolation builds, segregated local nests along flow paths. It could also be observed that the soil was segregated in those nests in an almost ascending superimposed order. On the top of these local ascending layered segregated nests, which replicate *ALS* some fine particles moved in the pore spaces in a rotational manner due to the water flow. Those particles sometimes could be transported due to the implementation of the next higher hydraulic gradients locally to the upcoming pore. However, occasionally the ascending layered particles existed in all of the directions so that the fine particles in the middle of the spherical nest could not be transported. This model is based on the cyclic nature of homogeneity and segregation processes. In dependency on length or time scale, the total homogeneity could be seen as entirely segregated and inversely, the total segregation can be distinguished as complete homogeneity. From this point of view, the proposed descending segregated layered soil packing is the ideal homogeneous soil packing, which can replicate a piece of a closed circular packing with a radius of infinity. Based on this model, a suffusion criterion is proposed. The criterion was experimentally validated for *PSD1*.

One of the challenges in assessing the suffusive processes is to determine or to estimate the relevant parameters, i.e. the mobile and suffusive particles of widely graded soils under consideration of particular uncertainty due to segregation. If these relations cannot be determined with an appropriate accuracy, laboratory tests as described in this study should be carried out to allow a quantitative assessment of the risk of suffusion with homogeneity consideration. Small differences in the shape of the particle size distribution affect whether a soil is internally stable or not. This research emphasizes that the soil fractions with diameters of D_{60} and bigger of a widely graded soil build virtually the soil skeleton. The mass and spatial distribution of these fractions govern the internal stability, and the mass and distribution of the fill fractions are a secondary matter. For such a soil, the homogeneity of the skeleton must be measured and verified.

Major findings of this thesis can be listed as following:

· **Finding 1**: Suffusion is a particle scale phenomenon. Particle transport depends on particle arrangement (section 2). Position of the soil skeleton particles determine the D_{min} of the skeleton Constriction Size Distribution (*CSD*) If the soil is segregated it cannot form the D_{min} in expected quantity based on the *PSD* Hence, it cannot be referred as the same soil with the given *PSD* Thus, the homogeneity of the soil skeleton must be satisfied for all soils before assessing its internal stability.

· **Finding 2**: The granular material forms its skeleton when a minimum required mass

is reached (*REV* for skeleton) (see section 4). This condition is the necessary condition for the investigation.

· **Finding 3**: An ideal homogeneous packing model for soils with *DCM* is proposed. The concept of this packing model is based on the cyclic nature of homogeneity and segregation processes which were observed qualitatively in the suffusion tests. The advantage of this model is the simpleness of it. This model was tested and supported with Suffusion Test (*ST*).

· **Finding 4**: A statistical method for quantification of homogeneity C_H for *2D* images in dependency of the *REV* size is proposed. The conception of calculating the variances between the sub-images is a very uncomplicated and conceivable method. This method was tested for complex stochastically homogeneous (*MFBA* packing), segregated (*PA* packing) as well as total homogeneous lattice packings. The results are comparable with the established method of Voronoi-Tessellation. The advantage of this method is that many parameters can be considered and included in the code. Other available methods for quantification of homogeneity are unsuitable for particle assemblies of a widely graded soil (section 4 and 5).

· **Finding 5**: An in-situ test method for quantification of homogeneity $C_{H,Exp}$ is proposed. In section 3.5, it is shown that the loosest and densest states of a widely graded soil, which can be measured according to standard guidelines, are not the ultimate states. These states can be found by proposed sample preparation methods (Sample Reconstitution Technique (*SRT*) and Descending layered segregated (*DLS*)). For the measurements of n_{max} and n_{min}, the skeleton of the widely graded soil with a *DCM* must be identified (see section 3) and the tests must be carried out for the soil skeleton (see also section 5.6.2).

· **Finding 6**: A new suffusion test method based on the proposed packing model is introduced. The Suffusion Test (*ST*)-D1 or Suffusion Test (*ST*)-D2 with the sample preparation method *ALS* delivered good results which were in solid agreement with the proposed ideal homogeneous packing. The advantage of the proposed suffusion test method is that the results show less fluctuation in comparison to the *ST* with an apparent homogeneous sample. This test method is reproducible and straightforward.

· **Finding 7**: A new suffusion criterion based on the proposed packing model is designed.

7.2. Future works

For the future research in the area of internal stability of widely graded soils, dam and road construction quality, redistribution and homogeneity characterization of granular packings, the following topics are of primary relevance:

1. The coefficient of homogeneity (C_H) or Experimental Homogeneity Coefficient ($C_{H,Exp}$) can be integrated into the proposed suffusion criterion. This can lead to

risk assessment of available earthworks, which is nowadays the main concern of many governments for their projects and insurance investments.

2. CFD-DEM coupled modeling of *ST* using *ALS* samples to visualize the transport of mobile and suffusive particles.

3. Refinement of the *MATLAB* shearing model such that the image may be rotated and sheared in small increments to estimate the coefficient of homogeneity (C_H).

4. Performing a case study and comparing the homogeneity estimations for an earthwork

5. Extension of the homogeneity model to soils containing particles with more than one type of material. The current approach would require that multiple particle types have some discriminating factor such as shape, size, or contrast to be detected separately.

6. Extension of the homogeneity model to *3D*, based on voxel generation for *3D* computer tomography images.

Bibliography

Allen, M. P. and Tildesley, D. J. (1989), *Computer simulation of liquids*, Oxford university press.

Andreasen, A. (1930), 'Über die Beziehung zwischen Kornabstufung und Zwischenraum in Produkten aus losen Körnern (mit einigen Experimenten)', *Kolloid-Zeitschrift* **50**(3), 217–228.

Arulanandan, K. and Perry, E. B. (1983), 'Erosion in relation to filter design criteria in earth dams', *Journal of Geotechnical Engineering* **109**(5), 682–698.

Bear, J. (2012), *Hydraulics of groundwater*, Courier Corporation.

Beck, J. (1967), 'Perceptual grouping produced by line figures', *Perception & Psychophysics* **2**(11), 491–495.

Bertram, G. E. (1940), An experimental investigation of protective filters, Soil Mechanics Series 7, Harvard University.

Beutel, R., Reinhardt, H.-W., Grosse, C. U., Glaubitt, A., Krause, M., Maierhofer, C., Algernon, D., Wiggenhauser, H. and Schickert, M. (2008), 'Comparative performance tests and validation of ndt methods for concrete testing', *Journal of Nondestructive Evaluation* **27**(1-3), 59–65.

Binner, R., Homberg, U., Prohaska, S., Kalbe, U., Berger, W. and Witt, K. J. (2010), Identification of descriptive parameters of gradated soils using column experiments and analysis of ct data, *in* 'EGU General Assembly Conference Abstracts', Vol. 12, p. 2305.

Bonelli, S. (2012), *Erosion of geomaterials*, John Wiley & Sons.

Bun (2013), *MMB*.

Bungey, J. H., Grantham, M. G. and Millard, S. (2006), *Testing of concrete in structures*, Crc Press.

Burenkova, V. V. (1993), Assessment of suffusion in non-cohesive and graded soils, *in* U. J. Brauns, M. Heibaum, ed., 'Filters in Geotechnical and Hydraulic Engineering', First International Conference "Geo-Filters", A.A Balkema, Rotterdam, Brookfield, Karlsruhe, Germany, pp. 357–360.

Callister, W. D., Rethwisch, D. G. et al. (2007), *Materials science and engineering: an introduction*, Vol. 7, Wiley New York.

Carrier III, W. D. (2003), 'Goodbye, hazen; hello, kozeny-carman', *Journal of Geotechnical and Geoenvironmental Engineering* .

Chapuis, R. P. (1992), 'Similarity of internal stability criteria for granular soils', *Canadian Geotechnical Journal* **29**(4), 711–713.

Chermant, J.-L., Chermant, L., Coster, M., Dequiedt, A.-S. and Redon, C. (2001), 'Some fields of applications of automatic image analysis in civil engineering', *Cement and Concrete Composites* **23**(2), 157–169.

Cundall, P. A. (1971), 'A computer model for simulating progressive large scale movements in blocky rock systems', *Proceedings of the Symposium of the International Society of Rock Mechanics* **29**(1), 47–65.

Cundall, P. A. (2004), 'Pfc user manual', *Itasca Consulting Group Inc., Mineapolis* .

Cundall, P. A. and Strack, O. D. (1979), 'A discrete numerical model for granular assemblies', *Geotechnique* **29**(1), 47–65.

Davidenkoff, R. (1964), *Deiche und Erddämme. Sickerströmung – Standsicherheit*, Werner-Verlag, Düsseldorf. book.

DIN18123 (2011), *Baugrund, Untersuchung von Bodenproben - Bestimmung der Korngrößenverteilung*.

DIN18130 (1998), *Bestimmung des Wasserdurchlässigkeitsbeiwertes*.

EDEM (2006), 'Edem 1.3 user's manual', *Edinburgh, UK* .

Edgar, G. and Measure, T. (n.d.), 'Fractal geometry. 1990'.

Fair, G. M., Hatch, L. P. and Hudson, H. E. (1933), 'Fundamental factors governing the streamline flow of water through sand [with discussion]', *Journal (American Water Works Association)* pp. 1551–1565.

Fell, R. and Fry, J.-J. (2007), *Internal Erosion of Dams and Their Foundations*, Taylor and Francis, London.

Foster, M. A., Fell, R. and Spannagle, M. (2000), 'The statistics of embankment dam failures and accidents', *Canadian Geotechnical Journal* **37**(1000-1024).

Fuller, W. B. and Thompson, S. E. (1907), 'The laws of proportioning concrete', *Transactions of the American Society of Civil Engineers* **59**(2), 67–143.

Goniva, C., Kloss, C., Hager, A. and Pirker, S. (2010), An open source cfd-dem perspective, *in* 'Proceedings of OpenFOAM Workshop, Göteborg', pp. 22–24.

Hales, T. C., Harrison, J., McLaughlin, S., Nipkow, T., Obua, S. and Zumkeller, R. (2011), 'A revision of the proof of the kepler conjecture'.

Henderson, A., Ahrens, J., Law, C. et al. (2004), *The ParaView Guide*, Kitware Clifton Park, NY.

Hodge, R. A. and Freeze, R. A. (1977), 'Groundwater flow systems and slope stability', *Canadian Geotechnical Journal* **14**(4), 466–476.

Hoła, J. and Schabowicz, K. (2010), 'State-of-the-art non-destructive methods for diagnostic testing of building structures–anticipated development trends', *Archives of Civil and Mechanical Engineering* **10**(3), 5–18.

Homberg, U., Binner, R., Prohaska, S., Dercksen, V. J., Kuß, A. and Kalbe, U. (2009), Determining geometric grain structure from x-ray micro-tomograms of gradated soil, *in* 'Workshop Internal Erosion', Vol. 21, Bauhaus-Universität Weimar.

Hubbert, M. K. and Rubey, W. W. (1959), 'Role of fluid pressure in mechanics of overthrust faulting i. mechanics of fluid-filled porous solids and its application to overthrust faulting', *Geological Society of America Bulletin* **70**(2), 115–166.

Indraratna, B., Nguyen, V. T. and Rujikiatkamjorn, C. (2011), 'Assessing the potential of internal erosion and suffusion of granular soils', *Journal of Geotechnical and Geoenvironmental Engineering* .

Jaeger, J. (2005), *New solutions in contact mechanics*, Wit Pr/Computational Mechanics.

Jazwinski, A. (1970), *Stochastic Processes and Filtering Theory*, Mathematics in Science and Engineering, Elsevier Science.
URL: *http://books.google.de/books?id=nGlSNvKyY2MC*

Jentsch, H., Salehi Sadaghiani, M. R. S., Winkler, P. and Witt, K. (2014), Experimental investigation–influence of the shape of the gradation curve on the soil structure, *in* 'Scour and Erosion: Proceedings of the 7th International Conference on Scour and Erosion, Perth, Australia, 2-4 December 2014', CRC Press, p. 105.

Kenney, T. C. and Lau, D. (1985), 'Internal stabilty of granular filters', *Canadian Geotechnical Journal* **22**, 215.–225. article.

Kenney, T. C. and Lau, D. (1986), 'Internal stability of granular filters: Reply', *Canadian Geotechnical Journal* **23**(3), 420–423.
URL: *http://dx.doi.org/10.1139/t86-068*

Kenney, T. C. and Westland, J. (1993), 'Labratory study of segregation of granular filter materials', *Filters in Geotechnical and Hydraulic Engineering* pp. 313–319.

Kenney, T., Chahal, R. and al., e. (1985), 'Controlling constriction sizes of granular filters', *Canadian Geotechnical Journal* **22**(1), 32.–43.

Kloss, C. and Goniva, C. (2011), 'Liggghts–open source discrete element simulations of granular materials based on lammps', *Supplemental Proceedings: Materials Fabrication, Properties, Characterization, and Modeling, Volume 2* pp. 781–788.

Kloss, C., Goniva, C., Hager, A., Amberger, S. and Pirker, S. (2012), 'Models, algorithms and validation for opensource dem and cfd-dem', *Progress in Computational Fluid Dynamics, an International Journal* **12**(2), 140–152.

Krumbein, W., Monk, G. et al. (1943), 'Permeability as a function of the size parameters of unconsolidated sand', *Transactions of the AIME* **151**(01), 153–163.

Kuhn, M. R. (2006), 'Oval and ovalplot: Programs for analyzing dense particle assemblies with the discrete element method'.

Lafleur, J. (1984), 'Filter testing of broadly graded cohesionless tills', *Canadian Geotechnical Journal* **21**(4), 634–643.
URL: *http://dx.doi.org/10.1139/t84-070*

Lafleur, J., Mlynarek, J. and Rollin, A. L. (1993), Filter criteria for well graded cohesionless soils, *in* H. . S. Brauns, ed., 'Filters in Geotechnical and Hydraulic Engineering', Belkema, pp. 97–106.

LAMMPS Users Manual / LIGGGHTS Documentation (2013). http://nf.nci.org.au/facilities/software/LIGGGHTS/doc/Manual.html.

Latham, J.-P., Xiang, J., Harrison, J., Munjiza, A. et al. (2010), Development of virtual geoscience simulation tools, vgest for irregular blocky rock applications in rock engineering using the combined finite discrete element method, femdem, *in* '44th US Rock Mechanics Symposium and 5th US-Canada Rock Mechanics Symposium', American Rock Mechanics Association.

Long, J., Remer, J., Wilson, C. and Witherspoon, P. (1982), 'Porous media equivalents for networks of discontinuous fractures', *Water Resources Research* **18**(3), 645–658.

Masad, E., Jandhyala, V., Dasgupta, N., Somadevan, N. and Shashidhar, N. (2002), 'Characterization of air void distribution in asphalt mixes using x-ray computed tomography', *Journal of materials in civil engineering* **14**(2), 122–129.

MATLAB (2013), *version 8.1.0.604 (R2013a)*, The MathWorks Inc., Natick, Massachusetts.

Mauldin, R. D. and Urbański, M. (1998), 'Dimension and measures for a curvilinear sierpinski gasket or apollonian packing', *Advances in Mathematics* **136**(1), 26–38.

Meier, H., Kuhl, E. and Steinmann, P. (2008), 'A note on the generation of periodic granular microstructures based on grain size distributions', *International journal for numerical and analytical methods in geomechanics* **32**(5), 509.

Milligan, V. (2003), 'Some uncertainties in embankment dam engineering', *Journal of Geotechnical and Geoenvironmental Engineering* **129**(9), 785–797.

Min, K.-B., Jing, L. and Stephansson, O. (2004), 'Determining the equivalent permeability tensor for fractured rock masses using a stochastic rev approach: method and application to the field data from sellafield, uk', *Hydrogeology Journal* **12**(5), 497–510.

Morrison, D. F. (1990), 'Multivariate statistical methods. 3', *New York, NY. Mc* .

Nielsen, K., Miller, C., Beck, D. and Lynch, J. (1998), 'Fractal geometry of root systems: field observations of contrasting genotypes of common bean (phaseolus vulgaris l.) grown under different phosphorus regimes.', *Plant and Soil* **206**, 9.

Oda, M. (1985), 'Permeability tensor for discontinuous rock masses', *Geotechnique* **35**(4), 483–495.

O'Sullivan, C. (2011), *Particulate discrete element modelling*, Taylor & Francis.

Phoon, K. (2008), *Reliability-Based Design in Geotechnical Engineering*, Abingdon: Oxon.

Plimpton, S., Crozier, P. and Thompson, A. (2007), 'Lammps-large-scale atomic/molecular massively parallel simulator', *Sandia National Laboratories* **18**.

Raschdorf, S. (2010), *Bestimmung der Raumausfüllung von Partikelmischungen: Modelle und Datenstrukturen für die Simulation durch Kugelpackungen*, Papierflieger-Verlag.

Ripley, C. F. (1986), 'Internal stability of granular filters: Discussion', *Canadian Geotechnical Journal* **23**(2), 255–258.
    URL: *http://dx.doi.org/10.1139/t86-037*

Salehi Sadaghiani, M. R., Jentsch, H., Faulstich, K., Winkler, P. and Witt, K. J. (2014), Dem modeling and identification of representative element volume of soil skeleton, *in* 'Numerical Methods in Geotechnical Engineering'.

Salehi Sadaghiani, M. R. and Witt, K. J. (2011), 'Experimental identification of mobile particles in suffusible non cohesive soils', *European Journals of Geotechnical Engineering* pp. 33–39.

Salehi Sadaghiani, M. R. and Witt, K. J. (2012), Analysis of internal stability of widely graded soils based on identification of mobile particles, *in* '6th International Conference of Scour and Erosion', pp. 257–264.

Salehi Sadaghiani, M. R., Witt, K. J. and Jentsch, H. (2012), A statistical approach to identify mobile particles of widely graded soils, *in* '6th International Conference of Scour and Erosion', pp. 839–845.

Salgado, R. (2007), *The Engineering of Foundations*, McGraw-Hill International Edition, McGraw Hill.
    URL: *https://books.google.de/books?id=3ZErAQAAMAAJ*

Saucke, U., Brauns, J. and Wibel, S. (1999), 'Zur Entmischungsneigung körniger Schüttstoffe', *Geotechnik* **22**(4), 259.–268.

Scheidegger, A. E. (1963), Geophysical data regarding the earth, *in* 'Principles of Geodynamics', Springer, pp. 47–105.

Semar, O., Witt, K. J. and Fannin, R. J. (2010), Suffusion evaluation - comparison of current approaches, *in* 'Internationa Conference on Scouer and Erosion', Vol. 12, pp. 251–262.

Sherard, J. (1979), Sinkholes in dams of coarse, broadly graded soils. 13th int, *in* 'Congress on Large Dams, New Delhi Q', Vol. 49, p. R2.

Sherard, J., Dunningan, L. and Talbot, J. (1984), 'Filters for silts and clays', *Journal of Geotechnical Engineering, ASCE* **110**(6), 701–718.

Silveira, A. F. (1965), An analysis of the problem of washing through in protective filters, *in* '6th Int. Conf. on Soil Mechanics and Foundation Engineering', Vol. 2, pp. 551.–555. inproceedings.

Skempton, A. and Brogan, J. (1994), 'Experiments on piping in sandy gravels', *Geotechnique* **44**(3), 449–460.

Šmilauer, V. and Chareyre, B. (2010), 'Yade dem formulation', *Yade Documentation* .

Spowart, J. E. (2006), 'Automated serial sectioning for 3-d analysis of microstructures', *Scripta Materialia* **55**(1), 5–10.

Spowart, J., Maruyama, B. and Miracle, D. (2001), 'Multi-scale characterization of spatially heterogeneous systems: implications for discontinuously reinforced metal–matrix composite microstructures', *Materials Science and Engineering: A* **307**(1), 51–66.

Sun, C.-B. B. (1989), Internal Stability of Clayey to Silty Sands, PhD thesis, University of Michigan.

Szpiro, G. G. (2011), *Die Keplersche Vermutung: wie Mathematiker ein 400 Jahre altes Rätsel lösten*, Springer-Verlag.

Terzaghi, K., Peck, R. B. and Mesri, G. (1996), *Soil Mechanics in Engineering Practice*, 3 edn, Wiley- Interscience. book.

To, H. D., Galindo-Torres, S. A. and Scheuermann, A. (2014), A numerical approach for the determination of the primary fabric of granular soils, *in* 'Applied Mechanics and Materials', Vol. 553, Trans Tech Publ, pp. 489–494.

Tory, E. M. (1990), 'A stochastic model for the slow sedimentation of small particles in a viscous fluid', *Ocean Waves Mechanics* **12**(2-3), 671–685.

Toth, J. (1970), 'A conceptual model of the groundwater regime and the hydrogeologic environment', *Journal of Hydrology* **10**(2), 164–176.

Tóth, L. F. (1953), 'Kreisausfüllungen der hyperbolischen ebene', *Acta Mathematica Hungarica* **4**(1-2), 103–110.

Vaughan, P. R. and Soares, P. (1982), 'Design of filters for clay cores of dams', *ASCE Journal of Geotech. Eng.* **108**, 17.–31. article.

Vincens, E., Witt, K. J. and Homberg, U. (2014), 'Approaches to determine the constriction size distribution for understanding filtration phenomena in granular materials', *Acta Geotechnica* pp. 1–13.

Wan, C. F. and Fell, R. (2008), 'Assessing the potential of internal instability and suffusion in embankment dams and their foundations', *Journal of Geotechnical and Geoenvironmental Engineering* **134 No. 3**, 401–407.

Weatherley, D., Hancock, W., Abe, S. and Boros, V. (2013), 'Esys-particle tutorial and user's guide version 2.2. 2'.

Webster's Revised Unabridged Dictionary (2010), University of Chicago. The ARTFL Project, University of Chicago.

Weisstein, E. W. (2003), 'Sphere packing'.

Winkler, P. (2013), Numerische Simulation zur Identifizierung der skelettbildenden Fraktionen eines weitgestuften Bodens unter dynamischer Beanspruchung, Diplomarbeit, Bauhaus Universität Weimar.

Winkler, P., Salehi Sadaghiani, M. R., Jentsch, H. and Witt, K. (2014), Granular packing generation using dem - modified-force biased-algorithm, *in* 'Scour and Erosion: Proceedings of the 7th International Conference on Scour and Erosion, Perth, Australia, 2-4 December 2014', CRC Press, p. 345.

Witt, K. J. (1986), Filtrationsverhalten und Bemessung von Erdstofffiltern, Veröffentlichung des Institutes für Bodenmechanik und Felsmechanik Dissertation Heft 104.

Witt, K. J. (2013), 'Der Selbstfiltrationsindex als Suffosionskriterium für nichtbindige Erdstoffe', *Geotechnik* **36**(3), 160–168.

Woertz, J., Menon, S. and McNelley, T. (2013), 'Microstructure refinement and homogenization of non-deforming constituent distributions during fsw/p', *Friction Stir Welding and Processing VII* pp. 1–8.

Yachida, M., Ikeda, M. and Tsuji, S. (1979), Boundary detection of textured regions, *in* 'Proceedings of the 6th international joint conference on Artificial intelligence-Volume 2', Morgan Kaufmann Publishers Inc., pp. 992–994.

Ziems.J. (1969), Beitrag zur Kontakterosion nichtbindiger Erdstoffe, ,diss.,, TUDresden.

Declaration of authorship

I, Mohamad Reza salehi sadaghiani, declare that this thesis and the work presented in it are my own. I confirm that:

· This work was done wholly while in candidature for a research degree at this University.

· Where any part of this thesis has previously been submitted for a degree or any other qualification at this University or any other institution, this has been clearly stated.

· Where I have consulted the published work of others, this is always clearly attributed.

· Where I have quoted from the work of others, the source is always given. With the exception of such quotations, this thesis is entirely my own work.

· I have acknowledged all main sources of help.

· Where the thesis is based on work done by myself jointly with others, I have made clear exactly what was done by others and what I have contributed myself.

Signed:
_____

Date:
_____

A. Appendix - Experimental investigation

A.1. *SFT*

A.1.1. *SFT* using *PSD1*

F_{PSD}	F_{chosen}	d_i	d_{i+1}	ρ_i	PDF	CDF	PDF	CDF
$[-]$	$[-]$	$[mm]$	$[mm]$	$[g.cm^{-3}]$	$[\%]$	$[\%]$	$[\%]$	$[\%]$
1	1	25.0	20.0	2.5141	52.42	100.00	52.38	100.00
2	2	20.0	16.0	2.5177	21.35	47.58	21.31	47.62
3	3	16.0	6.3	2.5205	5.07	26.23	5.06	26.31
4	4	5.0	5.0	2.5356	4.04	21.16	4.00	21.26
5	5	3.0	3.0	2.5538	2.01	17.12	1.98	17.25
6	6	1.3	1.0	2.5538	2.01	15.10	1.98	15.27
7	7	0.75	0.50	2.4764	4.03	13.09	4.08	13.29
8		0.50	0.25	2.4756	3.04	9.07	3.09	9.21
9	8	0.25	0.15	2.4721	3.04	6.02	3.09	6.12
10		0.15	0.125	2.4721	2.98	2.98	3.03	3.03
				$\sum$	100.00		100.00	

Table A.1.: Reconstitution of the *PSD1* with glass beads

F_{chosen}	h_i	V_w	V_{total}	V_w/V_{total}	ρ_i	h_i/h_{max}
$[-]$	$[cm]$	$[cm^3]$	$[cm^3]$	$[\%]$	$[g.cm^{-3}]$	$[\%]$
1	15.2	1061	2306.55	46.00	1.41	69.4
2	19.7	1104	2989.41	36.93	1.53	90.0
3	20.5	1018	3110.81	32.76	1.57	93.6
4	21.7	1066	3277.73	32.52	1.57	98.6
5	21.5	957	3262.56	29.33	1.62	98.2
6	21.9	1009	3323.25	30.36	1.62	100
7	20.9	745	3171.51	23.49	1.84	95.4
8	21.4	532	3247.38	16.38	1.91	97.7

Table A.2.: *SFT*1 for *PSD1*

F_{chosen}	h_i	V_w	V_{total}	V_w/V_{total}	ρ_i	h_i/h_{max}
$[-]$	$[cm]$	$[cm^3]$	$[cm^3]$	$[\%]\,[g.cm^{-3}]$	$[\%]$	$[\%]$
1	15.5	-	2352.55	-	1.38	72.3
2	19.6	1091	2974.24	36.54	1.54	91.4
3	20.6	1004	3125.98	34.90	1.57	96.0
4	21.1	1006	3201.86	31.36	1.61	98.4
5	21.2	920	3217.03	28.60	1.64	98.8
6	21.3	947	3224.62	29.37	1.67	99.1
7	20.6	802	3125.98	25.66	1.87	96.0
8	21.4	508	3254.97	15.61	1.91	100

Table A.3.: *SFT*2 for *PSD1*

F_{chosen}	h_i	V_w	V_{total}	V_w/V_{total}	ρ_i	h_i/h_{max}
$[-]$	$[cm]$	$[cm^3]$	$[cm^3]$	$[\%]\,[g.cm^{-3}]$	$[\%]$	$[\%]$
1	15.3	919	2352.55	39.81	1.43	68.9
2	20.1	1075	2974.24	35.54	1.54	93.9
3	20.6	1004	3125.98	34.90	1.57	96.0
4	21.1	1006	3201.86	31.36	1.61	98.4
5	21.2	920	3217.03	28.60	1.64	100
6	21.3	947	3224.62	29.37	1.67	100
7	20.6	802	3125.98	20.66	1.87	99.0
8	21.4	508	3254.97	12.61	1.91	99.2

Table A.4.: *SFT*3 for *PSD1*

F_{chosen}	h_i	V_w	V_{total}	V_w/V_{total}	ρ_i	h_i/h_{max}
$[-]$	$[cm]$	$[cm^3]$	$[cm^3]$	$[\%]\,[g.cm^{-3}]$	$[\%]$	$[\%]$
1	15.5	919	2352.55	38.99	1.45	72.1
2	20.1	1075	2974.24	35.54	1.54	93.9
3	20.6	1004	3125.98	33.95	1.57	96.0
4	21.1	1006	3201.86	32.76	1.61	98.4
5	21.2	920	3217.03	29.60	1.64	99.9
6	21.3	947	3224.62	28.57	1.67	100
7	20.6	802	3125.98	20.66	1.87	99.0
8	21.4	508	3254.97	12.61	1.91	99.2

Table A.5.: *SFT*4 for *PSD1*

A.2. Suffusion tests

A.2.1. *ST*-A1

Saturation phase

W_{tap}	W_{dio}	V_{sat}	V_{total}	n
$[cm^3]$	$[cm^3]$	$[cm^3]$	$[cm^3]$	$[\%]$
832.313	21.42	853.733	2760.39	30.93

Percolation phase

i	Δt	$V_{w,outlet}$	Q	k
$[-]$	$[sec]$	$[cm^3]$	$[m.sec^{-1}]$	$[cm_3.sec^{-1}]$
1.00	10	433.92	43.392	4.66×10^{-3}
1.04	10	420.26	42.026	4.45×10^{-3}
1.00	10	434.82	43.482	4.66×10^{-3}
1.02	10	430.70	43.07	4.34×10^{-3}
1.10	10	639.10	63.91	4.25×10^{-3}
1.07	10	631.90	63.19	4.65×10^{-3}
1.04	10	657.45	65.74	4.45×10^{-3}
1.02	10	634.10	63.41	4.51×10^{-3}

Table A.6.: Measured parameters during saturation and percolation of Suffusion Test (*ST*)-A1
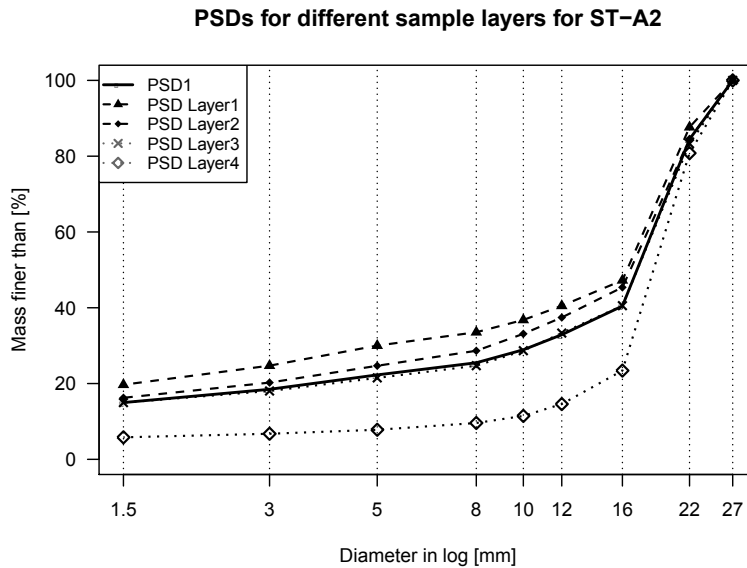
Figure A.1.: *PSDs* of the sample layer after the *ST*-A2

A.2.2. *ST*-A2

Saturation phase

W_{tap}	W_{dio}	V_{sat}	V_{total}	n
$[cm^3]$	$[cm^3]$	$[cm^3]$	$[cm^3]$	$[\%]$
938.68	53.35	885.33	2760.39	33,15

Percolation phase

i	Δt	$V_{w,outlet}$	Q	k
$[-]$	$[sec]$	$[cm^3]$	$[m.sec^{-1}]$	$[cm_3.sec^{-1}]$
0.90	10	706.6	70.66	5.17×10^{-3}
0.90	10	703.6	70.36	5.15×10^{-3}
0.99	10	707.2	70.72	4.69×10^{-3}
1.02	10	668.2	66.82	4.31×10^{-3}
1.02	10	706.9	70.69	4.56×10^{-3}
0.99	10	754.3	75.43	5.03×10^{-3}
1.06	10	703.4	70.34	4.35×10^{-3}
1.02	10	696.6	69.56	4.49×10^{-3}

Table A.7.: Measured parameters during saturation and percolation of Suffusion Test (*ST*)-A2
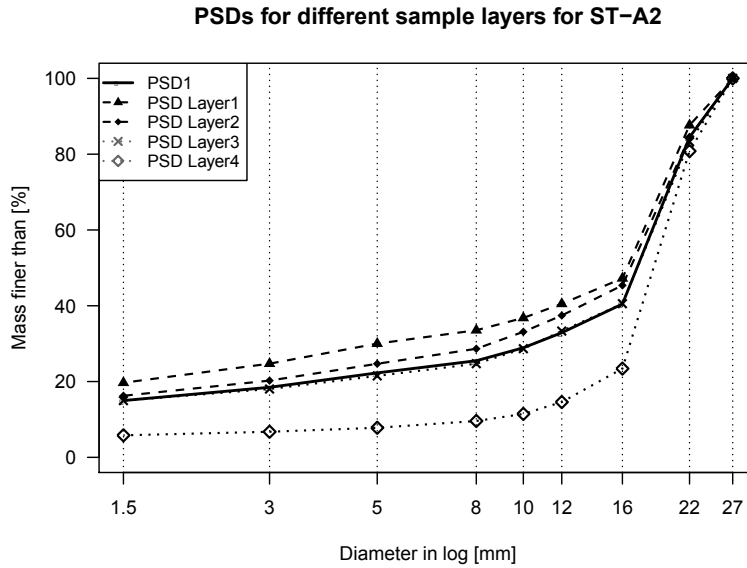
Figure A.2.: *PSDs* of the sample layer after the *ST*-A2

A.2.3. *ST*-A3

Saturation phase

W_{tap}	W_{dio}	V_{sat}	V_{total}	n
$[cm^3]$	$[cm^3]$	$[cm^3]$	$[cm^3]$	$[\%]$
939.62	53.35	886.27	2760.39	32.10

Percolation phase

i	Δt	$V_{w,outlet}$	Q	k
$[-]$	$[sec]$	$[cm^3]$	$[m.sec^{-1}]$	$[cm_3.sec^{-1}]$
0.553	10	327.08	32.708	3.90×10^{-3}
0.505	10	342.14	34.214	4.46×10^{-3}
0.505	10	325.76	32.576	4.25×10^{-3}
0.510	10	325.76	32.576	4.21×10^{-3}
1.000	10	648.43	64.843	4.28×10^{-3}
1.020	10	649.13	64.913	4.20×10^{-3}
1.030	10	655.42	65.542	4.20×10^{-3}
1.050	10	649.55	64.955	4.08×10^{-3}

Table A.8.: Measured parameters during saturation and percolation of Suffusion Test (*ST*)-A3
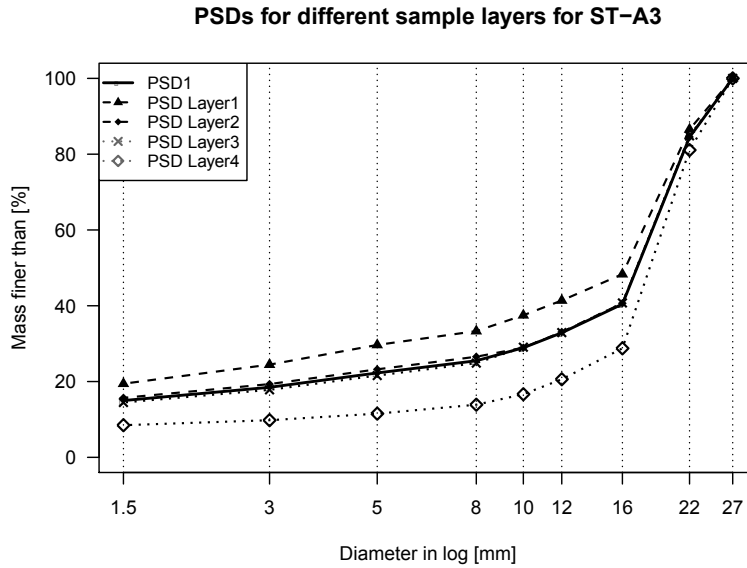
Figure A.3.: *PSDs* of the sample layer after the *ST*-A3

A.2.4. *ST*-B1

Saturation phase

W_{tap}	W_{dio}	V_{sat}	V_{total}	n
$[cm^3]$	$[cm^3]$	$[cm^3]$	$[cm^3]$	$[\%]$
938.60	53.35	885.25	2760.39	33.15

Percolation phase

i	Δt	$V_{w,outlet}$	Q	k
$[-]$	$[sec]$	$[cm^3]$	$[m.sec^{-1}]$	$[cm_3.sec^{-1}]$
1.00	10	706.60	70.66	4.66×10^{-3}
1.00	10	703.60	70.36	4.64×10^{-3}
1.00	10	707.20	70.72	4.66×10^{-3}
1.00	10	668.20	66.82	4.41×10^{-3}
1.10	10	706.85	70.69	4.24×10^{-3}
1.07	10	754.30	75.43	4.65×10^{-3}
1.04	10	703.40	70.34	4.46×10^{-3}
1.00	10	695.60	69.56	4.59×10^{-3}

Table A.9.: Measured parameters during saturation and percolation of Suffusion Test (*ST*)-B1
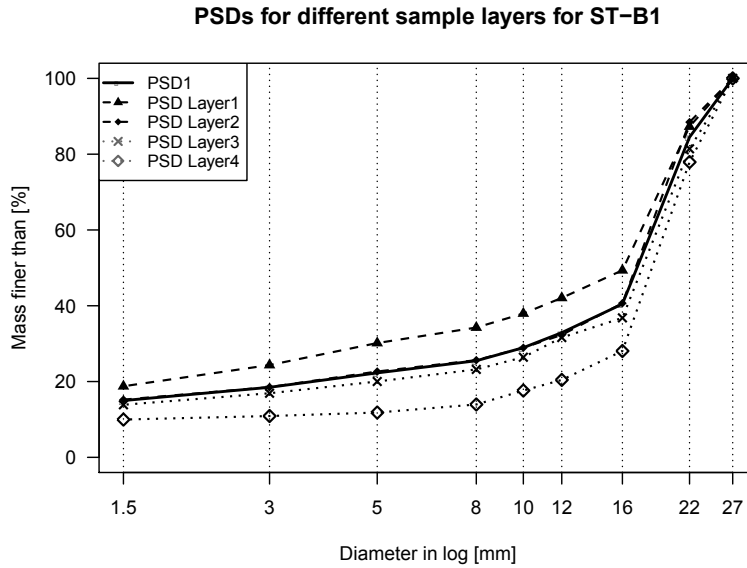
Figure A.4.: *PSDs* of the sample layer after the *ST*-B1

A.2.5. *ST*-C1

Saturation phase

W_{tap}	W_{dio}	V_{sat}	V_{total}	n
$[cm^3]$	$[cm^3]$	$[cm^3]$	$[cm^3]$	$[\%]$
822.60	87.18	735.42	2760.39	27.54

Percolation phase

i	Δt	$V_{w,outlet}$	Q	k
$[-]$	$[sec]$	$[cm^3]$	$[m.sec^{-1}]$	$[cm_3.sec^{-1}]$
1.00	10	725.25	72.53	4.78×10^{-3}
1.00	10	625.05	62.51	4.12×10^{-3}
2.00	10	609.10	60.91	2.01×10^{-3}
2.00	10	887.55	88.76	2.93×10^{-3}
2.00	10	915.20	91.52	3.02×10^{-3}
2.00	10	878.35	87.84	2.90×10^{-3}
2.87	9	896.35	99.59	2.29×10^{-3}
2.87	9	897.75	99.75	2.29×10^{-3}
2.87	8	807.15	100.89	2.32×10^{-3}

Table A.10.: Measured parameters during saturation and percolation of Suffusion Test (*ST*)-C1
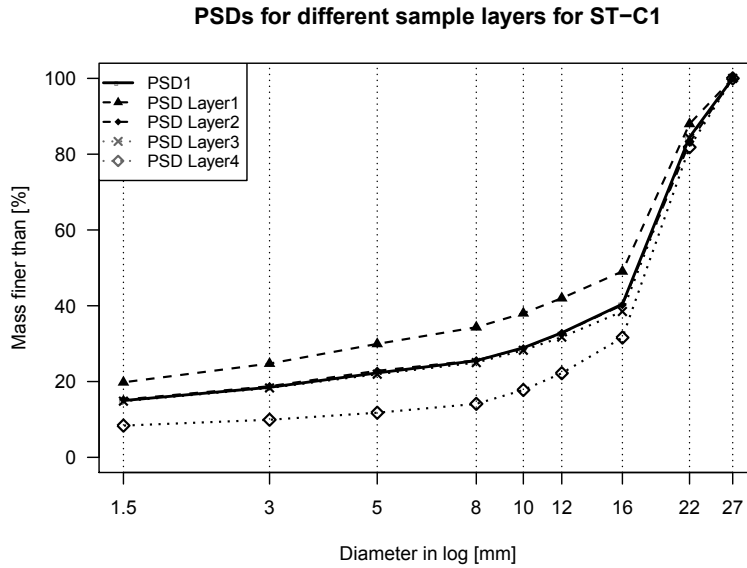
Figure A.5.: *PSDs* of the sample layer after the *ST*-C1

A.2.6. *ST*-D1

Saturation phase

W_{tap}	W_{dio}	V_{sat}	V_{total}	n
$[cm^3]$	$[cm^3]$	$[cm^3]$	$[cm^3]$	$[\%]$
822.60	87.18	735.42	2760.39	27.54

Percolation phase

i	Δt	$V_{w,outlet}$	Q	k
$[-]$	$[sec]$	$[cm^3]$	$[m.sec^{-1}]$	$[cm_3.sec^{-1}]$
1.00	10	725.25	72.53	4.78×10^{-3}
1.00	10	625.05	62.51	4.12×10^{-3}
2.00	10	609.10	60.91	2.01×10^{-3}
2.00	10	887.55	88.76	2.93×10^{-3}
2.00	10	915.20	91.52	3.02×10^{-3}
2.00	10	878.35	87.84	2.90×10^{-3}
2.87	9	896.35	99.59	2.29×10^{-3}
2.87	9	897.75	99.75	2.29×10^{-3}
2.87	8	807.15	100.89	2.32×10^{-3}

Table A.11.: Measured parameters during saturation and percolation of Suffusion Test (*ST*)-D1
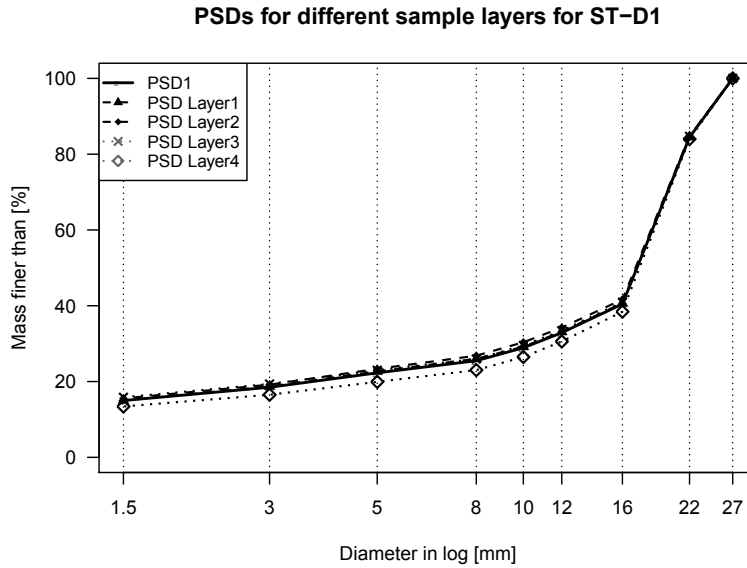
Figure A.6.: *PSDs* of the sample layer after the *ST*-D1

A.2.7. C_H-C1

One example for the calculation of C_H for the Suffusion Test (*ST*) with glass beads.
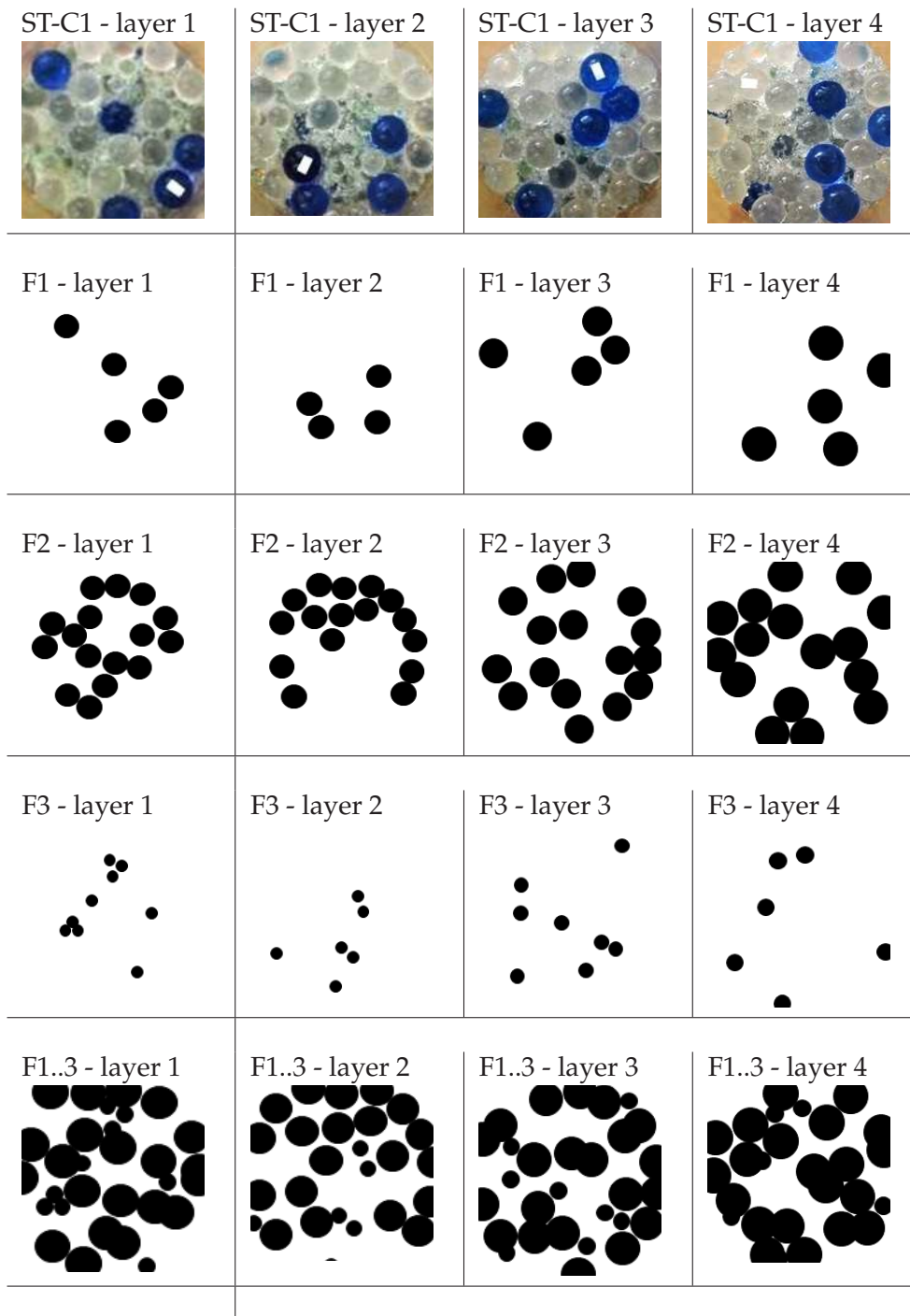
Figure A.7.: Images of the samples for *ST*-C1 and for quantification of C_H
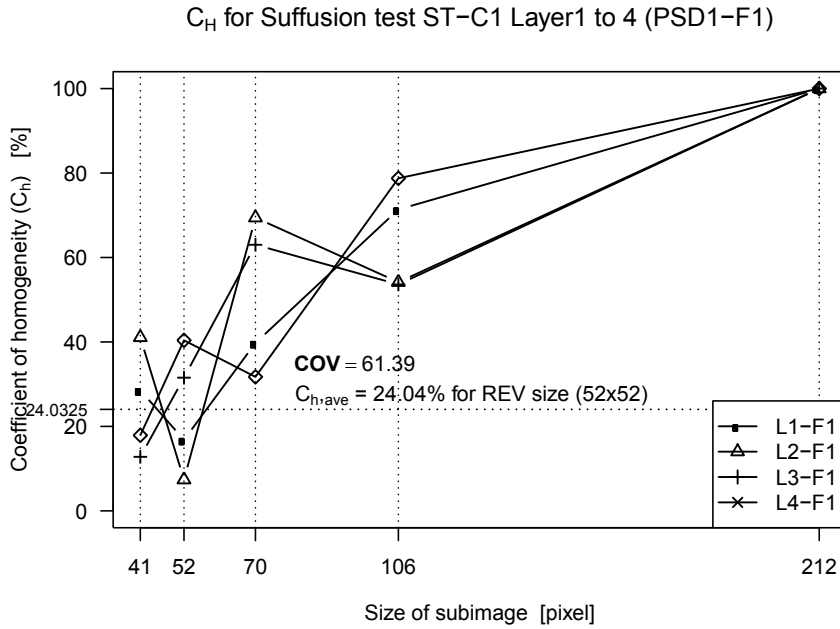
Figure A.8.: C_H calculations for sample *ST*-C1 for fraction *F1* (layers 1 to 4)
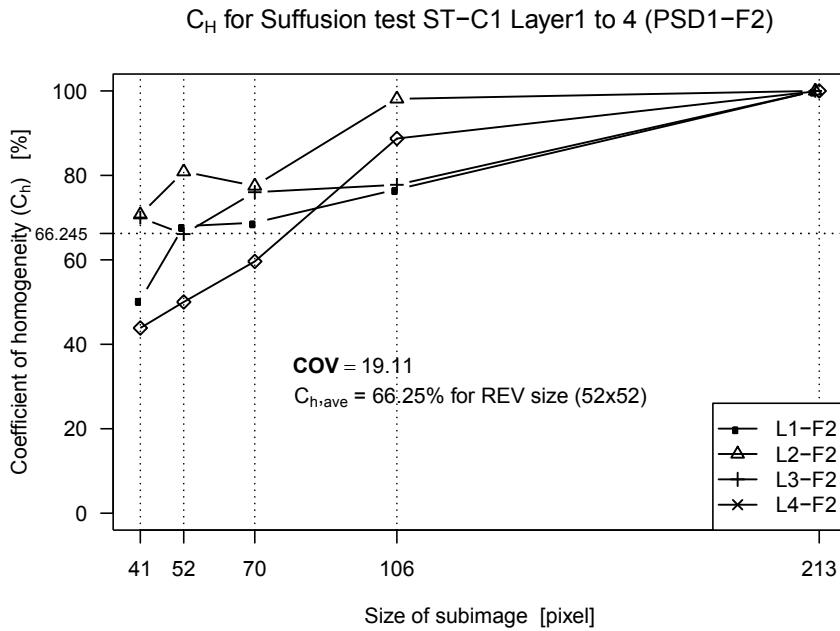
Figure A.9.: C_H calculations for sample *ST*-C1 for fraction *F2* (layers 1 to 4)
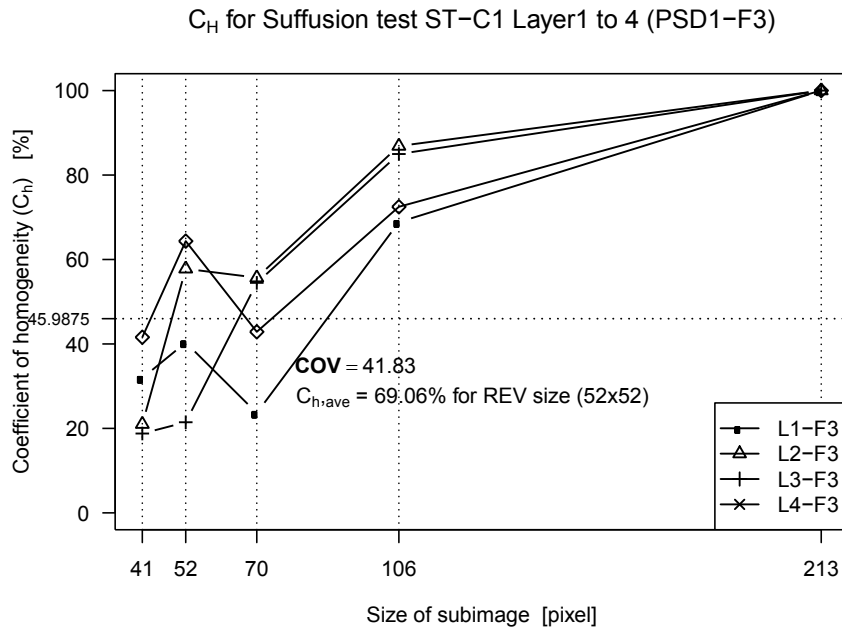
Figure A.10.: C_H calculations for sample *ST*-C1 for fraction *F3* (layers 1 to 4)
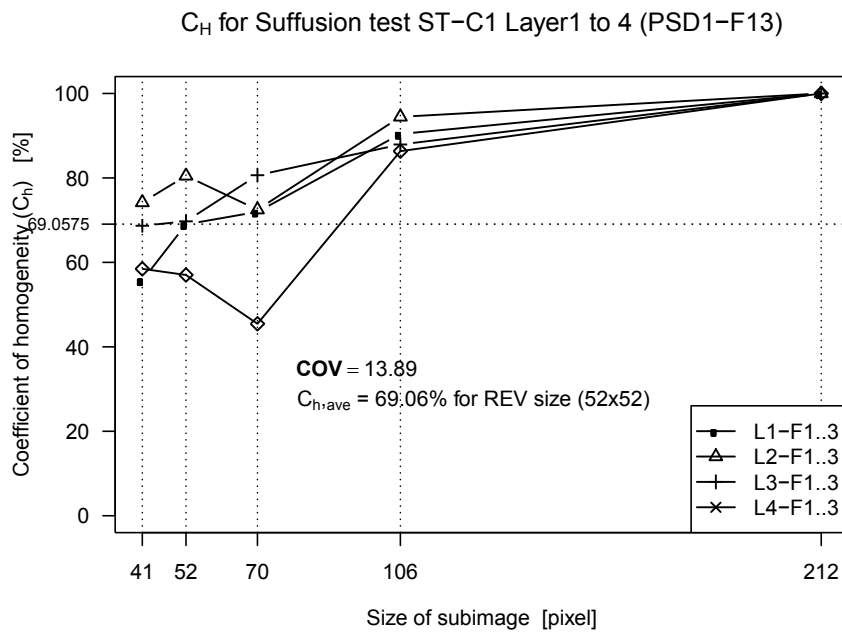
Figure A.11.: C_H calculations for sample *ST*-C1 for fractions *F*1..3 (layers 1 to 4)

B. Appendix - Numerical investigation

B.1. Packing generation - SFT

B.1.1. Model Construction in LIGGGHTS

This part pf appendix describes the input script for the Sequential Fill Test (*SFT*) in *LIGGGHTS* in detail. Note that the lines beginning with a # are either a title or comment for the section or are used to invalid the line. Due to original usage of the LAMMPS for molecular dynamics, the particles in the source code is called **atom**. A *LIGGGHTS* input script consists out of the parts initialization, particle definition, settings and run a simulation. This input script begins with a setting to control the input script from the terminal. Depending on how many fractions should be calculated, one can use the command:

```
time liggghts -var groupnr X < in.group
```

In the Terminal of the UBUNTU to start the simulation with *X* fractions. The variable for that, *groupnr*, also sets other values later in the script. *LIGGGHTS* creates a post file to put in log file.

```
shell rmdir post${groupnr}a.5
shell mv post${groupnr}a.4 post${groupnr}a.5
shell mv post${groupnr}a.3 post${groupnr}a.4
shell mv post${groupnr}a.2 post${groupnr}a.3
shell mv post${groupnr}a.1 post${groupnr}a.2
shell mv post${groupnr}a post${groupnr}a.1
shell mkdir post${groupnr}a
log post${groupnr}a/log.fraction${groupnr}a
```

In this first section it is also defined, that if there are more simulations than one for the same amount of fractions, the program automatically changes all other post file names to *a*.1 to *a*.5 depending on their creation time. All other files after *a*.5 is overwritten.

```
# set simulation domain
   echo            log
   units              si
   atom_style        granular
   atom_modify       map array
   boundary          m m m
```

```
    newton              off
    communicate         single vel yes
    neighbor            0.002 bin
    neigh_modify delay 0
# create simulation box
    region              reg block -0.0695 0.0695 -0.0695 0.0695 0. 0.261
    units box
    create_box        1 reg
```

In the next section the initialization takes place. The simulation domain including particle style, boundary conditions and units is defined.

Echo log means that a log file with all progress of the simulation will be crated. *units* command sets the style of units used for a simulation and its output. *si* means the standard international unit system in which the mass has a unit of Kilogram , length is defined in meter and time in second.

atom style defines the particle style that is chosen to be granular. An associated command describes LIGGGHTS to create a data structure used for indexing particles. *atom modify* assigns how properties of the particle style selected are modified. The keyword *map* determines how particle ID lookup is performed during the calculations. Such lookups are conducted by bond routines to find the local particle index associated with a global particle ID. When the *array* value is used, each processor stores a lookup table of length N, where N is the total number of particles in the system. This is the fastest method for most simulations, but a processor can run out of memory to store the table for very large simulations. Next, the style of boundaries for the global simulation box in each dimension (*x, y, z*) is set. The *m* indicates that the box is non-periodic, which means that particles do not interact across the boundary and do not move from one side of the box to the other.

Another way to make the simulation run faster is to set Newtons third law off by the command *newton off*. The *communicate single vel yes* command sets the style of interprocessor communication. The default style *single* means that each processor acquires information for ghost particles that are within a the distance of the maximum of the neighbor cutoff for all particle type pairs. The velocity information like translational velocity, angular velocity, and angular momentum of a particle are communicated with ghost particles by the setting *vel yes*. The command *neighbor* sets parameters that affect the building of pairwise neighbor lists. All particle pairs within a neighbor cutoff distance equal to their force cutoff plus the skin distance are stored in the list. This meas that *LIGGGHTS* creates a grid in the background of the simulation and checks how many neighbors of one particle are within the determined area. It does not necessarily mean that there is an actual contact of two particles. The larger the determined distance (here $0.002\,m$), the less often neighbor lists need to be built, but more pairs must be checked for possible force interactions every timestep. To create a list by binning which is an operation that scales linearly with the number of particles per processor the argument *bin* is used. The *neighmodify* command sets parameters that affect the building and use of pairwise neighbor lists. The *delay* setting means never build a new list until at least N steps after the previous build. After the initialization step, a simulation box will be created. In this case the region is a block with the base area of a square 13.9 cm times 13.9 cm and 26.1 cm high.

The axis lies in the middle of the square for following geometry inputs.

In the following section the particle properties are defined by the command *fix* with the argument *property/global*. The physical properties assigned here are Young's modulus (*E*), poisson's ratio, coefficient of restitution and coefficient of friction of the soil. The coefficient of rolling friction is neglected, to get the maximum density for the packing. Later, the linear cohesion model is activated for the Hertzian potential forces for interaction between particles. If two particle are in contact, it adds an additional normal force tending to maintain the contact, which means that the cohesion energy density must be defined first.

```
# define material properties
fix m1 all property/global youngsModulus peratomtype 7.e10
fix m2 all property/global poissonsRatio peratomtype 0.2
fix m3 all property/global coefficientRestitution peratomtypepair 1 0.94
fix m4 all property/global coefficientFriction peratomtypepair 1 0.1
fix m5 all property/global coefficientRollingFriction
peratomtypepair 1 0.5
fix m6 all property/global cohesionEnergyDensity
peratomtypepair 1 300000
```

The pair potential is defined using the *pair-style* command. The Hertzian model is one where the normal push-back force for two overlapping particles is proportional to the area of overlap of the two particles, and is thus a non-linear function of overlap distance. The Hertzian style uses this formula:

$$F_{hz} = \sqrt{\delta} * \sqrt{\frac{R_i * R_j}{R_i + R_j}} * F_{hk}$$

With δ being the overlap distance and R_i and R_j the radii of two particles. This formula is only valid, if the distance $r = R_i * R_j$ between those two particles is smaller than their contact distance $d = R_i + R_j$. The last factor is the result of the Hookean style formula. If all particles in the simulation interact via a this pair potential model, the command *pair-coeff * ** should be used.

```
# new pair style
pair_style  gran/hertz/history 1 1  # Hertzian with friction, cohesion
pair_coeff * *
```

The setting goes on by defining a time step for the simulation. It is difficult to find the right time step for the simulation because later with the "run" command the massflowrate plays an important roll as well. At first a total simulation time of 2.5 sec is chosen and a time step of $4.8 * 10^{-8}$. The dump-number *dmpnr*, also used in the *run* command, sets the amount of time steps after the results are saved, e.g. after each 400.000 steps. The argument *ts-check* is set to periodically calculate estimations of the Rayleigh- and Hertz time (dt_r and dt_h) for a granular system every 1000 time-steps. This offers the opportunity to find an error in the input script faster. A warning message is printed if the time-step size exceeds either of $dt_r * 0.02$ or $dt_h * 0.02$.

```
# dt * iteration = 2.5
variable dt equal 0.000000048
timestep ${dt}
variable iter equal 2.5/${dt}
variable dmpnr equal ${iter}/100
variable im equal ${iter}/1000000
variable simt equal 2.5
fix  ts_check all check/timestep/gran 1000 0.2 0.2
```

Now the limits of the simulation are set. Before a region in the shape of a block was defined and now the particles get their limits by a cylinder fitting exactly in this block. The cylinder has an open top and a fixed bottom. The walls have got the same pair potential setting as the particles. Besides the gravity is set to act downwards.

```
# defining gravitation and limits
fix gravi all gravity 9.81 vector 0.0 0.0 -1.0
fix zwalls all wall/gran/hertz/history 1 1 zplane 0.0 0.260 1
fix cylwalls all wall/gran/hertz/history 1 1 zcylinder 0.0695 1
```

The next section describes the descretized PSD1 for the simulations. All the fractions are defined in the first part of the script. The setting *radius uniform* means that LIGGGHTS generates particles, e.g. with radius between 0.008 and 0.01 randomly. This leads to different simulation results with the same input script which will be described in the next Section. Otherwise the argument *constant* means, that all particles of the named fraction have the same radius. Then the distribution of the defined fractions follows. For PSD1 the amount of the different fractions can be found in the next part of the input script. Depending on the groupnumber chosen at the start of the simulation via the Terminal, the masses are calculated.

```
# GSD2
fix frak1  all particletemplate/sphere 1 atom_type 1
density constant 2518 radius uniform 0.008 0.01
fix frak2  all particletemplate/sphere 1 atom_type 1
density constant 2521 radius uniform 0.00315 0.008
fix frak3  all particletemplate/sphere 1 atom_type 1
density constant 2536 radius constant 0.0025
fix frak4  all particletemplate/sphere 1 atom_type 1
density constant 2535 radius constant 0.0015
fix frak5  all particletemplate/sphere 1 atom_type 1
density constant 2554 radius uniform 0.0005 0.00065
fix frak6  all particletemplate/sphere 1 atom_type 1
density constant 2476 radius uniform 0.00025 0.000375

fix kgv1 all particledistribution/discrete 42 1 frak1 1.0
fix kgv2 all particledistribution/discrete 42 2 frak1 0.7829
frak2 0.2171
```

```
fix kgv3 all particledistribution/discrete 42 3 frak1 0.7481
frak2 0.2075 frak3 0.0444
fix kgv4 all particledistribution/discrete 42 4 frak1 0.6878
frak2 0.1908 frak3 0.0408 frak4 0.0806
fix kgv5 all particledistribution/discrete 42 5 frak1 0.6674
frak2 0.1851 frak3 0.0396 frak4 0.0783 frak5 0.0296
fix kgv6 all particledistribution/discrete 42 6 frak1 0.6424
frak2 0.1782 frak3 0.0381 frak4 0.0753 frak5 0.0285 frak6 0.0375

# variable i equal 0.494 #8/16.2
# variable i equal 0.370 #6/16.2
# variable i equal 0.247 #4/16.2
variable i equal 0.185 #3/16.2

if ${groupnr} == 1 then "variable frakmass equal 3.472*${i}"
if ${groupnr} == 2 then "variable frakmass equal 4.435*${i}"
if ${groupnr} == 3 then "variable frakmass equal 4.641*${i}"
if ${groupnr} == 4 then "variable frakmass equal 5.048*${i}"
if ${groupnr} == 5 then "variable frakmass equal 5.202*${i}"
if ${groupnr} == 6 then "variable frakmass equal 5.405*${i}"
variable i delete
```

At the next step, a region of insertion for the particles is chosen from the former defined region. The total cylinder height was set to 0.251 m and now the upper part measuring 9 cm is used to generate the particles. The *pour/dev* command is responsible for pouring the particles from the recently defined insertion region into the cylinder. The mass and grain size distribution is related to the groupnumber. The first setting for *vol* or volume is the percentage which should be filled with material, here it is 60 percent of the insertion area, which is the maximum possible. The value 200 is the amount of attempts, to insert a single particle without overlap. The *massflowrate* determines the mass of particles that should be inserted in one second. Here the chosen time step is important, because the generated particles should leave the insertion area before new particles are generated. Otherwise an error occurs. Therefor the particles get a start velocity *vel* of -1.1 m/sec. Then the gravity accelerates the particles.

Because problems occurred by pouring the finer fractions the command *insert/pack* instead of *pour/dev* was used. Hence the insertion area is the same as the whole simulation domain and all particles are generated at the same time. The input script for this simulation can be found in at the end of this appendix.

```
#region and insertion
group nve_group region reg
region bc cylinder z 0.0 0.0 0.0695 0.16 0.25 units box
fix ins nve_group pour/dev mass ${frakmass} 1
distributiontemplate kgv${groupnr} vol 0.6 200
massflowrate 4.2 vel uniform 0. 0. 0. 0. -1.1 region bc
```

```
# apply nve integration to all particles
that are inserted as single particles
fix integr nve_group nve/sphere
```

Finally the input script is concluded with a run command. At first a computation is defined that calculates the rotational kinetic energy of a group of spherical particles. The *run* command follows and in the dump file all results after the defined time increment *dumpnr* are saved. The information about every particle like particle ID, position, velocity, forces on the particles and their radius can be found in the dump file. The process of pouring ends after the specified end point with *unfix* the insertion. Finally a restart file will be saved after the first part of the simulation is finished. The second and third part of the simulation is about compaction of the sample*LAMMPS Users Manual / LIGGGHTS Documentation* (2013).

```
# save
compute 1 all erotate/sphere
run 1
dump dmp all custom ${dmpnr} post${groupnr}a/dump.fraction${groupnr}a
id type type x y z ix iy iz vx vy vz fx fy fz radius

#insert particles und Output
run ${iter} every 50000 "print dumpnumber ${dmpnr} iterationN
${im} [Mil] - Simu-Time ${simt}
aktuelle Fraktion: ${groupnr} H43cm|
aktuelle Masse: ${frakmass}"
unfix ins

# print on screen
print "aktuelle Fraktion : ${groupnr}"
print "aktueller Pfad : post${groupnr}a"
print "aktuelle KGV : kgv${groupnr}"
print "aktuelle Masse : ${frakmass}"

# write restart file
write_restart post${groupnr}a/fraction${groupnr}a.restart
```

Input script of the first step a:

```
# Inputscript Schritt a
# Dateioperationen auf Betriebssystem-Ebene
shell rmdir post${fraknumber}a.5
shell mv post${fraknumber}a.4 post${fraknumber}a.5
shell mv post${fraknumber}a.3 post${fraknumber}a.4
shell mv post${fraknumber}a.2 post${fraknumber}a.3
```

```
shell mv post${fraknumber}a.1 post${fraknumber}a.2
shell mv post${fraknumber}a post${fraknumber}a.1
shell mkdir post${fraknumber}a
log post${fraknumber}a/log.frak${fraknumber}a
echo log

#Initialisierung Programmparameter
units si
atom_style granular
atom_modify map array
boundary m m m
newton off
communicate single vel yes
neighbor 0.002 bin
neigh_modify delay 0
variable intubeheight equal 0.42

# Erstellen von Gitterstruktur, Simulationsbox, Teilchen und Teilcheneigenschaften
region region_box cylinder z 0 0 0.1 0 2.0 units box
create_box 1 region_box

variable timesteps equal 1e7
variable timestepstartinsertion equal 1
variable timestepstopinsertion equal ${timesteps}
variable timesteplength equal 1/${timesteps}
variable dumpsteps equal ${timesteps}/100

# Materialeigenschaften festlegen
fix  m1 all property/global youngsModulus peratomtype 7.e10
fix  m2 all property/global poissonsRatio peratomtype 0.2
fix  m3 all property/global coefficientRestitution peratomtypepair 1 0.94
fix  m4 all property/global coefficientFriction peratomtypepair 1 0.1
#Gleitreibung, Glas nass
fix  m5 all property/global coefficientRollingFriction
 peratomtypepair 1 0.5 #
fix m6 all property/global cohesionEnergyDensity peratomtypepair 1 300000

# Neuen pair style anlegen
pair_style  gran/hertz/history 1 1  # Hertzian with friction,
 cohesion
pair_coeff * *

# Gravitation einschalten, Begrenzungen festlegen
fix gravi all gravity 9.81 vector 0.0 0.0 -1.0
fix zwalls all wall/gran/hertz/history 1 1 zplane 0.0 ${intubeheight} 1
fix cylwalls all wall/gran/hertz/history 1 1 zcylinder 0.07 1
fix intube all mesh/gran insertion_tube.stl 1 1. 0. 0. 0. 0. 0. 0.
fix intube_wall all wall/gran/hertz/history 1 1 mesh/gran 1 intube

# Korngrössenverteilung KGV-1Semar
fix frak1  all particletemplate/sphere 1 atom_type 1 density constant 2500 radius
```

```
constant 0.00895
fix frak2  all particletemplate/sphere 1 atom_type 1 density constant 2500 radius
constant 0.0050
fix frak3  all particletemplate/sphere 1 atom_type 1 density constant 2500 radius
constant 0.0025
fix frak4  all particletemplate/sphere 1 atom_type 1 density constant 2500 radius
constant 0.0015
fix frak5  all particletemplate/sphere 1 atom_type 1 density constant 2500 radius
constant 0.00057
fix frak6  all particletemplate/sphere 1 atom_type 1 density constant 2500 radius
constant 0.00031
fix frak7  all particletemplate/sphere 1 atom_type 1 density constant 2500 radius
constant 0.00018
fix frak8  all particletemplate/sphere 1 atom_type 1 density constant 2500 radius
constant 0.000097

fix kgv1 all particledistribution/discrete 42 1 frak1 1.0
fix kgv2 all particledistribution/discrete 42 2 frak1 0.711 frak2 0.289
fix kgv3 all particledistribution/discrete 42 3 frak1 0.665 frak2 0.271
frak3 0.064
fix kgv4 all particledistribution/discrete 42 4 frak1 0.632 frak2 0.258
frak3 0.061 frak4 0.049
fix kgv5 all particledistribution/discrete 42 5 frak1 0.617 frak2 0.252
frak3 0.060 frak4 0.048 frak5 0.024
fix kgv6 all particledistribution/discrete 42 6 frak1 0.603 frak2 0.246
frak3 0.058 frak4 0.047 frak5 0.023 frak6 0.023
fix kgv7 all particledistribution/discrete 42 7 frak1 0.558 frak2 0.227
frak3 0.054 frak4 0.043 frak5 0.021 frak6 0.021 frak7 0.075
fix kgv8 all particledistribution/discrete 42 8 frak1 0.524 frak2 0.214
frak3 0.051 frak4 0.040 frak5 0.02 frak6 0.02 frak7 0.07 frak8 0.06
variable i equal 1/3
if ${fraknumber} == 1 then "variable frakmass equal 3.255*$i"
if ${fraknumber} == 2 then "variable frakmass equal 4.581*$i"
if ${fraknumber} == 3 then "variable frakmass equal 4.896*$i"
if ${fraknumber} == 4 then "variable frakmass equal 5.147*$i"
if ${fraknumber} == 5 then "variable frakmass equal 5.272*$i"
if ${fraknumber} == 6 then "variable frakmass equal 5.397*$i"
if ${fraknumber} == 7 then "variable frakmass equal 5.836*$i"
if ${fraknumber} == 8 then "variable frakmass equal 6.210*$i"
variable i delete

group nve_group region region_box
fix integr nve_group nve/sphere
fix ins nve_group insert/pack seed 42 distributiontemplate kgv${fraknumber}
maxattempt 2000 insert_every once overlapcheck yes all_in yes
vel constant 0 0 -1.0  region region_intube mass_in_region ${frakmass}

# Berechnungseinstellungen, Berechnung, Ausgabe
fix ts_check all check/timestep/gran 1000 0.2 0.2
compute 1 all erotate/sphere
timestep ${timesteplength}
```

```
print ""
print "aktuelle Fraktion : ${fraknumber}"
print "aktueller Pfad : post${fraknumber}a"
print "aktuelle KGV : kgv${fraknumber}"
print "aktuelle Masse : ${frakmass}"
print "timesteps : ${timesteps}"
print "timesteplength : ${timesteplength}"
print "Start : ${timestepstartinsertion}"
print "Ende : ${timestepstopinsertion}"
print ""

run ${timestepstartinsertion}
dump dmpa all custom ${dumpsteps} post${fraknumber}a/dump.frak${fraknumber}a
id type type x y z ix iy iz vx vy vz fx fy fz omegax omegay omegaz radius
run ${timestepstopinsertion} upto
write_restart post${fraknumber}a/restart.frak${fraknumber}a.bin
undump dmpa



# created stl-file using software gmsh
solid Created by Gmsh
facet normal -0.980785 -0.19509 0
  outer loop
    vertex 0.0323358 0.0133939 0.0625
    vertex 0.035 0 0.125
    vertex 0.0323358 0.0133939 0.125
  endloop
endfacet
facet normal -0.980785 -0.19509 0
  outer loop
    vertex 0.0323358 0.0133939 0.0625
...
    vertex 0.0323358 -0.0133939 0.8125
  endloop
endfacet
endsolid Created by Gmsh
```

Input script for the step b of the simulation.

```
# Initialisierung Programmparameter

shell rmdir post${fraknumber}b.5
shell mv post${fraknumber}b.4 post${fraknumber}b.5
shell mv post${fraknumber}b.3 post${fraknumber}b.4
shell mv post${fraknumber}b.2 post${fraknumber}b.3
shell mv post${fraknumber}b.1 post${fraknumber}b.2
shell mv post${fraknumber}b post${fraknumber}b.1
shell mkdir post${fraknumber}b
log post${fraknumber}b/log.frak${fraknumber}b
```

```
echo log
units si
atom_style granular
atom_modify map array
boundary m m m

# Ergebnisse von Schritt a laden
read_restart post${fraknumber}a/restart.frak${fraknumber}a.bin
newton off
communicate single vel yes
neighbor 0.002 bin
neigh_modify delay 0

# Erstellen von Gitterstruktur, Simulationsbox, Teilchen und
Teilcheneigenschaften
region region_box cylinder z 0 0 0.1 0 1.5 units box
region region_intube cylinder z 0 0 0.034 0.0 0.5 units box

variable timesteps equal 1e7
variable timestepstartinsertion equal 1
variable timestepstopinsertion equal 1e7
variable timestepmovetube equal 1
variable timestepstoptube equal ${timestepstopinsertion}
+${timesteps}*3
variable timesteplength equal 1/${timesteps}
variable dumpsteps equal ${timesteps}/100

# Materialeigenschaften festlegen
fix  m1 all property/global youngsModulus peratomtype 7.e10
fix  m2 all property/global poissonsRatio peratomtype 0.2
fix  m3 all property/global coefficientRestitution
peratomtypepair 1 0.94
fix  m4 all property/global coefficientFriction peratomtypepair 1 0.1
fix  m5 all property/global coefficientRollingFriction
peratomtypepair 1 0.001
fix m6 all property/global cohesionEnergyDensity peratomtypepair 1 300000

# Neuer pair style
pair_style  gran/hertz/history 1 1  # Hertzian with friction, cohesion
pair_coeff * *

# Gravitation einschalten, Begrenzungen festlegen
fix gravi all gravity 9.81 vector 0.0 0.0 -1.0
fix zwalls all wall/gran/hertz/history 1 0 zplane 0.0 1.5 1
fix cylwalls all wall/gran/hertz/history 1 0 zcylinder 0.07 1
fix intube all mesh/gran insertion_tube.stl 1 1. 0. 0. 0. 0. 0. 0.
fix intubewall all wall/gran/hertz/history 1 0 mesh/gran 1 intube

group nve_group region region_box
fix integr nve_group nve/sphere
```

```
# Berechnungseinstellungen, Berechnung, Ausgabe
fix ts_check all check/timestep/gran 1000 0.2 0.2
compute 1 all erotate/sphere
timestep ${timesteplength}
print ""
print "aktuelle Fraktion : ${fraknumber}"
print "aktueller Pfad : post${fraknumber}b"
print "timesteps : ${timesteps}"
print "timesteplength : ${timesteplength}"
print "Start : ${timestepmovetube} "
print "Ende : ${timestepstoptube}"
print ""
```

Input script for the step c of the simulation.

```
shell rmdir post${fraknumber}c.5
shell rmdir post${fraknumber}c.5.short
shell mv post${fraknumber}c.4 post${fraknumber}c.5
shell mv post${fraknumber}c.4.short post${fraknumber}c.5.short
shell mv post${fraknumber}c.3 post${fraknumber}c.4
shell mv post${fraknumber}c.3.short post${fraknumber}c.4.short
shell mv post${fraknumber}c.2 post${fraknumber}c.3
shell mv post${fraknumber}c.2.short post${fraknumber}c.3.short
shell mv post${fraknumber}c.1 post${fraknumber}c.2
shell mv post${fraknumber}c.1.short post${fraknumber}c.2.short
shell mv post${fraknumber}c post${fraknumber}c.1
shell mv post${fraknumber}c.short post${fraknumber}c.1.short
shell mkdir post${fraknumber}c

log post${fraknumber}c/log.frak${fraknumber}c
echo log
units si
atom_style granular
atom_modify map array
boundary m m m

read_restart post${fraknumber}b/restart.frak${fraknumber}b.bin

newton off
communicate single vel yes
neighbor 0.002 bin
neigh_modify delay 0

# Erstellen von Bereichen
region region_box cylinder z 0 0 0.1 0 1.5 units box
region region_intube cylinder z 0 0 0.034 0.0 0.5 units box

# Vorgabe der Zeitschritt-Variablen
variable timesteps equal 1e7
variable timestepstartinsertion equal 1
```

```
variable timestepstopinsertion equal 1e7
variable timestepmovetube equal 1
variable timestepstoptube equal ${timestepstopinsertion}+${timesteps}*3
variable timestepstartcomp equal 1
variable timestepstopcomp equal ${timestepstoptube}+${timesteps}*1
variable timesteplength equal 1/${timesteps}
variable dumpsteps equal ${timesteps}/100

# HÃfÂ¶he der Kompressionsplatte bei Begin
if ${fraknumber} == 1 then "variable start_comp_height equal 0.065"
if ${fraknumber} == 2 then "variable start_comp_height equal 0.085"
if ${fraknumber} == 3 then "variable start_comp_height equal 0.088"
if ${fraknumber} == 4 then "variable start_comp_height equal 0.085"
if ${fraknumber} == 5 then "variable start_comp_height equal 0.086"
if ${fraknumber} == 6 then "variable start_comp_height equal 0.2"
if ${fraknumber} == 7 then "variable start_comp_height equal 0.2"
if ${fraknumber} == 8 then "variable start_comp_height equal 0.2"

# Materialeigenschaften festlegen
fix  m1 all property/global youngsModulus peratomtype 7.e10
fix  m2 all property/global poissonsRatio peratomtype 0.2
fix  m3 all property/global coefficientRestitution peratomtypepair 1 0.94
fix  m4 all property/global coefficientFriction peratomtypepair 1 0.1
fix  m5 all property/global coefficientRollingFriction peratomtypepair 1 0.001
fix m6 all property/global cohesionEnergyDensity peratomtypepair 1 300000
fix  m7 all property/global k_finnie peratomtypepair 1 1.0
#fÃ¼r mesh/gran/stressanalysis finnie model

# Neuer pair style
pair_style  gran/hertz/history 1 1  # Hertzian with friction, cohesion
pair_coeff * *

# Gravitation einschalten, Begrenzungen festlegen
fix gravi all gravity 9.81 vector 0.0 0.0 -1.0
fix zwalls all wall/gran/hertz/history 1 0 zplane 0.0 1.5 1
fix cylwalls all wall/gran/hertz/history 1 0 zcylinder 0.07 1
fix comp_plate all mesh/gran/stressanalysis square_plate.stl 1 1. 0. 0.
${start_comp_height} 0. 0. 0. finnie yes
fix comp_plate_wall all wall/gran/hertz/history 1 0 mesh/gran 1 comp_plate

group nve_group region region_box
fix integr nve_group nve/sphere

# Berechnungseinstellungen
fix ts_check all check/timestep/gran 1000 0.2 0.2
compute gran all erotate/sphere
compute stressgran all stress/atom

timestep ${timesteplength}
print ""
print "aktuelle Fraktion : ${fraknumber}"
```

```
print "aktueller Pfad : post${fraknumber}c"
print "timesteps : ${timesteps}"
print "timesteplength : ${timesteplength}"
print "Start : ${timestepstartcomp}"
print "Ende : ${timestepstopcomp}"
print ""

# Berechnung, Ausgabe
#run ${timestepstartcomp}
dump dmpc all custom ${dumpsteps} post${fraknumber}c/dump.frak${fraknumber}c
id type x y z ix iy iz vx vy vz fx fy fz omegax omegay omegaz radius
c_stressgran[1] c_stressgran[2] c_stressgran[3]
dump  dmpstressmesh all mesh/gran/VTK ${dumpsteps}
post${fraknumber}c/stressmesh*.vtk stress id wear vel stresscomponents comp_plate
fix  moveplate all move/mesh/gran linear 0. 0. -0.01 units box comp_plate
run ${timestepstopcomp} upto
undump dmpc
undump dmpstressmesh
write_restart post${fraknumber}c/restart.frak${fraknumber}c.bin
```
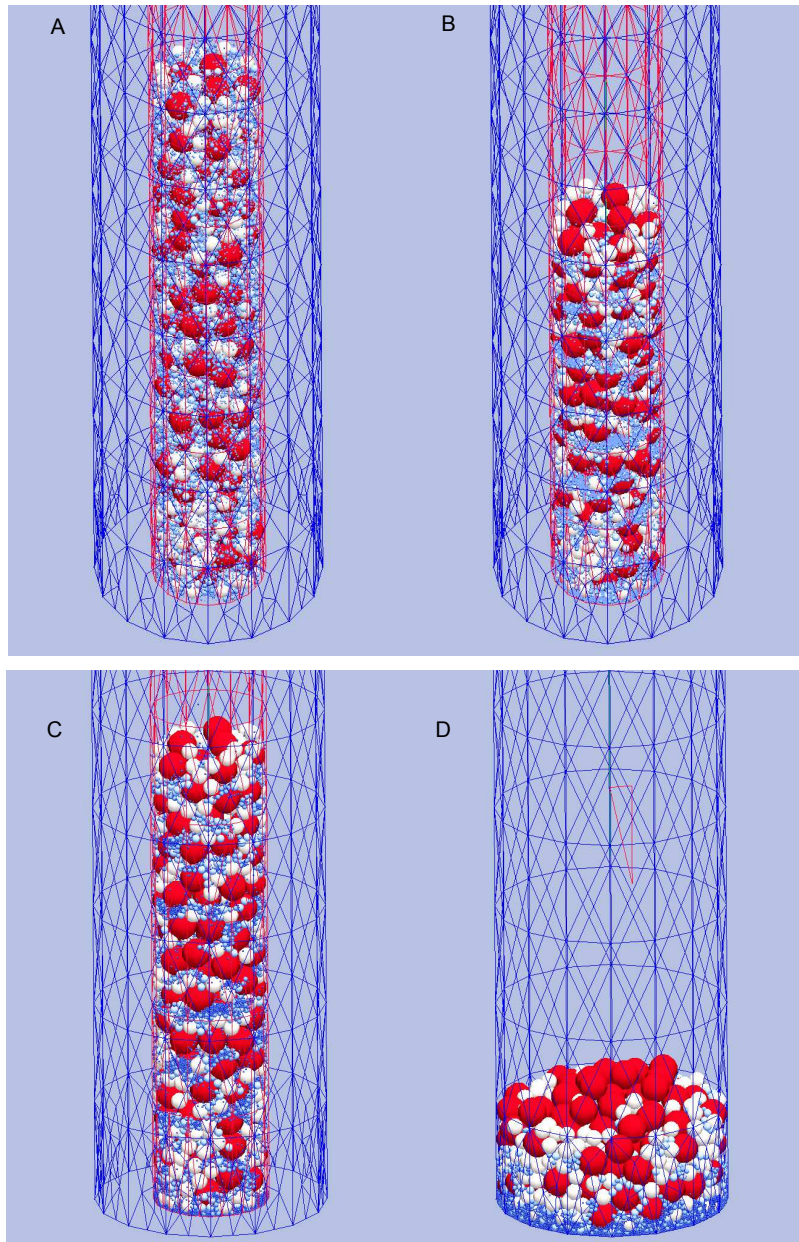
Figure B.1.: SFT- Simulation steps. Image A shows the filling process of the funnel. Image B shows that the funnel is filled and the particles are at their equilibrium. Image D shows that the funnel starts to move upward slowly and the image D shows that the funnel is totally out of the cylinder and all particles are at the rest. In the next image the compaction is shown.
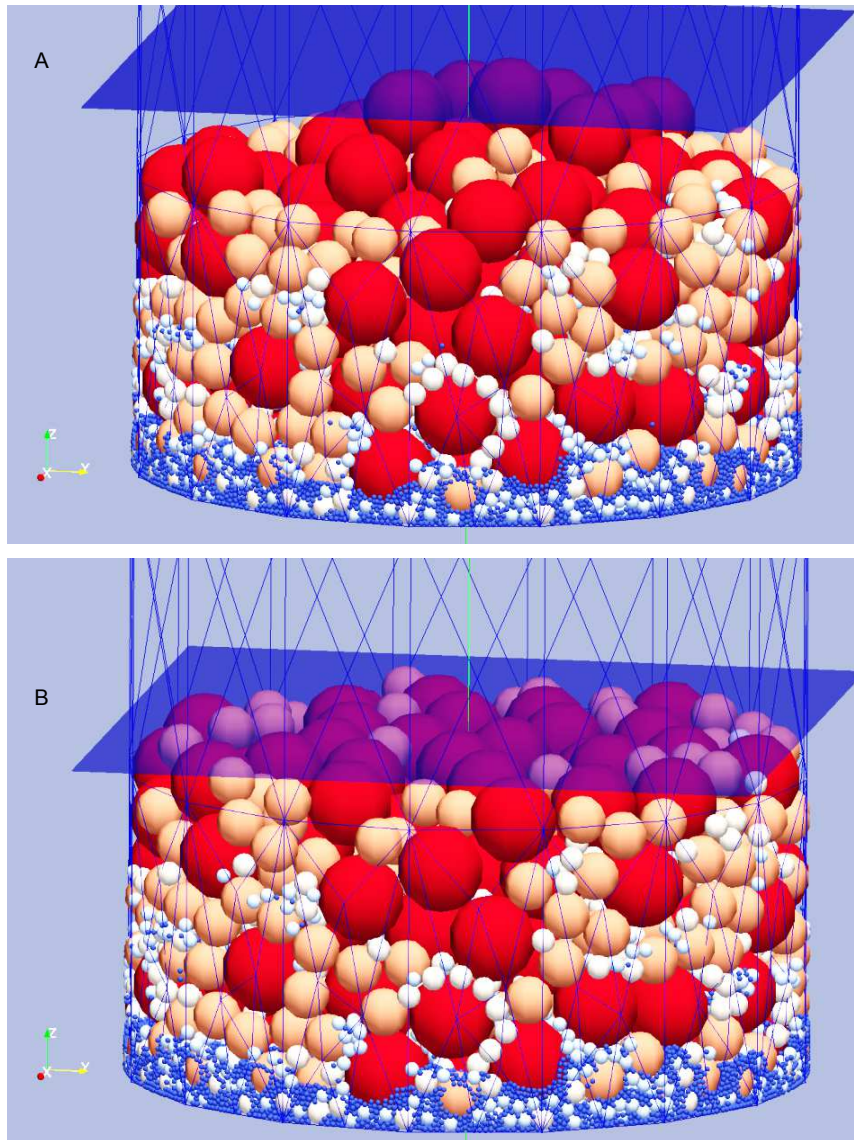
Figure B.2.: SFT- Image A shows the starting position of the compaction plate. Image B shows the final position of the plate after compaction. In the previous image the filling process is shown.

B.2. Packing generation - MFBA

B.2.1. The input script of MFBA packing generation

```
echo log
variable insvfrac equal 0.6 #insert_volume_fraction

## Variablen
```

```
variable ts_length equal 1e-7
variable ts_dump equal 1/${ts_length}/10000
variable ts_grow equal ${ts_dump} #timesteps between grows
variable ts_relax equal ${ts_dump}*10 #timesteps to relax
variable growsmax equal 1000
variable growpress equal 10e6 #10MPa
variable growpressdelta equal ${growpress}/1e4
variable growrate equal
1.01^((${growpress}+${growpressdelta}-v_cpress)/${growpress})
if "${psd} > 100" then "variable psdname string kgv10"
if "${psd} > 200" then "variable psdname string semar"
if "${psd} > 300" then "variable psdname string dinger"
if "${psd} > 400" then "variable psdname string fuller"
variable psdnr equal ${psd}-floor(${psd}/10)*10
variable modelname string ${psdname}${psdnr}a

## Systembefehle
shell "rm -rf" ${modelname}
shell "mkdir" ${modelname}
shell "mkdir" ${modelname}/jpga
shell "mkdir" ${modelname}/jpgb
shell "mkdir" ${modelname}/jpgc
shell "mkdir" ${modelname}/voro
shell "mkdir" ${modelname}/vtk
log ${modelname}/tmp.log
shell mv log.liggghts ${modelname}/${modelname}.log
shell date +%_a_%_d_%_b_%R > ${modelname}/tmp.time
shell date +%s > ${modelname}/tmp.0

## Modellinitialisierung
units si
atom_style granular
atom_modify map array
boundary p p p
newton off
communicate single vel yes
neighbor 0.002 bin
neigh_modify check yes page 1000000 one 100000 #1e6 1e5
region region_box block 0. 0.1 0. 0.1 0. 0.1 units box
create_box 1 region_box
variable catoms equal atoms
variable cstep equal step
variable cetotal equal etotal
variable centhalpy equal enthalpy
variable ctemp equal temp
variable cpress equal press
variable vreg equal vol
variable nreg equal (${vreg}-(mass(all)/2500))/${vreg}
variable mass_all equal mass(all)

## Materialeigenschaften
```

```
fix  m1 all property/global youngsModulus peratomtype 50e9
fix  m2 all property/global poissonsRatio peratomtype 0.35
fix  m3 all property/global coefficientRestitution peratomtypepair 1 0.3
fix  m4 all property/global coefficientFriction peratomtypepair 1 0.1
fix  m5 all property/global coefficientRollingFriction peratomtypepair 1 0.5
fix m6 all property/global cohesionEnergyDensity peratomtypepair 1 0

## Particle properties
pair_style gran/hertz/history
#rolling_friction = 'off'
cohesion = 'off'
tangential_damping = 'on'
absolute_damping = 'off'
store_force = 'no'
viscous = 'off'
pair_coeff * *
# fractions
fix f1  all particletemplate/sphere 1 atom_type 1 density
 constant 2500 radius constant 0.01118
fix f2  all particletemplate/sphere 1 atom_type 1 density
 constant 2500 radius constant 0.00894
fix f3  all particletemplate/sphere 1 atom_type 1 density
 constant 2500 radius constant 0.00447
fix f4  all particletemplate/sphere 1 atom_type 1 density
 constant 2500 radius constant 0.00194
fix f5  all particletemplate/sphere 1 atom_type 1 density
 constant 2500 radius constant 0.00099
fix f6  all particletemplate/sphere 1 atom_type 1 density
 constant 2500 radius constant 0.00049
fix f7  all particletemplate/sphere 1 atom_type 1 density
 constant 2500 radius constant 0.00031
fix f8  all particletemplate/sphere 1 atom_type 1 density
 constant 2500 radius constant 0.00018
fix f9  all particletemplate/sphere 1 atom_type 1 density
 constant 2500 radius constant 0.00009
# kgv10
fix kgv106 all particledistribution/discrete 42 6 f1 0.030 f2
 0.062 f3 0.416 f4 0.157 f5 0.037 f6 0.298
fix kgv107 all particledistribution/discrete 42 7 f1 0.030 f2
 0.062 f3 0.416 f4 0.157 f5 0.037 f6 0.010 f7 0.288
fix kgv108 all particledistribution/discrete 42 8 f1 0.030 f2
 0.062 f3 0.416 f4 0.157 f5 0.037 f6 0.010 f7 0.002 f8 0.286
fix kgv109 all particledistribution/discrete 42 9 f1 0.030 f2
 0.062 f3 0.416 f4 0.157 f5 0.037 f6 0.010 f7 0.002 f8 0.004 f9
  0.282
# kgv20 = 20 kleinere Fraktionen zu letzter aufaddiert
fix semar6 all particledistribution/discrete 42 6 f2 0.524 f3
 0.214 f4 0.052 f5 0.040 f6 0.020 f7 0.150
fix semar7 all particledistribution/discrete 42 7 f2 0.524 f3
 0.214 f4 0.052 f5 0.040 f6 0.020 f7 0.020 f8 0.130
fix semar8 all particledistribution/discrete 42 8 f2 0.524 f3
```

```
   0.214 f4 0.052 f5 0.040 f6 0.020 f7 0.020 f8 0.070 f9 0.060
# dinger.funk = 30 kleinere Fraktionen zu letzter aufaddiert
fix dinger6 all particledistribution/discrete 42 6 f1 0.127
 f2 0.314 f3 0.259 f4 0.143 f5 0.104 f6 0.053
#fix dinger6 all particledistribution/discrete 42 6 f1
 0.116 f2 0.289 f3 0.239 f4 0.131 f5 0.096 f6 0.129
fix dinger7 all particledistribution/discrete 42 7 f1 0.116
 f2 0.289 f3 0.239 f4 0.131 f5 0.096 f6 0.049 f7 0.080
fix dinger8 all particledistribution/discrete 42 8 f1 0.116
 f2 0.289 f3 0.239 f4 0.131 f5 0.096 f6 0.049 f7 0.044 f8 0.036
# fuller = 40 kleinere Fraktionen zu letzter aufaddiert =
 Neuberechnung
fix fuller6 all particledistribution/discrete 42 6 f1 0.106
 f2 0.262 f3 0.216 f4 0.119 f5 0.087 f6 0.210
fix fuller7 all particledistribution/discrete 42 7 f1 0.106
 f2 0.262 f3 0.216 f4 0.119 f5 0.087 f6 0.045 f7 0.165


## Model
fix ins_pack all insert/pack seed 42 distributiontemplate
 ${psdname}${psdnr} verbose yes maxattempt 2000 insert_every
  once overlapcheck yes all_in yes random_distribute
  exact region  region_box volumefraction_region ${insvfrac}
fix limitnve all nve/limit absolute 1e-6 # displacement
 limit
fix nve_sphere all nve/sphere


## Berechnungseinstellungen
timestep ${ts_length}
fix ts_check all check/timestep/gran 1000 0.2 0.2
compute  dia all property/atom diameter # diameter
compute temp all temp     # temp
compute press all pressure temp # pressure
compute contact all contact/atom # c. number
compute avecont all reduce ave c_contact # ave coordination number
variable cavecont equal c_avecont
thermo_style custom step atoms etotal enthalpy temp press
 v_cavecont v_nreg v_growrate
thermo 1000
thermo_modify lost ignore norm no
compute_modify thermo_temp dynamic yes
# dump lpp
dump dmp_lpp all custom ${ts_dump} ${modelname}/vtk/${modelname}.dump
id type x y z ix iy iz vx vy vz fx fy fz
omegax omegay omegaz radius c_contact
dump_modify dmp_lpp first yes  pad 7 sort
id format "%d %d %.9f %.9f %.9f %.9f
%.9f %.9f %.9f %.9f %.9f %.9f %.9f %.9f
 %.9f %.9f %.9f %.9f %.0f"
# dump images
dump dmp_image_a all image ${ts_dump} ${modelname}/jpga/${modelname}.*a.jpg type
diameter size 1024 1024 shiny 0.5 box yes
```

```
0.01 axes yes 0.25 0.005 view 90 -90 center s 0.5 0.5 0.5
dump_modify dmp_image_a first yes pad 7
acolor 1 lightgrey backcolor white boxcolor blue
dump dmp_image_b all image ${ts_dump}
 ${modelname}/jpgb/${modelname}.*b.jpg type
diameter size 1024 1024 shiny 0.5 box
yes 0.01 axes yes 0.25 0.005 view 0 -90 center s 0.5 0.5 0.5
dump_modify dmp_image_b first yes pad 7
acolor 1 lightgrey backcolor white boxcolor blue
dump dmp_image_c all image ${ts_dump}
 ${modelname}/jpgc/${modelname}.*c.jpg type
diameter size 1024 1024 shiny 0.5 box
yes 0.01 axes yes 0.25 0.005 view 60 -75 center s 0.5 0.5 0.5
dump_modify dmp_image_c first yes pad 7 acolor 1 lightgrey
 backcolor white boxcolor blue

# dump input file voro++
dump dmp_voro_in all custom ${ts_dump}
 ${modelname}/voro/${modelname}.*.voi id x y z radius
dump_modify dmp_voro_in first yes sort id format "%d %.6f %.6f
 %.6f %.6f"

# print thermo
fix prn_thermo all print ${ts_dump} "${cstep} ${catoms}
 ${cetotal} ${centhalpy} ${ctemp} ${cpress} ${cavecont} ${nreg}
  ${growrate}" file ${modelname}/${modelname}.print

## Output for the screen and log file
# insertion
print '------------------------------------------------------------'
print '------ ${modelname} particle insertion ...
 --------------------'
variable m_start equal ${mass_all}
variable c_start equal ${catoms}
variable ts_start equal ${cstep}
run 1 post no
variable m_ins equal ${mass_all}
variable c_ins equal ${catoms}
variable ts_ins equal ${cstep}
variable p_ins equal ${cpress}
print '------------------------------------------------------------'


# Wachsen
print '------------------------------------------------------------'

print '------ ${modelname} growing... -----------------------------'
variable g loop ${growsmax}
label grow
variable grownd atom ${growrate}*c_dia
fix grow all adapt 0 atom diameter v_grownd
```

```
print '--------------------------------------------------------------'

print '------ ${modelname} growing... loop: $g with
 growrate: ${growrate}'
run ${ts_grow} post no
print '--------------------------------------------------------------'
if "$g == ${growsmax}" then "jump SELF growerror"
if "${cpress} < ${growpress}" then "next g" &

"jump SELF grow" else "jump SELF growdone"

label growerror
print 'WARNING: Error growing particles, after

$g attemps pressure of ${growpress} not reached!'

label growdone
unfix grow
variable m_grown equal ${mass_all}
variable c_grown equal ${catoms}
variable ts_grown equal ${cstep}
variable p_grown equal ${cpress}

# Relaxation
print '--------------------------------------------------------------'
print '------ ${modelname} relaxing...
 ---------------------------'
run ${ts_relax} post no
print '--------------------------------------------------------------'

variable m_relaxed equal ${mass_all}
variable c_relaxed equal ${catoms}
variable ts_relaxed equal ${cstep}
variable p_relaxed equal ${cpress}

variable growratevol equal ${m_grown}/${m_ins}
variable growratelin equal ${growratevol}^(1/3)
variable nreg_ins equal (${vreg}-(${m_ins}/2500))/${vreg}
variable nreg_grown equal (${vreg}-(${m_grown}/2500))/${vreg}
variable nreg_relaxed equal
 (${vreg}-(${m_relaxed}/2500))/${vreg}
print "mass start: ${m_start}   mass ins:
${m_ins}   mass grown: ${m_grown} mass relaxed:
${m_relaxed}"
print "count start: ${c_start}   count ins:

${c_ins}   count grown: ${c_grown}   count relaxed: ${c_relaxed}"

print "steps start: ${ts_start}   steps ins: ${ts_ins}
 steps grown: ${ts_grown}   steps relaxed: ${ts_relaxed}"
```

```
print "press start: --   press ins: ${p_ins}

press grown: ${p_grown}   press relaxed: ${p_relaxed}"

print "poro0: --   poro ins: ${nreg_ins}   poro grown:
 ${nreg_grown} poro relaxed: ${nreg_relaxed}"

print "growrate_linear: ${growratelin}

growrate_volume: ${growratevol}"
variable dmp_ins equal ${ts_dump}
variable dmp_grown equal floor(${ts_grown}/${ts_dump})*${ts_dump}
variable dmp_relaxed equal floor(${ts_relaxed}/${ts_dump})*${ts_dump}
write_restart ${modelname}/${modelname}.restart
shell date +%_a_%_d_%_b_%R >> ${modelname}/tmp.time
shell date +%s >> ${modelname}/tmp.0
log none
```

C. Appendix - Image analysis

All of the written codes are developed based on the online help of *MATLAB*, various Youtube examples and different available partial codes from *MATLAB* community. In the following 3 *MATLAB*-codes for visualization of the packing, capturing section-images and calculation of coefficient of homogeneity (C_H) is presented:

1. *MATLAB*-code written by author for visualization of the particle assemblies and capturing section-images from numerically generated packings.

2. *MATLAB*-code written by author for calculation of *DF* for section-images.

3. *MATLAB*-code written by author for calculation of coefficient of homogeneity (C_H).

C.1. Visualization of the particle assemblies

```
close all               % CLOSES ALL THE PROGRAMS
clear all               % CLEARS ALL THE VARIABLES
clc                     % CLEAR THE CONSOLE


load SFT_5.txt          %open file packing2.txt without any
text data and headers

x = SFT_5(:,1)*945      % multiply the 3rd row by 1000 and store it in x
y = SFT_5(:,2)*945      % multiply the 4th row by 1000 and store it in y
z = SFT_5(:,3)*945      % multiply the 5th row by 1000 and store it in z
r = SFT_5(:,6)*945      % multiply the 18th row by 1000 and store it in r

xyz = cat(2,x,y,z)      % make two dimentional matrix from x,y,z

[NumSpheres, nDims] = size(xyz);          % store the dimention of matrix xyz
%NumSpheres = rows    of xyz
%nDims      = columns of xyz

Radius=r                                  % store r row in radius

% A 3-D matrix 'F' which has its value at particular
coordinate set to 255 if it belongs to any one of the spheres and 0 otherwise.

[X,Y,Z] = meshgrid(1:100, 1:100, 1:140);   % make 100*100*100
matrix for each X,Y,Z   3D matrix

F = zeros(size(X));            % make a 3d matrix like X but all zero values

% loops from 1 until NumSpheres
for SpNum = 1:NumSpheres
```

```
    F( sqrt((X - xyz(SpNum,1)).^2 + (Y - xyz(SpNum,2)).^2 + (Z - xyz(SpNum,3)).^2)
     <=Radius(SpNum) ) = 255;

end

% Extract cross sections from F using interp3 function along the z-axis.

I = zeros(size(X));          % make a zero valued matrix of size (X)
which is same size of F

for i = 1:50

    % after each 5
    sample_space = 5;
    modresult = mod(i,sample_space);

    if modresult == 0
        % make the file name
        fname = sprintf('./Z_SFT_3B_3/image%04d.tiff', i);

        I(:,:,i) = interp3(X, Y, Z, F, 1:100, (1:100)', i, 'spline');

        % store the image in a file
        imwrite(I(:,:,i),fname,'tiff');
    end

end

hold on
[X,Y,Z] = ellipsoid(0,0,0,1,1,1,50);               % ellipsoid(xc,yc,zc,xr,yr,zr,n)
%cols = interp1(0:6, lines(7), rand(NumSpheres,1)*6);

for i = 1:NumSpheres

    m = repmat(Radius(i)/100,NumSpheres,1);
    cols = interp1(0:6, lines(7), m*18);

    surface(X*Radius(i) + xyz(i,1),...
    Y*Radius(i) + xyz(i,2),...
    Z*Radius(i) + xyz(i,3),...
    'facecolor',cols(i,:), 'EdgeColor','none');

end

 view(3), axis image, camlight
% % % % wb2 = imcomplement(I);
% % % % P = imresize(wb2, 8.0);
% % % % P2 = bwareaopen(P, 150,4);
% % % implay(P,5)
```

C.2. Capturing of the section-images soil surface

```
  close all
  clear all
  clc
  a = imread('Layer4_before.JPG');
  figure
imshow(a);

disp('If it is a test of glass beads, please enter 1');
disp('If it is a test of granular materials, please enter 2')

z=input('please input number:');


switch z
    case 1
        disp('GLASS BEADS')
        disp('SOME RECOMMANDATIONS:');
disp('For very dark images use LI = 0.05')
disp('  For very bright images use LI > 0.6 ')
disp('For the images neither very dark nor very bright use a value ');
disp('           between LI = 0.05 and 0.6');
disp('Recomend try to use LI=0.1 firstly')
Light_intensity=input('please input the light intensity (LI):');
title('Original Photo')
I = rgb2gray(a);
bw = im2bw(I,Light_intensity);
figure
imshow(bw)
title('Black and White Photo')

disp('If this is a satisfied Light Intensity value, please enter 1');
disp('others, please enter 2');
w=input('please input number:');


while w==2;

Light_intensity=input('please input the light intensity (LI):');

I = rgb2gray(a);

bw = im2bw(I,Light_intensity);
bw = bwareaopen(bw,140);
se = strel('arbitrary',2);
bw = imclose(bw,se);

bw = imfill(bw,'holes');

imshow(bw)
```

```
title('Black and White Photo')

disp('If this is a satisfied Light Intensity value, please enter 1');
disp('others, please enter 2');
w=input('please input number:');

end

d = imdistline;


min=input('please input the minimun size of the scale in pixel:');
max=input('please input the maximun size of the scale in pixel:');
delete(d);
J = imresize(bw, 0.4);
figure
imshow(J);
title('Black and White Photo&Detected Circles')

Rmin = min*0.4/2;
Rmax = max*0.4/2;
[centers, radii] = imfindcircles(J,[Rmin Rmax],'ObjectPolarity',
'bright','Sensitivity',0.9);
h = viscircles(centers,radii,'EdgeColor','b');

x=[centers, radii];
particle_number=size(x);
diameter=radii*2;
d_mm=round((diameter)/(0.4*24));
d_cm=d_mm*0.1;
d_cm=unique(d_cm);
q = unique(d_mm);
out = [q,histc(d_mm(:),q)];
mass_g=(2.5*pi/6)*d_cm.^3;
out1=[out,mass_g];
total_mass=out1(:,3).*out1(:,2);
sum_mass=sum(total_mass);
mass_percent=total_mass/sum_mass*100;
Size=size(mass_percent);
loopsize=Size(1,1);
cum=mass_percent(1,1);
for i=2:loopsize
cum(i)=cum(i-1)+mass_percent(i,1);
end
out2=[out1,total_mass];
out3=[out2,mass_percent];
out4=[out3,cum'];
figure
e=plot(out4(:,1),out4(:,6));
```

```
axis([16,inf,0,inf]);
title('diameter & cumulative mass percentage')
xlabel('diameter[mm]')
ylabel('cumulative mass percentage[%]')
grid on
out4=[cellstr('diameter[mm]'),cellstr('number'),cellstr('mass of
each kind(g)'),cellstr('total mass(g)'),cellstr('percentage of
mass(%)'),cellstr('cumulative mass(g)');num2cell(out4)]


    otherwise
         disp('GRANULAR MATERIALS');
         disp('SOME RECOMMENDATIONS:');
disp('For very dark images use LI = 0.05')
disp('  For very bright images use LI > 0.6 ')
disp('For the images neither very dark nor very bright use a value ');
disp('          between LI = 0.05 and 0.6');
disp('Recomend try to use LI=0.1 firstly')
Light_intensity=input('please input the light intensity (LI):');


title('Original Photo')
I = rgb2gray(a);

bw = im2bw(I,Light_intensity);
bw = bwareaopen(bw,400);
se = strel('arbitrary',2);
bw = imclose(bw,se);

bw = imfill(bw,'holes');
figure
imshow(bw)
title('Black and White Photo')

disp('If this is a satisfied Light Intensity value, please enter 1');
disp('others, please enter 2');
w=input('please input number:');


while w==2;

Light_intensity=input('please input the light intensity (LI):');

I = rgb2gray(a);

bw = im2bw(I,Light_intensity);
bw = bwareaopen(bw,140);
se = strel('arbitrary',2);
bw = imclose(bw,se);

bw = imfill(bw,'holes');
```

```
imshow(bw)
title('Black and White Photo')

disp('If this is a satisfied Light Intensity value, please enter 1');
disp('others, please enter 2');
w=input('please input number:');

end

[B,L] = bwboundaries(bw,'holes');
figure
imshow(label2rgb(L, @jet, [.5 .5 .5]))
hold on
for k = 1:length(B)
  boundary = B{k};
  plot(boundary(:,2), boundary(:,1), 'w', 'LineWidth', 2)
end



J = imresize(bw, 0.4);




    CC = bwconncomp(J,8);
    RGPROP_Area = regionprops(CC, 'Area');
    areas = cat(1, RGPROP_Area.Area);
areas_size=size(areas);

for j=1 : areas_size(1,1)
    radii(j)=(areas(j,1)/pi).^0.5;
end



particle_number=areas_size(1,1);
diameter=radii*2;
d_mm=round((diameter)/(0.4*24));
d_mm(d_mm==0) = [];
d_mm(d_mm==1) = [];
d_mm(d_mm==2) = [];
d_mm(d_mm==3) = [];
d_cm=d_mm*0.1;
d_cm=unique(d_cm);
q = unique(d_mm);
q=q';
d_mm=d_mm';
```

```
b=histc(d_mm(:),q);
out = [q,b];
mass_g=(2.5*pi/6)*d_cm.^3;
out1=[out,mass_g'];
total_mass=out1(:,3).*out1(:,2);
sum_mass=sum(total_mass);
mass_percent=total_mass/sum_mass*100;
Size=size(mass_percent);
loopsize=Size(1,1);
cum=mass_percent(1,1);
for i=2:loopsize
cum(i)=cum(i-1)+mass_percent(i,1);
end
out2=[out1,total_mass];
out3=[out2,mass_percent];
out4=[out3,cum'];
figure
e=plot(out4(:,1),out4(:,6));
g=min(out4(:,1))-3;
h=max(out4(:,1))+3;
axis([g,h,0,inf]);
title('diameter & cumulative mass percentage')
xlabel('diameter[mm]')
ylabel('cumulative mass percentage[%]')
grid on
out4=[cellstr('dimater[mm]'),cellstr('number'),cellstr('mass of
each kind(g)'),cellstr('total mass(g)'),cellstr('percentage of
mass(%)'),cellstr('culmilative mass(g)');num2cell(out4)]
end

disp('If you want to save the Figures, please enter 1');
disp('others, please enter 2');
kk=input('please input number:');

if kk==1

    saveas(gcf,'output.jpg') ;
end
```

C.3. Calculation of C_H for section-images

```
%Program  first opens an image and then make some corrections
% for the calculateion of CH (Coefficent of Homogeneity)
%-------------------------------------------------------------
clear all
close all
clc
%-------------------------------------------------------------
% the image of the particles has to  have bright backgraund and dark
```

145

```
% particles
%Get original image from file
[filename, pathname] = uigetfile( ...
{'*.jpg;*.tif;*.png','Image Files (*.jpg;*.tif;*.png)';
'*.png','png files (*.png)';
'*.jpg','Jpeg files (*.jpg)';
'*.tif','Tiff files (*.tif)'; ...
'*.*', 'All Files (*.*)'}, ...
'Select the image',...
'\\in.uni-weimar.de\fs\home\b\m\lpqx5569\dokumente\PHD
\Homogeneity\Pack_Semar3f_zSec\all Alices');

img = (imread([pathname, filename]));

Filter_level=0.5;
bw1 = im2bw(img,Filter_level);
wb2 = imcomplement(bw1);
L = bwlabel(bw1);
Image_size=size(bw1);
n=Image_size(1,1);
    figure
    %imshow(bw1);
    img = wb2;  %# Load a sample 3-D RGB image
img(n/4:n/4:end,:,:) = 0;        %# Change every tenth row to black
img(:,n/4:n/4:end,:) = 0;        %# Change every tenth column to black
imshow(img) %# Display the image
    axis on
    title(['REV is equal to image size/4 - file name is: ',filename,'  '])


% the wihte pixels will be calculated

% by default regions are consisted of 25 equal units based on 5 d_max
% Image / (u=5)
u = input('Enter a number between 1 to 5 to dvivide the image in each direction: ');

switch u
    case 1
        disp('original image will be divided into 1 subimage(s)')
    case 2
        disp('original image will be divided into 1 to 4 subimage(s)')
    case 3
        disp('original image will be divided into 1 to 9 subimage(s)')
    case 4
        disp('original image will be divided into 1 to 16 subimage(s)')
    otherwise
        disp('original image will be divided into 1 to 25 subimage(s)')
end

for j=1:1:u
    %% prelocation for speed
```

```
ecs=zeros(1,j^2);
edias=zeros(1,j^2);
f=zeros(1,j^2);
areas=zeros(1,j^2);
%% cropping in a way that the CH can be calculated in most effetively
if rem(n,j)==0
myImage = imcrop(wb2,[0 0 n n]); %here for cropping image
else
    n=n-rem(n,j);
    myImage = imcrop(wb2,[0 0 n n]); %here for cropping image
end
u_width=n/j;
REV_size(j)=u_width;

%% starting blocking the image

xBlockSize = u_width;
yBlockSize = u_width;
xOverlap = 0;
yOverlap = 0;

x = 1:(xBlockSize - xOverlap):n;
y = 1:(yBlockSize - yOverlap):n;

[X,Y] = meshgrid(x,y);

subImages = arrayfun( @(x,y) myImage( x:min( end, x +
xBlockSize - 1), y:min( end, y + yBlockSize - 1) ), X, Y,
'UniformOutput', false )';
A=size(subImages);
loopsize=A(1,1)*A(1,2);

%% start calculating the units properties
for i=1:loopsize


    CC = bwconncomp(subImages{i},8);
    RGPROP_C = regionprops(CC, 'Centroid');
    centroids = cat(1, RGPROP_C.Centroid);
    CENTdist=(pdist(centroids,'euclidean'));

    m_dist(i,j)=mean(CENTdist);
    std_dist(i,j)=std(CENTdist);
    var_dist(i,j)=var(CENTdist/max(CENTdist),1);

    % finding the number of particles
    NUM(i,j) = max(size(centroids));

    m_dist(isnan(m_dist)) = 0;
    std_dist(isnan(std_dist)) = 0;
```

```
        var_dist(isnan(var_dist)) = 0;
        %-Normalize Values and shape into a vector
        %-Normalize centroid distances
        if j==1
         Norm_dist_v1= m_dist(:,j)/max(m_dist(:,j));
         NDist1=var(Norm_dist_v1);
        end
        if j==2
Norm_dist_v2= m_dist(:,j)/max(m_dist(:,j));
         NDist2=var(Norm_dist_v2);
        end
        if j==3
Norm_dist_v3= m_dist(:,j)/max(m_dist(:,j));
         NDist3=var(Norm_dist_v3);
        end
        if j==4
Norm_dist_v4= m_dist(:,j)/max(m_dist(:,j));
         NDist4=var(Norm_dist_v4);
        end
        if j==5
Norm_dist_v5= m_dist(:,j)/max(m_dist(:,j));
         NDist5=var(Norm_dist_v5);
        end



        %-Normalize particle Number

        if j==1
         Norm_particle_num_v1= NUM(:,j)/max(NUM(:,j));
         ND1=var(Norm_particle_num_v1);
        end
        if j==2
        Norm_particle_num_v2= NUM(:,j)/max(NUM(:,j));
        ND2=var(Norm_particle_num_v2);
        end
        if j==3
        Norm_particle_num_v3= NUM(:,j)/max(NUM(:,j));
        ND3=var(Norm_particle_num_v3);
        end
        if j==4
        Norm_particle_num_v4= NUM(:,j)/max(NUM(:,j));
        ND4=var(Norm_particle_num_v4);
        end
        if j==5
        Norm_particle_num_v5= NUM(:,j)/max(NUM(:,j));
        ND5=var(Norm_particle_num_v5);
        end


Num1=size(centroids);
```

```
a = Num1(1,1)+ Num1(1,2);
if a==0
    xc(i)=u_width/2;
    yc(i)=u_width/2;
end
if a==2
    xc(i)= centroids(1,1);
    yc(i)= centroids(1,2);
end
if a>=2
    xc(i)= mean(centroids(:,1));
    yc(i)= mean(centroids(:,2));
end

    %% Fraction Area
        RGPROP_A = regionprops(CC, 'Area');
        areas = cat(1, RGPROP_A.Area);
    sum_area_white_pix=sum(areas); %solid Areas
    Area_Total=u_width^2;
    Porosity(i,j)=(Area_Total-sum(areas))/Area_Total;
    m_fraction_area(i,j)=mean(areas);
    std_fraction_area(i,j)=std(areas);
    var_fraction_area(i,j)=var(areas,1);
        m_fraction_area(isnan(m_fraction_area)) = 0;
        std_fraction_area(isnan(std_fraction_area)) = 0;
        var_fraction_area(isnan(var_fraction_area)) = 0;

        %-Normalize Values and shape into a vector
        if j==1
         Norm_poros_vector1= Porosity(:,j)/max(Porosity(:,j));
         NP1=var(Norm_poros_vector1);
        end
        if j==2
        Norm_poros_vector2= Porosity(:,j)/max(Porosity(:,j));
        NP2=var(Norm_poros_vector2);
        end
        if j==3
        Norm_poros_vector3= Porosity(:,j)/max(Porosity(:,j));
        NP3=var(Norm_poros_vector3);
        end
        if j==4
        Norm_poros_vector4= Porosity(:,j)/max(Porosity(:,j));
        NP4=var(Norm_poros_vector4);
        end
        if j==5
        Norm_poros_vector5= Porosity(:,j)/max(Porosity(:,j));
        NP5=var(Norm_poros_vector5);
        end

    %% Equivalent Diamters
        RGPROP_ED= regionprops(CC, 'EquivDiameter');
```

```
            edias = cat(1, RGPROP_ED.EquivDiameter);



     m_edia(i,j)=mean(edias);
     std_edia(i,j)=std(edias);
     var_edia(i,j)=var(edias,1);
         m_edia(isnan(m_edia)) = 0;
         std_edia(isnan(std_edia)) = 0;
         var_edia(isnan(var_edia)) = 0;
         %-Normalize Values and shape into a vector
         if j==1
          Norm_edia_vector1= m_edia(:,j)/max(m_edia(:,j));
          NED1=var(Norm_edia_vector1);
         end
         if j==2
          Norm_edia_vector2= m_edia(:,j)/max(m_edia(:,j));
          NED2=var(Norm_edia_vector2);
         end
         if j==3
          Norm_edia_vector3= m_edia(:,j)/max(m_edia(:,j));
          NED3=var(Norm_edia_vector3);
         end
         if j==4
          Norm_edia_vector4= m_edia(:,j)/max(m_edia(:,j));
          NED4=var(Norm_edia_vector4);
         end
         if j==5
          Norm_edia_vector5= m_edia(:,j)/max(m_edia(:,j));
          NED5=var(Norm_edia_vector5);
         end


      %% Particle Ecentrecities
         RGPROP_EC = regionprops(CC, 'Eccentricity');
         ecs = cat(1, RGPROP_EC.Eccentricity);

     m_ecs(i,j)=mean(ecs);
     std_ecs(i,j)=std(ecs);
     var_ecs(i,j)=var(ecs,1);



%          if size(ecs)==[0,0]
%              ecs(i)= 0;
%          else
%               ecs(i)= ecs(1,1);
%          end

%-------------------------------------------------------------------
%        %% Axis Ratio s
%          MajAxL = regionprops(CC, 'MajorAxisLength');
%          majaxls = cat(1, MajAxL.MajorAxisLength);
```

```
%
%          MinAxL= regionprops(CC, 'MinorAxisLength');
%          minaxls = cat(1, MinAxL.MinorAxisLength);
%
%          AxisRatio=majaxls./minaxls;
%          axisratio=mean(AxisRatio);
%
%    std_axisratio(i,j)=std(axisratio);
%    m_axisratio(i,j)=mean(axisratio);
%    var_axisratio(i,j)=var(axisratio,1);
%
    %% Orientation
    Ori = regionprops(CC, 'Orientation');
    oris = cat(1, Ori.Orientation);

    m_ori(i,j)=mean(oris);
    std_ori(i,j)=std(oris);
    var_ori(i,j)=var(oris,1);
    %%

switch j
    case 1
        X1 = Norm_particle_num_v1;
        X2 = Norm_poros_vector1;
        X3 = Norm_edia_vector1;
       % X4 = Norm_dist_v1; <----- additional parameter of the normalized
       % distance of centroid of each particle
        c1=cat(2,X1,X2,X3);%,X4); <--- Here, the additional
        paramters can be added

    case 2
        X1 = Norm_particle_num_v2;
        X2 = Norm_poros_vector2;
        X3 = Norm_edia_vector2;
       % X4 = Norm_dist_v2;
        c2=cat(2,X1,X2,X3);%,X4); <--- Here, the additional
        paramters can be added

    case 3
        X1 = Norm_particle_num_v3;
        X2 = Norm_poros_vector3;
        X3 = Norm_edia_vector3;
       % X4 = Norm_dist_v3;
        c3=cat(2,X1,X2,X3);%,X4); <--- Here, the additional
        paramters can be added

    case 4
        X1 = Norm_particle_num_v4;
        X2 = Norm_poros_vector4;
        X3 = Norm_edia_vector4;
       % X4 = Norm_dist_v4;
```

```
                c4=cat(2,X1,X2,X3);%,X4); <--- Here, the additional
                paramters can be added

        otherwise
            X1 = Norm_particle_num_v5;
            X2 = Norm_poros_vector5;
            X3 = Norm_edia_vector5;
          % X4 = Norm_dist_v5;
            c5=cat(2,X1,X2,X3);%,X4); <--- Here, the additional
            paramters can be added

end

        f=figure;
         imshow(subImages{i})
          hold on
s=size(centroids);
          if s(1,1)>0
              plot(centroids(:,1), centroids(:,2), 'b*')
              title(['Equivalent Diameter is: ',num2str(mean(edias)),' Pixels'])
          end

          hold off


    end



    %plotting the centroids

    f(i)=figure
        set(gcf,'PaperUnits','inches');
        set(gcf,'PaperSize', [8 8]);
        set(gcf,'PaperPosition',[0.5 0.5 7 7]);
        set(gcf,'PaperPositionMode','Manual');
    scatter(xc,yc,120,'b','filled');
    axis([0 u_width 0 u_width]);
    title(['Unit size is',num2str(u_width),'Pixels']);

    %% writing the centroids in a textfile
    %dlmwrite('x_centroids.txt',xc(i,j),'-append','delimiter',' ','roffset',j);
    %type('x_centroids.txt');
%    dlmwrite('y_centroids.txt',yc(i,j),'-append','delimiter',' ','roffset',j);
%    type('y_centroids.txt');
%    dlmwrite('centroids_distances.txt',CENTdist,'-append',
'delimiter',' ','roffset',j);
%    type('centroids_distances.txt');
    %% reading the textfiles of centroides
    %x_centroids=dlmread('x_centroids.txt');
```

```
    %y_centroids=dlmread('y_centroids.txt');
    %centroids_distances=dlmread('centroids_distances.txt');

end

%% Variation Particle Numbers
%-----------------------------------------------------------



if exist('c1','var')>0 && exist('c2','var')==0
    figure
    plotmatrix(c1)

    end
    if exist('c2','var')>0 && exist('c3','var')==0
    figure
    plotmatrix(c2)

    end
    if exist('c3','var')>0 && exist('c4','var')==0
    figure
    plotmatrix(c3)
    COVMATRIX=cov(c3);
    end
    if exist('c4','var')>0 && exist('c5','var')==0
    figure
    plotmatrix(c4)
    COVMATRIX=cov(c4);
    end
    if exist('c5','var')>0
    figure
    plotmatrix(c5)
    COVMATRIX=cov(c5);
    end

    %Calculate Covariances for all parameters (X1 = Norm_particle_num_v1 &
    % X2 = Norm_poros_vector1) relations and sum them
    % calc of CH
    if exist('c1','var')>0
    COVMATRIX1x1=cov(c1);

     idx = find(COVMATRIX1x1<0);
 while any(idx)
     COVMATRIX1x1(idx) = COVMATRIX1x1(idx)*-1;
     idx = find(COVMATRIX1x1<0);
 end

    sumc1x1=sum(COVMATRIX1x1);
    sum1x1=sum(sumc1x1);
    C_H_1x1=(1-sum1x1)*100;
```

```
        end

        if exist('c2','var')>0
        COVMATRIX2x2=cov(c2);
            idx = find(COVMATRIX2x2<0);
    while any(idx)
        COVMATRIX2x2(idx) = COVMATRIX2x2(idx)*-1
        idx = find(COVMATRIX2x2<0);
    end

        sumc2x2=sum(COVMATRIX2x2);
        sum2x2=sum(sumc2x2);
        C_H_2x2=(1-sum2x2)*100;
        end

        if exist('c3','var')>0
        COVMATRIX3x3=cov(c3);
            idx = find(COVMATRIX3x3<0);
    while any(idx)
        COVMATRIX3x3(idx) = COVMATRIX3x3(idx)*-1;
        idx = find(COVMATRIX3x3<0);
    end

        sumc3x3=sum(COVMATRIX3x3);
        sum3x3=sum(sumc3x3);
        C_H_3x3=(1-sum3x3)*100;
        end

        if exist('c4','var')>0
        COVMATRIX4x4=cov(c4);
            idx = find(COVMATRIX4x4<0);
    while any(idx)
        COVMATRIX4x4(idx) = COVMATRIX4x4(idx)*-1;
        idx = find(COVMATRIX4x4<0);
    end

        sumc4x4=sum(COVMATRIX4x4);
        sum4x4=sum(sumc4x4);
        C_H_4x4=(1-sum4x4)*100;
        end

        if exist('c5','var')>0
        COVMATRIX5x5=cov(c5);
            idx = find(COVMATRIX5x5<0);
    while any(idx)
        COVMATRIX5x5(idx) = COVMATRIX5x5(idx)*-1;
        idx = find(COVMATRIX5x5<0);
    end

        sumc5x5=sum(COVMATRIX5x5);
        sum5x5=sum(sumc5x5);
```

```
        C_H_5x5=(1-sum5x5)*100;
    end
    CH=C_H_1x1;
      if exist('C_H_2x2','var')>0
    CH=[CH,C_H_2x2];
      end
      if exist('C_H_3x3','var')>0
    CH=[CH,C_H_3x3];
      end
      if exist('C_H_4x4','var')>0
    CH=[CH,C_H_4x4];
      end
      if exist('C_H_5x5','var')>0
    CH=[CH,C_H_5x5];
      end
 figure
plot(REV_size,CH,'-ks','LineWidth',1.5 )
title([' Coefficient of Homogeneity vs REV Size in Pixel'],'FontSize',12)
xlabel('REV Size [Pixel]')
ylabel('Coefficient of Homogeneity (CH) [%]')
grid on
```

C.4. Code for calculation of *DF*

```
function [ D ] = hausDim( Image )
% HAUSDIM Returns the Haussdorf fractal dimension of an object represented by
% a binary image.
%    Returns the Haussdorf fractal dimension D of an object represented by the
%    binary image I. Nonzero pixels belong to an object and 0 pixels
%    constitute the background.
%
%    Algorithm
%    ---------
%    1 - Pad the image with background pixels so that its dimensions are a
%        power of 2.
%    2 - Set the box size 'e' to the size of the image.
%    3 - Compute N(e), which corresponds to the number of boxes of size 'e'
%        which contains at least one object pixel.
%    4 - If e > 1 then e = e / 2 and repeat step 3.
%    5 - Compute the points log(N(e)) x log(1/e) and use the least squares
%        method to fit a line to the points.
%    6 - The returned Haussdorf fractal dimension D is the slope of the line.
%
%    Author
%    ------
%    Alceu Ferraz Costa
%    email: alceufc [at] icmc [dot] usp [dot] br
%
```

```
% Pad the image with background pixels so that its dimensions are a power of 2.
maxDim = max(size(Image));
newDimSize = 2^ceil(log2(maxDim));
rowPad = newDimSize - size(Image, 1);
colPad = newDimSize - size(Image, 2);
Image = padarray(Image, [rowPad, colPad], 'post');

boxCounts = zeros(1, ceil(log2(maxDim)));
resolutions = zeros(1, ceil(log2(maxDim)));

boxSize = size(Image, 1);
boxesPerDim = 1;
idx = 0;
while boxSize >= 1
    boxCount = 0;

    for boxRow = 1:boxesPerDim
        for boxCol = 1:boxesPerDim
            minRow = (boxRow - 1) * boxSize + 1;
            maxRow = boxRow * boxSize;
            minCol = (boxCol - 1) * boxSize + 1;
            maxCol = boxCol * boxSize;

            objFound = false;
            for row = minRow:maxRow
                for col = minCol:maxCol
                    if Image(row, col)
                        boxCount = boxCount + 1;
                        objFound = true; % Break from nested loop.
                    end;

                    if objFound
                        break; % Break from nested loop.
                    end;
                end;

                if objFound
                    break; % Break from nested loop.
                end;
            end;
        end;
    end;

    idx = idx + 1;
    boxCounts(idx) = boxCount;
    resolutions(idx) = 1 / boxSize;

    boxesPerDim = boxesPerDim * 2;
    boxSize = boxSize / 2;
end;
```

```
    D = polyfit(log(resolutions), log(boxCounts), 1);
    D = D(1);
end
```

D. Appendix - Significance of suffusion criterion

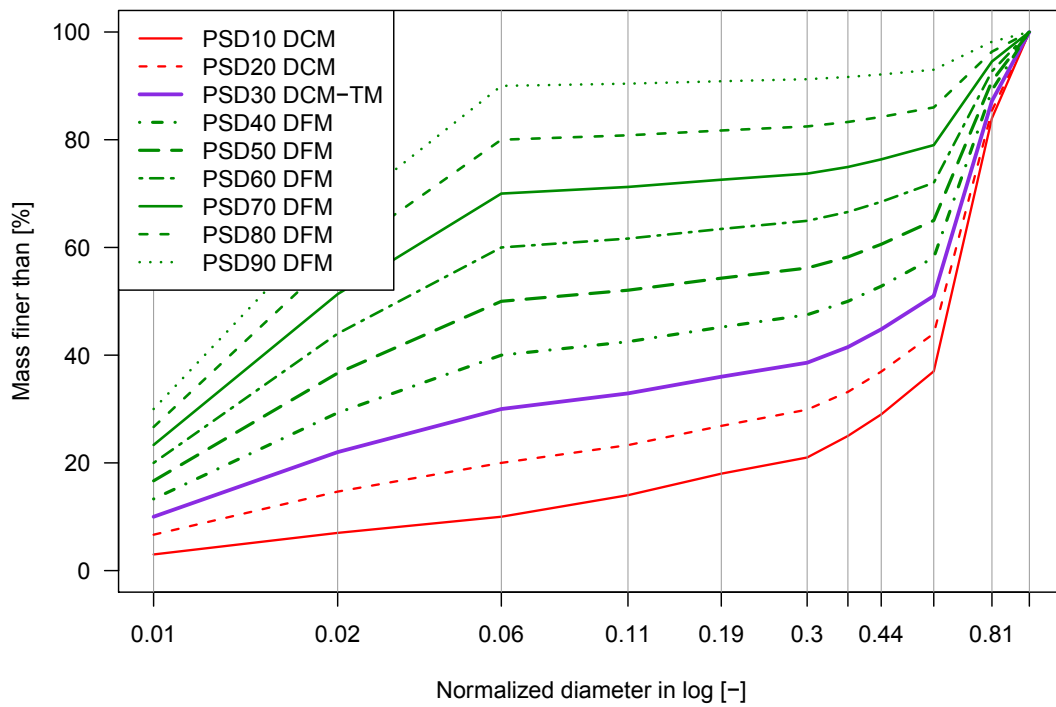## D.1. Example - Application of proposed suffusion criterion for a band of PSD

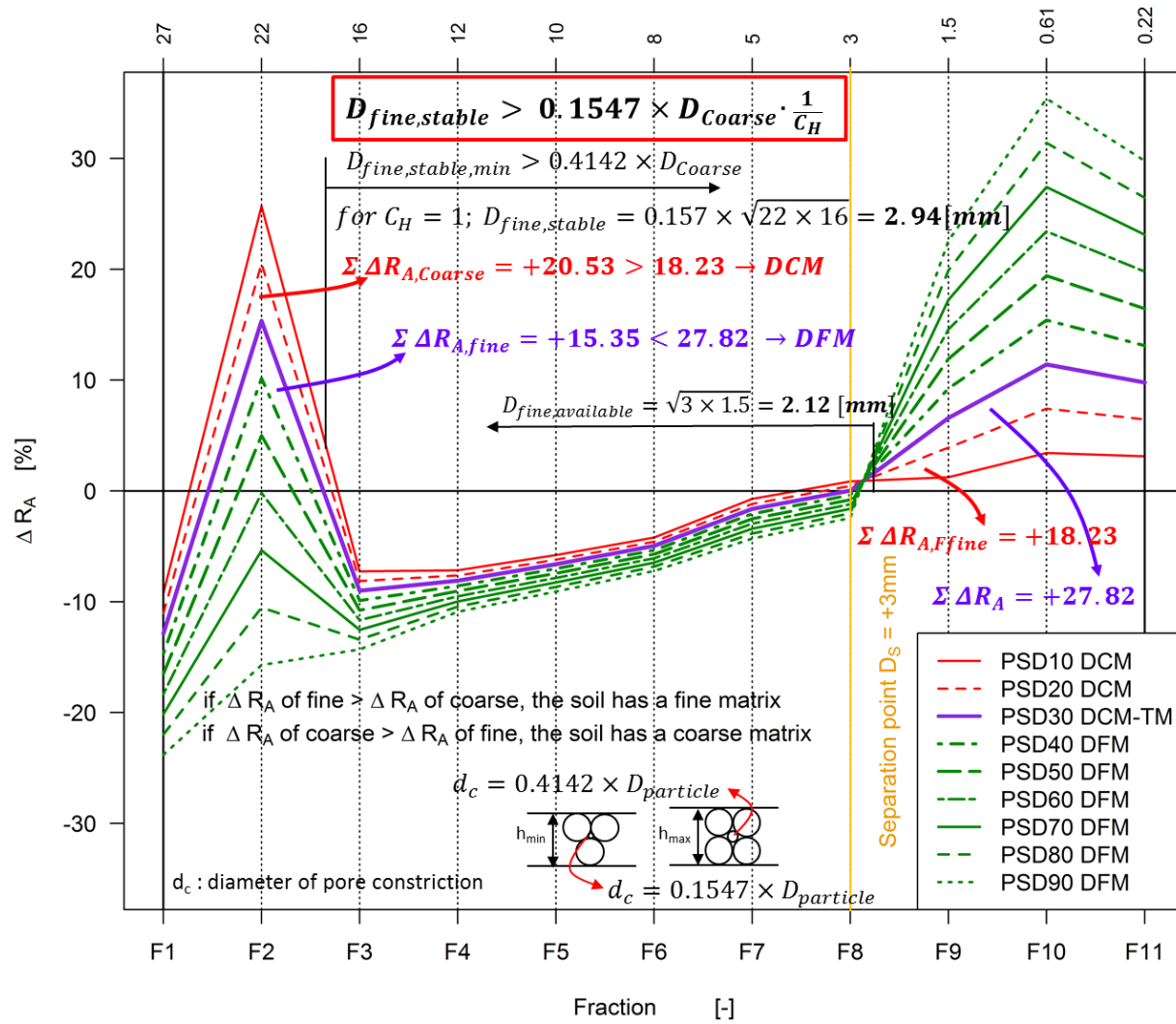Figure D.1.: Significance of the proposed suffusion criterion - PSD1 with different amount of fines

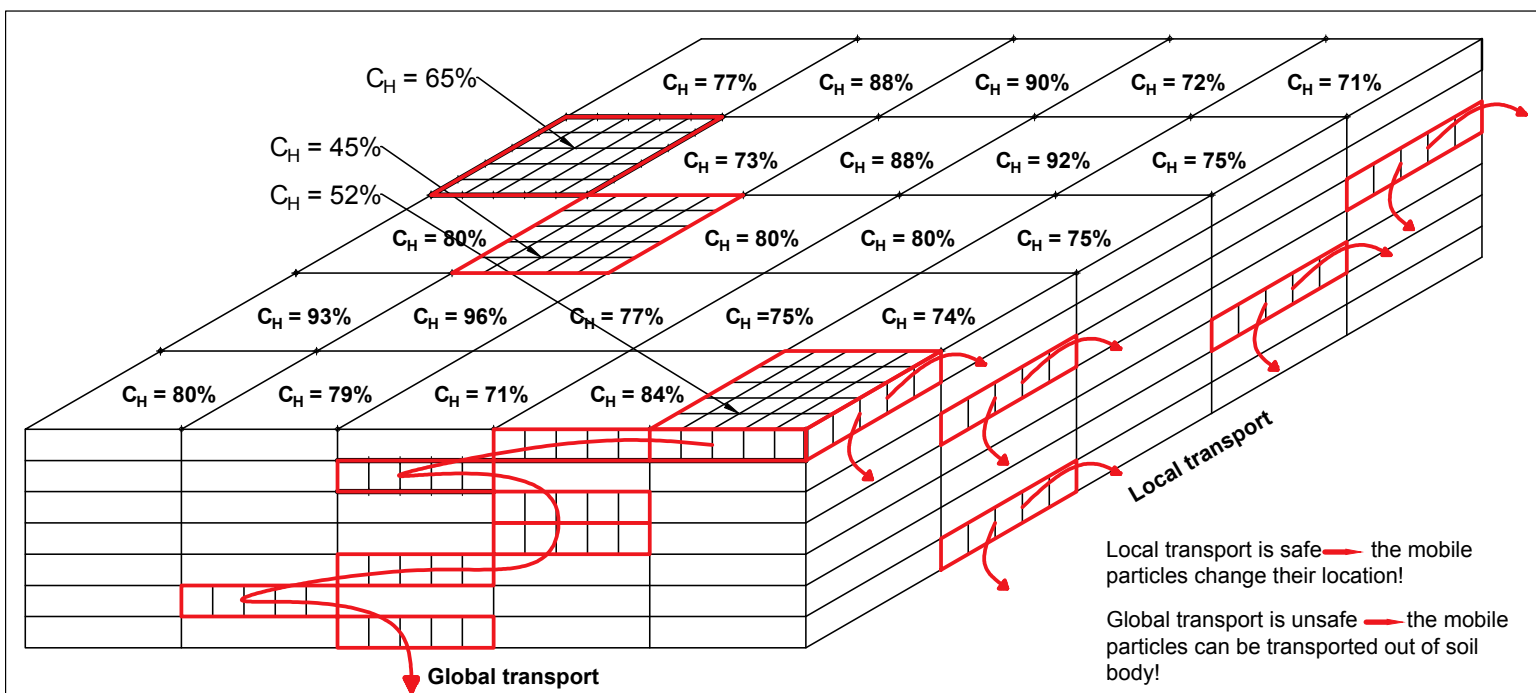Figure D.2.: proposed suffusion criterion - PSD1 with different amount of fill

Figure D.3.: Illustration of the measured C_H and its relationship to local and global particle transport